Study of Volatile Organic Compounds (VOC) in the cloudy atmosphere : air/droplet partitioning of VOC

Miao Wang

UNIVERSITE CLERMONT AUVERGNE

DOCTORAL SCHOOL OF FUNDAMENTAL SCIENCES

PhD Thesis

in partial fulfilment of the requirements for the degree of

Doctor of University Clermont Auvergne

Specialty : Physics-Chemistry of the Atmosphere and Climate

Submitted and presented by
« WANG Miao »

Graduate of the Master Physics and Chemistry for the Environment

Study of Volatile Organic Compounds (VOC) in the cloudy atmosphere : air/droplet partitioning of VOC

To be defended the 16th of December 2019

Jury member of the committee:

Huret Nathalie	President
Leriche Maud	Reviewer
Sauvage Stéphane	Reviewer
Mailhot Gilles	Examiner
Beekmann Matthias	Examiner
Colomb Aurélie	Invited
Borbon Agnès	Co-supervisor
Deguillaume Laurent	Supervisor

UNIVERSITE CLERMONT AUVERGNE

ECOLE DOCTORALE DES SCIENCES FONDAMENTALES

THESE

présentée pour obtenir le grade de

DOCTEUR D'UNIVERSITE CLERMONT AUVERGNE

Spécialité : Physique-chimie de l'atmosphère et climat

Par « **WANG Miao** »

Diplômée du Master Physique et Chimie pour l'Environnement

Etude des Composés Organiques Volatils (COV) dans l'atmosphère nuageuse au sommet du puy de Dôme : partition air/goutte des COV et impact sur la chimie atmosphérique

Soutenance prévue publiquement le 16 Décembre 2019 devant le jury :

Huret Nathalie	Président
Leriche Maud	Rapporteur
Sauvage Stéphane	Rapporteur
Mailhot Gilles	Examinateur
Beekmann Matthias	Examinateur
Colomb Aurélie	Invitée
Borbon Agnès	Co-directrice de thèse
Deguillaume Laurent	Directeur de thèse

Table of contents

Table of figures

Table of tables

Introduction

Volatile Organic Compounds (VOC), including saturated, unsaturated, and other substituted hydrocarbons, play a major role in atmospheric chemistry (Atkinson, 2000). They are primarily emitted by anthropogenic and biogenic sources into the atmosphere; they are also transformed *in situ* by chemical reactions, and more specifically, by photo-oxidation leading to the formation of ozone (O_3) and Secondary Organic Aerosol (SOA) (Atkinson and Arey, 2003; Kanakidou et al., 2005; Goldstein and Galbally, 2007; Carlton et al., 2009; Hallquist et al., 2009; Chen et al., 2018; Palm et al., 2018). By altering the organic fraction of aerosol particles, VOC modify the Earth's radiative balance through a direct effect (absorption and scattering of solar radiation) or through indirect effect by altering cloud microphysical properties (Scott et al., 2014). They also present a direct effect on human health and on the environment (Zhu et al., 2018).

During their atmospheric transport, VOC and their oxidation products, Oxygenated Volatile Organic Compounds (OVOC), may partition between the gaseous and aqueous phases depending on their solubility. **Clouds have a significant effect on tropospheric chemistry** by redistributing trace constituents between phases and by providing liquid water in which aqueous phase chemistry can take place (Herrmann et al., 2015). Indeed, during the cloud lifetime, chemical compounds and particularly VOC are efficiently transformed since clouds favor the development of complex "multiphase chemistry". The latter presents several particularities. First, photochemical processes inside the droplets are important in the transformation of chemical compounds (Barth, 2006; Vione et al., 2006). Second, aqueous chemical reactions are efficient and can be faster than the equivalent reactions in the gas phase. This can be related to the presence of strong oxidants such as hydrogen peroxide H_2O_2 or Transition Metal Ions (TMI), which participate in the formation of radicals such as hydroxyl radicals ($HO^\bullet$) that favor oxidation processes (Deguillaume et al., 2005). Furthermore, the presence of viable microorganisms has been highlighted and shown to participate in transformations of the chemical species (Vaïtilingom et al., 2013; Bianco et al., 2019). Finally, these transformations in clouds are also strongly perturbed by microphysical processes that control formation, lifetime and dissipation of clouds. These processes will redistribute the chemical species between the different reservoirs (cloud water, rain, particle phase, gaseous phase, and solid ice phase) (Marécal et al., 2010; Rose et al., 2018). In this frame, the transformation of VOC in the cloud medium can lead to the production of secondary compounds contributing to SOA formation, reported as "cloud aqSOA" (Ervens, 2015). This secondary organic aerosol mass produced during the cloud lifetime could explain in part the ubiquity of small dicarboxylic and keto acids and high molecular-weight compounds measured in aerosol particles, fog water, cloud water, or rainwater at many locations, as they have neither substantial direct emission sources nor any identified important source in the gas phase. This aqSOA mass stays in the particle phase after cloud evaporation implying a modification of the (micro)physical and chemical properties of aerosol particles (particle size, chemical composition, morphology). This leads to modifications of their impacts on consecutive cloud or fog cycles (aerosol indirect effects) and of their interactions with incoming radiation by scattering/absorbing (aerosol direct effect).

Measurements of chemical compounds in cloud aqueous phase have been conducted for decades and have been more recently focused on the characterization of the dissolved organic matter (Ervens et al., 2013; Cook et al., 2017; Zhao et al., 2013; Bianco et al., 2018). Among this complex matrix, a significant fraction of organic compounds comes from the gas phase. Indeed, many secondary organic species such as carbonyls and carboxylic acids are formed during the gas phase oxidation of hydrocarbons; since they are highly soluble, they solubilize into the aqueous phase. They also result from aqueous phase processes (chemical and biological transformations). This explains why those compounds have been commonly measured in atmospheric waters (van Pinxteren et al., 2005; Matsumoto et al., 2005; Sorooshian et al., 2006; Deguillaume et al., 2014). However, **few studies have been conducted looking in parallel both compartments (gas and aqueous phases) in order to estimate how VOC compounds are partitioned**. This can be partly explained by the inherent difficulty of sampling clouds. However, this is of major importance since this gives indication of how the cloud is able to scavenge and transform them during their lifetimes.

Using a rough approach, the partitioning of organic compounds between gas and aqueous phases can be described by Henry's law constants that is to assume thermodynamic equilibrium for all species. However, cloud chemistry models (Lim et al., 2005; Barth, 2006; Ervens, 2015; Rose et al., 2018) and few observational studies (Facchini et al., 1992; Winiwarter et al., 1992; van Pinxteren et al., 2005; Li et al., 2008) have highlighted deviations from the Henry's law equilibrium. Many factors control the partitioning between these two phases such as the pH, the droplet size, and the reactivity in both phases. Kinetic transport limitations through the droplet surface have to be considered, as they can be perturbed by the presence of hydrophobic molecules at the air/water interface. In this frame, cloud chemistry models simulate the mass transfer between the two phases but those models have to be evaluated towards *in situ* estimates that are actually scarce (Winiwarter et al., 1994; van Pinxteren et al., 2005).

My thesis work aims at **improving the knowledge on the air-water partitioning of VOC in the cloud multiphasic system**. To investigate partitioning, simultaneous air/cloud samplings need to be carried out. Two classes of VOC have been chosen. First, we decided to focus upon the analysis of VOC of atmospheric interest from **anthropogenic and biogenic origin**. They include benzene, toluene, ethylbenzene and xylenes (BTEX) as well as biogenic species like isoprene and other terpenes. These compounds are usually detected in the gas phase but are not expected to be present in the aqueous phase due to their low solubility. Beyond the health impact for some of them, like benzene (Cocheo et al., 2000), these compounds are also well-known to contribute to the formation of secondary pollutants like ozone and SOA (Hu et al., 2008; Fu et al., 2009). This first choice was motivated by previous works that highlighted the accumulation of hydrophobic compounds in the aqueous phase (Valsaraj, 1988a,b; Valsaraj et al., 1993). A second category of VOC of atmospheric interest has been selected for their ability to efficiently dissolve in the aqueous phase due to their high solubility. Those compounds are **OVOC such as carbonyls, carboxylic acids and alcohols**. Those compounds are known to be primary emitted and also produced by homogenous gas phase reactivity and they are suspected to lead to aqSOA mass formation in the aqueous phase.

LaMP has a long experience in the off-line sampling of gaseous VOC on sorbent tubes. VOC samples are analyzed by Gas Chromatograph–Mass Spectrometer system (GC-MS) connected to a Thermal Desorption unit (TD) **TD-GC-MS**. However the OVOC analysis needed more developments based on a molecular derivatization step before TD-GC-MS analysis. To investigate VOC and OVOC in cloud water, a new extraction method, **Stir Bar Sorptive Extraction (SBSE)** has been developed. All these developments have been part of my thesis work. Then, two sites presenting different environmental conditions (seasons, origin of air masses, and level of pollution...) have been chosen for testing the new experimental developed devices developed for VOC/OVOC characterization. The **puy de Dôme station** has been naturally selected because it offers all the facilities for sampling natural clouds (gas and aqueous phases) and this station is a reference site for cloud studies (Baray et al., 2019). The second site is La **Réunion** Island (Pacific Ocean) where a field campaign (BIOMAIDO campaign, ANR program) was performed in spring 2019 for studying the atmospheric organic matter transformation during a cloud cycle. In this frame, VOC and OVOC were sampled and recently quantified by our analytical methods. All those elaborated data will allow to evaluate cloud chemistry models for their ability to reproduce air/water partitioning. In this frame, the new cloud chemistry model CLEPS (Cloud Explicit Physico-Chemical Scheme) developed at LaMP will be used to simulate cloud events on these two sites in the future.

In CHAPTER I, VOC "history" in the atmosphere are presented: sources, transformations and incorporation into the atmospheric condensed phases (particles, cloud). Associated uncertainties to these processes are highlighted since they motivates the goal of my thesis. In CHAPTER II, instrumental developments both in the field and in the laboratory are presented. In the laboratory, new analytical procedures have been developed to quantify VOC and OVOC in both gas and cloud water phases by TD-GC-MS analysis. These developments have been tested on real matrices sampled at the top of the puy de Dôme station (France) and/or at the Maïdo observatory at La Réunion Island). The results are detailed in CHAPTER III.

CHAPTER I Atmospheric VOC: sources & multiphasic transformations

I.1 General physical and chemical properties of Volatile Organic Compounds (VOC)

I.1.1 Definition

Chemically, a volatile organic compound (VOC) is a compound containing at least one carbon atom together with atoms of hydrogen, oxygen, nitrogen, sulfur, halogens, phosphorous and silicon, excluding carbon monoxide, carbon dioxide, carbonic acid, metallic carbides or carbonates and ammonium carbonate. Hydrocarbons are included but are often mistakenly equated with it. This is probably because VOC are often expressed as total methane- or propane-equivalent hydrocarbons. Methane (CH_4), which is a specific VOC and a greenhouse gas naturally widely present in the air, is often considered apart from the other VOC, which are referred to as non-methane volatile organic compounds (NMVOC). VOC are generally considered as NMVOC.

Physically, VOC are organic chemical compounds whose composition makes it possible for them to evaporate under "normal" atmospheric conditions of temperature and pressure. Following European directives, VOC means "any compound organic having a vapor pressure of 0.01 kPa or more at a temperature of 293.15 K or having a corresponding volatility under the particular conditions of use". "Volatility" can be quantitatively defined, either by its vapor pressure that is more than 0.01 kPa (European Directive; National Pollutant Inventory (NPI) of Australia www.npi.gov.au), or by its boiling point that is between 50–250 °C (United States Environmental Protection Agency (EPA) www.epa.gzov; Health Canada (HC) www.hc-sc.gc.ca).

The vapor pressure value is used to characterize the tendency of a substance to vaporize. At a given temperature, a substance with a higher vapor pressure will vaporize more readily than a substance with a lower vapor pressure. The vapor pressure of a substance is the pressure at which its gaseous (vapor) phase is in equilibrium with its liquid or solid phase. It is a measure of the tendency of molecules and atoms to escape from a liquid or solid matrix. At atmospheric pressures, when a liquid's vapor pressure increases with increasing temperature to the point at which it equals the atmospheric pressure, the liquid has reached its boiling point, namely, the temperature at which the liquid changes its state to a gas throughout its bulk. That temperature is commonly referred to as the "liquid's normal boiling point". The higher is the vapor pressure of a liquid, the higher is the volatility and the lower is the normal boiling point of the liquid.

For example, at any given temperature, methyl chloride (CH_3Cl) has the highest vapor pressure in comparison to other VOC in Figure I-1. CH_3Cl also has the lowest normal boiling point (-26 °C), which corresponds to the intercept between its vapor pressure curve (the blue line) and the horizontal pressure line of one atmosphere (atm) of absolute vapor pressure. This compound, widely used as a refrigerant, is therefore very volatile and is emitted in the air.

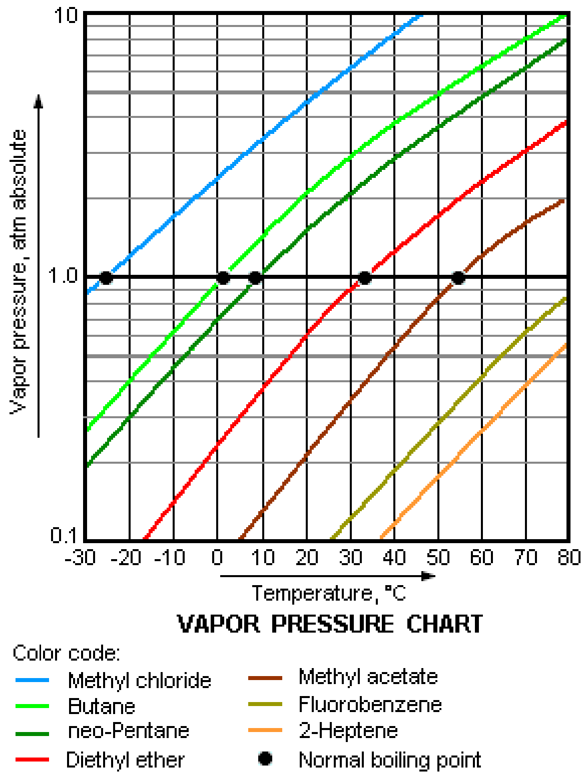

Figure I-1 Example of vapor pressure of organic compounds at different temperatures. Normal boiling points are represented with black dots; the vapor pressure curve intersects the horizontal pressure line at 1 atm of absolute vapor pressure (https://chem.libretexts.org/Bookshelves/Physical_and_Theoretical_Chemistry_Textbook_Maps/Supplemental_Modules_(Physical_and_Theoretical_Chemistry)/Physical_Properties_of_Matter/States_of_Matter/Properties_of_Liquids/Vapor_Pressure).

I.1.2 Chemical VOC diversity

VOC are a vast and diverse group of compounds presenting various physical-chemical properties. Physical properties include melting point and boiling point and chemical properties include reactivity and flammability. All of these properties are linked with the chemical structure of the compound. The chemical structure presents high variability with different bonding angles, type of bonds, carbon chain sizes, chemical functions, *etc.* Changes in the chemical structure drastically affect the properties of the compound. Even isomers, compounds with the same chemical formula but different structures, can have very different properties. Some of main classes of VOC emitted into the atmosphere are presented in Table I-1. They are classified based on their chemical structure.

Table I-1 Classification of major atmospheric VOC into categories based on their chemical structures and examples of compounds are given.

Family	**Selection of VOC compounds with various chemical structure**	
Hydrocarbons	Alkanes, alkenes, alkynes	 Propane 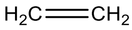 Ethene 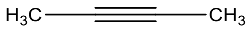 2-butyne
	Aromatics	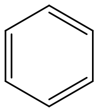 Benzene 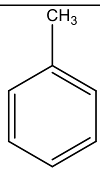 Toluene 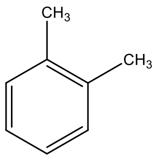 o-xylene 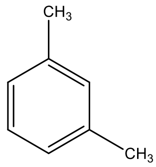 m-xylene 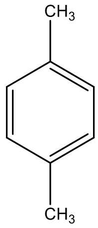 o-xylene
Terpenes	Isoprenoids $(C_5H_8)_n$	
	Hemiterpenoids (n=1, C_5H_8)	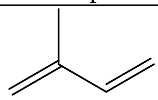 Isoprene
	Monoterpenoids (n=2, $C_{10}H_{16}$)	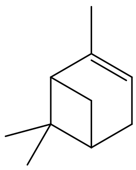 α-pinene 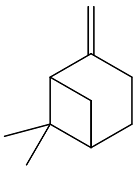 β-pinene 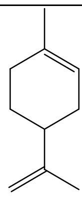 Limonene
	Sesquiterpenoids (n=3, $C_{15}H_{24}$)	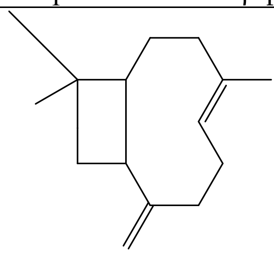 β-Caryophyllene
	Oxygenated terpenoids	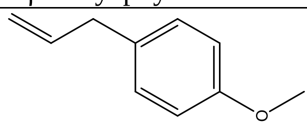 Methylchavicol
Oxygenated VOC (OVOC)	Carbonyl compounds	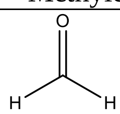 Formaldehyde 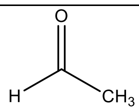 Acetaldehyde 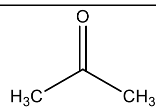 Acetone
	Carboxylic acids	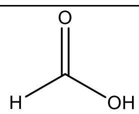 Formic acid 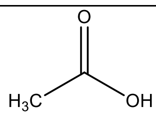 Acetic acid

	Alcohols	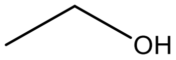 Ethanol 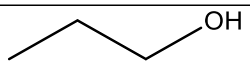 Propanol
Others	Organic compounds with heteroatoms (S, N, Cl, Br, ...) Organosulfates Organonitrates Organohalides Pesticides Polychlorinated biphenyls (PCBs) Polycyclic aromatic hydrocarbons (PAHs)	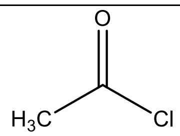 Acetyl chloride 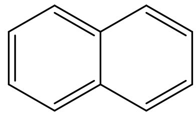 Napthalene 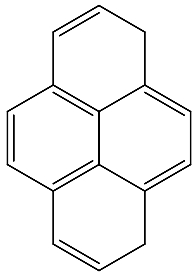 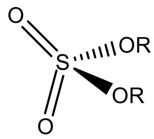 Organosulfate Pyrene

Hydrocarbons, more specifically Non-Methane Hydrocarbon Compounds (NMHCs), include several chemical families of species that consist only of carbon and hydrogen atoms: alkanes, alkenes, alkynes and aromatic compounds:

- Alkanes are saturated compounds, consisting of covalent bonds C–C and C–H, and their structures may be linear (*e.g.*, ethane, propane see in Table I-1), branched (*e.g.*, i-butane, 2-methylpentane) or cyclic (*e.g.*, cyclopentane). These compounds are relatively stable and not very reactive. Indeed, it is necessary to provide a substantial energy to dissociate the atoms of a single bond. Carbon–hydrogen bonds have a bond energy of about 483 kJ mol^{-1} and carbon-carbon of about 347 kJ mol^{-1}.

- Alkenes and alkynes are unsaturated compounds having respectively at least one double or one carbon-carbon triple bond. Unsaturation includes a simple bond (σ-bonding) to which is added one or two bonds of π-bonding. Like the alkanes, they can also be linear (*e.g.*, ethylene, propene and acetylene), branched (*e.g.*, trans-2-pentene) or cyclic (*e.g.*, cyclopentene). At the same number of carbon atoms, the alkenes and the alkynes are more reactive than the alkanes because the energy to be supplied to break their liaison is lower (259 kJ mol^{-1} to break the first π-bonding of C=C and 226 kJ.mol^{-1} for the second π-bonding of C≡C).

- Aromatic compounds are cyclic compounds, including in particular benzene, toluene, xylenes and trimethylbenzenes (see in Table I-1). These compounds have a benzene ring with delocalized double bonds responsible for their high stability.

Terpenes are a large and diverse class of natural products derived from the branched C5 carbon skeleton of isoprene (2-methyl-1,3-butadiene (C_5H_8), see its structure in Table I-1) (Arroo, 2007). They are synthesized within plant cells according to mechanisms closely associated with their metabolism. The synthesis of isoprenoids takes place in organelles called plastids. The cells of these organelles are essential for photosynthesis because they contain chloroplasts. From the primary substrates of photosynthesis, two key molecules for the synthesis of isoprenoids are formed: isopentenyl pyrophosphate (IPP) and its isomer dimethylallyl pyrophosphate (DMAPP). Then, isoprene is formed through an enzymatic process (triggered by the enzyme isoprene synthase). All terpenoids come from the same IPP and DMAPP precursors assembled and modified in thousands of ways (Dewick, 2002).

Sesquiterpenes (n=3) are major components of essential oils stored by some plants, especially broadleaf trees. They are part of the biogenic VOC (BVOC), which can be produced by plants involved in plant growth, development, reproduction and defense. They also serve for communication between plants and between plants and living organisms. Sesquiterpenes were the less studied to date: this is explained both by their more recent highlighting, and by their very high reactivity constraining their analytical quantification. Finally, some oxygenates, are also grouped in the family of terpenes, such as methyl chavicol (essential oil of tarragon (comprising 60–75%), also present in pine oil, turpentine, fennel, anise (2%), *Clausena anisata* and *Syzygium anisatum*) and α-thujene (essential oils of a variety of plants, and contributes pungency to the flavor of some herbs such as Summer savory).

Oxygenated VOC (OVOC) concern organic compounds with at least one oxygen atom. They are therefore polar and relatively hydrophilic compounds. They can be classified, depending on their chemical functions, as aldehydes (such as formaldehyde, acetaldehyde and acetone), alcohols (such as propanol and butanol), carboxylic acids (formic acid, acetic acid, for example) (see in Table I-1), organic hydroperoxide and multifonctionnel OVOC. The possible bonds between a carbon atom and oxygen require more energy to be dissociated (with respect to the C–C and C=C bonds) whereas an -OH bond is more fragile. Hence a higher reactivity for the alcohols and aldehydes is observed in comparison to that of ketones.

There are other families of organic compounds presenting in their structure other atoms than C, H and O atoms. Some examples are organosulfates, organonitrates and organohalides or chemicals like insecticides, fungicides or herbicides, polychlorinated biphenyls (PCBs), polycyclic aromatic hydrocarbons (PAHs) and Peroxyacyl nitrates (PANs). Their properties are various and complex due to their chemical structure.

The above section presents the main classes of VOC encountered in the atmosphere with some examples of molecules of atmospheric interest. However, they represent only a small part of the myriad of VOC emitted in the atmosphere. Sources of VOC are discussed in the next section.

I.2 Sources of VOC into the atmosphere

VOC emissions come from extremely numerous and varied sources. However, there are secondary sources aside from primary sources. “Primary sources” directly release compounds into the atmosphere. These primary sources can be of two types: (1) anthropogenic sources, which are relatives to human activities, and are subdivided into different categories like the industrial, residential and/or traffic sector, and (2) biogenic sources. Secondary sources of VOC are related to VOC production by oxidation reactions of primary VOC. On a global scale, biogenic emissions are higher than anthropogenic emissions (Goldstein and Galbally, 2007; Müller, 1992). However, anthropogenic emissions usually dominate in urban areas (Borbon et al., 2013). The identification and quantification of emission sources provide the scientific basis for strategies for reducing pollutant emissions. VOC emissions are described in the following sections as well as the factors controlling their intensity and speciation. Finally, difficulties associated with the quantification of these emissions are presented.

I.2.1 Natural emissions

Estimations of global emissions of natural volatile organic compounds (*e.g.*, woods, crops, shrubs, oceans, cultivated soil, meadow and others) are about 1150 TgC yr^{-1} and made up of 44% isoprene, 11% monoterpenes, 22.5% other reactive BVOC. In particular, tree emissions account for about 75% of the atmospheric BVOC emitted at the global scale. Table I-2 gives an overview of the estimated annual global emissions of major natural VOC. It is widely recognized that terrestrial ecosystems provide the largest source of VOC to the global atmosphere, mainly through foliar emissions but also *via* microbial decomposition of organic material with an estimated flux of 750–1000 TgC yr^{-1} (Safieddine et al., 2017; Guenther et al., 2012), which include the isoprenoids as well as hydrocarbons, carbonyls, alcohols, esters, ethers, and acids. Among them, the most emitted are isoprene and monoterpenes such as α-pinene, β-pinene, δ-3-carene or limonene (see their structures in Table I-1) (Guenther et al., 2012; Lathière et al., 2010; Kesselmeier and Staudt, 1999).

Table I-2 Estimated annual global emissions of major BVOC (based on Fall et al., 1999).

Compounds	**Primary natural sources**	**Estimated annual global emissions (TgC yr^{-1})**
Isoprene	Plants	175–503
Monoterpenes	Plants	127–480
Other reactive VOC (*e.g.* acetaldehyde, 2-methyl-3-buten-2-ol, hexenal family)	Plants	~260
Other less reactive VOC (*e.g.*, methanol, ethanol, formic acid, acetic acid, acetone)	Plants, soils	~260
Dimethylsulfide	Oceans	15–30
Ethylene	Plants, soils, oceans	8–25

I.2.1.1 Plant emissions

It is observed that isoprene is mainly emitted by broadleaved deciduous trees such as Oaks and Eucalyptus while monoterpenes are largely emitted by pines and other coniferous trees (Steiner and

Goldstein, 2007). In addition, coniferous forests could represent a significant fraction of OVOC emissions (Seco et al., 2007; Jacob, 2005). Despite the limited number of studies on BVOC emissions from shrubs, they are also considered to be a significant source of BVOC (Guenther et al., 1995). In particular, in Mediterranean-type ecosystems, some monoterpenes such as α-pinene, β-pinene and limonene are emitted in large quantities by shrubs (Owen et al., 2001). Other plant organisms, including ferns and mosses, also emit isoprene (Steiner and Goldstein, 2007; Hanson et al., 1999). More recent studies have also revealed an increase in emissions, especially in oxygenated compounds when the leaves of plants are under "mechanical" stress or are damaged. Thus, increasing emissions of OVOC and monoterpenes were observed during the harvest periods of cultivated species (Holopainen and Gershenzon, 2010; Jardine et al., 2010). Although the emission rates of single oxygenated BVOC species can be relatively small, their total amount can reach the same order of magnitude as those of isoprene and monoterpenes. Methanol, acetone and acetaldehyde (see their structures in Table I-1) are the most abundant oxygenated BVOC in the C_1–C_3 group of carbon release by many ecosystems, including forests and grasslands (Hörtnagl et al., 2011; Schade et al., 2011; Seco et al., 2007). In particular, formic and acetic acid has been found to be emitted by European oak and pines trees (Kesselmeier and Staudt, 1999). Another set of oxygenated BVOC released mainly after leaf damage is a group of C_5–C_6 compounds, known as the hexenal family (Hatanaka, 1993). Almost all plants seem to produce these compounds, of which (2E)-hexenal and (3Z)-hexenol are the most important.

I.2.1.2 Soil emissions

The soil is also a reservoir and source of BVOC, which are formed from decomposing litter and dead organic material or are synthesized by underground living organism or organs and tissues of plants. Soil VOC emissions to the atmosphere are often 1–3 orders of magnitude lower than those from aboveground vegetation (Peñuelas et al., 2014).

Plant roots system represent a strong source of VOC such as terpenes (Liu et al., 2007). However, the assessment of the contribution of root emissions to the overall soil VOC fluxes is difficult because of their linkage with soil microbes. Of the biotic processes, the microbial decomposition of soil organic matter is one of the most important contributions to soil VOC emissions (Leff and Fierer, 2008). Several microbial VOC are released as intermediate or end products of fermentative and respiratory (aerobic or anaerobic) microbial metabolic pathways. Because plant litter inputs (aboveground and belowground dead material) and root exudates contribute highly to soil organic matter (Kögel-Knabner, 2002), a large fraction of soil VOC results from the microbial degradation of plant-derived substrates. Goldstein and Schade (2000) measured the soil VOC fluxes with and without the top litter layer in a ponderosa pine (*Pinus ponderosa*) plantation and found that the litter layer in this ecosystem acts as the main source of methanol, whereas the acetone emissions are high in the bare soil without litter, indicating the existence of a different source of acetone in the subsoil. During their metabolism, plant roots, which have between one (fine roots) and two (total roots) orders of magnitude larger biomass than microbial biomass in most biomes (Jackson et al., 1997), also contribute to the release of VOC with different chemical origins (Lin et al., 2007; Gfeller et al., 2013). Of the abiotic processes contributing to soil VOC emissions, the evaporation of VOC from plant litter storage pools or soil solutions and Maillard-type reactions have been described (Gray et al., 2010; Greenberg et al., 2012). These physical processes contribute, for example, to the typical burst of VOC from dry soils after a rain or dew event. Some VOC in the soil pores can become quickly dissolved in water after the first drops (particularly polar oxygenated VOC) and further evaporate from the soil solution into the atmosphere, giving rise to a flush of oxygenated VOC from soils. However, the fast activation of microbial activity during a rain event also contributes to this phenomenon (Wang et al., 2010).

Few studies such as the one from Peñuelas and Staudt (2010) discuss the impacts of biogenic VOC emitted by soils. Bachy et al. (2016) recently discussed the possible under-estimation of flux emission from soil. These authors have compared VOC emissions from agricultural ecosystems over one year of plant growth between on bare soil and on well-developed vegetation corn soil and found that BVOC exchanges were of the same order of magnitude, suggesting that soil is a major BVOC reservoir in agricultural ecosystems. This means that the soil could be an important under-estimated source in the atmosphere, especially for methanol, acetic acid, acetaldehyde, acetone and other OVOC, also the terpenes, benzene and toluene. However, the studies on VOC emitted by ecosystems were mainly focused on terpenes, isoprene, monoterpenes and sesquiterpenes (Harley et al., 1999; Tiiva et al., 2008; (Ludley et al., 2009) and OVOC are less studied but emitted by soils as well (see in Table I-2).

I.2.1.3 Ocean emissions

Oceans can also contribute to global fluxes of BVOC but this contribution remains a very small fraction in comparison with the terrestrial vegetation. Indeed, at the surface layer of the ocean, the produced reactive gases are essentially hydrocarbons and sulfur compounds (hydrogen sulphide and especially dimethyl sulphide (DMS)). Isoprene is also produced from the seabed, particularly as a product of phytoplankton and algal activity (Bonsang et al., 1992; Broadgate et al., 2004). For example, marine emissions of isoprene in the western Mediterranean basin are estimated to be between 1.0 10^8 and 6.0 10^9 molecules cm^{-2} s^{-1}, which is two orders of magnitude lower than the fluxes of the terrestrial biosphere in the same region (Liakakou et al., 2007). Isoprene has also been measured in the depths of the Arctic Ocean, with maximum concentrations between -10 and -40 m depth directly related to the abundance of the phytoplankton biomass (Tran et al., 2013). Global ocean isoprene emissions have recently been estimated at 0.1 TgC yr^{-1} or less than 0.025% of total isoprene (Palmer, 2005). Total emissions of light hydrocarbons (2 to 5 carbons) by oceans are estimated at ~ 2.1 TgC yr^{-1} (Bonsang et al., 1992; Shaw et al., 2010). The oceans have also the capacity to store methanol and acetone with an estimation of the respective deposition speed of 0.10 cm s^{-1} and 0.08 cm s^{-1}. Indeed, the surface of the oceans plays a significant role in the overall budget of trace organic oxygenates such as acetone (Singh et al., 2003). Within the ocean-atmosphere interface, photosynthetic organisms are the main producers of VOC (Schall et al., 1997; Sinha et al., 2007). For example, the level of phytoplankton activity is strongly correlated with the flow of OVOC such as acetone and acetaldehyde (Sinha et al., 2007). Very large uncertainties, related to a lack of knowledge, exist regarding the estimation of VOC fluxes emitted by the oceans. For example, total flow estimates for acetone range from 37 to 148 Tg yr^{-1} according to the different studies (de Laat et al., 2001; Jacob et al., 2002).

I.2.1.4 Variability of natural emissions from terrestrial ecosystems

Emissions from terrestrial ecosystems of VOC vary widely by species and depends on biotic (metabolism, plant physiology…) and abiotic (temperature, light intensity, humidity and other physical parameters) conditions.

The starting unit for the synthesis of monoterpenes (and then sesquiterpenes) is obtained by adding a second (then third) IPP unit to the DMAPP.

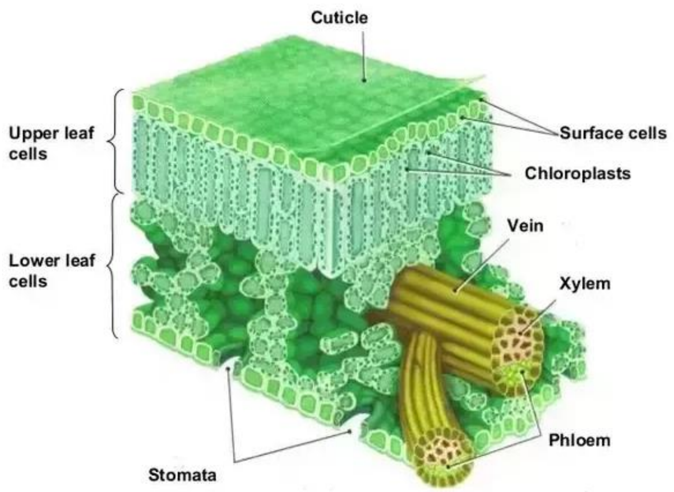

Figure I-2 Anatomy of a eudicot leaf (https://plantstomata.wordpress.com/) (eudicot: clade of flowering plants).

After production, VOC move from inter-cellular air spaces and storage cellular structures to the atmosphere. There are three processes of VOC release: diffusion through stomata of the leaves, diffusion through plant cuticles or woody parts of the plant and release *via* plant storage structures (see in Figure I-2). Diffusion is the fundamental process that governs the emission of VOC, such as isoprene. Diffusion is the result of a positive gradient of concentration between the cells of the leaf (high concentrations) and the air around (relatively low concentrations).

The reasons and mechanisms of the synthesis and emission of volatile organic compounds into the atmosphere by plants has been a debate subject for many years. Initially it's considered as simple metabolic product, but VOC seem to be agents of protection of terrestrial plants. They would allow plants to defend against biotic stresses, for example against attacks by pathogens or herbivores thanks to their antimicrobial and antifungal activity (Wang et al., 2013). Other studies suggest that isoprene and monoterpenes would protect the plant's photosynthetic apparatus against heat stress damage during high temperature episodes and could thus prevent the progressive reduction of their photosynthetic capacity (Behnke et al., 2007; Loreto et al., 1998). Finally, flowering plants would release a myriad of aromatic VOC (such as limonene) to attract pollinators and thus ensure their reproduction (Wright and Schiestl, 2009).

The plants cell production efficiency of isoprenoids and their emissions depend on the amount and activity of this enzyme, which is directly influenced by temperature and light. In the case of isoprene, the emissions increase instantaneously when temperature increases, but for a certain optimal temperature (35–45 °C), the plants undergo a "heat stress" and then their emissions decrease (see in Figure I-3). Isoprene emissions are also highly dependent on photosynthetically active radiation (PAR), which refers to the spectral range (wave band) of solar radiation from 400 to 700 nm involved in the process of photosynthesis of crops and plants. The response of isoprene emissions to the PAR is hyperbolic, which means that emissions increase for a certain spectral range until saturation is reached (see in Figure I-3). Temperature and light intensity influence the emission potential of plants also over the longer term (a few hours to several days) (Geron et al., 2000; Sharkey et al., 1996). Similarly, leaves exposed to light may have higher emission potential than shaded leaves (Kesselmeier and Staudt, 1999; Steiner and Goldstein 2007).

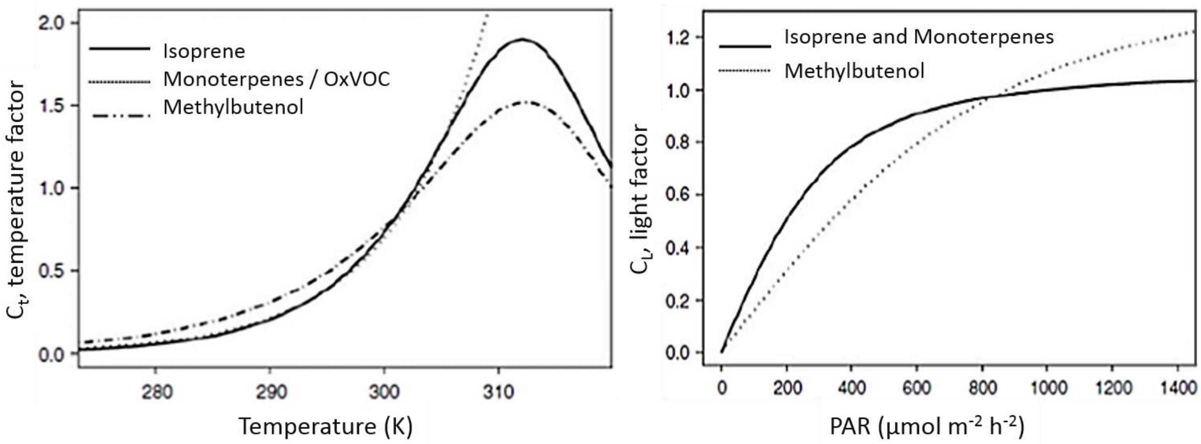

Figure I-3 Dependence of BVOC emissions on temperature in K (left) and light (right) by PAR (photosynthetically active radiation) in µmol m^{-2} h^{-2}. Adapted from Steiner and Goldstein (2007).

In case of monoterpene, its emitters do not have a storage mechanism (Niinemets et al., 2004; Schurgers et al., 2009), but they have a temperature and solar radiation dependence similar to isoprene emitters. However, for plants who have storage structures, they emit monoterpenes independently from PAR. Their dependence on temperature is also different. The release of monoterpenes from storage structures is controlled by their volatility. As a result, their emission rates are exponentially dependent on temperature (see in Figure I-3). The dependence of OVOC on light is not yet clearly established.

However, increasing emissions of OVOC (acetaldehyde and hexanal) have been observed for very short durations during day-to-night passage (Graus et al., 2004; Loreto et al., 2006).

For many years, the effects of radiation and temperature on isoprene emissions have been parameterized to allow the representation of VOC emission fluxes in modeling tools (Guenther et al., 1995, 2012). More recently, the parameterization of isoprene emissions has been extended in the Model of Emissions of Gases and Aerosols from Nature (MEGAN) to take into account variations in temperature, solar radiation, humidity of soil for short and medium term (see in Figure I-3) and the maturity of the emitting leaves (Guenther et al., 2006). This modeling tool can also be applied to monoterpene emissions, for plants with similar dependence on temperature and radiation. Other models have also been established for plants with storage structures, where monoterpene emissions are independent of the radiation (Guenther et al., 1993; Tingey et al., 1980).

Figure I-4 shows the seasonal time series of isoprene flux measurements compared with models (MEGAN) and satellite (GOME), featuring an increase from leaf-out to early August followed by a sharp decline, with large day-to-day variability superimposed. MEGAN (in green) shows generally under-estimation when compared with direct measurements (in black) and also with measurements retrieved by remote sensing (Palmer et al., 2006).

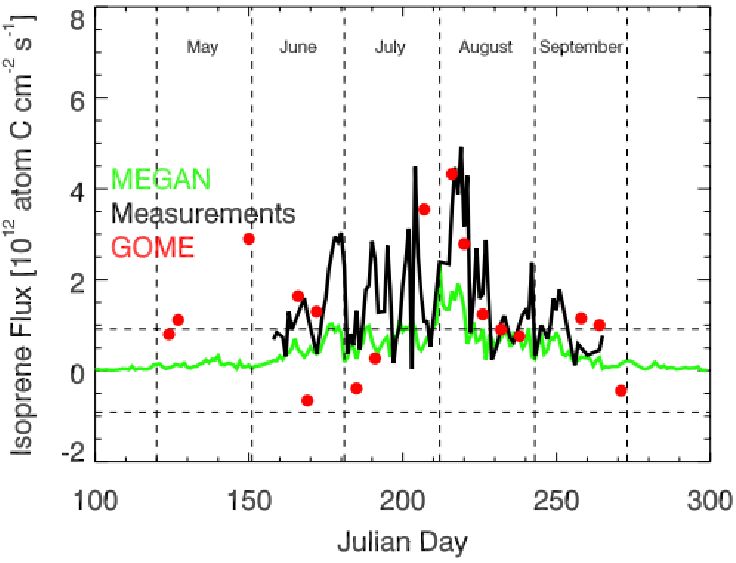

Figure I-4 Isoprene fluxes at the forest site (PROPHET), Michigan during the 2001 growing season. Green and black lines denote MEGAN and measured isoprene fluxes, respectively. Red circles denote isoprene fluxes retrieved from a 6-year (1996–2001) formaldehyde (HCHO) column data set from the Global Ozone Monitoring Experiment (GOME) satellite instrument. Horizontal dashed lines denote uncertainty in the retrieved HCHO vertical columns (Palmer et al., 2006).

In soils, microorganisms are the major players in the production of VOC. This production is linked to several processes grouped into two major pathways (Figure I-5):

- A first VOC production pathway is linked to the incomplete biodegradation of soil organic matter by microorganisms (Leff and Fierer, 2008). A change in the microbial habitat may induce changes in the mobilized microbial metabolic pathways and hence changes in the produced VOC. For example, in the case of a soil that becomes saturated with water (lack of oxygen), soil microorganisms move from an aerobic to anaerobic system which prevents the complete degradation of organic matter in the environment. This is the case for example for ethanol production.
- The second path of VOC production is related to microbial communication processes (Wheatley, 2002) within communities, particularly in a competitive context. It is illustrated by the set of green and red arrows in Figure I-5.

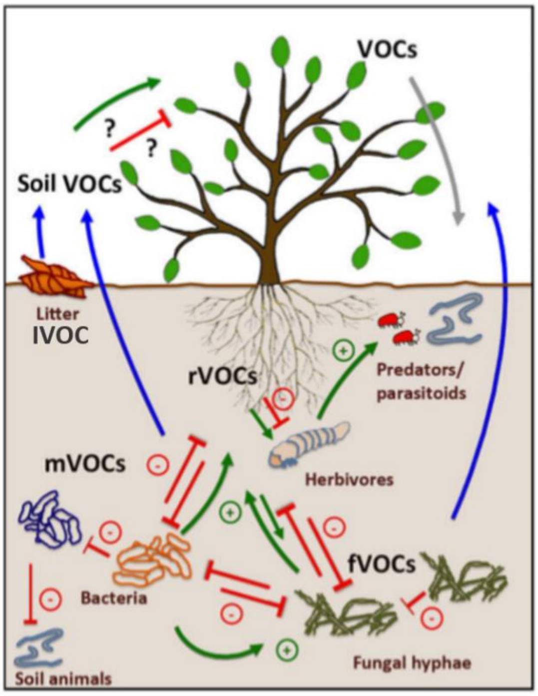

- *Figure I-5 Representation of VOC emissions linked with biotic interactions in soils. VOC in the soil (blue arrows) are emitted by bacteria (mVOC), fungi (fVOC), roots (rVOC) and litter (lVOC). Direct negative effects (e.g., growth inhibition, toxicity) of VOC are indicated by red arrows; direct and indirect positive effects are indicated by green arrows (Peñuelas et al., 2014).*

Microorganisms are VOC producers by degrading the soil organic matter or by communicating with other organisms in their environment. Thus, their production will depend on the degraded soil organic matter and on the biotic and abiotic parameters (pH, soil moisture, temperature, *etc.*) that regulate the microbial communities and their interactions.

The influence of the abiotic compartment on VOC emissions depends on the regulation of the gaseous or liquid state of the VOC and the adsorption mechanisms. In fact, once in the poral space of the soil, the temperature of the soil will regulate in which phase the compound is. For example, some VOC will need a higher temperature than others to be in gaseous form and emitted to the atmosphere (Schade and Custer, 2004).

The adsorption mechanisms of VOC depends also on sol texture. They can be adsorbed on minerals and organic matter (Ruiz et al., 1998; van Roon et al., 2005). Adsorbed VOC can be desorbed depending on the particle size of the minerals influence the adsorption capacity of VOC (Morrissey and Grismer, 1999). Thus, clay has the highest adsorption capacity and sand has the weakest one (Breus et al., 2014). In addition, the humidity of the soil influences the VOC adsorption. Hydration of soil can inhibit adsorption of hydrocarbons and increases adsorption for alcohol like methanol (Morozov et al., 2014). The type of VOC also plays a role in the VOC adsorption/desorption phenomenon, especially for polar compounds that are better retained than aliphatic and aromatic molecules (Ruiz et al., 1998).

I.2.2 Anthropogenic emissions

Emissions of anthropogenic VOC (AVOC) are composed of various sources resulting from human's activity including, for example, biomass burning, road transport sector, residential sector and industrial sector. To better estimate those complex emissions, "emission inventory" are developed to estimate the quantity of a pollutant emitted by a given emitter for a given geographical area and a given time period. For this, it is necessary to identify the emitting sources (emitter), to determine the activity of each source (type of activity, emission flow) and emission factor. The emission of a compound "i" by an activity is expressed by the equation (Eq.1):

$$E_{i,s,t} = EF_{i,s} \times A_{s,t} \qquad \text{(Eq.1)}$$

where $E_{i,s,t}$ is the quantity of compound i emitted by source s during time t;

$A_{s,t}$ is the activity of the source s during the time t;

$EF_{i,s}$ is the emission factor of the compound i by the source s.

Finally, the global emissions of the compound i by n different source s are described by the equation (Eq.2):

$$E_{i,t} = \sum_{s=1}^{s=n} E_{i,s,t} \qquad \text{(Eq.2)}$$

where $E_{i,t}$ is the total quantity of pollutant i emitted by the n sources during time t.

Estimating emissions is complex since several parameters have to be considered: the variety of sources, possible factors controlling these sources and their composition (or speciation). To illustrate this, the following sections present the main anthropogenic sources and their temporal and spatial variability.

I.2.2.1 Biomass burning

At the global level, biomass burning is the second largest source of VOC behind natural sources, which leads to an estimated 60–500 Tg yr^{-1} of emitted VOC (Yokelson et al., 2008; Akagi et al., 2011). Biomass burning can be broadly defined as open or quasi-open combustion of any non-fossilized vegetative or organic fuel. Examples range from open fires in forests, savannas, crop residues, semi-fossilized peatlands, *etc.* to biofuel burning (*e.g.*, cooking fires, dung burning, charcoal or brick making, *etc.*). Savanna fires, domestic and industrial biofuel use, tropical forest fires, extratropical (mostly boreal) forest fires, and crop residue burning are thought to account for the most global biomass consumption (in the order given) (Andreae and Merlet, 2001; Guenther et al., 2006). More than 80% of biomass burning of anthropogenic origin takes place in the tropical zone. In these areas, biomass burnings are much related to the need for energy sources because of growing populations in developing countries.

Table I-3 shows the global emissions of a selection of VOC emitted by biomass burning estimated by Andreae (2019). Averages of the available activity estimates of source and emission factors (Akagi et al., 2011) are used for the principal combustion categories (savanna and grassland, tropical forest, temperate forest, boreal forest, peat fires, open agricultural waste burning, biofuels, charcoal making, charcoal burning) to derive global emission values for VOC emitted from biomass burning. NMOGs noted in the Table I-3 is composed of non-methane hydrocarbons including unidentified VOC species.

Table I-3 Global emission of selected species based on the emission factors and the biomass burning estimates (in Tg y^{-1}) (Andreae, 2019).

	Savanna and grassland	Tropical forest	Temperate forest	Boreal forest	Peat fires	Agricultural residues	Biofuel burning	Charcoal making	Charcoal burning	Total
Tg dry matter burned	2400	2880	300	450	172	240	2134	180	45	8800
CO_2	3980	4670	470	690	270	340	3310	90	110	13 900
CO	170	300	34	55	45	18	180	17	9.4	820
CH_4	6.5	19	1.6	2.5	1.6	1.4	15	3.4	0.27	50
Total VOCs	12.2	16	4.0	2.7	3.7	1.8	17	4.8	0.3	62
Total NMOGs*	72	149	11.7	26	23	12.3	123	58	0.5	480
C_2H_2	0.75	1.0	0.09	0.13	0.02	0.07	1.4	0.05	0.012	3.6
Methanol	3.2	8.1	0.7	1.0	0.4	0.8	4.3	2.3	0.04	21
Formaldehyde	2.9	6.9	0.6	0.8	0.2	0.4	1.9	–	0.02	14
Acetaldehyde	2.0	6.5	0.36	0.37	0.20	0.43	0.87	–	0.01	10.8
Acetone	1.1	1.81	0.23	0.72	0.16	0.17	0.74	0.05	0.07	5.1
Acetonitrile	0.40	1.42	0.07	0.14	0.10	0.06	0.21	–	–	2.4
Formic acid	0.5	1.4	0.3	0.5	0.1	0.1	0.49	0.03	0.00	3.3
Acetic acid	5.5	9.5	0.8	1.7	0.8	1.5	8.4	8.4	0.08	37

VOC emitted by biomass smoke undergo smog photochemistry in the atmosphere, leading to the production of secondary compounds such as ozone, secondary organic aerosols (SOA), and other pollutants (Pacifico et al., 2015; Hatch et al., 2017; Yue and Unger, 2018). These gaseous pollutants pose grave risks to human health (Knorr et al., 2017; Apte et al., 2018) and also impact plant productivity (Carter and Foster, 2004; Kirkman and Jack, 2017). Recent estimates of global excess mortality from outdoor air pollution range from 4.2 to 8.9 million annually (Cohen et al., 2017; Burnett et al., 2018; Lelieveld et al., 2019), with smoke from vegetation burning accounting for up to 6.0 10^5

premature deaths per year globally (75th percentile of model estimates) (Johnston et al., 2012). Even significant impacts of biomass burning emissions on climate, ecosystem function, and human wellbeing have been highlighted, large uncertainties, persist regarding the amounts emitted and their spatial and temporal distribution.

I.2.2.2 Other anthropogenic emissions

There are three other predominant sectors in terms of anthropogenic VOC (AVOC) emissions in urban areas: the road transport sector, the residential sector and the industrial sector. Those various sectors are described below:

Road transport sector

Sources of VOC from the transport sector are numerous, ranging from mobile sources (vehicle exhaust and fuel evaporation) to stationary sources (evaporation at the level of a storage or distribution facility at stations). Different emission profiles can be associated with this sector, depending on whether exhaust emission, which involves combustion, or by evaporation.

The combustion processes can lead to the formation of carbon monoxide (CO), carbon dioxide (CO_2), and hydrocarbons (VOC). Emitted hydrocarbons consist of compounds present in the fuel that are partially oxidized (carbonyl compounds) or non-oxidized (alkanes, aromatics) and of compounds resulting from combustion reactions (alkenes: ethylene, 1,3-butadiene, alkynes: acetylene, aromatics: toluene, benzene, ethylbenzene and xylenes, propylbenzene, 1,3,5-trimethylbenzene) (Nguyen et al., 2009; Parra et al., 2009). Commonly, compounds such as acetylene and benzene are used as emission tracers from road transport (Borbon et al., 2003; Hoshi et al., 2008).

The composition of the exhaust emissions depends on several factors: type of vehicles (engine, technology, maintenance, aging, presence or absence of catalytic converters) (Montero et al., 2010; Nelson et al., 2008) speed of the vehicles, engine temperature, fuel composition and also the ambient temperature controlling the VOC volatility.

Concerning the profiles estimated for evaporation-type emissions, they include essentially alkanes having 4 to 5 carbon atoms (butane, isobutane, pentane, isopentane) (Borbon et al., 2002; Liu et al., 2008). Compounds aromatics are also present. The composition of these emissions will depend on the initial composition of the fuel, its volatility related to its nature and the ambient temperature. Thus, evaporative emissions may be higher in summer (Wang et al., 2012).

An example is given in Figure 1-6 that presents the contribution of different types of fuel to anthropogenic VOC emissions of the road transport sector in UK from 1970 to 2012. Overall, road transport emissions are dominated by C_2–C_5 and C_{6+} alkanes and aromatics (*e.g.* toluene); in addition contributions from alk(adi)enes/alkynes (olefins) and alkenes (ethane) are observed. For road transport emissions, the reduction in VOC emissions has been driven by the requirement for all new petrol cars to be fitted with three-way catalysts since 1989 and by fuel switching from petrol to diesel.

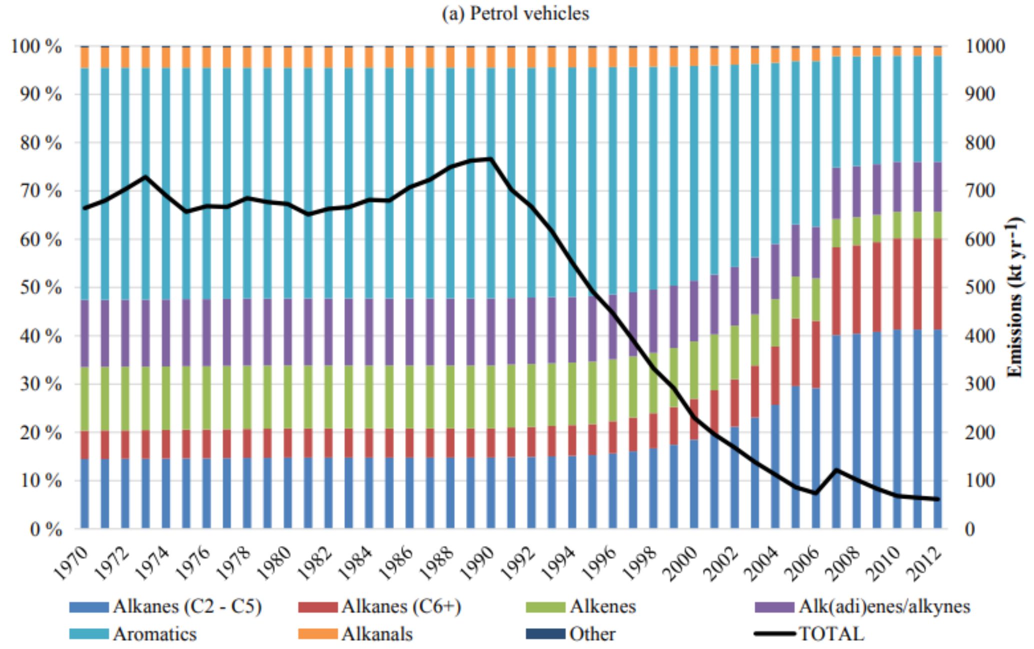

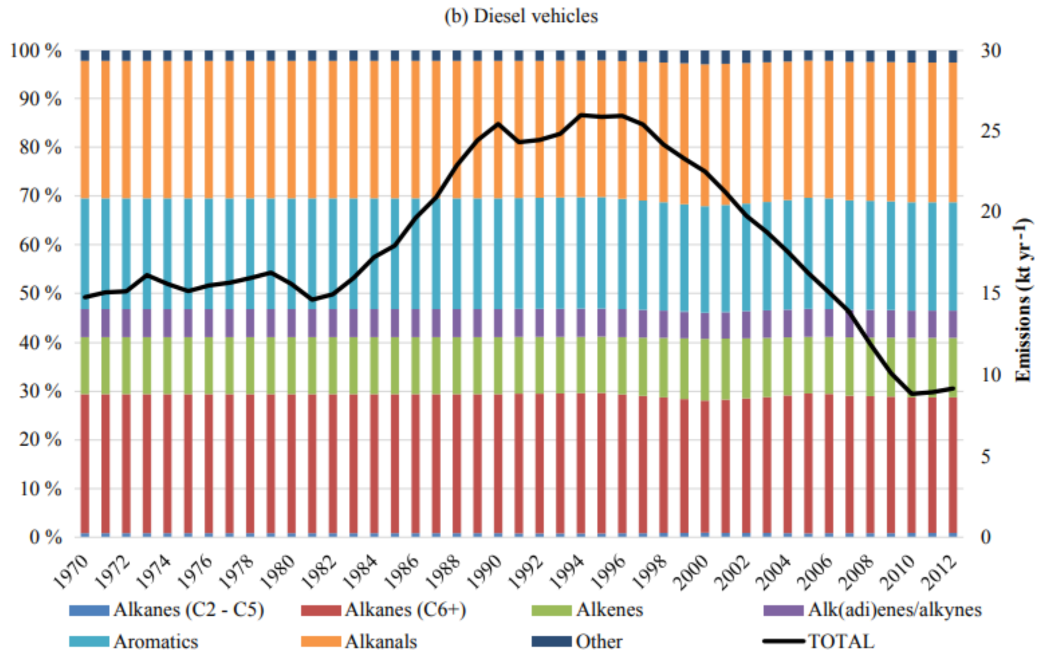

Figure I-6 Total anthropogenic VOC combustion emissions and their speciation for (a) petrol vehicles and (b) diesel vehicles of the road transport sector in the UK during 1970–2012 (Huang et al., 2017).

Residential sector

This sector brings together a range of different sources: domestic heating or urban, solvent use (domestic or tertiary), combustion of the commercial sector, cooking. These are areal sources as they cannot be treated individually.

According to Passant (2002), the combustion of gas and fuel oil indicates the presence of a large unburned fraction with significant amounts of alkanes, benzene, toluene and also ethylene for the fuel oil. The emissions associated with residential heating are more pronounced in winter. VOC emissions related to household cleaning products include alcohols (ethanol, isopropanol) and ketones (*e.g.*, acetone, 2-butanone) (Passant, 2002). They may also contain glycol ethers and ethyl ester in smaller proportions. The cosmetic products emit a high proportion of ethanol. The main VOC present in the solvents used are C_2Cl_4 (dry cleaning) (Doherty, 2000), n-hexane, n-heptane, n-octane and BTEX (Borbon et al., 2002; Wang et al., 2010).

Road traffic is an important source even though its relative importance in comparison to the contribution from the residential sector in particular is being questioned. A key conclusion in McDonald et al. (2018) is that VOC emission factors (emission amount per unit product use) resulting from the use of many volatile chemical products such as solvents are one to two orders of magnitude higher than VOC emission factor from automobile exhaust. In Figure I-7, total VOC emission factors include mobile sources and volatile chemical products. This figure is based on results from various field or laboratory studies that report total gas-phase VOC emission factors in industrialized cities. The green symbol and dashed arrow illustrate the large reductions in tailpipe VOC emission factors as precatalyst on-road gasoline vehicles were replaced by present-day vehicle fleets.

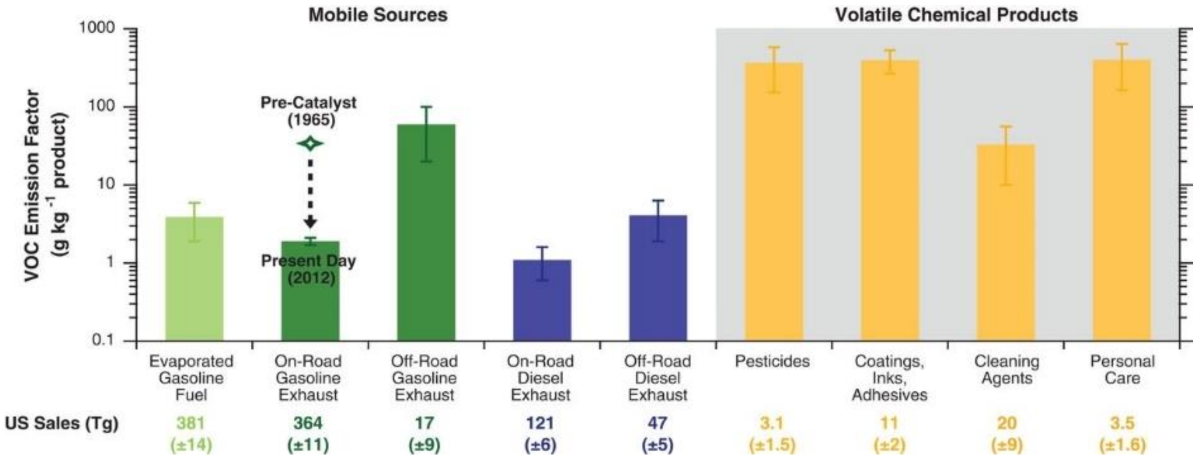

Figure I-7 Total VOC emission factors with distinction between mobile sources (left) and volatile chemical products (right). The green symbol and dashed arrow illustrate the large reductions in tailpipe VOC emission factors as precatalyst on-road gasoline vehicles were replaced by present-day vehicle fleets (McDonald et al., 2018). Error bars reflect the 95% confidence interval of the mean or expert judgment.

The relatively low VOC emission factor for on-road gasoline engines today can be concluded from: (i) combustion leads more efficiently to carbon dioxide formation by oxidation of hydrocarbons present in fuel, and (ii) the increasing effectiveness of modern three-way catalytic converters in reducing tailpipe VOC emissions over multiple decades (McDonald et al., 2015; McDonald et al., 2013). Consequently, the relative importance of solvents emissions has grown. For example, mixing ratios of acetone, a marker of coating-related solvent in this study and in the past (Harley et al., 1992), increased in ambient air in Los Angeles (US) from 1990 to 2010. This is in sharp contrast to VOC present in gasoline exhaust, which decreased markedly during the same period (Warneke et al., 2012), except for ethanol (de Gouw et al., 2012).

A study conducted by Baudic et al. (2016) in Paris megacity shows that traffic-related activities still remain a major source (including motor vehicle exhaust, 15% and evaporative sources, 10% of the total mass on an annual average) but also describes that the remaining sources are important: natural gas and background (23%), solvent use (20%), wood-burning (18%) and a biogenic source (15%). An important finding of this work is the significant contribution from wood-burning, especially in winter, where it could represent up to ~ 50% of the total mass of VOC.

Industrial sector

This includes a large number of sources, corresponding to various activities (solvent use, printing, glasses and materials, plastics, paper, cardboard, agro-food industries ...). Solvent use is an important source of ambient VOC in industrial sector. Source apportionment studies point to solvent evaporation sources of VOC in China (Cai et al., 2010), Hong Kong (Ou et al., 2015), Aliaga, Turkey (Dumanoglu et al., 2014), San Diego, USA and Tijuana, Mexico (Zheng et al., 2013), Athens, Greece (Moschonas and Glavas, 1996), Helsinki, Finland (Hellen et al., 2003), Lille, France (Borbon et al., 2003), Wuppertal, Germany (Niedojadlo et al., 2007) and Houston, Texas (Leuchner and Rappengluck, 2010). These solvents include hydrocarbon, oxygenated and chlorinated solvents but currently exclude ethanol and methanol which are outside the scope of ESIG (European Solvent Industry Group).

The nature of the emitted compounds as well as the associated quantity vary according to the type industry. Numerous studies on the subject have led to a better understanding of these emissions; however, the lists of these emissions cannot be exhaustive because of the myriad of sources and the associated quantities often correspond to estimates. Moreover, there is a great diversity in a specific activity because the processes emitting VOC can vary a lot from one industry to another. It is therefore difficult to define a typical profile for the entire sector. Some of these activities have been more specifically studied, so that a typical profile by activity could be established for example, for refineries (Seila et al., 2001), coal-fired power plants (Fernández-Martínez et al., 2001), hydrocarbon cracking (Badol et al., 2008), *etc.* As a conclusion, many factors influence emissions levels and composition.

I.2.2.3 Temporal and spatial variability of anthropogenic emissions

To illustrate the temporal variability of the anthropogenic emissions, some examples are shown below. Figure I-8 (a) presents the diurnal time evolution of VOC concentrations with a maximum at morning and late afternoon corresponding to traffic rush hours. This profile is typical of traffic-emission-related compounds (Borbon et al., 2013; Gros et al., 2011; Gentner et al., 2009). The histograms (b) show the seasonal change in the composition of VOC in urban area. In winter, an enrichment in the fraction of combustion products (alkenes and acetylene) of 4% in comparison to summer is observed. Same trend is observed for the C_2–C_3 alkane fraction related to the use of natural gas (ethane and propane) with an increase up to 30% in winter. Conversely, in summer, an enrichment in the unburned gasoline related fraction is observed for C_4–C_8 alkanes and >C_7–aromatics. These seasonal changes are either due to changes in source types or source composition. Given the nature of the compounds affected by seasonal variations, the additional contributions of combustion sources in winter and of losses by evaporation in summer are suspected.

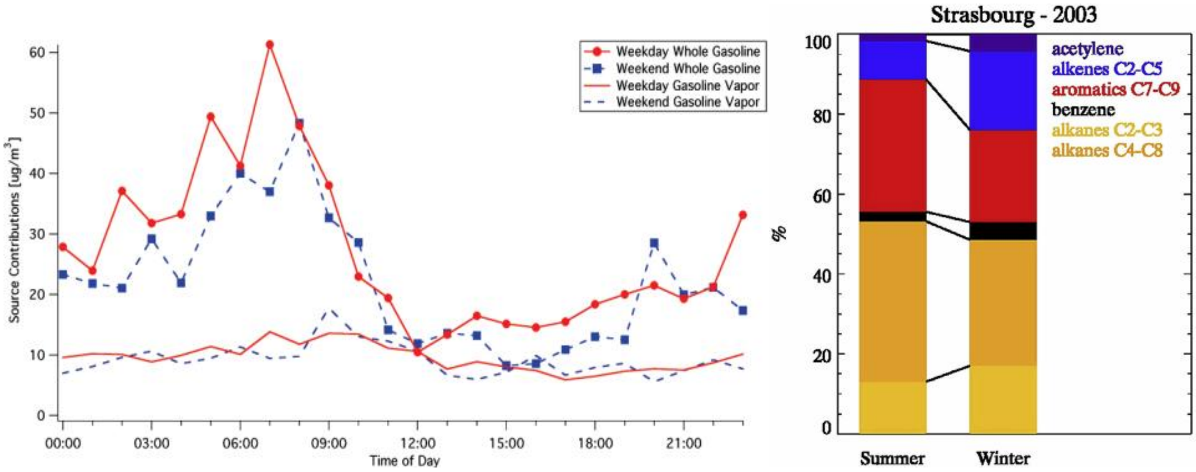

Figure I-8 (a) The diurnal profile of ambient VOC from whole gasoline and gasoline vapor emissions (Gentner et al., 2009); (b) the seasonal change in the composition of the urban VOC (Boynard et al., 2014).

Inter-annual profile of VOC concentrations in UK (see in Figure I-6) between 1990 and 2010 shows that approximately 90% of VOC emissions from road transport are attributed to petrol vehicles; however, this contribution has been steadily declining over this period due to the increasing usage of diesel, liquefied petroleum gas, and biogasoline in road transport. The percentage contribution of short-chain alkanes from petrol emissions has increased since 1990, and the proportion of aromatics has declined.

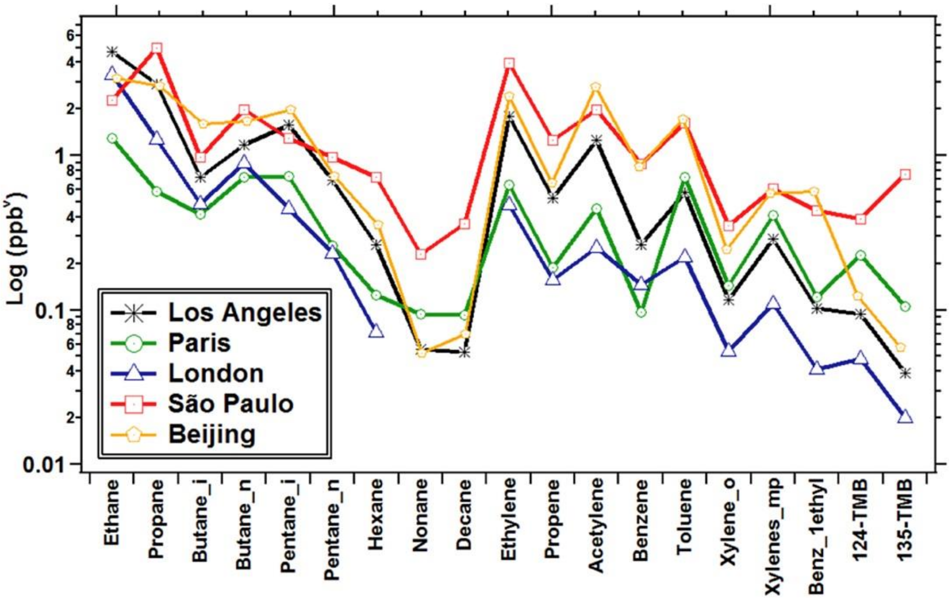

Figure I-9 VOC average mixing ratios in megacities (Dominutti et al., 2016). VOC average mixing ratios have been followed in several megacities such as in São Paulo (Brazil), Beijing (China), London (United-Kingdom), Los Angeles (USA) and Paris (France) in the frame of international projects.

The spatial variability of VOC urban emission has been also investigated in several studies over the past decades (Li et al., 2019; Lu et al., 2019). A recent study from Dominutti et al. (2016) suggests that VOC distribution in megacities is dominated by traffic emissions, especially from gasoline powered vehicles, regardless of regional practices and regulations such as fuel types and vehicle technologies. In spite of this distribution agreement, the average mixing ratios of all VOC were generally higher in São Paulo when compared to those in other megacities (see in Figure I-9).

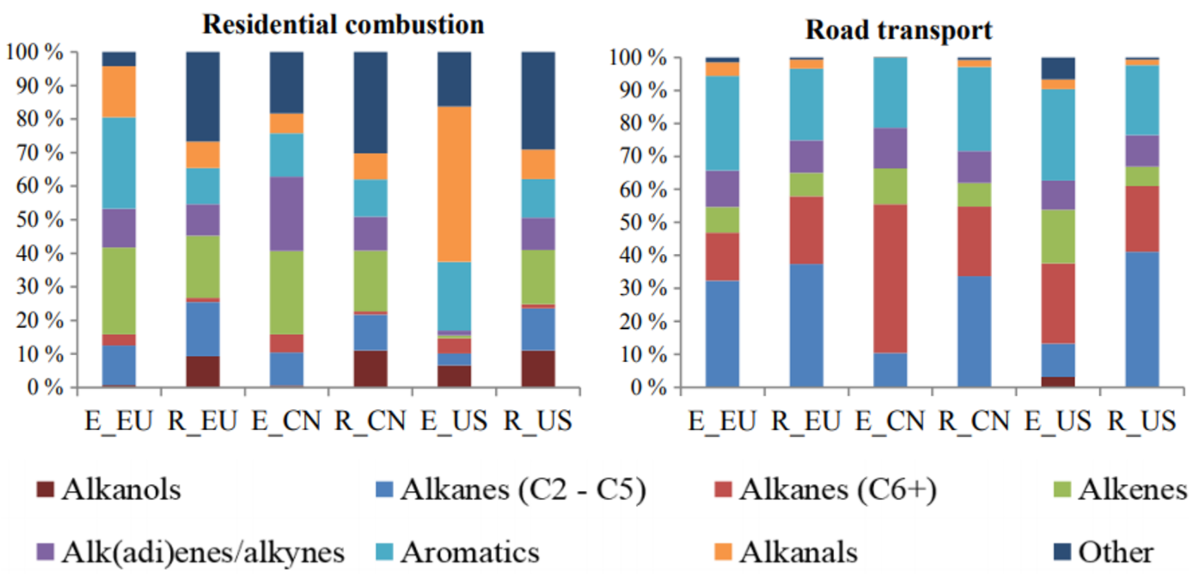

Figure I-10 Comparison of VOC distribution considered in two different inventories (EDGAR and RETRO) and for two distinct sectors by: Residential combustion and Road transport. EDGAR (E) and RETRO (R) data sets are indicated for Europe (EU), China (CN), and the United States (US) in 2000 (Huang et al., 2017).

In particular, the speciation of VOC emissions is still challenging. Figure I-10 is extracted from the work of Huang et al. (2017); it shows the comparison of VOC species emitted by two sectors (residual combustion and road transport) and considered in two different global inventories (EDGAR (Emissions Database for Global Atmospheric Research) and RETRO (REanalysis of TROpospheric chemical composition)). Those data sets are presented for Europe, China, and the United States in 2000. The speciation profiles are strongly different from one inventory to another except for Europe (EU). EDGAR presents the advantage in comparison to RETRO to consider regional specificities (technologies, fuel type) with different speciation profiles from one region to another.

I.3 VOC transformations in the atmosphere

Once emitted into the atmosphere, VOC can undergo chemical transformations and are also transported due to atmospheric dynamic. Their atmospheric concentrations are therefore driven by both physical and chemical processes. Chemical reactivity will modify the chemical structure of VOC and thus its physical-chemical properties (volatility and solubility, for example). Atmospheric transport will dilute or concentrate VOC in the atmosphere and dry and wet deposition can occur, representing a sink for VOC in the atmosphere. Their atmospheric lifetimes can be estimated considering their degradation kinetic constants (mainly by oxidants) and indirectly their residence times in the atmosphere. This is described in the following section and the current knowledge of homogeneous gas phase VOC reactivity is detailed afterwards.

I.3.1 VOC chemical transformations: lifetime estimation

VOC can absorb UV light and therefore undergo photolysis or can react with radicals, mainly the hydroxyl radical ($HO^{\bullet}$) and the nitrate radicals ($NO_3^{\bullet}$) and ozone (and, for some aldehydes, also with $HO_2^{\bullet}$ radicals) (Finlayson-Pitts and Pitts, 2000; Atkinson, 2000; Atkinson and Arey, 2003) (see in Sections I.3.1.1, I.3.1.2 and I.3.1.3). The lifetime τ of a chemical compound with respect to its reactivity with a chemical species X (such as $HO^{\bullet}$ and $NO_3^{\bullet}$ radicals and ozone) is given by equation Eq.3:

$$\tau = k_X \ \ ([X])^{-1} \qquad \text{(Eq.3)}$$

It depends on the kinetic constant k_X (expressed in cm^3 $molecules^{-1}$ s^{-1}) of the reaction of a VOC with X and the ambient atmospheric concentration of X ([X]) (reactions R.1-R.4). The $HO^{\bullet}$ and $NO_3^{\bullet}$ radical and ozone concentrations vary temporally and spatially, and hence the "instantaneous" lifetime τ and the loss rate τ^{-1} of a chemical also vary with space and time. The oxidation of VOC and their photolysis affect their lifetime τ in the atmosphere, presented in following equation (Eq.4), thus limiting their atmospheric transport and affecting their impact on the environment.

$$VOC_i + HO^{\cdot} \xrightarrow{k_{HO^{\cdot}}} P_1 \qquad \text{(R.1)}$$

$$VOC_i + O_3 \xrightarrow{k_{O_3}} P_2 \qquad \text{(R.2)}$$

$$VOC_i + NO_3^{\cdot} \xrightarrow{k_{NO_3^{\cdot}}} P_3 \quad \text{(R.3)}$$

$$R_1 - R_2 \xrightarrow{J_{photo}} R_1^{\cdot} + R_2^{\cdot} \quad \text{(R.4)}$$

$$\tau = (k_{OH^{\cdot}} \times [HO^{\cdot}] + k_{O_3} \times [O_3] + k_{NO_3^{\cdot}} \times [NO_3^{\cdot}] + J_{photo})^{-1} \quad \text{(Eq.4)}$$

I.3.1.1 Hydroxyl radicals HO$^{\bullet}$

Photolysis of ozone is an important source of hydroxyl radicals HO$^{\bullet}$. Ozone and dioxygen in the stratosphere absorb ultraviolet radiations (λ ≤ 290 nm) and only higher wavelengths are transmitted to the troposphere (Atkinson, 2000). This radiation is energetic enough to activate the photolysis of ozone (Tang et al., 1998). The O (^{1}D) formed during the photolysis of ozone can react in the presence of water vapor (R.5):

$$O(\,^1D) + H_2O \rightarrow 2\,HO^{\cdot} \quad \text{(R.5)}$$

Hydroxyl radicals can also be formed during the day, from the photolysis of nitric acid and the photolysis of aldehydes. Reactions between ozone and alkenes or monoterpenes (Atkinson and Arey, 2003) and reactions between hydroperoxyl radicals (HO$_2^{\bullet}$) and NO also lead to HO$^{\bullet}$ both during the day and during the night. Concentrations of hydroxyl radicals exhibit a great spatial and temporal variability with a strong diurnal production. The HO$^{\bullet}$ radicals are maintained at global diurnal concentrations of the order of 1.0 10^6 molecules cm^{-3} in the troposphere (Spivakovsky et al., 2000).

I.3.1.2 Nitrate radicals NO$_3^{\bullet}$

The formation of nitrate radicals NO$_3^{\bullet}$ is initiated by the presence of NO in the atmosphere (emitted by anthropogenic and/or natural sources) reacting with ozone (see R.6-R.9). During the day, the level of NO$_3^{\bullet}$ radical concentration is very low because its lifetime is in the order of few seconds (≈ 5 s at the sunniest hours) because they degrade rapidly by photolysis in the presence of solar radiation. On the other hand, NO$_3^{\bullet}$ concentrations can increase at night, reaching measurable levels. Indeed, their concentration can reach few ppt at night (of the order of 20 ppt) and become an important pathway for the degradation of VOC, especially unsaturated compounds. Nighttime maximum NO$_3^{\bullet}$ radical mixing ratios measured in the lower troposphere over continental areas range from lower than 2 ppt to 430 ppt; the mixing ratio in marine air masses has been measured to be inferior 0.5 ppt (Atkinson, 1997).

$$NO + O_3 \rightarrow NO_2 + O_2 \quad \text{(R.6)}$$

$$NO_2 + O_3 \rightarrow NO_3^{\cdot} + O_2 \quad \text{(R.7)}$$

$$NO_3^{\cdot} \xrightarrow{h\upsilon} NO + NO_2 \; (10\%) \quad \text{(R.8)}$$

$$NO_3^{\cdot} \xrightarrow{h\upsilon} NO_2 + O(\,^3P) \; (90\%) \quad \text{(R.9)}$$

I.3.1.3 Ozone O_3

The presence of ozone in the troposphere was first attributed to dynamic stratospheric ozone transfers. In fact, vertical exchanges of ozone between the low-lying (troposphere) and high-altitude regions are low and contribute only to an estimated 20–30% of tropospheric ozone; the rest is formed near the ground by chemical processes.

The production of tropospheric ozone is primarily based on precursors, the most important is nitrogen oxides: monoxide and nitrogen dioxide, respectively NO and NO_2, which are primary pollutants. These molecules result from the combination of oxygen and nitrogen, elements that are widespread in the troposphere in the natural state, a combination that occurs most often in the context of high-temperature combustion phenomena in the presence of an excess of oxygen. This type of combustion can occur in the context of natural phenomena (thunderstorms, because of the very high temperature that prevails in the vicinity of lightning, forest fires...) or result from human activities (combustions, especially during the operation of engines or heating devices, agriculture...).

Once released, the nitrogen dioxide is photo-dissociated in the presence of a short wavelength radiation between 280 and 430 nm (R.10):

$$NO_2 + h\upsilon \rightarrow NO + O(\,^3P) \qquad \text{(R.10)}$$

Then, the oxygen atom $O^{\bullet}$ is released under a particular excitation state and reacts with the oxygen to produce ozone (R.11):

$$O(\,^3P) + O_2 + M \rightarrow O_3 + M\ (M = air) \qquad \text{(R.11)}$$

The O_3 thus formed are rapidly destroyed by photolysis between 290 and 330 nm (R.12) producing oxygen and atomic oxygen in the metastable state O (^{1}D).

$$O_3 + h\upsilon \rightarrow O_2 + O(\,^1D) \qquad \text{(R.12)}$$

$$O(\,^1D) + M \rightarrow O(\,^3P)\ (M = air) \qquad \text{(R.13)}$$

$$NO + O(\,^3P) \rightarrow NO_2 \qquad \text{(R.14)}$$

The latter will return to its O (^{3}P) state (R.13), and then react with the NO to reform NO_2 (R.14).

This cycle called the "Leighton" cycle thus explains the low levels of ground-level ozone because a balance is created between ozone formation and degradation processes (Atkinson, 2000; Jacob, 2000). Ozone can also be deposited on the surface of the Earth. The resulting ozone concentrations are in the order of 10–40 ppb in background sites, but can reach more than 100 ppb in urban and polluted areas (Logan, 1985; Oltmans and Levy, 1994).

The formation of ozone takes place during daytime. However, the lifetime of ozone is several hours or even days. Therefore, its oxidative action can also take place at night. In summary, atmospheric gaseous oxidants are $HO^{\bullet}$ and O_3 for daytime and $NO_3^{\bullet}$ and O_3 for nighttime.

Table I-4 illustrates the variability of the tropospheric lifetimes of VOC depending on the oxidants, for a selection of VOC from anthropogenic and biogenic sources. These have been calculated assuming classically measured ambient concentrations of $HO^•$ and $NO_3^•$ radicals and ozone and the kinetic constants of those VOC at 20 °C with those oxidants. These lasts can vary across several orders of magnitude (Parrish et al., 2007) controlling VOC lifetimes. Of course, any variations of the $HO^•$, $NO_3^•$ and O_3 concentrations can translate directly into variations in the instantaneous loss rate and lifetime of VOC.

Table I-4 Calculated tropospheric lifetimes of selected VOC due to photolysis and reaction with $HO^•$ and $NO_3^•$ radicals and ozone O_3 ($HO^•$, 12-hour average concentration of 1.5 10^6 molec cm^{-3} (0.06 ppt) (Prinn et al., 1987); $NO_3^•$ 12-hour average concentration of 5.0 10^8 molec cm^{-3} (20 ppt) (Atkinson, 1991); O_3 24-hour average concentration of 7.0 10^{11} molec cm^{-3} (28 ppb) (Logan, 1985). Calculated from 20 °C rate data of Atkinson (1988, 1990a, 1991), Plum et al. (1983), and Rogers (1990). "/"was expected to be of negligible importance.) (https://www.nap.edu/read/1889/chapter/7#123).

VOC	Lifetimes estimated by reaction with:			
	$HO^•$	**$NO_3^•$**	**O_3**	**hν**
Ethane	60 days	12 years	4500 years	
Propane	13 days	2.5 years	4500 years	
n-Butane	6.1 days	2.5 years	4500 years	
n-Octane	1.8 days	260 days	4500 years	
Ethene	1.8 days	225 days	9.7 days	
Propene	7.0 hours	4.9 days	1.5 days	
Isoprene	1.8 hours	5 hours	1.2 days	
α-Pinene	3.4 hours	15 min	1.0 days	
Acetylene	19 days	2.5 years	5.8 years	
Formaldehyde	1.6 days	77 days	4.5 years	
Acetaldehyde	1.0 days	17 days	4.5 years	4 hours
Acetone	68 days	/	4.5 years	15 days
Methyl ethyl ketone	13.4 days	/	4.5 years	
Methylglyoxal	10.8 hours	/	4.5 years	2 hours
Methanol	17 days	77 days	/	
Ethanol	4.7 days	51 days	/	
Methyl t-butyl ether	5.5 days	/	/	
Benzene	12.5 days	6 years	4.5 years	
Toluene	2.6 days	1.9 years	4.5 years	
m-Xylene	7.8 hours	200 days	4.5 years	

Residence times of VOC vary from minutes to days or even years depending on their reactivity. For a selected VOC, its lifetime calculated by its reactivity with $NO_3^{\bullet}$ is shorter than the one calculated with other oxidants. Less VOC compounds can undergo direct photolysis (see more in Section I.3.2.3). Compounds less reactive in the atmosphere tend to accumulate more and thus present higher background levels. They can be transported over longer distances and therefore present impacts over regional or global scales. On the other hand, compounds less reactive such as terpene compounds or certain OVOC will have more local impact.

I.3.2 VOC reactivity

This section describes the mechanisms of transformations that VOC undergo in the homogeneous gas phase leading to the formation of secondary VOC presenting physical and chemical properties highly different from their precursors.

I.3.2.1 VOC oxidation

As discussed above, the oxidation of VOC is initiated by the main oxidants in the atmosphere: the hydroxyl radicals ($HO^{\bullet}$) (Atkinson and Arey, 2003), ozone (O_3) (Johnson and Marston, 2008) and the nitrate radical ($NO_3^{\bullet}$) (Wayne et al., 1991). Currently, the oxidation mechanisms of VOC is relatively well identified. It comes in three key steps governing the distribution of reaction products ("branching ratio") (Figure I-11): (a) initial attack of the oxidant, (b) evolution of peroxyl radicals ($R(OO)^{\bullet}$) and (c) evolution of alkoxy radicals ($R(O)^{\bullet}$).

(a) The reaction mechanism is initiated by the reaction of a VOC with one of the atmospheric oxidants ($HO^{\bullet}$, $NO_3^{\bullet}$, O_3). This first step leads to the formation of an alkyl radical $R^{\bullet}$ which will rapidly react with oxygen (O_2) to produce a peroxyl radical $R(OO)^{\bullet}$ (R.15).

(b) The photochemical conditions and the NO_X concentrations will then control the evolution of the peroxyl radicals $R(OO)^{\bullet}$:

- in the presence of NO_X or at high concentration of NO_X, $R(OO)^{\bullet}$ reacts preferentially with nitric oxide (NO) to form an alkoxy radical ($R(O)^{\bullet}$) and an organic nitrate $RONO_2$ (R.16). At the same time, $R(OO)^{\bullet}$ can react with NO_2 leading to the production of $ROONO_2^{\bullet}$ peroxynitrates, but this reaction is negligible compared to other pathways because, at ambient temperature, these species tend to decompose thermally to give $R(OO)^{\bullet}$ and NO_2 (R.23);

- at low concentrations of NO_X (sub-ppb), $R(OO)^{\bullet}$ evolves by self-reaction with another peroxyl radical towards stable compounds such as an alcohol or a carbonyl or towards an alkoxy radical $R(O)^{\bullet}$ (R.17). It can also be involved in a reaction with the hydroperoxyl radical $HO_2^{\bullet}$ which leads to the formation of a hydroperoxide ROOH (R.18);

- under diurnal condition, the nitrate radical $NO_3^{\bullet}$ formed by the reaction of NO_2 with O_3, is rapidly photolyzed which considerably reduces its concentration in the atmosphere. On the other hand, during nighttime, since its concentration is more elevated, it reacts with $R(OO)^{\bullet}$ to also form an alkoxy radical $R(O)^{\bullet}$ and gives NO_2 (R.19).

(c) The radicals $R(O)^{\bullet}$ thus formed can evolve in three different reactional pathways:

- $R(O)^{\bullet}$ reacts with O_2 to form a stable product characterized by the presence of a carbonyl group (aldehyde or ketone). This reaction is favored only in the case of very poorly branched compounds and having a low molecular weight (Atkinson and Arey, 2003) (R.20);
- they can lead to the production of a new peroxyl radical and a carbonyl compound by breaking a C–C bond (R.21);
- in the case of long chain carbon compounds (more than 5 carbon atoms), the hydrogen atom migration (isomerisation) leads to the production of a hydroxycarbonyl compound (R.22).

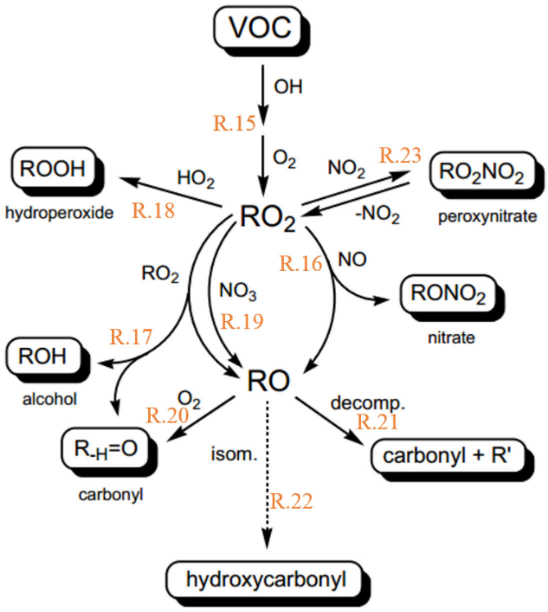

Figure I-11 Simplified pathways for the oxidation of VOC by the radical $HO\cdot$ in the gas phase from Hallquist et al. (2009).

In summarize, the oxidation of VOC leads to the formation of more oxidized compounds presenting new chemical functions such as carbonyl or alcohol groups and also to the formation of organo-nitrate compounds.

I.3.2.2 VOC oxidation by ozonolysis

Ozone is also relatively well known for its ability to oxidize unsaturated compounds (having a C = C double bond) such as alkenes, terpenes and aromatic compounds (Atkinson and Arey, 2003). It also represents a source of hydroxyl radicals $HO^{\bullet}$ and peroxyl radicals $R(OO)^{\bullet}$ (Anglada et al., 2002; Ariya et al., 2000). Ozone first adds across a carbon–carbon double bond to form an unstable primary ozonide (or 1,2,3-trioxolane) (see in R.24) that readily decomposes to form an aldehyde and a vibrationally excited carbonyl oxide (referred to as the "Criegee intermediate" (CIs) see in R.25). This Criegge Intermediate can react in different ways and form different products:

- the CIs can react with water (R.26 a) or with oxygenated organic compounds (R.26 b) respectively forming an α-hydroxyhydroperoxide and a more stable secondary ozonide (Johnson and Marston, 2008; Hallquist et al., 2009) when under some conditions such as on surfaces and in solution where a solvent cage exists, the aldehyde and carbonyl oxide intermediates are held in close proximity. Ozonolysis on surfaces such as aerosol particles also facilitates the formation of stable secondary ozonides by providing alternative pathways for the energy from the initial ozone addition to be dispersed. Karagulian et al. (2008) have observed the formation of secondary ozonides from unsaturated lipids at the surfaces of model sea salt aerosol, whereas we have observed secondary ozonide formation on various surfaces following ambient ozonolysis of unsaturated phospholipids (Ellis et al., 2012).

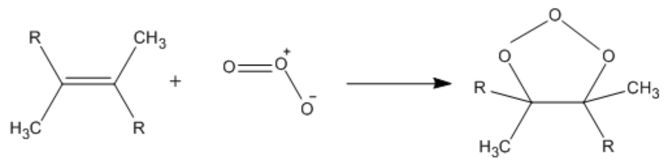

(R.24)

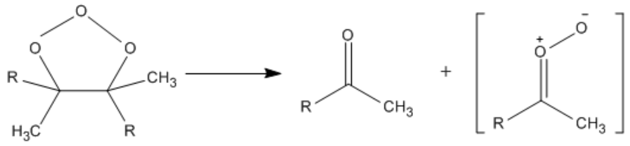

(R.25)

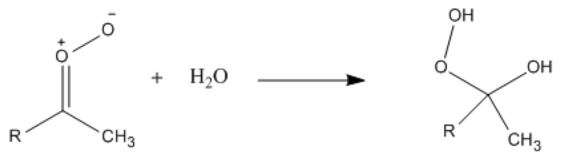

(R.26 a)

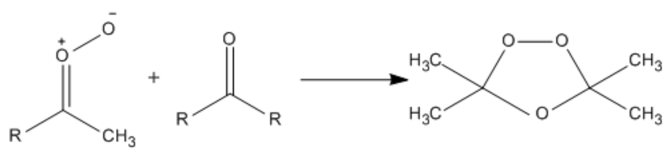

(R.26 b)

- the CIs can become rapidly separated in gas phase, allowing for comparatively little recombination (see in Figure I-12). They are thought to predominantly decompose through isomerization give an excited vinyl hydroperoxide intermediate, which subsequently decomposes to give HO$^{\bullet}$ and a vinoxy radical (R.27 a; the hydroperoxide mechanism). The proportion of the vibrationally excited CIs that have insufficient energy to isomerize/decompose may form so-called stable Criegee intermediates (SCIs), either directly following decomposition of the primary ozonide or through collisional stabilization of the CI (R.28), which can subsequently undergo bimolecular reactions (R.29) or decomposition (leading to further, delayed production of HO$^•$, again *via* a vinyl hydroperoxide intermediate (R.27 b), or potentially to $HO_2^•$, *via* a dioxirane/hot acid intermediate (R30)). The vinoxy radical formed alongside HO$^•$ will react with oxygen in the atmosphere to form an excited β-oxo peroxy radical, which may be stabilized or undergo decomposition forming CO, a (secondary) stable carbonyl species and HO$^•$.

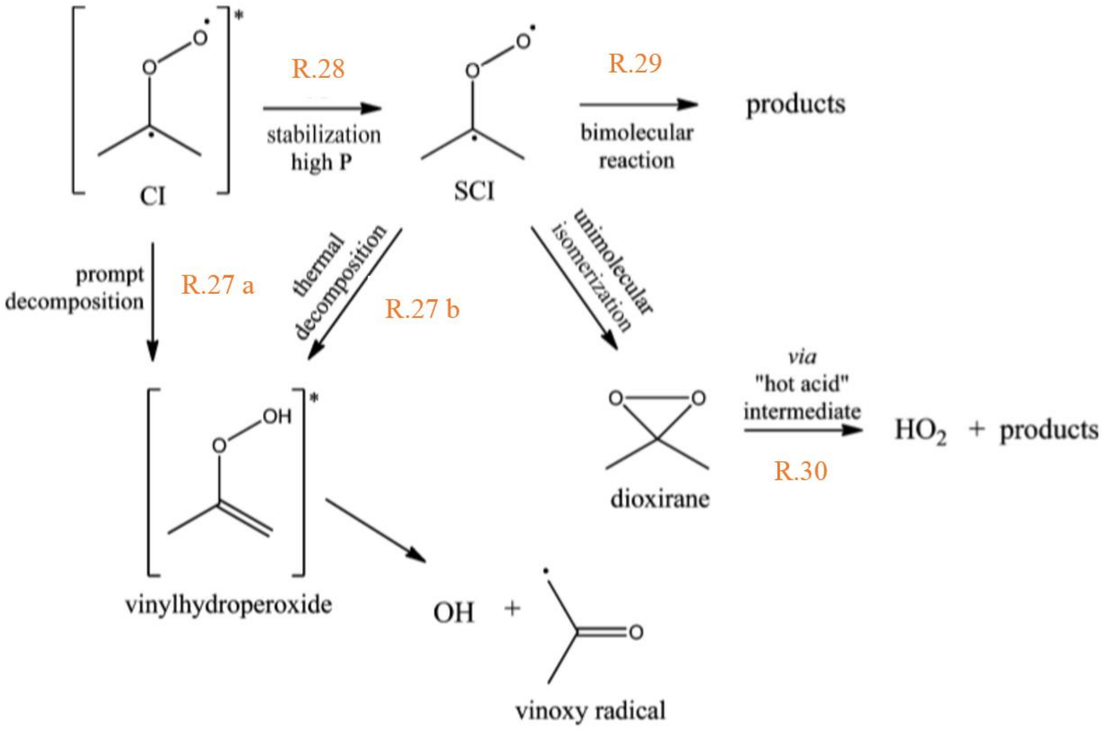

Figure I-12 Potential fates of the Criegee intermediate (from Alam et al., 2013).

All of these mechanisms lead to the formation of organic compounds having one or more oxygenated functions: aldehyde (–CHO), ketone (–CO–), alcohol (–C(OH)), nitrate (–ONO_2), PeroxyAcyl Nitrate (PAN) (–COO(ONO_2), carboxylic acid (–CO(OH)), hydroperoxide (–C(OOH)), and percarboxylic acid (–CO(OOH)).

I.3.2.3 VOC photolysis

A VOC in the atmosphere can be photo-dissociated following the absorption of a light radiation sufficiently intense to rupture one of its chemical bonds (R.31). This photolysis results in the formation of very reactive radical species.

$$R_1 - R_2 \rightarrow R_1^{\cdot} + R_2^{\cdot} \qquad \text{(R.31)}$$

These reactive radical species can react with O_2 by forming the radical R(OO)$^•$. The evolution of R(OO)$^•$ is the same as described in Section I.3.2.1 b. Photolysis is an important removal process for VOC which are likely to strongly absorb ultraviolet or visible radiation. This process is therefore an important sink for the carbonyl compounds present in the troposphere, such as for acetone (Seco et al., 2007) and for formaldehyde (Anderson et al., 1996).

I.3.2.4 Comparison of VOC oxidation mechanisms

VOC oxidation mechanisms with $HO^{•}$, O_3 and $NO_3^{•}$ lead to the formation of different oxidation products with concentrations depending on the branching ratios. In the presence of O_3 and $NO_3^{•}$, organic nitrate can be formed by VOC transformations, which cannot be produced directly by photolysis. The oxidation mechanisms previously described (see in Section I.3.2.1, I.3.2.2 and I.3.2.3) result in the formation of a large variety of first generation oxidation products having either an identical number of carbon atoms as their parent VOC (also called VOC precursors), nor a smaller number of carbon atoms when resulting from a fragmentation process. Fragmentation therefore leads to the formation of compounds with lower molecular weight that are more volatile. On the other hand, oxidation process leads also to the functionalization of the molecules (addition of new functional groups) that decreasing their volatility (Donahue et al., 2019).

These first-generation products may undergo oxidation processes resulting in the formation of new polyfunctional compounds. The identification of the functional group added to a species during oxidation mechanisms plays an important role in its volatility. Table I-5 shows the effects of various functional groups on the vapor pressure of organic compounds (Kroll and Seinfeld, 2008). The addition of an oxygenated functional group has a stronger effect on the vapor pressure of the compound than if a carbon atom is added. This phenomena is less obvious for carbonyls and ketones but much more important for hydroxyl, hydroperoxide or carboxylic groups, that can reduce the vapor pressure by more than two orders of magnitude. Thus, the reaction pathways that lead to the addition of these functional groups, with few or no fragmentation by breaking C = C bonds, tends to reduce the volatility and thus promote the transfer to the particulate phase or to the liquid phase because they are often more soluble than VOC precursors. This potential gas to particle conversion of VOC is described in more details in the following section.

Table I-5 Modification of the vapor pressure for organic compounds when adding a functional group. The indicated values correspond to a multiplicative factor applied to the vapor pressure of the compound (in atm). The addition of a carbon on the molecular chain is given as an indication. This table is derived from Kroll and Seinfeld (2008).

Functional groups	**Structure**	**Corrective factor (298K)**
Ketone	$-CO-$	0.1
Aldehyde	$-CHO$	0.085
Hydroxyl	$-OH$	5.7 10^{-3}
Hydroperoxide	$-OOH$	2.5 10^{-3}
Nitrate	$-ONO_2$	6.8 10^{-3}
Carboxylic acid	$-C(O)OH)$	3.1 10^{-4}
Peroxy acid	$-C(O)OOH)$	3.2 10^{-3}
Peroxyacylnitrate	$-C(O)OONO_2$	2.7 10^{-3}
Carbone	$-CH_2$	0.35

I.4 Transfer from the gas phase to the particulate phase

As described in Section I.3, multi-step oxidation in the gas phase leads to the generation of a set of organic products containing one or more polar oxygenated functional groups (see table above), which tend to make the products less volatile and more water soluble. In this context, Secondary Organic Aerosols (SOA) are formed from the gas-to-particle transfer of partially oxidized organic material, occurring in competition with further oxidation in the gas phase.

Due to the complexity of VOC mixture in the atmosphere, the partitioning of VOC between the gas and the solid phase is difficult to estimate. SOA formation depends on VOC precursors, on oxidation processes and also on environmental parameters such as NOx level, relative humidity (RH), solar intensity, for examples. In addition, since VOC modulate ozone formation and free radical budget, they can have also indirect effects on SOA formation by modulating oxidation efficiency.

I.4.1 Gas to particle partitioning theory

Due to oxidative phenomena described above (see in Section I.3.2), a large variety of first-generation oxidation products are obtained which have either the same number of carbon atoms as their parent VOC, or a lower number of carbon if fragmentation occurred. Those having the same carbon skeleton are systematically less volatile than their parent compound because of higher molecular weight and having one or more polar functional groups. This process is accelerated by the oxidation of first-generation products, forming new polyfunctional compounds that are even less volatile. The species thus formed are generally referred to as semi-volatile organic compounds (SVOC). The formed oxidation products of the SVOC type will then potentially transfer to the particulate phase. Aerosols that result from the condensation of SVOC are commonly referred to SOA.

Several condensation processes govern the passage of the SVOC from the gas phase to the particulate phase resulting in the formation of SOA: they can be adsorbed on the surface of pre-existing particles or absorbed in the particulate phase. The dominant process that controls partitioning of these species between gas and particulate phase is an absorption mechanism (Pankow, 1997). This distribution can be defined by a thermodynamic phase equilibrium represented by the Raoult's Law. This can be defined by the following equation (Eq.5):

$$P_i = \gamma_i x_i P_i^{vap} \qquad \text{(Eq.5)}$$

with:

P_i the partial vapor pressure (atm) of a compound i in equilibrium with the particulate phase;

P_i^{vap} the saturation vapor pressure of the compound i (atm);

γ_i and x_i (without unit) respectively the activity coefficient and the molar fraction of the compound i in the condensed phase.

The value of the activity coefficient γ_i determines the stability of the compound towards the phase in which it is located. Thus a compound, with a low γ_i value (less than 1), will be more stable in the particle phase and will have more affinities with the other compounds present in this phase and inversely.

I.4.2 SOA precursors

The importance of emitted VOC as SOA precursors is quite variable; certain classes of VOC have long been identified as more likely to lead to SOA formation by virtue of their general high gas phase reactivity and oxidation products formed. In this frame, cyclic compounds are known to be efficient SOA precursors. Indeed, the oxidation products (*i.e.*, ring opening) often present the same (or similar) carbon number as their parent compound. Furthermore, in the cases of cycloalkenes, aromatic hydrocarbons and terpenes (the majority of which are cyclic), oxidation occurs predominantly by an addition mechanism, so that the first-generation products generally contain two (or more) polar functional groups. Consequently oxidation of these classes of compounds is more likely to lead to the generation of low-volatility products. The characterization of SOA formation (mechanism and yields) from the degradation of cyclic hydrocarbons, such as BVOC (sesquiterpenes, cyclic diolefins (*i.e.*, limonene), bicyclic olefins (*i.e.*, α-pinene, β-pinene, Δ^3-carene, and sabinene), acyclic (*i.e.*, ocimene)) and AVOC (*i.e.*, toluene, m-xylene, m-ethyltoluene, propylbenzene, and 1,2,4-trimethylbenzene), has therefore been the focus of numerous investigations over the years (Fry et al., 2014; Tu et al., 2016).

The large majority of our knowledge about SOA formation from VOC oxidation derives from laboratory studies. Most of these studies make use of simulation chambers, ranging in volume from 1 to 270 m^3 (Folkers et al., 2003; Chen et al., 2019; Schwantes et al 2019) allowing to estimate SOA yields from various precursors under different experimental conditions. There are many factors that control the SOA yields and therefore complicate their understanding/interpretation. First is to constrain the yields (αi) of a set of (semi- or non-) volatile products as a function of the appropriate variables (temperature, relative humidity, NO_x and hydrocarbon mixing ratios, UV intensity, *etc.*). Second is to elucidate fundamental aspects such as chemical mechanisms and phase partitioning of a given mixture of products in an experiment and then extend that knowledge to the atmosphere.

I.4.3 Parameters influencing SOA formation

Temperature and water vapor are known to influence both the chemical mechanism and thermodynamics and hence the phase partitioning. SOA formation is modulated by the temperature since it modifies the chemical reactivity (Jonsson et al., 2007, 2008; Pathak et al., 2007, 2008). A higher SOA yield is obtained at lower temperature and with a higher concentration of SOA generated. For example, under the same experimental conditions, SOA yields at 283 K are approximately twice than that at 303 K for a selection of aromatic hydrocarbons (toluene, m-xylene and 1,2,4-trimethylbenzene) and biogenic alkene (α-pinene) (Takekawa et al., 2003). Humidity also modifies SOA production: for example, high relative humidity (RH) (60–69%) increases SOA yields from photo-oxidation of α-pinene by a factor up to 6 (1.5–6.4) compared to low RH (23–29%) (Stirnweis et al., 2017). During the ozonolysis of α-pinene, β-pinene, and limonene, the impact of RH during SOA formation on the volatility of SOA was small and often within the uncertainty limits (Lee et al., 2011). The aerosol produced at 50% RH is little more volatile (<10% difference in volume fraction remaining) than the one produced at low RH. Part of the difference might be due to the small but nonzero water content of the SOA at 50% RH. The evaporation of the particles in the system takes place at lower temperature compared to Jonsson et al. (2007) in the same conditions; this difference is due to the kinetics of the evaporation (An et al., 2007). Ye et al. (2016) have performed experiments where SOA derived from toluene and α-pinene were mixted with semi-volatile compounds. The objective was to evaluate mass transfer limitation according to RH level. They showed that uptake of semivolatile constituents by SOA particles at low relative humidity (RH) (above 20%) was much less efficient than for RH between 40 and 90%.

SOA formation also depends on parameters like VOC precursor vapor pressure and the concentration of reactive species (*e.g.*, $HO^{\bullet}$, O_3, NO_x) (Heringa et al., 2011). The yields at low NOx/VOC ratios were in general higher compared to yields at high NO_x/VOC ratios. This NOx dependence follows the same trend as seen in previous studies for α-pinene SOA. SOA yields of many VOC species present a strong dependence on NO_x level. Ng et al. (2007) have conducted experiments under two limiting NO_x conditions. For all studied hydrocarbons, considerably more SOA is formed under low-NO_x than under high-NO_x conditions. Under high-NO_x conditions, the SOA yields from m-xylene and toluene photooxidation are about 10%; they are 36% and 30%, respectively, under low-NO_x conditions. Similar NO_x dependences have been observed in other SOA-forming systems (Presto et al., 2005; Kroll et al., 2006).

During field campaigns, small VOC species (glyoxyl, methyglyoxal, acetylene, *etc.*) have been also identified as important SOA precursors (Volkamer et al., 2007, 2009). For example, a previous study showed that glyoxal can contribute at least to 15% of SOA formation in Mexico City (Volkamer et al., 2007). High relative humidity was observed during the Changdao campaign and the uptake of glyoxal by aqueous aerosol has been revealed as a significant source of SOA (Yuan et al., 2013). In the same campaign, concentrations of biogenic species, including isoprene, methyl vinyl ketone (MVK), methacrolein (MACR) and monoterpenes, precursors of SOA, were found low.

The recent review from Wu et al. (2018) summarizes multiple investigations that have been led in China to characterize organic aerosols. They indicate that secondary organic aerosol, averaged across China, derived from biogenic precursors accounts for 24–75% of total SOA, while estimates of the anthropogenic fraction are from 25–76%. Of course, those results strongly depend on the season and the measurement site (remote *vs.* urban site). They highlight the fact that chemical tracers for SOA precursors need to be developed to characterize SOA sources. This task is difficult due to the complexity of SOA composition that is often a mixture of chemicals from AVOC and BVOC oxidation products. This statement is linked to the fact that comprehension of SOA formation mechanisms are still weak.

I.4.4 Global SOA production estimates

Estimates of global SOA production have been made using two different approaches. The traditional approach is a bottom-up estimate where known or inferred biogenic (most notably isoprene and terpenes) and/or anthropogenic VOC precursor fluxes are considered in global models using laboratory data (SOA yields) derived from oxidation experiments (Chung, 2002; Kanakidou et al., 2005; Henze and Seinfeld, 2006). An alternative approach is a top-down inverse estimate based on constraining the eventual fate of known precursor emissions to infer the total SOA production rate (Goldstein and Galbally, 2007).

A recent intercomparison study of more than 20 state-of-the-art global aerosol models showed that estimates of the SOA annual production rate vary among models by an order of magnitude, from ~ 13 to 119 Tg yr^{-1}, and estimates of its lifetime range from 5 to 15 days (Tsigaridis et al., 2014). This wide spread in model results arises from a limited knowledge of underlying processes controlling both SOA formation and removal in the atmosphere. SOA formation rates used in current large-scale models are commonly based on yields derived from chamber experiments, which might be severely underpredicted (up to a factor of 4) due to loses of organic vapors onto chamber walls (Zhang et al., 2014; Matsunaga and Ziemann, 2010). As a consequence, these models often significantly underestimate ambient SOA concentrations (Heald et al., 2011; Spracklen et al., 2011).

To compensate for these model underestimations in an effort to match surface organic aerosol (OA) and SOA measurements, models increasingly include unconstrained aging parameterizations in which more volatile organic constituents are converted to less volatile ones (Shrivastava et al., 2011; Tsimpidi et al., 2010).

Wet scavenging is typically the major direct loss (90%) of SOA in global models (Tsigaridis et al., 2014), with dry deposition representing a much smaller sink (< 10%) due to the small dry deposition velocities predicted for accumulation mode aerosols (Seinfeld and Pandis, 2006). SOA loss can also occur indirectly by wet and dry removal of gas-phase semi-volatile oxidized species, which act to suppress the amount of condensable material available for SOA formation through gas-particle partitioning.

Global models typically treat the removal of these gas-phase oxidized volatile organic compounds (OVOC) in an ad hoc manner using constant Henry's law solubility coefficients between 10^3 and 10^6 M atm^{-1} (Knote et al., 2014). However, recent explicit modeling results (Hodzic et al., 2016) show that Henry's law solubility coefficients can vary significantly as a function of the volatility of OVOC, indicating the need for a reassessment of effective wet and dry removal lifetimes of SOA. In addition to wet and dry removal, there is increasing evidence of other potentially important SOA loss mechanisms that are, rarely implemented in global model calculations (see in Figure I-13).

Laboratory studies suggest that photolytic processing of organic gases and particles can remove tropospheric aerosols on timescales comparable to those of wet deposition, although the chemical transformations involved are not well understood (Henry and Donahue, 2012; Epstein et al., 2014). Model estimates performed by Hodzic et al. (2015) indicate that SOA photolytic frequencies equivalent to 0.04% of typical NO_2 photolysis frequencies can decrease SOA tropospheric concentrations by 20–60%.

Furthermore, organic compounds at or near the surface of particles were also found to be sensitive to heterogeneous (surface) oxidation by $HO^•$ and O_3 (George and Abbatt, 2010; Kroll and Seinfeld, 2008b). An attempt to include this process in a global model by oxidizing SOA with $HO^•$ with an effective gas-phase-equivalent rate constant of 10−12 cm^3 $molecule^{-1}$ s^{-1} and assuming that only 5% of reacted molecules is lost, suggested a 25% loss of SOA in the upper troposphere and 15% elsewhere (Heald et al., 2011).

Moreover, the aerosol aging in the atmosphere also lead to a modification of the gas-aerosol equilibrium. Vapor-particle transformations are bidirectional: organic aerosol formation can be induced by gas-phase aging reactions that yields to products with lower vapor pressures than their parents. On the other hand, heterogeneous oxidation of organic particles can generate products with higher vapor pressures that can evaporate from the particles. Those processes are studied at molecular level but are still badly constrained in regional/global models.

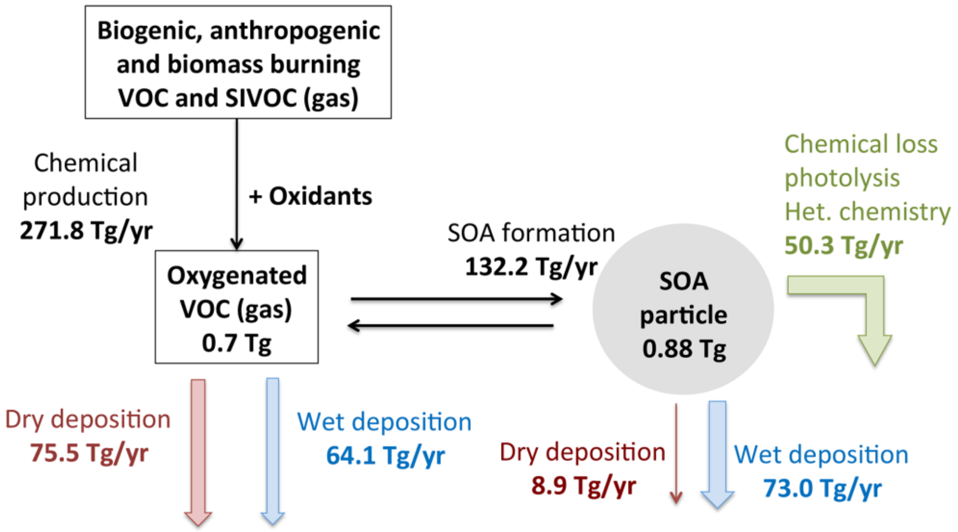

Figure I-13 Global budgets (sources/sinks Tg yr^{-1} and burden Tg) of condensable secondary organic gas and particle compounds as predicted by GEOS-Chem simulations for 2005–2008 from Hodzic et al. (2016).

Hodzic et al. (2016) have updated the global GEOSChem model considering new constrains based on recent studies: wall-corrected yields and emissions of semi-volatile and intermediate volatility organic compounds and on removal processes (photolysis and heterogeneous oxidation). They predicted that global SOA burden in the updated model is 0.88 Tg and the corresponding direct radiative effect at top of the atmosphere is −0.33 W m^{-2}, which is comparable to recent model estimates constrained by observations (Spracklen et al., 2011; Hallquist et al., 2009; Heald et al., 2011). The updated model predicts a population-weighed global mean surface SOA concentration that is a factor of 2 higher than in the reference model (without updates). This highlights the need for more extensive field and laboratory studies.

I.5 Transfer to the aqueous phase

As mentioned in Section I.3, the oxidation of VOC in the gas phase leads to the formation of more oxygenated compounds, usually less volatile, more polar than the starting species and generally more soluble (Herrmann et al., 2015; Raventos-Duran et al., 2010).

Field investigations on fog and cloud characterization demonstrated the presence in elevated concentrations of carboxylic acids such as formic, acetic, oxalic or succinic acids (Deguillaume et al., 2014; van Pinxteren et al., 2005). Other studies showed that carbonyls are also present in the atmospheric aqueous medium such as for example formaldehyde, glyoxal, methylglyoxal, *etc.* (Ervens et al., 2013; Houdier et al., 2011). These low molecular weight compounds are highly abundant since they are present in the gas phase and are soluble. Besides these highly polar species, polycyclic aromatic hydrocarbons (PAH) received some attention in recent years (Ehrenhauser et al., 2012; Herckes et al., 2007) with a focus on studying their occurrence and transformation in fog/cloud cycles (Ehrenhauser et al., 2012). Other species observed in fog/cloud droplet like nitrosamines (Hutchings et al., 2010), phenols, nitrophenols, phthalates (Lebedev et al., 2018), BTEX species (Hutchings et al., 2009) and pesticides (Glotfelty et al., 1987; Schomburg et al., 1991) have been investigated for health reasons.

Organic compounds detected in cloud waters can enter into droplets through particle dissolution or through mass transfer from the gas phase to the aqueous phase. Due to the inherent difficulty to sample clouds and to sample at the same time the gas phase, data on the partitioning of organic compounds between the cloud phases (gas, liquid) are scarce. However, this is of prior importance since cloud chemistry strongly perturbs the homogeneous gas phase chemistry and can potentially modify the chemical and physical properties of tropospheric aqueous phase aerosols. The next sections are devoted to a global overview of parameters that are known to drive the transfer of molecules between the gas and the aqueous phases (solubility described by Henry's law, accommodation coefficient). This will be followed by a global description of the way this transfer can be kinetically described by different steps. Finally, uncertainties/difficulty associated to the evaluation of the partitioning of chemical compounds between phases will be addressed.

I.5.1 Henry's Law equilibrium

Henry's Law describes the thermodynamic equilibrium between an ideal gas in contact with an ideal solution (*i.e.*, infinite dilution) and its dissolved quantity; physically, it represents the solubility of the gas. Thus, it makes a link between the partial pressure $p_{X,gas}$ of the gas X and its concentration in the aqueous phase $[X]$ by the Henry's $H(X)$ constant:

$$H(X) = \frac{[X]_{aq}}{p_{X,gas}} \qquad \text{(Eq.6)}$$

where $p_{X,gas}$ is the partial pressure of species X in the gas phase (atm),

$[X]_{aq}$ is the concentration of species X in the aqueous phase (mol L^{-1}),

$H(X)$ is the Henry's constant (mol L^{-1} atm^{-1}), defined for species X at a given temperature.

In atmospheric chemistry, these constants are used to describe the theoretical distribution of trace species between the air and liquid cloud droplets or aerosol particles. In another context, these constants are useful for calculating the vaporization of chemical compounds from various aqueous surfaces such as rivers or waste waters. Different definitions of the Henry's Law constant are used in the literature depending on the units as described in Sander (2015). This review article is the most complete compilation of Henry's law constant of chemical compounds presenting potential relevance for atmospheric chemistry (14 775 Henry's Law constants for 3214 inorganic and organic compounds); it also provides details on temperature dependencies of Henry's Law constants. It must be noted that Henry's Law is generally only applicable for dilute solutions. For concentrated solutions, dependencies of the Henry's Law constants on the chemical composition and ionic strength of the electrolyte must be considered. These dependencies, which are typically referred to as "salting in" and "salting out" effects (Sander, 1999).

Henry's law constant depends on the temperature T, which can be expressed following the integration of Van't Hoff's equation:

$$H_T = H_{298} \times \exp\left[-\frac{\Delta H}{R}\left(\frac{1}{T} - \frac{1}{298}\right)\right] \qquad \text{(Eq.7)}$$

where H_{298} is the Henry's constant at 298 K. ΔH is the dissolution enthalpy (enthalpy variation of the system). R is the perfect gas constant equal to 8.3145 J K^{-1} mol^{-1}.

ΔH corresponds to the variation of enthalpy accompanying the dissolution of the gases. Since those values are rather high, H therefore varies rapidly with the temperature. Henry's Law constants generally increase when the temperature decreases, reflecting a greater solubility of the gas at lower temperatures. The dissolution enthalpies are always negative and the solubility of the gases increases when the temperature decreases (see in Table I-6). For example, the Henry's Law constant increases for formaldehyde by a factor of 8.08 from 298 to 273 K.

Table I-6 Henry's law constants at 298 K and ΔH enthalpy variation for a selection of chemical species.

Species	Henry's Law constant H (M atm^{-1}) at 298 K	ΔH (kJ mol^{-1}) at 298 K	Henry's Law constant H (M atm^{-1}) at 273 K
SO_2	1.23	-6.25	1.55
HCOOH	3.75 10^3	-11.4	5.59 10^3
CH_3COOH	4.66 10^3	-7.57 10^2	3.23 10^4
HCHO	3.24 10^3	-8.18 10^2	2.62 10^4

When the gas X dissociates or hydrates in solution, an effective Henry's law constant (also called pseudo Henry's law constant H_X^* or $H_{eff,X}$) is defined which relates the total concentration of the dissolved compound in the aqueous phase $[X]_{tot}$ to its partial pressure in the gas phase (the total concentration is the concentration accessible by the measure and the sum of each individual concentration of each aqueous forms of a compound X). In this case, as dissociation and hydration can occur, the solubility of the gas can be increased by these rapid chemical equilibria. We then define the effective Henry's constant by the relation:

$$H_X^* = \frac{[X]_{tot}}{p_{X,gas}} \qquad \text{(Eq.8)}$$

For an acid, acid/base equilibria have to be considered. For example, if compound X is a mono-acid called HA which dissociates according to the acid/base equilibrium:

$$[HA]_{gas} \overset{H_{HA}}{\longleftrightarrow} [HA]_{aq} \qquad \text{(L.1)}$$

$$[HA]_{aq} \overset{K_{AH}}{\longleftrightarrow} [A^-]_{aq} + [H^+]_{aq} \qquad \text{(L.2)}$$

$$with\ K_{AH} = \frac{[A^-][H^+]}{[HA]}$$

The effective Henry's law constant H_{HA}^* is then defined as:

$$H_{HA}^* = \frac{[HA]_{tot}}{p_{HA,gas}} = \frac{[HA]_{aq} + [A^-]_{aq}}{p_{HA,gas}} = H_{HA}(1 + \frac{K_{HA}}{[H^+]})$$

This equation of Henry's law constant can also be generalized in the case of a second dissociation such as di-acids called H_2A.

$$[H_2A]_{gas} \overset{H_{H2A}}{\longleftrightarrow} [H_2A]_{aq} \qquad \text{(L.3)}$$

$$[H_2A]_{aq} \overset{K_{HA1}}{\longleftrightarrow} [HA^-]_{aq} + [H^+] \tag{L.4}$$

$$with\ K_{HA1} = \frac{[HA^-][H^+]}{[H_2A]}$$

$$[HA^-]_{aq} \overset{K_{HA2}}{\longleftrightarrow} [A^{2-}]_{aq} + [H^+] \tag{L.5}$$

$$\text{with } K_{HA2} = \frac{[A^{2-}][H^+]}{[HA^-]}$$

The effective Henry's law constant can be expressed, after calculations as following:

$$H_{H2A}^* = H_{H2A}(1 + \left(\frac{K_{HA1}}{[H^+]}\right) + \left(\frac{K_{HA1}\, K_{HA2}}{[H^+]^2}\right))$$

As an example of hydration:

$$HCHO \quad + H_2O \overset{K_H}{\leftrightarrow} HCH(OH)_2 \tag{L.6}$$

The hydration constant is defined as:

$$K_H \ = \frac{[HCH(OH)_2]}{[HCHO]}$$

By combining with Henry's Law, the effective Henry's constant is expressed,

$$H_{HCHO}^* = \frac{[HCHO]_{tot}}{P_{HCHO,gas}} = \frac{[HCHO] \quad + \ [HCH(OH)_2]}{P_{HCHO,gas}} = \frac{[HCHO] \quad + K_H \ [HCHO]}{P_{HCHO,gas}}$$

$$H_{HCHO}^* = H_{HCHO}(1 + K_H\ )$$

As an example, the theoretical effective Henry's Law constants can be calculated as a function of pH for both formic and acetic acids. Figure I-14 represents this dependency: the solid line represents the theoretical Henry's law constant, while the symbols represent the experimental results obtained from concurrent gas and liquid phase measurements during campaign measurements for 1 h (Facchini et al., 1992). The effective Henry's Law constant is strongly dependent on pH (especially when pH > 4) since these species undergo rapid acid-base equilibrium in solution.

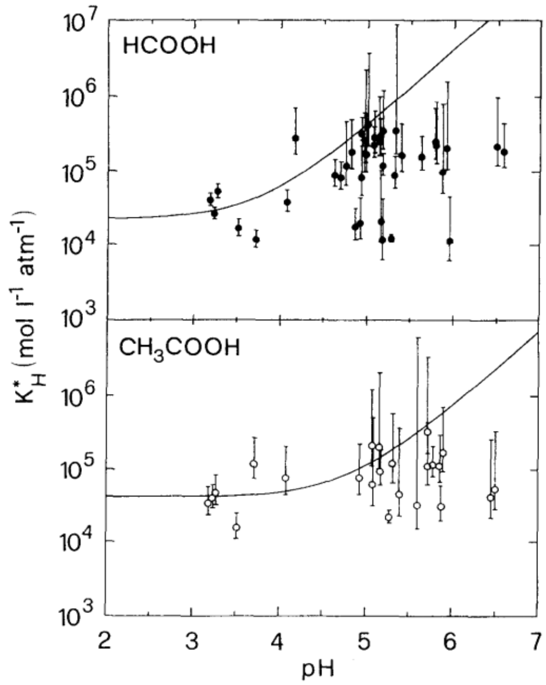

Figure I-14 Effective Henry's Law Constant for organic acids as a function of pH at a temperature of 278 K. The solid line represents the theoretical effective Henry's Law constant, while the symbols represent the experimental results obtained from gas and liquid phase measurements (1-h time basis). The error bars account for sampling and analytical errors from Facchini et al. (1992).

The liquid water content (LWC) of typical clouds varies from approximately 0.05 to 3 g (water) m^{-3}(air). The cloud liquid water content value allows to know the volume of liquid that is in that volume of air. The cloud water mixing ratio defines as w_L = (volume of liquid) / (volume of air) can be linked to the LWC:

$$LWC = \rho_w w_L \qquad \text{(Eq.9)}$$

The distribution of a species between the gas and the aqueous phases can be evaluated by a distribution factor:

$$f_X = \frac{C_{X,aq}}{C_{X,gas}} \qquad \text{(Eq.10)}$$

The distribution factor f_X is defined as the ratio of its aqueous-phase mass concentration $C_{X,aq}$ in g (L of air)$^{-1}$ to its gas-phase mass concentration $C_{X,gas}$ in g (L of air)$^{-1}$. Assuming Henry's law equilibrium one can show that, by combining Ideal Gas theory and LWC:

$$p_{gas}V_{gaz} = n_{gaz}RT \qquad \text{(Eq.11)}$$

$$H(X) = \frac{[X]_{aq}}{p_{X,gas}} = \frac{n_{X,aq}/V_{X,aq}}{p_{X,gas}} = \frac{n_{X,aq}}{V_{X,aq}} \div \frac{n_{X,gaz}RT}{V_{X,gaz}} = \frac{n_{X,aq}}{n_{X,gaz}RT} \times \frac{V_{X,gaz}}{V_{X,aq}}$$

$$H(X) = \frac{n_{X,aq}}{n_{X,gaz}RT} \times \frac{1}{LWC} = \frac{f}{RTLWC}$$

The distribution factor can be expressed as:

$$f_X = 10^{-6} H(X) RTLWC \quad \text{(Eq.12)}$$

where H is in M atm^{-1}; R is the ideal-gas constant equal to 0.08205 atm L mol^{-1} K^{-1}; T is the temperature in K, and LWC is the cloud/fog liquid water content in g m^{-3}.

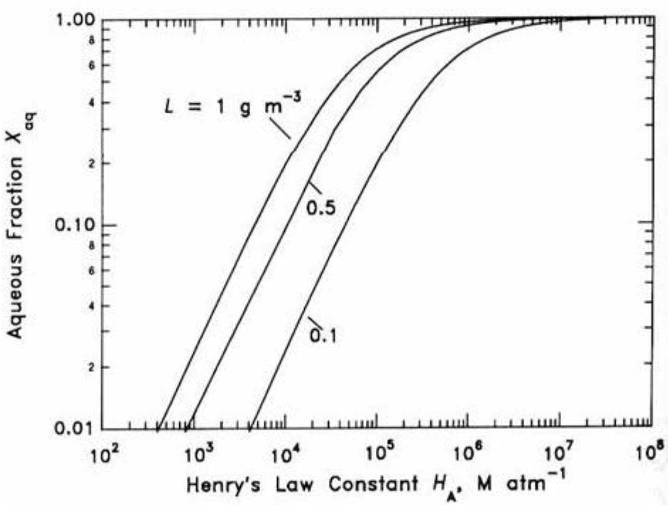

Figure I-15 Aqueous fraction of a chemical species X as a function of the cloud water content (noted as "L" on the figure) and the Henry's law constant at 298 K (Seinfeld and Pandis, 2016).

The Figure I-15 shows the variation of the aqueous fraction of a compound as a function of the cloud liquid water content and its Henry's Law constant. As expected, more the LWC is important, more the aqueous fraction increases.

Commonly, depending on the Henry's law constant values, solubility of the compounds are shared into 3 classes:

- H < 10^3 M atm^{-1}, the dissolved fraction does not exceed a few percent. The compounds can be considered as poorly soluble;
- 10^3 < H < 10^5 M atm^{-1} the dissolved fraction shows some percent or more. The compounds can be qualified as moderately soluble and partitioned between the two phases;
- H > 10^5 M atm^{-1} the dissolved fraction is dominant and the compounds is considered as very soluble.

Atmospheric chemistry models require the knowledge of the Henry's law constants for organic species considered in the chemical mechanism and that potentially dissolve into cloud droplets. Detailed gas phase or multiphase chemical mechanisms involve a vast number of species (Mouchel-Vallon et al., 2017; Herrmann et al., 2005; Aumont et al., 2005) that are not documented regarding their solubility. Moreover, there is also a critical lack of knowledge concerning the detailed water soluble organic fraction in clouds. As mentioned before, targeted analysis have been conducted allowing to quantify both soluble compounds (*e.g.*, organic acids, carbonyls, *etc.*) but also compounds presenting low or intermediate solubility (*e.g.*, PAHs). For the most part, those compounds with effective Henry's constants larger than 10^3 M atm^{-1} are considered readily subject to scavenging by cloud droplets and to wet deposition. The collection of Henry's law constants required to develop detailed models far exceeds the number of species for which experimental data is available. Numerous structure activity relationships (SARs) have been developed to determine the Henry's law constants in a response to the difficulties associated with its laboratory measurement, in particular, for compounds with higher solubility (Mouchel-Vallon et al., 2017; Raventos-Duran et al., 2010; Suzuki et al., 1992).

I.5.2 Mass transfer: a kinetical process

In the atmosphere, Henry's equilibrium is rarely reached (Iribarne and Cho, 1989). In fact, the cloud medium is poly-disperse and represents therefore a complex air/water interface. Moreover, complex multiphase cloud chemistry takes place in clouds. Physical and chemical parameters control the mass transfer from chemical compounds at the air/water interface. This mass transfer should be studied kinetically as discussed below.

Figure I-16 summarizes the processes that may influence uptake of chemical species: (1) diffusion of the trace species through the gas phase to the surface, (2) adsorption and desorption at the air/liquid surface, (3) reaction at the surface, (4) solvation of the trace species and incorporation into the bulk liquid, (5) diffusion of the trace species in the bulk liquid, and (6) reaction in the bulk liquid. Some of these processes can be considered as non-limiting steps because they are kinetically fast.

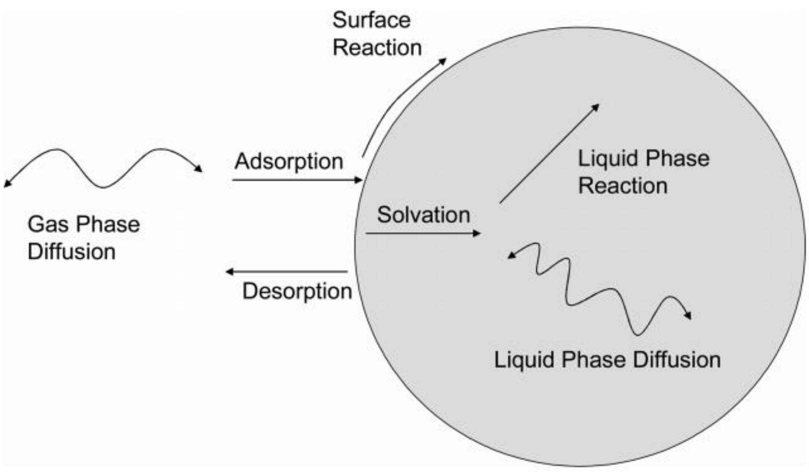

Figure I-16 Schematic of transport and reactive processes which determine the net uptake in gas–liquid interactions (from Davidovits et al., 2006).

Schwartz (1986) proposed to describe the air/droplet mass transfer in several successive steps and to estimate limiting and non-limiting steps. These steps are schematically illustrated in Figure I-17 for a species A in the presence of a droplet of radius a. They are described below:

(1): Transport of species A in the gas phase to the air-water interface governed by the differential gas phase diffusion equation associated with the gas phase diffusion coefficient D_g. $p_{A(\infty)}$ represents the partial pressure of species A in air and $p_{A(a)}$ the partial pressure of A at the surface of the droplet.

(2): Transport through the air/liquid interface and possible establishment of a local equilibrium. [A](a) is the concentration of species A in the aqueous phase at the interface in mol L^{-1} and $p_{A(a)}$ the partial pressure of A at the interface in atm.

(3): Possible establishment of a rapid equilibrium (hydration or dissociation) in the aqueous phase involving the dissolved gas. [B](a) is the concentration of species B in equilibrium with A dissolved in the droplet with radius r = a and [B](r) for the interior of the droplet.

(4): Dissolution of the dissolved species A and/or species B in the aqueous phase in equilibrium with A within the droplet governed by the differential equation of diffusion in the aqueous phase determined by the diffusion coefficient D_a.

(5): Chemical reactions in the aqueous phase. [C](r) is the concentration in mol L^{-1} of one of the products resulting from a reaction of dissolved species A or B; this concentration depends on the radius r.

(6): Transport of the products in the aqueous phase according to the differential equation of the diffusion in the aqueous phase.

(7): Possible transfer of volatile products from the aqueous phase to the gas phase.

(8): Transport of products in the gas phase according to the differential equation of gas phase diffusion.

Limiting steps have been evaluated and discussed by Schwartz (1986). This is achieved by calculating characteristic times for each step. Mathematical formulations of each step are indicated in Table I-7 below.

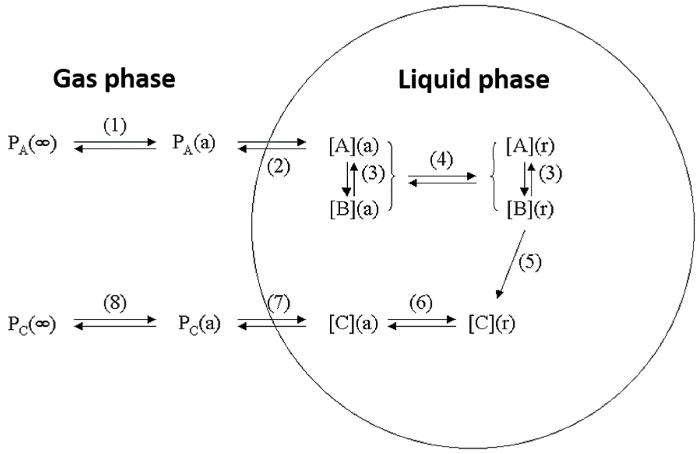

Figure I-17 Physical and chemical processes driving the mass transfer of species A between the gas phase and the liquid phase (adapted from Schwartz, 1986).

Table I-7 Characteristic times associated to each steps describing the mass transfer of a species A between the gas phase and cloud droplets.

Process	**Characteristic time**	**Formulation**
Gas phase diffusion	τ_{dg}	$\frac{a^2}{3D_g}$
Transfer at the air/water interface	τ_i	$\frac{4a}{3v\alpha}$
Diffusion in the aqueous phase	τ_{da}	$\frac{a^2}{\pi^2 D_a}$
Aqueous phase reactivity	τ_r	$\frac{[A]}{v_A R_A}$
Gas phase diffusion + transfer at the air/water interface	τ_t	$\frac{a^2}{3D_g} + \frac{4a}{3v\alpha}$

a is the radius of the droplet in cm; D_g is the diffusion coefficient in the gas phase a species A in cm^2 s^{-1}; v is the mean quadratic speed following the kinetic theory of gases in cm s^{-1}; α is the accommodation coefficient; D_a is the diffusion coefficient in the aqueous phase in cm^2 s^{-1}; $[A]$ is the aqueous concentration in mol L^{-1}; v_A is its associated stoichiometric coefficient in the aqueous phase; R_A is the reaction rate in the aqueous phase in mol L^{-1} s^{-1}.

$$v = \sqrt{\frac{8R'T}{\pi M_A}} \quad \text{(Eq.13)}$$

The parameter "mean quadratic speed" can be expressed as following:

R' = 8.3145 10^7 g cm^2 s^{-2} K^{-1} mol^{-1}, T is the temperature in K and M_A represents the molecular weight in g mol^{-1}.

The gas phase diffusion coefficient has an average value of about 0.1 cm^2 s^{-1} (Schwartz, 1986). The aqueous phase diffusion of the dissolved gases has an average value of about 2 10^{-5} cm^2 s^{-1} at 25 °C. (Schwartz, 1986).

The mass accommodation coefficient, α, is the probability that a molecule that collides the liquid surface enters into the bulk liquid.

$$\alpha = \frac{number\ of\ molecules\ entering\ into\ the\ aqueous\ phase}{total\ number\ of\ molecules\ colliding\ the\ liquid\ surface} \quad \text{(Eq.14)}$$

The value of α is generally of the order of 10^{-2} but can vary by several orders of magnitude ranging from 1 to 10^{-4}. Since few data exists in the literature, the accommodation coefficients are set to a default value of α = 0.05 (Davidovits et al., 2006, 2011), especially for modelling studies.

By studying the characteristic times in Table I-7, it is demonstrated that the gas phase diffusion and the transfer at the air/water interface are limiting steps depending on the values of α and of the droplet radius a. To summarize, for small droplets, the transfer is a limiting step and that for larger droplets, diffusion in the limiting step. Those two steps have therefore to be considered and can be grouped into one step corresponding to the transfer of the chemical species in the air to the droplet surface with a characteristic time τ_t (see in Table I-7). The characteristic time τ_{da} corresponds to the time required for obtaining a homogenous concentration of the chemical species in the cloud droplet, independently of the radius. This step is not a limiting step since most of the time $\tau_{da} << \tau_r$. This means that the concentration of the chemical species is homogenous in the cloud droplet volume. Finally, two steps need to be taken into account: the transfer of the chemical species from the air to the interior of the cloud droplet (aqueous phase diffusion is non-limiting) with a characteristic time τ_t and the aqueous phase reactivity with a characteristic time τ_r.

In order to evaluate the contribution of the gas phase to the cloud water composition, numerical models have been developed for simulating multiphase cloud chemistry. They consider complex gas phase and aqueous phase mechanisms and they parametrize the mass transfer of chemical compounds according to the available data (Henry's law constants, accommodation coefficient, *etc.*). They often consider kinetical approaches, notably the one from Schwartz (1986) described above. These models allow estimating gas/liquid partitioning of chemical compounds. They have to be confronted to *in situ* measurements of those partitioning. This point is detailed in the next section.

I.5.3 Evaluation of gas/liquid partitioning

Both gas-phase and liquid-phase chemical kinetics have been studied in their separated states for many years and extensive databases of kinetic parameters are available. However, the study of the two phases in interaction with each other is relatively recent and not nearly as well developed. Such heterogeneous studies are significantly more complex both theoretically and experimentally.

The partitioning of chemical compounds between gas and aqueous phases can be described in a first approach by Henry's law constants that is to assume thermodynamic equilibrium for all species.

To describe the deviation from thermodynamic equilibrium, the partitioning of chemical compounds between the gas and aqueous phases can be represented by a partitioning coefficient q, first defined by Audiffren et al. (1998) and used in other studies such as in van Pinxteren et al. (2005) and Rose et al. (2018) which is defined as:

$$q = \frac{H_{exp}}{H_{theory}} \qquad \text{(Eq.15)}$$

H_{exp} represents the experimental "pseudo"-Henry's law constant calculated with the aqueous and gaseous experimental concentrations and H_{theory} is the Henry's law constant estimated in the laboratory.

$$q = \frac{C_{aq}}{LWC \times H_{eff} \times R \times T \times C_{gas}} \qquad \text{(Eq.16)}$$

Where C_{aq} and C_{gas} are, respectively, the experimental gaseous and aqueous concentrations of the studied compound in molec cm^{-3}. LWC is the liquid water content of the cloud event in vol.(water)/vol.(air). H_{eff} is the effective Henry's law constant evaluated in the laboratory in M atm^{-1}. T is the temperature. R is equal to 0.08206 atm M^{-1} K^{-1}.

This factor q indicates whether the measured compound is at the Henry's law equilibrium (q = 1), undersaturated in the aqueous phase (q < 1) or supersaturated in the aqueous phase (q > 1).

Observations have shown that for many species the assumption of thermodynamic equilibrium between gas and aqueous phases is not appropriate and often leads to a biased estimate of the aqueous phase concentrations and reactions rates. Values for observed q values for various species at different locations in cloud and fogwater are summarized in Figure-18. Oxalic acid ($H_2C_2O_4$) is found with q = 1, in agreement with their effective Henry's law constants (Winiwarter et al., 1994; Sellegri et al., 2003). Formic (HCOOH) and acetic (CH_3COOH) acids are often found q ≤ 1. They can be subsaturated in the water phase by a factor about 3−5. This phenomena can be explained by the effect of pH (Facchini et al., 1992). At more acidic pH values (<3), these acids can be slightly supersaturated in the aqueous phase (Winiwarter et al., 1994). The deviation from partitioning according to Henry's law increases with increasing pH for species over a wide range of solubility. The partitioning of carbonyl compounds have been investigated by van Pinxteren et al. (2005) for clouds sampled during orographic events in the frame of the FEBUKO/MODMEP (Field investigations of budgets and conversions of particle phase organics in tropospheric cloud processes)/(Modeling of Tropospheric Multiphase Processes: Tools and Chemical Mechanisms)project in Germany. For the relatively polar compounds, formaldehyde (HCHO) and glycolaldehyde (GA), they showed that the measured liquid phase fractions are equal or lower in comparison the calculated fractions assuming thermodynamic equilibrium conditions ($q \leq 1$). However, for larger and less soluble carbonyl compounds (methyl vinyl ketone (MVK), heptanal and octanal), a supersaturation by a factor of 100−1000 was observed.

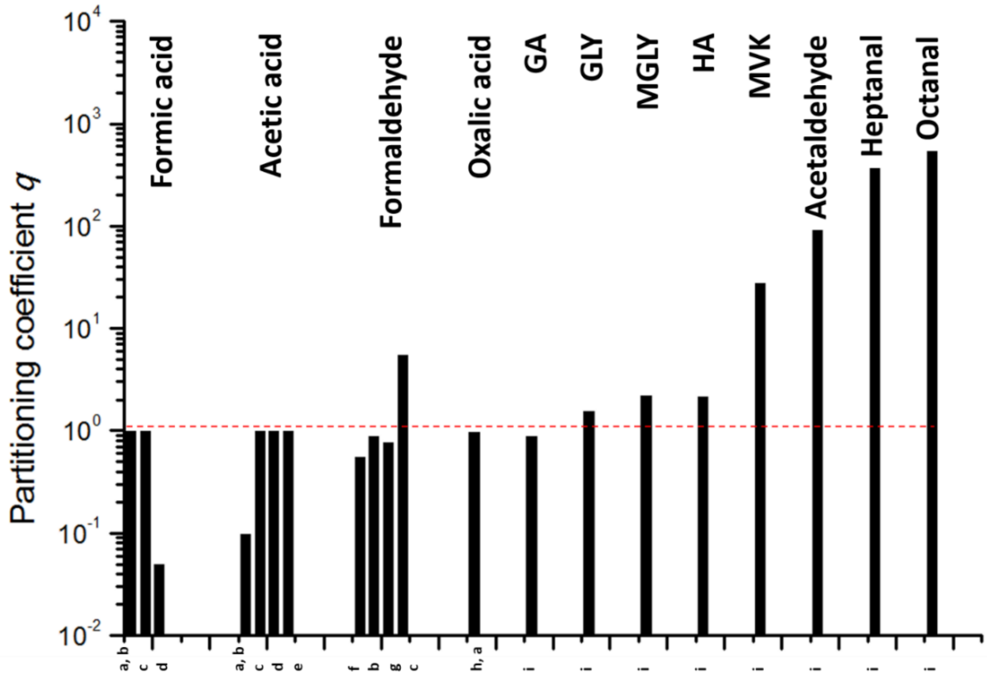

Figure I-18 Observed q values for various species at different locations in cloud/fog conditions (a–i: Winiwarter et al., 1994; Munger et al., 1995; Facchini et al., 1992; Voisin et al., 2000; Keene et al., 1995; Ricci et al., 1998; Li et al., 2008; Sellegri et al., 2003; van Pinxteren et al., 2005). GA: glycolaldehyde; GLY: glyoxal; HA: hydroxyacetone; MVK: methyl vinyl ketone.

Cloud chemistry models (Chaumerliac et al., 2000; Leriche, 2003; Lim et al., 2005; Barth, 2006; Ervens, 2015; Rose et al., 2018) have also highlighted deviations from the Henry's law equilibrium for some targeted chemical compounds, but, among them, few investigated the partitioning of organic compounds in clouds. Many factors control the partitioning between these two phases such as the pH, the droplet size, and the reactivity in both phases and are described more or less explicitly depending on the model. Historically, those models have targeted small organic compounds such as formic acid, acetic acid or formaldehyde that are commonly measured in the cloud medium (Ervens et al., 2003; Leriche, 2003). These models kinetically consider the mass transfer as described in Section I.5.2 and show that Henry's law to predict the partitioning of the compounds is sufficient, if the pH dependence of the acid solubility or hydration of formaldehyde is considered. Recently, Rose et al. (2018) with the

CLEPS (Cloud Explicit Physico-Chemical Scheme) model have shown that the partitioning ratio is evaluated to be at Henry's law equilibrium for carboxylic acids originating from the particulate phase. However, some deviations are observed for highly soluble carbonyl compounds (glyoxal, formaldehyde, *etc.*) that are simulated to be undersaturated with respect to the equilibrium predicted by the Henry's law.

The results obtained with the models exhibit large uncertainties explained by the variety of the physical and chemical processes that need to be considered to reproduce the cloud medium. Among this complex processes, those models do not consider for example how the kinetic transport limitations through the droplet surface are perturbed by the presence of hydrophobic molecules at the air/water interface. In this frame, it is of high importance that cloud chemistry models have to be evaluated towards *in situ* estimates that are actually particularly scarce.

I.6 Transformations in the aqueous phase

Once in the aqueous phase, VOC can be transformed efficiently by various processes briefly described below. Those processes are much different (mechanisms and kinetics) than the ones occurring in the gas phase; some differences can be highlighted such as the presence on ionic species, the efficient photolytic transformations and the presence of microorganisms that can use VOC for their metabolic activity.

I.6.1 Abiotic transformations

The atmospheric aqueous phase contains oxidants that will transform dissolved VOC. In this frame, H_2O_2 and metals drive the oxidative capacity of the aqueous phase (Deguillaume et al., 2005). They lead to the production of the hydroxyl radical $HO^•$, which is responsible for the oxidation of organic matter. The so-called "Fenton" reaction between H_2O_2 and iron(II) and the photolysis of iron(III)-hydroxy complexes are significant source of $HO^•$ radicals. $HO^•$ in the aqueous phase results also from its mas transfer from the gaseous phase. Finally, the photolysis of aqueous H_2O_2, $NO_3^{•-}$ and $NO_2^{•-}$ serves as an effective source of $HO^•$ in the aqueous phase (Bianco et al., 2015). Metals and especially iron can be complexed by the organic matter. These complexations are not well characterized in natural cloud water and the photochemistry of these metal-organic compounds is also not thoroughly understood. This can reduce the contribution of iron to produce $HO^•$. The oxidation of organic matter by ozone and hydrogen peroxide can also occur in the aqueous phase but rate constants are roughly 10 orders of magnitude smaller than the ones from radical reactions (Schöne and Herrmann, 2014).

Aqueous reactivity of VOC then results in the production of shorter (fragmentation process) and more oxygenated molecules (functionalization). Accretion processes can also take place in cloud droplets, with the production of organic compounds presenting higher molecular mass than their precursors. Those molecules are mainly produced for wet aerosols, in which concentrations of organic compounds are higher. Many organic precursors are suspected such as carbonyls (glyoxal, *etc.*) or carboxylic acids (acetic acids, *etc.*).

The two known mechanisms of $HO^{\bullet}$ radicals with organic compounds in aqueous solutions are: H–abstraction reactions with saturated compounds and addition reactions (*e.g.*, C=C double bonds in unsaturated compounds). Electron transfer processes of $HO^{\bullet}$ radicals can also occur but depends on reduction potentials and on reactant structures. For example, $HO^{\bullet}$ can undergo an electron transfer in the presence of anions (*e.g.*, carboxylate compounds). The alkyl radical $R^{\bullet}$ produced directly reacts with oxygen to form a peroxyl radical $RO_2^{\bullet}$. Peroxyl radical mainly reacts with another peroxyl radical to form a tetroxide that quickly decomposes. The decomposition of tetroxide can occur through various pathways depending on the nature of the initial peroxyl radical. When a hydroxyl moiety occupies the α-position of the peroxyl function, the peroxyl radical can undergo $HO_2^{\bullet}$ elimination. To briefly summarize, the transformation of organic compounds *via* radical chemistry occurs when alcohols in the aqueous phase are oxidized into carbonyls that form carboxylic acids (Mouchel-Vallon et al., 2017).

$HO^{\bullet}$ radical reactions have been deeply investigated in the past: the reactivity of alcohols, carboxylic acids, carbonyls, certain aromatic compounds, and certain halogenated alkanes in aqueous solutions has been studied in the laboratory because they have been detected into cloud water (Deguillaume et al., 2014; Li et al., 2019). However, due to the numerous organic compounds found in cloud water, not all oxidation pathways have been documented. To compensate this, structure activity relationships (SAR) as well as reactivity correlations have been developed for estimating missing parameters: kinetic constants, branching ratios, hydration constants, acidity constants, *etc.* (Doussin and Monod, 2013). However, the aqueous organic composition is complex (Bianco et al., 2018, 2019) and for example reactivity of aromatic compounds, sugars, amino acids, organo-nitrates and sulfates and other functionalized aliphatic reactants have not been deeply studied. For example, products and branching ratios must be identified and quantified. Uncertainties also remain in regards to the reactivity, formation and distribution of transient species and stable reaction products. Furthermore, temperature and pH levels can influence reaction rates, though these effects are not typically measured in laboratory settings.

I.6.2 Biotic transformations

As microorganisms are alive and metabolically active in clouds, they interact with the cloud medium, and thus microbial metabolism may serve as an alternative route to pure abiotic processes involved in cloud chemistry. Cloud microorganisms degrade organic compounds present in cloud waters and can interact with H_2O_2 and iron.

As described before, short chain mono- and di-carboxylic acids as well as C1 compounds (methanol and formaldehyde) are present in the aqueous phase. They result from VOC dissolution from the gas phase to the aqueous phase by mass transfer and they are also formed during successive oxidation processes in cloud waters. Consequently, they are found at rather high concentrations (range of µM) and can be used as nutrients by microorganisms present in cloud droplets (Vaïtilingom et al., 2011; Vaïtilingom et al., 2012; Husárová et al., 2011; Bianco et al., 2019). Indeed, most of those compounds can enter into the central metabolism of several microorganisms, and these metabolites can be used to maintain energy levels through the production of ATP (Adenosine Tri-Phosphate) to synthesize larger molecules and produce biomass (proteins, nucleic acids, membranes, *etc.*). Microorganisms can, for example, synthesize biosurfactants (surface active agents) that are highly complex molecules, presenting considerable levels of structural variability. Biosurfactants are amphiphilic compounds with hydrophobic (*e.g.*, lipids) and hydrophilic (*e.g.*, sugars, amino-acids) moieties. They can also produce exopolysaccharides (EPSs) that are highly functionalized molecules including sugar alcohols, monosaccharides, disaccharides, trisaccharides, and anhydrosugars.

Microorganisms can interact directly with extracellular Reactive Oxidant Species (ROS) (H_2O_2, $HO_2^{\bullet}/O_2^{\bullet-}$, and $HO^{\bullet}$), which can diffuse into cells. Aerobic microorganisms are equipped to face against ROS, because they produce the same molecules intracellularly during respiration when O_2 diffuses inside the cell. This protective mechanism against ROS, is referred to as “oxidative stress metabolism”. ROS can be deleterious to cells by damaging major cellular components (proteins, DNA, lipids, *etc.*). It has been shown that the cloud microflora is able to degrade H_2O_2 then reducing a major source of radicals (Vaïtilingom et al., 2013; Wirgot et al., 2017). Microorganisms are also able to synthetize siderophores that are complex molecules with a large variety of chemical structures (Vinatier et al., 2016). These biological molecules have a high affinity for iron (Cheize et al., 2012). Siderophore photochemistry may change the redox cycling of iron and the production of ROS in clouds.

I.7 Objectives of the thesis: effect of clouds on the atmospheric VOC budget?

CHAPTER I has highlighted that VOC in the atmosphere are a vast and diverse group of compounds emitted by anthropogenic and natural sources. They play a key role on climate, environment and health issues. However, many uncertainties still exist concerning the quantification of their sources, and their transformations in the multiphasic atmosphere (gas, cloud droplets, aerosol particles).

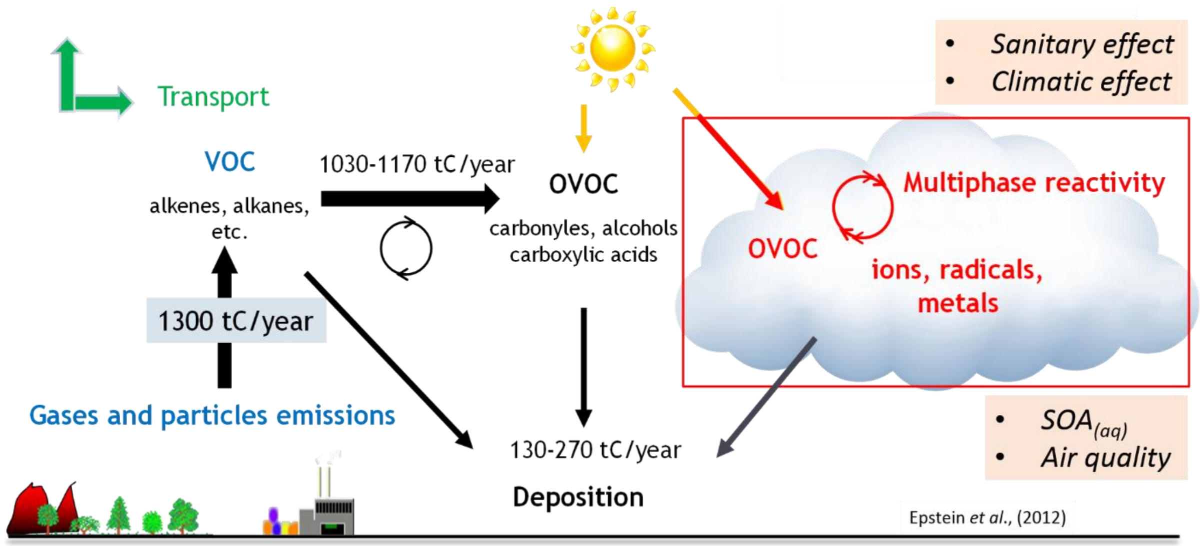

Figure I-19 Scientific context: VOC in the atmosphere and their climate and sanitary effects.

During their atmospheric transport, VOC can undergo multiphasic chemical transformations. Chemical reactivity will modify the chemical structure of VOC and thus its physical and chemical properties. Atmospheric transport will dilute or concentrate VOC in the atmosphere and dry and wet deposition can occur, representing a sink for VOC. Complex multi-steps oxidation of VOC leads to the generation of a set of organic products containing one or more polar oxygenated functional groups, which tend to make the products less volatile and more water soluble. SOA are formed from the gas-to-particle transfer of partially oxidized organic material, occurring in competition with further oxidation in the gas phase. SOA formation by many VOC precursors have been deeply investigated in the past and many studies demonstrated the complexity of this phase change controlled by many environmental parameters.

Moreover, cloud droplets constitute one of the most reactive medium with their ability to capture and dissolve numerous gaseous and particulate compounds. Thus, the cloud droplet can be considered as an extremely efficient chemical reactor that will be the seat of many transformations (chemical and biological). In addition, the microphysical processes of clouds redistribute the chemical species between different reservoirs (cloud water, rain droplet, particulate phase, gas phase, solid phase ice). Physico-chemical processes in clouds will consequently strongly perturb the VOC budget in the atmosphere. Due to the inherent difficulty to sample clouds and to sample at the same time the gas phase, data on the partitioning of VOC between the cloud phases (gas, liquid) are scarce. However, this is of prior importance since cloud chemistry strongly perturbs the homogeneous VOC gas phase chemistry and can potentially modify the chemical and physical properties of organic aerosols.

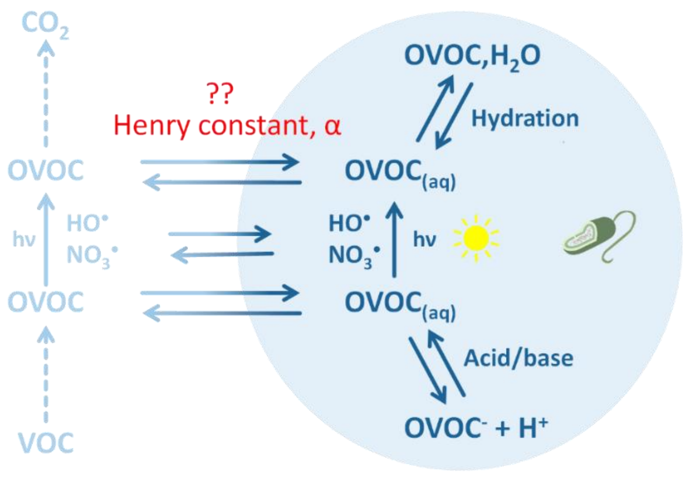

Figure I-20 VOC multiphase chemistry: reactivity and air/droplet exchanges.

In this frame, my thesis work aims at improving knowledge on the characterization and reactivity of VOC in the cloud system (air and cloud droplets). Targeted species are from both anthropogenic and biogenic sources with a focus on OVOC that are known to be highly soluble and to play a role on the SOA budget. In cloud droplets, aqueous phase reactivity of VOC will also lead to a production of secondary compounds that can contribute to SOA and are reported as “aq SOA” (Ervens, 2015). To evaluate the role of cloud on VOC, *in situ* measurements are required to document their partitioning between the gas and the aqueous phase. In the frame of my thesis at LaMP, instrumental developments both in the field and in the laboratory have been conducted. In the laboratory, new analytical procedures have been developed to characterized VOC and OVOC in both phases by gas chromatography (CHAPTER II). These developments have been tested on real matrices sampled at the top of the puy de Dôme station (France) and/or at the Maïdo observatory Réunion Island) presenting highly different environmental conditions (temperature, solar irradiation, seasons, origin of air masses, level of pollution, ...). Results are presented in CHAPTER III.

CHAPTER II Analytical developments for quantification of multiphasic VOC/OVOC in cloud

II.1 Framework of the analytical developments

II.1.1 Which target compounds?

As discussed in CHAPTER I, Volatile Organic Compounds (VOC) encompass a large spectrum of species with various origins and properties. Here target compounds are the ones of atmospheric interest regarding their (i) atmospheric abundance, (ii) primary, secondary ,biogenic and anthropogenic sources, (iii) reactivity towards major atmospheric oxidants, (iv) volatility (see in Section I.4) and (v) solubility (see in Section I.5). All these properties, together with environmental conditions, will define the multiphasic fate of the compounds, *i.e.* their ability to partition between gas phase and condensed phases (particulate and aqueous phases).

These compounds include:

- **Non-Methane Hydrocarbons (NMHC)**: alkanes, alkenes and aromatics like benzene, toluene, ethylbenzene and xylenes (BTEX) of anthropogenic origin and isoprene and other terpenes of biogenic origin (Leuchner et al., 2015; Michoud et al., 2017). These compounds which are usually detected in the atmospheric gas phase are the most abundant. However, they are not expected to be present in the aqueous phase due to their low solubility. Beyond their health impact, like benzene (Cocheo et al., 2000), these compounds are also well-known to contribute to the formation of secondary pollutants like ozone and SOA (Hu et al., 2008; Fu et al., 2009) as described in CHAPTER I.
- **Oxygenated VOC with carbonyls, alcohols and carboxylic acids** (see in Table II-1). These compounds are fairly common primary compounds (mainly as residues from incomplete combustion) and even more frequently secondary compounds as intermediates in the photo-oxidation of organic compounds. As they can be easily photolyzed, they are also an essential source of free radicals (George and Abbatt, 2010). Due to their polarity, they easily interact with the condensed phases and, in particular, the cloud phase. As discussed in Section I.4 and Section I.4, these compounds represent an important fraction of the organic matter in the cloud droplet phase due to their high solubility. In addition, observational and model studies have shown that for these compounds, the assumption of thermodynamic equilibrium between gas and aqueous phases is not appropriate and often leads to a biased estimate of the aqueous phase concentrations and reactions rates (Ervens, 2015).

The target compounds are listed in Table II-1.

Table II-1 List of target compounds in our study.

Classification	Compounds	Criteria	References
NMHC			
Anthropogenic VOC (AVOC)	Alkanes, alkenes, C_6–C_9 aromatics (benzene, toluene, ethylbenzene and xylenes (BTEX))	Combustion processes including vehicle exhaust and biomass combustion Precursors of SOA Varied lifetimes: indicator of photochemical aging	Lanz et al., 2008
Biogenic VOC (BVOC)	Isoprene, monoterpenes, (α/β-)pinene, limonene	Biogenic emissions from vegetation Precursors of SOA	Holopainen et al., 2017
	Nopinone	Oxidation product of isoprene and β-pinene Precursor of SOA	Neeman et al., 2017
OVOC			
Carbonyl compounds	Linear aldehydes	Biogenic source and secondary precursors of SOA	Colmán et al., 2015
	Acetaldehyde	Biogenic sources	Millet et al., 2010
	Formaldehyde	Tracer of photochemical process	Zeng et al., 2019
	Acetone	Possible variable sources Possible tracer of pollution background	Singh et al., 2003 Goldstein and Schade, 2000 Legreid et al., 2007
	Methyl vinyl ketone (MVK) Methacrolein (MACR) Glyoxal (GLY) Methylglyoxal (MGLY)	Oxidation products of isoprene Biogenic precursors of SOA	Nguyen et al., 2014 Lim et al., 2005
Alcohols	Methanol Ethanol	Primary and secondary biogenic sources	Michoud et al., 2017
Carboxylic acids	Carboxylic acids (C_3–C_5)	Important fraction of organic matter in cloud droplets. Contribution to SOA formation.	Deguillaume et al., 2014 Lim et al., 2005 Ervens et al., 2013

II.1.2 Which expertise at LaMP?

- In the cloud water phase

The LaMP laboratory (Laboratoire de Météorologie Physique) has a long experience for cloud sampling and different bio-physical-chemical parameters are determined systematically on cloud water samples. Cloud water sampling is regularly performed using a dynamic one-stage cloud water impactor (Brantner et al., 1994), with a cut off diameter of approximately 7 µm. Cloud liquid water content (LWC) and droplet radius are measured by Gerber PVM-100, a ground-direct scattering laser spectrophotometer. pH is determined immediately after sampling. Main inorganic cations (Na^+, NH_4^+, K^+, Mg^{2+}, Ca^{2+}) and anions (Cl^-, NO_3^-, SO_4^{2-}, PO_4^{3-}) as well as short chain carboxylic acids (formate, acetate, succinate, oxalate) are measured by ion chromatography (IC). A Shimadsu TOC analyzer allows to evaluate the total organic matter amount in cloud water. Hydrogen peroxide (H_2O_2), a strong oxidant in the cloud water, is determined by spectrofluorometric quantification method (Li et al., 2007). The concentration of Fe(II) and Fe(III), a key parameter for the cloud water oxidative capacity evaluation (Deguillaume et al., 2005), is determined by spectrophotometric method after chemical complexation (Stookey, 1970). More recently, the analysis of the chemical composition of the cloud waters sampled has been strongly improved with the quantification of 16 amino acids (AAs) determined using a new complexation method coupled with high-performance liquid chromatography (HPLC) (Bianco et al., 2016); the concentrations of 33 metal elements have been determined using Inductively Coupled Plasma Mass Spectrometry (ICP-MS) (Bianco et al., 2017). The oxidative capacity of the cloud water has also been evaluated following the hydroxyl radical ($HO^•$) formation rates during the irradiation of cloud waters under sun-simulated radiation (Bianco et al., 2015). Ultrahigh-resolution mass spectrometry has been recently used to get a better identification of the dissolved organic compounds. Using GC×GC-HRMS technique, more than 100 semi-volatile compounds were detected and identified (Lebedev et al., 2018). Among them, phenols and phthalates that are strong pollutants were quantified. Ultrahigh-resolution Fourier-transform ion cyclotron resonance mass spectrometry (FT-ICR) has also been used to identify a wide spectrum of organic compounds (up to 5000 assigned molecular formula) that have been shared into several classes depending on their H/C and O/C ratio (Bianco et al., 2019, 2018). Since 2003, the biodiversity of microorganisms in cloud waters and their activity have been also investigated (Vaïtilingom et al., 2012; Amato et al., 2017, 2019).

Finally, the combined analysis of both VOC and OVOC of atmospheric interest in cloud water samples was not yet investigated at LaMP and new analytical development were required. As part of my PhD thesis, a first prerequisite was the development of VOC/OVOC extraction from the cloud liquid phase before analysis.

- For the gas phase

Over the last decade, LaMP has deployed the off-line active sampling of NMHC on sorbent cartridges filled with Tenax® TA at the puy de Dôme station in the frame of the ACTRIS European network (the European Research Infrastructure for the observation of Aerosol, Clouds and Trace Gases) and during intensive field campaigns. Tenax® is chemically inert, highly hydrophobic and widely used for VOC measurements of more than 4 carbon atoms (Rothweiler et al., 1991; Schieweck et al., 2018; Ho et al., 2018). Air pumping is either performed with an automatic sampling module developed by TERA Environment - a SASS (Smart Automatic Sampling System) (see in Figure II-1) or with an automatic Gilian pump at controlled flow rates of usually 100 mL min^{-1}. Sampling duration is flexible depending on the nature of the compound and air volume, which must be lower than the breakthrough volume for target species.

The instrumentation used for the cartridge analysis consists of a gas chromatograph - mass spectrometer system (GC-MS, Perkin Elmer) connected to an automatic Thermal Desorption (TD). GC is a separation technique capable of separating highly complex mixtures based primarily upon differences of boiling point/vapor pressure and of polarity. GC-MS is a hyphenated technique developed from the coupling of GC and MS. The acquired mass spectra offer more structure-related information based on the interpretation of ion fragments. The TD is a common technique that utilizes heat to increase the volatility of the trapped compounds to desorb them from the solid support (such as Tenax® adsorbent tubes) and that concentrates the compounds in gas streams prior to injection into the GC. At LaMP, the TD TurboMatrix 650 TD system is composed of a multi-tubes auto-sampler equipped with an injected sample split flow automated re-collection system. The GC system is a Perkin Elmer Clarus 600 equipped with an Elite-5MS capillary column (60 m, 0.25 mm i.d. (inner diameter), film thickness: 0.25 µm, Restek Corporation, Bellefonte, USA) (see the TD-GC-MS system in Figure II-1). NMHC are directly thermally desorbed from the cartridges and chromatographically separated with the following temperature program: from 35 to 250 °C with thermal ramps of 5 °C min^{-1} and hold about 2 min. The MS system is equipped with an electron ionization source (operated at an energy of 70 eV) for structural identification and quantification.

There are many advantages to use GC-MS for compound analysis, including its ability to separate complex mixtures, to identify and quantify analytes, and to determine trace levels of organic contamination. Molecular characterization of atmospheric organic compounds has its roots in GC-MS, which in many respects is ideally suited for organic compound analysis owing to high chromatographic resolution coupled with library searchable electron ionization (EI) mass spectra. Thermal Desorption (TD) is a very convenient extraction method as it can be fully automated and is inexpensive, sensitive and solvent-free. VOC sampling through active sorbent tubes and a further analysis of the tubes with a TD-GC-MS system allows for a good chromatographic separation and a reliable identification and quantification of the target compounds through their characteristic mass spectra. Additionally, this method presents low limits of detection and breakthrough, and high reproducibility (Ribes et al., 2007; Gallego et al., 2010). The most widely applied quantitative analytical technique for VOC remains GC-MS and GC-FID-MS (the system that combines the separation properties of GC with the detection feature of MS and Flame Ionization Detector (FID)) in order to unambiguously identify compounds from consideration of their retention times and mass spectra. However, the closely related methods of Chemical Ionisation Mass Spectrometry (CIMS) and Proton Transfer Reaction-Mass Spectrometry (PTR-MS) are becoming increasingly used (*e.g.*, Hansel et al., 1995, 1999; Holzinger et al., 2019).

Figure II-1 The analytical TD-GC-MS system available at LaMP (left) and the automatic sampling module-SASS (Smart Automatic Sampling System) installed et the puy de Dôme station (right).

While GC-MS is a mature and robust method, significant limitations still exist. Not all VOC can be chromatographically separated, resolved and identified by the GC column due to their high polarity and/or thermal lability. This is the case for OVOC. The polarity of more polar compounds such as some carbonyl compounds (*e.g.*, formaldehyde, glyoxal, and methylglyoxal) hinders direct analysis by GC, because they are easily lost onto the surfaces of injectors and columns. Consequently, polar analytes are not suitable for TD-GC analysis. However, polar analytes can be converted, through derivatization, into chemical forms that are thermally instable, more volatile and suitable for GC analysis (Nozière et al., 2015). An analytical scheme, which is able to couple derivatization sampling and thermal desorption, would exploit the advantages of thermal desorption for more polar analytes.

II.1.3 Derivatization techniques for OVOC measurement by GC-MS

Molecular derivatization methods have been developed for OVOC analysis. The 2,4-dinitrophenylhydrazine (DNPH) and the pentafluorobenzylhydroxylamine (PFBHA) are two derivatization reagents that are commonly used for the derivatization of aldehydes and ketones in various matrices. The DNPH is widely used coupled with liquid chromatography (LC) with detection by UV-Visible spectrophotometry or mass spectrometry (Chi et al., 2007). It is, however, rarely used in gas chromatography because of the low thermal stability of formed derivatives (Ho and Yu, 2004).

The DNPH derivatizing technique, however, fails to distinguish α-hydroxy carbonyls and the corresponding dicarbonyls, thus confusing glycolaldehyde and glyoxal (or hydroxyacetone and methylglyoxal) because they form the same osazone when the derivatization reaction proceeds in an organic solvent. Another problem with DNPH-HPLC techniques is the coelution or poor resolution of similar carbonyls such as acrolein, acetone and propanal, and methyl ethyl ketone and butanal (Ho and Yu, 2004). In addition, identification of unknown carbonyls by the DNPH method is difficult, even if coupled with a secondary method such as multiple columns or mass spectrometry. Several studies have shown that the oxime formation of aldehydes and ketones by reaction with O-(2,3,4,5,6 pentafluorobenzylhydroxylamine (PFBHA) coupled with GC-MS offers an excellent alternative to the DNPH-HPLC method (Yu et al., 1995; Ho and Yu, 2004). The reaction is detailed in Figure II-2.

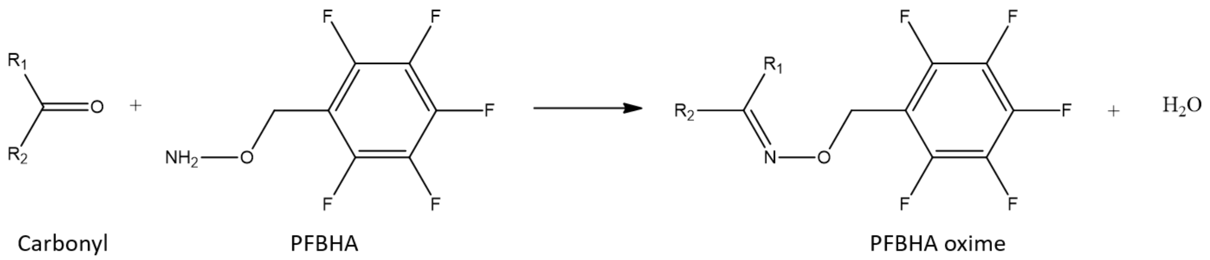

Figure II-2 Derivatization reaction of carbonyl compounds -C=O by the O-(2,3,4,5,6 pentafluorobenzylhydroxylamine (PFBHA) reagent.

Moreover, it is known that the combination of solid sorbent sampling and GC analysis enables the direct introduction of the entire sample for analysis through TD. Thermal desorption uses no solvent, making it more environmentally friendly. It also avoids extra sample handing as required with solvent extraction techniques. TD is a well-established sample-introducing technique in the GC analysis of nonpolar and low-polarity organic compounds in the air (Nollet, 2005).

An established GC-MS method for carbonyls is to convert them to their O-(2,3,4,5,6-pentafluorobenzyl)hydroxylamine (PFBHA) derivatives in a liquid medium and then to analyze the derivatives by GC with MS detection. The PFBHA derivatives allow sensitive GC/MS-selected ion monitoring of m/z 181 ions ($[C_6F_5CH_2]^+$) at the picogram (10^{-12} g) level (Wu and Hee, 1995). The reaction mechanism in the liquid phase has long been established, but little is known about the reaction between gaseous carbonyl and solid PFBHA. It is feasible to trap carbonyls on PFBHA-coated solid sorbents through their reaction with PFBHA. A two-step reaction mechanism is suggested for the vapor-solid derivatization reaction. In the first step, gaseous carbonyl molecules diffuse onto the solid sorbent surface where PFBHA is immobilized onto and react with PFBHA to form a tetrahedral carbinolamine intermediate. The reaction rate for this step is expected to play a key role in the collection efficiency of carbonyls. In the second step, the carbinolamine intermediate loses a molecule of water to form the oxime derivative (Cordes and Jencks, 1962).

For other polar compounds such as alcohols and carboxylic acids, N,O-bis(trimethylsilyl)trifluoroacetamide (BSTFA) and N-Methyl-N-(t-butyldimethylsilyl)trifluoroacetamide (MTBSTFA) (Figure II-3) are often used (Schummer et al., 2009). In the derivatization with BSTFA or MTBSTFA, silylation reactions, a labile hydrogen from acids or alcohols is replaced by a trimethylsilyl group. Reaction occurs through nucleophilic attack (SN2), and the presence of a strong leaving group often improves the reaction yield. Silylation normally does not require a purification step, and the derivatives can be injected directly into the GC. MTBSTFA should be preferred since its derivatives display a simplified fragmentation pattern yielding fragments with very high relative abundances, especially for $[M-57]^+$, that generates good detection limits. However, it was found that steric hindrance and molecular mass play a very important role in the choice of the best suited derivatization reagent: MTBSTFA derivatization of compounds with sterically hindered sites produces very small analytical responses or no signal at all, and BSTFA derivatization of compounds with high molecular mass produces no characteristic fragmentation pattern.

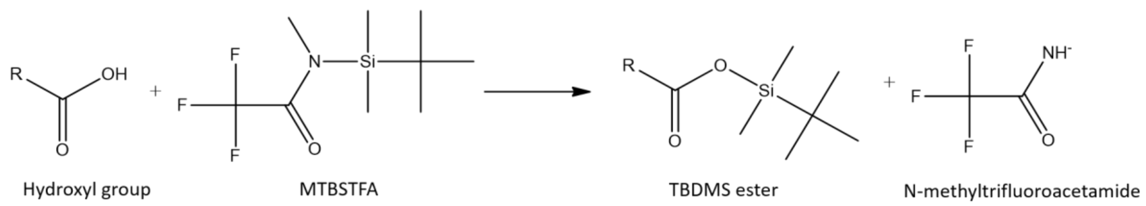

Figure II-3 Derivatization reaction of carboxyl or hydroxyl compounds -OH by the N-Methyl-N-(t-butyldimethylsilyl)trifluoroacetamide (MTBSTFA) reagent.

There are just a few approaches using derivatization strategies for OVOC directly from the gas phase (Ho and Yu, 2004; Temime et al., 2007; Pacolay et al., 2008) by analysis with TD-GC-MS. A recent study by Rossignol et al. (2012) has shown a method development and validation for an atmospherically relevant range of organic acids and carbonyl and hydroxyl compounds, which is based on TD-GC-MS, with derivatization on sampling sorbent tubes. Gaseous compounds were trapped on Tenax® adsorbent tubes pre-coated with PFBHA or MTBSTFA. The reliability of this method was demonstrated in simulation chambers (simulation EUPHORE, CEAM site, Valence, Spain) and in real atmospheric conditions (Haute Corse, France).

Given the technical resources and expertise at LaMP in TD-GC-MS analysis and as part of my PhD, we decided to explore the potentiality of the derivatization pretreatment for OVOC measurements in both gaseous and aqueous phases.

II.1.4 Design of the analytical set-up for VOC/OVOC measurement in gas and cloud phases

The analytical set-up is based on the existing TD-GC-MS system which will be optimized for the analysis of both VOC and OVOC from the gas and aqueous phases. The main steps are reported on Figure II-4.

While the analytical conditions for VOC identification and separation was already handled at the laboratory, the optimization of analytical conditions for the identification and separation of derivatized OVOC by TD-GC-MS was first required.

Secondly, the gas-phase sampling using Tenax TA sorbent tubes pre-coated with derivatization agent for OVOC needed to be adapted following Rossignol et al. (2012). From her study, two derivatization reagents (pentafluorobenzylhydroxylamine (PFBHA) and N-Methyl-N(t-butyldimethylsilyl)trifluoroacetamide (MTBSTFA)) were chosen for C=O, -OH/-COOH compounds. The performances of the method for light carbonyls will be tested.

Finally, for the analysis of cloud water samples, an intermediate extraction step of VOC/OVOC was required and needed to be developed with an extraction support compatible with thermal desorption. This extraction is based on Stir Bar Sorptive Extraction (SBSE) which will be described in the following sections. Derivatization of dissolved OVOC is also part of such development following the one for the gaseous phase.

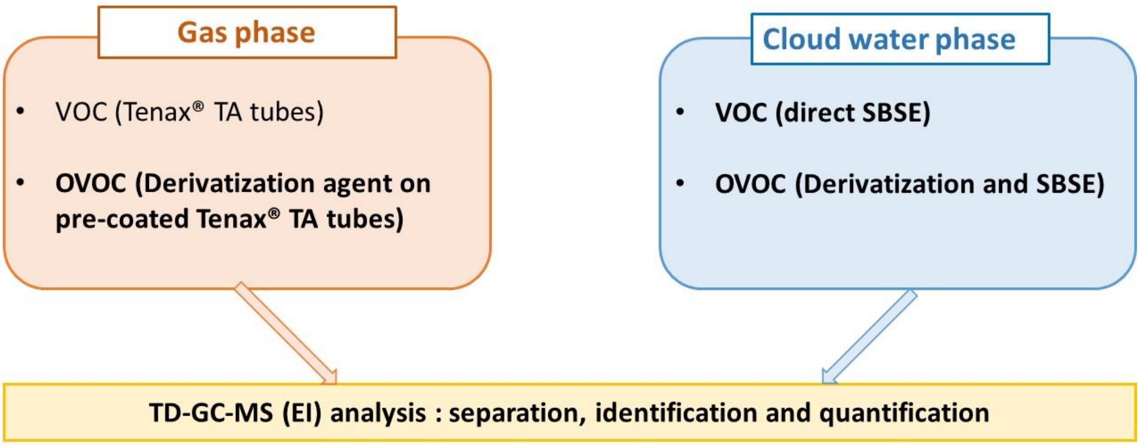

Figure II-4 Steps (in bold characters) of the analytical developments addressed during my PhD thesis. The measurement of VOC on Tenax TA tubes was already handled.

The developments are described in the following section while atmospheric applications will be discussed in CHAPTER III.

II.2 Identification and separation of the derivatized OVOC

II.2.1 Preparation of the derivatized standards

The identification and separation follows the procedure of Rossignol et al. (2012) by derivatizations in solution. O-(2, 3, 4, 5, 6-pentafluorobenzyl)hydroxylamine (PFBHA, purchased from Sigma-Aldrich: PFBHA hydrochloride, derivatization grade for GC, ⩾99.0%) was used to derivatise carbonyl compounds (aldehydes and ketones). N-Methyl-N-(t-butyldimethylsilyl)trifluoroacetamide (MTBSTFA, purchased from Regis® Technologies Inc., MTBSTFA +1% t-BDMCS) was used to derivatise carboxyl and hydroxyl compounds.

A carbonyl compound standard (C=O standard solution) was prepared at 0.01 M in H_2O/acetonitrile (5/95), consisting of glyoxal (GLY, Sigma-Aldrich, 40%), methylglyoxal (MGLY, Sigma-Aldrich, 40%), glycolaldehyde (GA, Sigma-Aldrich, 99%), formaldehyde (Sigma-Aldrich, 38%), hydroxyacetone (HA, Sigma-Aldrich, 90%), acetaldehyde (Sigma-Aldrich, 99%), acetone (Sigma-Aldrich, 99%), methyl vinyl ketone (MVK, Sigma-Aldrich, 99%), methacrolein (MACR, Sigma-Aldrich, 99%), butanal (ACROS Organics, 99%), pentanal (ACROS Organics, 99%), hexanal (ACROS Organics, 99%), heptanal (ACROS Organics, 99%) and octanal (ACROS Organics, 99%).

In a 10 mL size glass bottle, a 4.5 mL of PFBHA solution at 5 10^{-3} M and 0.5 mL diluted C=O standard solution were added for a total mixture solution volume at 5 mL with a molar excess of PFBHA corresponding to ten times the molar concentration of derivatisable functions. The excess of PFBHA to carbonyl derivatizations was favorable for the formation of carbonyl derivatives in high yield near to 100%. The mixture solution in the bottle was left about 24 h for the complete derivatization reaction between carbonyls and PFBHA. 1 µL of the mixture solution was then transferred into a clean Tenax® TA cartridge and analyzed by TD-GC- MS.

A hydroxyl standard solutions (–OH and –COOH) from commercial standards were prepared at 0.01 M in H_2O/acetonitrile (5/95) and composed of methanol (ACROS Organics, 99%), ethanol (Fisher Chemical, 99%), propanol (Fisher Chemical, 99%), butanol (Fisher Chemical, 99%), pentanol (ACROS Organics, 99%), formic acid (ACROS Organics, 99%), acetic acid (ACROS Organics, 99%), propionic acid (ACROS Organics, 99%), pyruvic acid (ACROS Organics, 99%), glycolic acid (ACROS Organics, 99%) and glyoxylic acid (ACROS Organics, 99%). 50 µL of the pure liquid MTBSTFA (corresponding to ten times the molar concentration of derivatisable functions) was added in 5 mL the diluted hydroxyl standard solutions in a 10 mL size glass bottle. The solution is left for one hour for the complete derivatization. One µL of the mixture solution was then transferred into a clean Tenax® TA cartridge and analyzed by TD-GC-MS.

The primary thermal desorption efficiency is evaluated for all available derivatized standards by performing as second thermal desorption. For none of the thermal desorbed derivatized compounds, a signal above detection limits is depicted, suggesting a desorption efficiency of 100% under the prescribed desorption conditions.

II.2.2 Identification and separation of carbonyl compounds

A good separation for carbonyl-PFBHA derivatives was achieved by utilizing the following temperature program: from 40 to 305 °C with a thermal ramp of 5 °C min^{-1}, making it possible to analyze them within a single GC run about 60 min in total. Derivatives were analyzed by electron impact (EI) in the full scan mode in order to obtain the fragmentation pattern of each compound. Similar carbonyls such as butanal and pentanal are well separated. Except for symmetrical carbonyls such as formaldehyde and acetone, PFBHA forms two geometric isomers due to the rigid nitrogen-carbon double bond. More than two isomers are possible for dicarbonyls such as glyoxal and methylglyoxal. Some of the isomers could be distinguished by using the GC temperature conditions described above. α-hydroxy carbonyls and the corresponding α-dicarbonyls such as glycolaldehyde and glyoxal and hydroxyacetone and methylglyoxal have distinctive derivatives and are well separated by the GC column under our conditions (see in Figure II-5).

As seen in previous studies, the El mass spectra of PFBHA oximes has a strong peak, usually a base peak, at m/z 181. This fragment is the pentafluorotropylium ion $C_6F_5CH_2^+$, originating from the derivatization reagent PFBHA. Because of its intensity, the m/z 181 fragment provides an immediate indication of the presence of a carbonyl group in the original molecule and can be utilized to differentiate carbonyl compounds from other classes of organics in complex samples. The high intensity of this ion also makes it well suited for selected ion monitoring quantification. More details about carbonyl compound identification are shown in Table II-2 and Table II-3.

Table II-2 Obtained fragmentation pattern and observed structure for PFBHA.

m/z	Characteristic ions	Observed structure observed
$[M]^+$	Molecular ion of derivatives	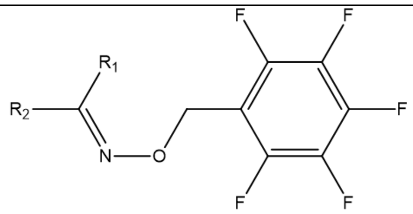
$[C_6F_5CH_2]^+$ 181	Fragmentation of the pentafluorotropylium ion $C_6F_5CH_2^+$	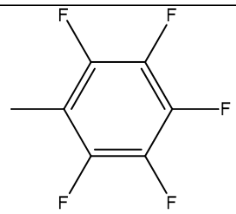

Table II-3 Molecular structure, parent mass weight (MW), derivative MW, GC retention times and characteristic mass of PFBHA derivatives of carbonyl compounds.

Compounds	**Molecular structure**	**Parent MW**	**Derivative MW**	**Retention time (min)**	**Characteristic ions**	
					$[M]^+$	
Formaldehyde	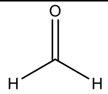	30	225	16.44	225	181 195
Acetaldehyde	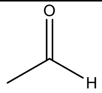	44	239	19.47 19.60	239	181 209
Acetone	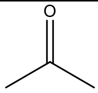	58	253	20.83	253	181 223
Glyoxal (GLY)	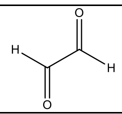	58	448	39.78	448	181
Methylglyoxal (MGLY)	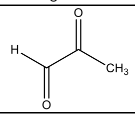	72	462	41.01	462	181
Methyl vinyl ketone (MVK)	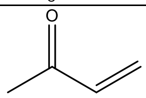	70	265	23.44	265	181 248
Methacrolein (MACR)	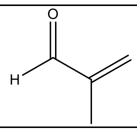	70	265	23.71	265	181
Glycolaldehyde (GA)	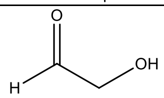	60	255	24.14 24.46	255	181 225
Hydroxyacetone (HA)	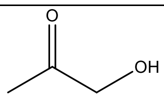	74	269	29.11	269	181 239
Butanal	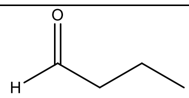	72	267	23.90 24.03	267	181
Pentanal	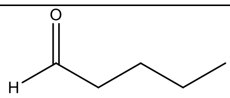	86	281	26.31 26.44	281	181
Hexanal	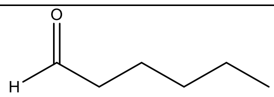	100	295	28.70 28.81	295	181
Heptanal	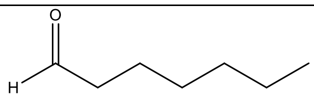	114	309	31.03 31.08	309	181
Octanal	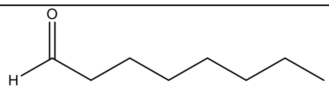	128	323	33.31 33.38	323	181

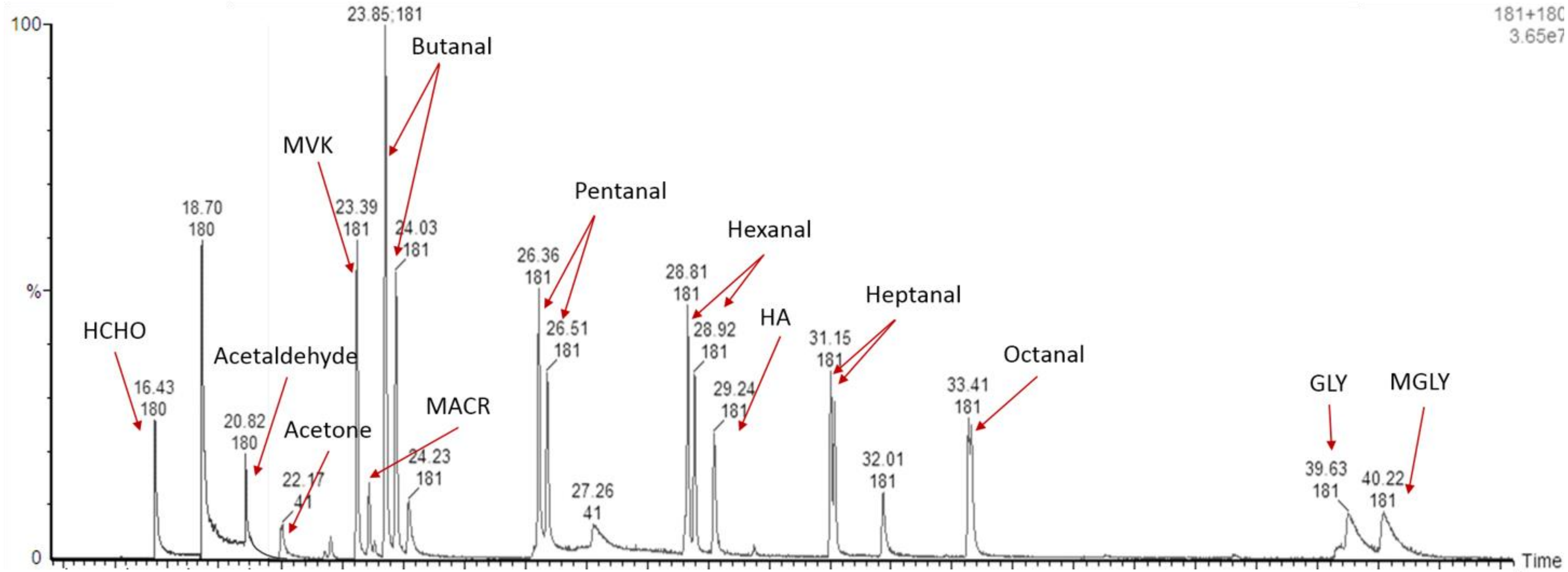

Figure II-5 Chromatogram of carbonyl compound standards prepared and derivatized with PFBHA (extracted by m/z 181 from total SIM ion chromatogram). Peak identification is noted with corresponding compound by red arrow. HCHO: formaldehyde; MACR: methacrolein; MVK: methyl vinyl ketone; HA: hydroxyacetone; GLY: glyoxal; MGLY: methylglyoxal.

II.2.3 Identification and separation of alcohols and carboxylic acids

All the hydroxyl groups are converted into their corresponding t-butyldimethylsilyl (tbdms) ethers during the silylation reaction, as derivatization with MTBSTFA *via* an SN_2 substitution reaction, yielding a single derivative for each compound. The separation of the compounds is achieved with the following temperature program: from 40 to 310 °C with a thermal ramp of 10 °C min^{-1}.Derivatized standards are analyzed in the full scan mode in order to obtain the fragmentation pattern of each compound. The derivatization reaction produces different fragmentation pattern. When the derivatization with MTBSTFA was effected for the mixture –OH and –COOH, we have found that the more derivatisable functional groups are added, the more fragments of derivative can produce. Then we decided to work on derivatization in solution one compound by one compound to make sure of the identification of each compound. Derivatization duration was also tested for 1-3h, because the selected compounds behave differently during derivatization. For acid compounds, pH in derivatization medium was also verified and controlled. Examples of mass spectrograms are given in Figure II-6 and Figure II-7. It is found that MTBSTFA-derivatives produce characteristic fragmentation patterns presenting mainly the fragments $[M]^+$, $[M-57]^+$, $[M-115]^+$ and $[M-131]^+$. The fragment [M−57]+ is generally dominant on the mass spectrogram (see more details about identification of hydroxyl compounds in Table II-4 and Table II-5).

Table II-4 Obtained fragmentation pattern and observed structure for MTBSTFA derivatives.

m/z	Fragmentation	Observed structure
$[M]^+$	Molecular ion	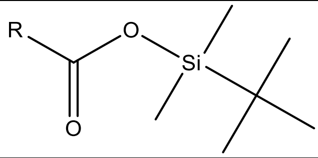
$[M-57]^+$	Cleavage of the t-butyl moiety ($-C(CH_3)_3$)	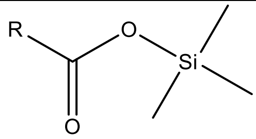
$[M-115]^+$	Cleavage of the t-butyl-dimethyl silyl moiety including the phenolic oxygen ($OSi(CH_2)C(CH_3)_3$)	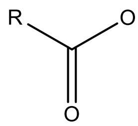

Table II-5 Molecular structure, parent mass weight (MW), derivative MW, GC retention times and characteristic mass of MTBSTFA derivatives of hydroxyl compounds.

Compounds	Molecular structure	Parent MW	Derivative MW	Retention time (min)	Characteristic ions			
					$[M]^+$	$[M-57]^+$	$[M-115]^+$	$[M-131]^+$
Methanol	H_3C-OH	32	146	8.47	146	89	31	15
Ethanol	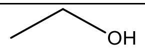	46	160	11.35	160	103	45	29
Propanol	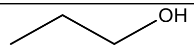	60	174	10.37	174	117	59	43
Butanol	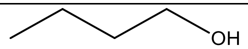	74	188	11.73	188	131	73	57
Pentanol	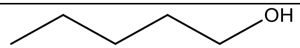	88	202	8.24	202	145	87	71
Formic acid	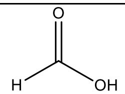	46	160	9.83	160	103	45	29
Glyoxylic acid	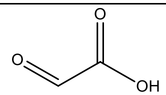	74	188	16.01	188	131	73	57
Glycolic acid	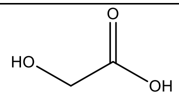	76	190; 304	13.57; 16.06	190; 304	247	189	173
Propionic acid	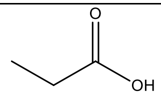	74	188	11.90	188	131	73	57
Acetic acid	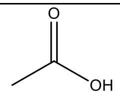	60	174	10.60	174	117	59	43
Pyruvic acid	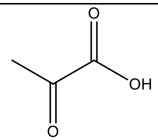	30	144	13.05	144	87	29	13

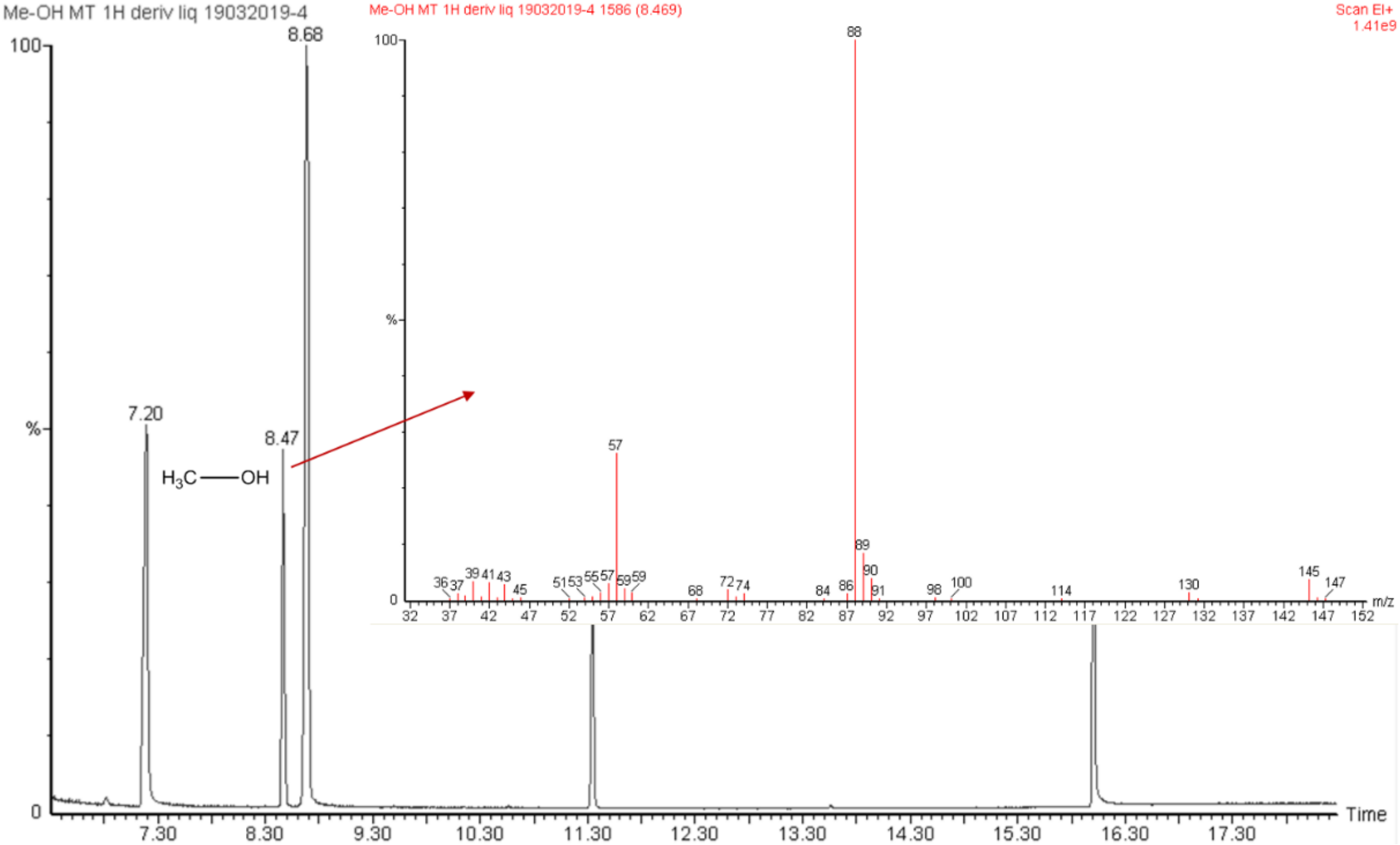

Figure II-6 Chromatogram of methanol derivatized with MTBSTFA from total SIM ion chromatogram. Peak identification is noted with red arrow and its mass spectrum.

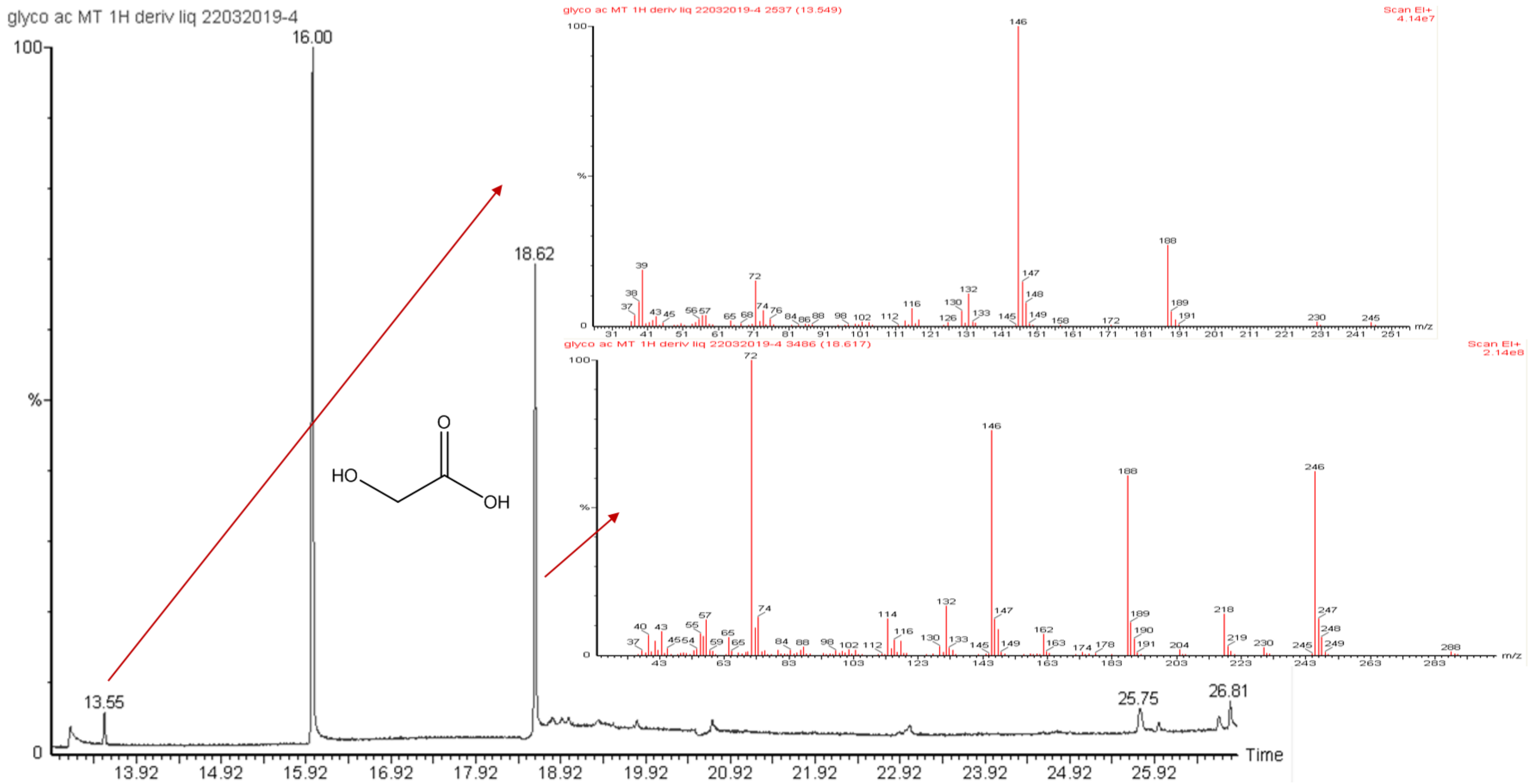

Figure II-7 Chromatogram of glycolic acid derivatized with MTBSTFA from total SIM ion chromatogram. Peak identification is noted with red arrow and its mass spectrum.

II.3 Analysis of carbonyls in the gas phase

II.3.1 Preamble

The optimization of OVOC analysis mostly relies on the protocols developed by Rossignol et al. (2012). The reliability of the protocols needed to be tested for lighter compounds (Cn ≤ C4). The breakthrough volume (BV) is a critical parameter when carrying out sampling on sorbent tubes, especially for the most volatile compounds. It is defined as the volume of air required to completely elute a compound through an adsorbent tube (Baltussen et al., 2002). It defines a limit volume beyond which the trapping of the analytes is no longer fully efficient and where losses may be encountered. For a given compound, it is defined for a given mass of adsorbent and environmental conditions of temperature and relative humidity (CEN, 2005).

The values of breakthrough volumes of Tenax TA sorbent are usually reported by manufacturers in L per grams of sorbent resin at different temperatures. Some of these volumes for carbonyls and alcohols are reported in Figure II-8 for 250 mg of Tenax which corresponds to the mass of sorbent introduced in tubes used for atmospheric sampling (upper panel). In the lower panel of Figure II-8, the exponential dependency of BV to temperature is illustrated for a selection of OVOC. At first glance, the breakthrough volume might be an issue when sampling light OVOC with a carbon number lower than 4 as shown in the upper panel of Figure II-8. This volume lower than 3 L for C1–C3 aldehydes and alcohols is lower than the air sampling volumes required for atmospheric applications. Even when going down to 0 °C, this volume remains very low for methanol and acetaldehyde (< 0.5 L). For C4-compounds like butanal, decreasing the temperature allows to increase BV at acceptable values above the air sampling volumes.

Despite these specifications do not support the use of Tenax sorbent for light OVOC sampling, experimental studies using pre-coated Tenax TA sorbent tubes moderate such statement. In the study by Pang et al. (2011), light carbonyls from C1 to C9 were collected on a sampling tube filled with 100 mg Tenax TA (60–80mesh) sorbent coated with pentafluorophenyl hydrazine (PFPH), followed by analysis with solvent-desorption GC-MS. The authors report that at 2 L of air sampling volume, none of the carbonyls break through the pre-coated Tenax tube even the most volatiles. Rossignol et al. (2012) have shown that the only compound breaking through is methacrolein, a C4-aldehyde, at 80% relative humidity level and for a volume of air below 6 L; other studied compounds have BV higher than 30 L. The BV does not seem to be dependent on the range of relative humidity levels (from 30% to 80%). As a consequence, we decided to test the reliability of this technique for C1–C4 carbonyls.

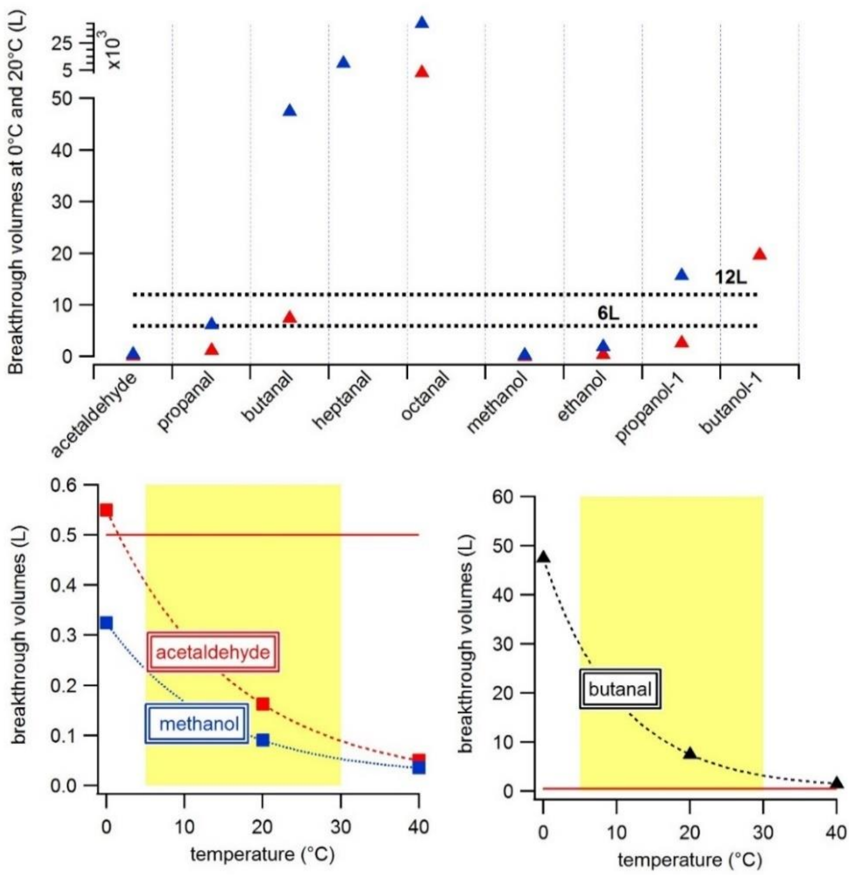

Figure II-8 Calculated breakthrough volumes (BV) and for 250 mg of Tenax tubes for C1–C8 carbonyls and alcohols (red triangles for at 20 °C and blue for 0 °C). The air sampling volumes (dotted lines) of 6 L and 12 L correspond, respectively, to a sampling duration of 40 min and 120 min at a flow rate of 100 mL min^{-1}. Source: https://www.sisweb.com/index/referenc/tenaxta.htm#aldehydes. The BV exponentially decreases with temperature. The red full line corresponds to a sampling volume of 0.5 L i.e., 5 min sampling at a flow rate of 100 mL min^{-1}.

II.3.2 Sorbent coating and derivatization

Following Rossignol et al. (2012), the derivatization of gaseous OVOC is directly performed on the solid Tenax® TA tubes after the atmospheric sampling. Before sampling, the Tenax sorbent need to be pre-coated at the laboratory. The sorbent coating is achieved in 20 min, without using any solvent, by sublimation of PFBHA: a nitrogen stream (100 ml min^{-1} tube^{-1}) is passed through a glass bulb that contained solid PFBHA and connected to 8 Tenax® sorbent tubes within an oven maintained at 110 °C. The home-made coating device is shown on Figure II-9. A PFBHA mass of 300 µg per connected tube is introduced into the glass bulb (Figure II-9). For a 24-L sampling volume at 10 ppb condition (corresponding to a sampling flow rate of 100 mL min^{-1} for 4 h), this PFBHA mass is sufficient to derivatise a carbonyl compound at a concentration of about 1 mg m^{-3} (for an average molecular weight of 100 g mol^{-1}). After the coating process, the pre-coated tube is sealed and left at room temperature. The coating efficiency and quality (no contamination) are tested by TD-GC-MS. Then the tube is ready for atmospheric gas sampling.

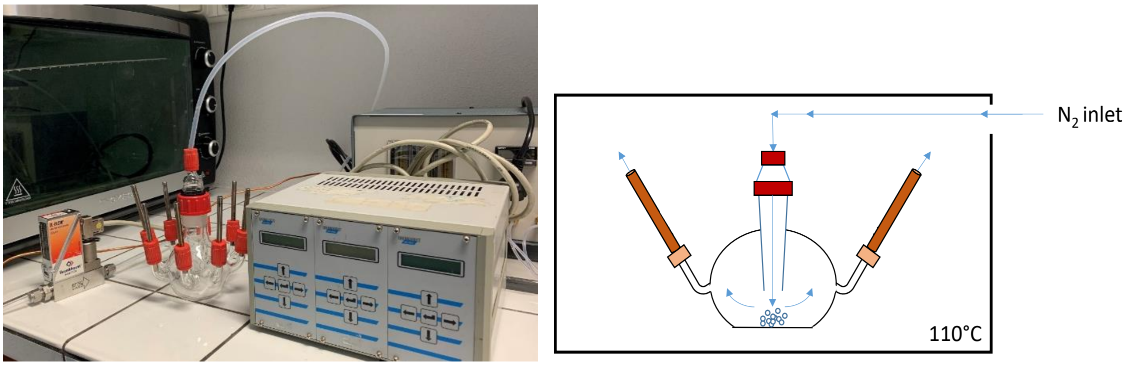

Figure II-9 Laboratory set-upfor the PFBHA coating process on Tenax® tubes. A controlled nitrogen flow at 100 ml min⁻¹ tube⁻¹ passes through the glass bulb that contains solid PFBHA powder connected to 8 Tenax® sorbent tubes.

II.3.3 Humidity influence

PFBHA derivatization is usually performed in aqueous or water containing solutions (Cancilla and Que Hee, 1992) and a molecule of water is formed for each derivative compound. Humidity can modify the derivatization efficiency (Rossignol et al., 2012). The cloudy atmosphere usually presents high RH levels and its influence is tested at the laboratory for PFBHA coated tubes.

We designed the humid air generating system as illustrated in Figure II-10. It is composed of a purified air generator (Fusion 1010, PEAK, France), a water micro-droplet generator filled with MilliQ water, two mass flow controllers, and an automatic Gilan pump to which the tubes are connected. The system is adjusted to generate 50% relative humidity (RH) and 90% RH clean air flow. This is achieved by combining the flows from the purified air generator and the micro-droplet generator at a flow largely exceeding the one of the tube connected to the Gilan pump of 100 mL min^{-1}.

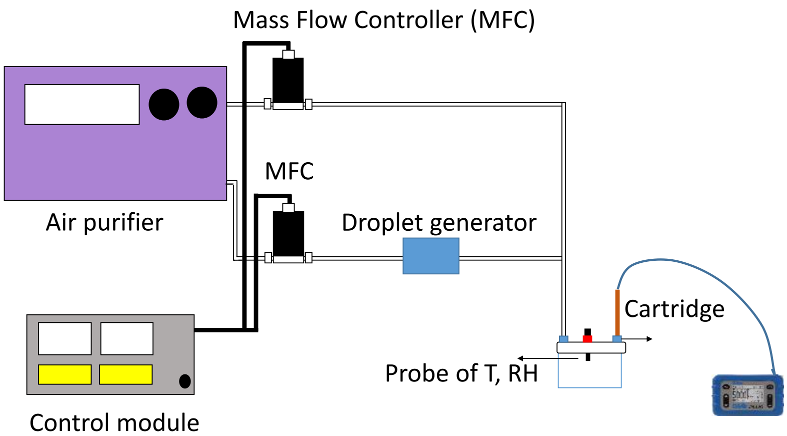

Figure II-10 Design of the humid air generating system.

The experiment is firstly carried out by preparing PFBHA pre-coated cartridges (8 tubes every time using the glass bulb). Then, each 1 µL diluted C=O standard solutions of 0.01 M is deposited onto the PFBHA pre-coated tube. The tube is connected to the relative humid air generating system where the humid clean air flow (100 mL min^{-1}) is flown through the tube for 40 min. A first series of tubes is not flushed with the clean air flow, noted as 0% RH group (2 tubes). The second and third series of tubes are connected to the system and flushed by the clean air flow at 50% RH (3 tubes) and at 90% RH (3 tubes), respectively. The tubes are stored at room temperature for five-day-derivatization before TD-GC-MS analysis. Several triplicates were conducted for the 0%, 50% and 90% RH experiments. The results are shown in Figure II-11 for a selection of OVOC compounds.

Except for formaldehyde, responses of the compounds do not seem to be influenced by RH levels within the determined repeatability range. In the case of formaldehyde, the peak area at 90% is two to three times higher at 50% and 90% HR than at 0%.

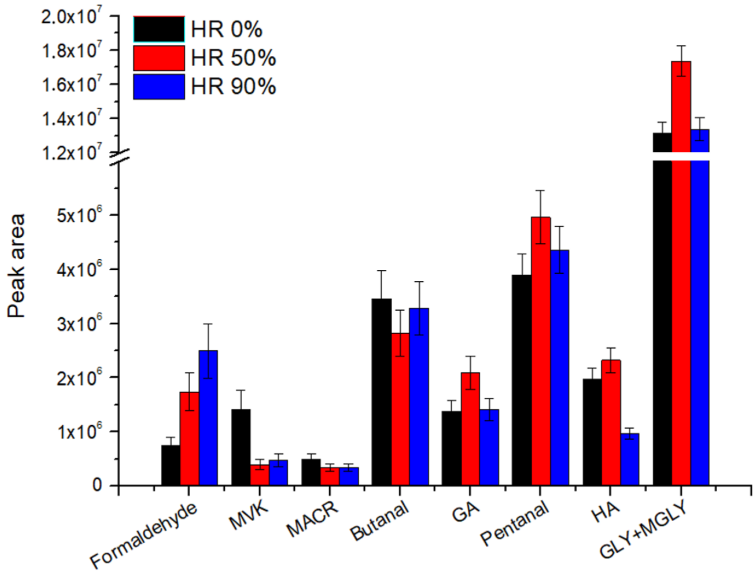

Figure II-11 Humidity influence (0% RH, 50% RH and 90% RH) of derivatized carbonyl compounds on-Tenax tube. "Peak area" refers to the 181 m/z with chromatogram obtained in the electron ionization mode, in area units. Error bars represent ± one standard deviation determined from 5 triplicates.

While the present study of the influence of relative humidity is not performed on gaseous OVOC, it is consistent with Rossignol et al. (2012)'s results. Gaseous carbonyl compounds were generated at the INERIS simulation chamber at various controlled humidity (30, 50 and 80% RH). The results revealed the absence of significant bias linked to humidity variation for the studied compounds and despite an increase in the repeatability at 80% RH, probably due to competition between water and adsorbed organic molecules on adsorbent surface sites.

II.3.4 Derivatization efficiency: liquid derivatization *versus* on sorbent tube derivatization

Following Rossignol (2012), the derivatization efficiency between liquid and on-sorbent-tube derivatization are compared. Standard solutions used for the comparison are prepared in a 5/95 water/acetonitrile mixture at a concentration of 0.01 M with the same selected carbonyl compounds (see in Section II.2.1). One µL of the diluted carbonyl solution 1 mM is injected into a pre-coated PFBHA tube for five days on-sorbent-tube derivatization. For in-solution derivatization, the same protocols as the ones described in Section II-2-1 are applied. The repeatability of the in-solution or on-sorbent-tube derivatization is also evaluated by estimating the relative standard deviation of the analytical response of each derivative from standard solutions (several replicates). These relative standard deviations are found to be satisfactory for all of the compounds, ranging from 5 to 25%.

The derivatization efficiency is shown in Figure II-12. On-sorbent-tube derivatization shows that the responses of oximes are higher than the ones from in-solution derivatization with ratio ranging from +134% (glyoxal) to +500% (hydroxyacetone) (red histograms). This is consistent with Rossignol's work, for most aldehyde compounds. However, for ketones higher than C4, they found that on-sorbent-tube derivatization leads to a derivatization efficiency lower than for in-solution derivatization, which is different from what we observe for acetone in Figure II-12. Probably, there is a different behavior during derivatization of lower molecular weight carbonyl compounds and higher molecular weight ones. Differences in derivatization efficiencies point out that the two procedures (in-solution and on-sorbent-tube derivatizations) provide different responses of the same oximes. Consequently, for OVOC quantification of atmospheric OVOC for atmospheric sampling, only the on-sorbent-tube calibration curve has to be used.

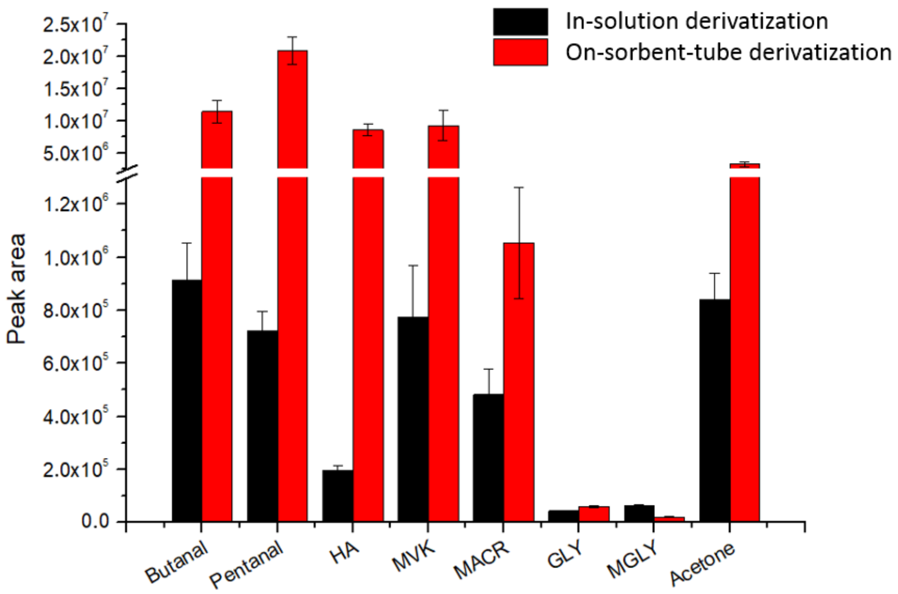

Figure II-12 Comparison of responses for in-solution and on-sorbent-tube PFBHA derivatization of carbonyls: "Peak area" refers to chromatogram with 181 m/z, in area units. Error bars represent ± standard deviation determined from repeatability tests. Both in-solution and on-sorbent-tube derivatization were performed more than four times.

II.3.5 Linearity of the method

For calibration curve of carbonyl compounds on-sorbent-tube derivatization, a diluted C=O standard solutions 2 µM - 10 mM is prepared with the carbonyl compound standards (C=O standard solution) prepared at 0.01 M in H_2O/acetonitrile (5/95). One µL of the diluted carbonyl standard solution is injected into every clean Tenax® TA tubes pre-coated with PFBHA. These tubes are stored at room temperature for five-day-derivatization before TD-GC-MS analysis. The calibration curves of MACR and butanal are shown in Figure II-13 and others are shown in Figures A.7 in Appendices. The linearity of the method is good with $R^2 > 90\%$.

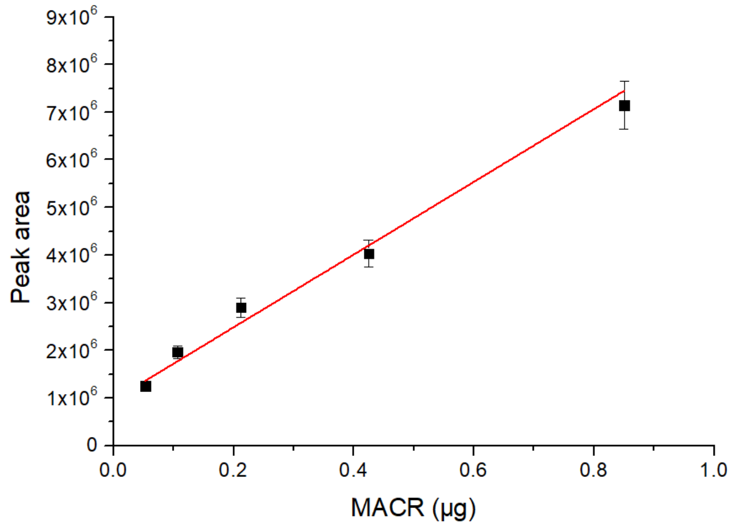

$$y = 7633530x + 959661$$
$$R^2 = 0.99$$

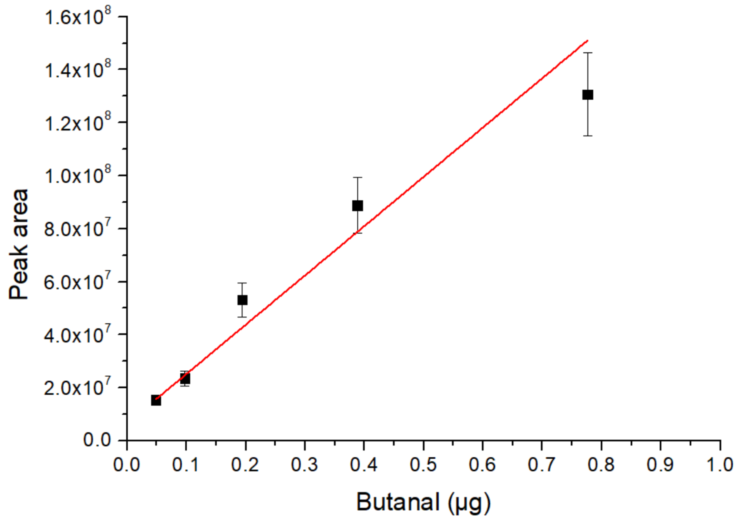

$$y = 186013000x + 6594000$$
$$R^2 = 0.98$$

Figure II-13 Calibration curves of methacrolein (MACR) and butanal after derivatization on Tenax® tube pre-coated with PFBHA. "Peak area" refers to chromatogram with 181 m/z, in area units.

II.3.6 Time of storage

Ho and Yu (2004) and Rossignol (2012), showed that a minimum of five days before TD-GC-MS analysis is required for full derivatization of the sampled OVOC. The storage duration of the sampled tubes has been tested for one month maximum (see in Figure II-14). Our test show that the response of the derivatized compounds is even better after 10 days of storage. However, a 5-day period is preferred in order to take into account analytical optimization delays and field constraints.

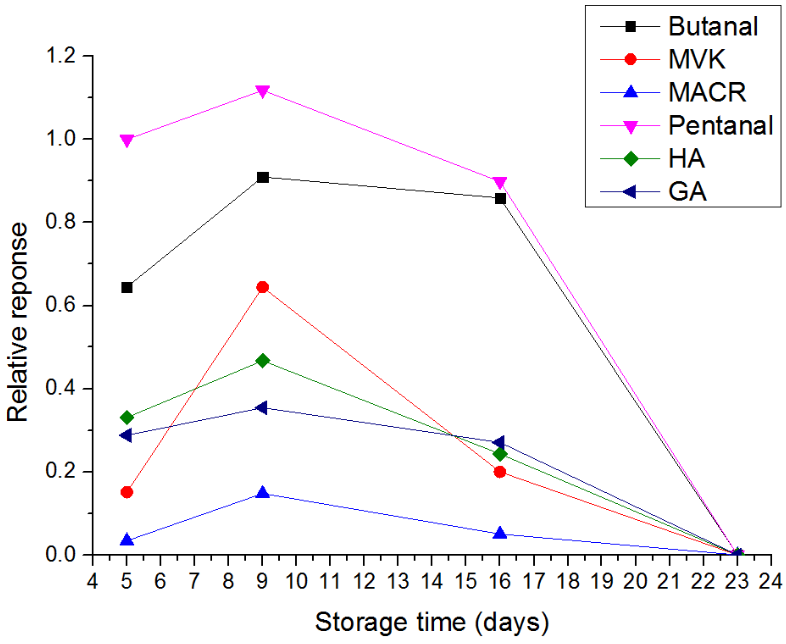

Figure II-14 Influence of storage time from five days to twenty three days. Relative response refers to a ratio between peak area of a derivative compound and the one of pentanal (in order to show these compounds in the same figure clearly).

II.3.7 The breakthrough volume (BV)

II.3.7.1 Preliminary tests for ambient air

The breakthrough volume tests are performed in real atmospheric conditions with two Tenax tubes PFBHA pre-coated in series (the front and the back sampling tubes) and operated at a flow rate of 100 ml min^{-1} by a Gilan pump. The gaseous sampling is performed for 5 min, 40 min, 1 h and 2 h corresponding respectively to the sampling volumes of 0.5 L, 4 L, 6 L, and 12 L, at UCA Cézeaux campus and at the station ATMO Auvergne in the urban centre of Clermont-Ferrand.

For a given compound, the breakthrough volume is reached when the response of the compound in the back sampling tube (or second coated tube) is higher than 5% of the one in the front tube. Two representative cases have been selected in Figure II-15 for formaldehyde (HCHO) and C4-C5 carbonyls.

For the light carbonyl compound HCHO, the BV seems to be always overpassed even at a small volume of 0.5 L. For C4-C5 carbonyls, C4-compounds breakthrough at 6L while pentanal (C5) does not. Six liters (60-min sampling duration at 100 mL min^{-1}) seem to be the minimum sampling volume in order to ensure that enough compound of interest can be trapped into the sorbent tube and detected by TD-GC-MS. While this first evaluation needs additional tests under controlled conditions, we have to keep in mind that carbonyls with a number of carbon lower than C5 may breakthrough. The use of several back tubes (at least three back tubes) could be employed for the quantification of C1−C4 carbonyl compounds.

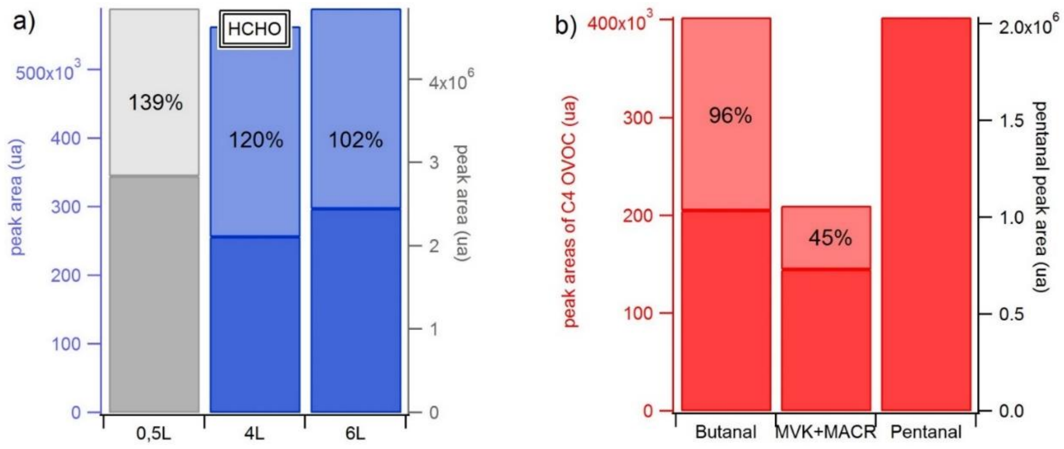

Figure II-15 First evaluation of the breakthrough volume of some aldehydes. Dark color: signal in the front tube. Light color: signal in the back tubes (when observed, value in % of the signal on the sampling tube). a) Testing formaldehyde BV for different air volume sampling; b) testing BV of some C4−C5 carbonyl for a 6 L-air volume sampling. Note that for the a) case, each BV test is carried out under different sampling concentrations.

II.3.7.2 2,4-dinitrophenylhydrazine (DNPH) sorbent tubes: an alternative for the future?

As described in Section II.1.3, the use of sorbent tubes coated with 2,4-DNPH coupled to HPLC analysis is a commonly used technique for the measurement of light carbonyls. In collaboration with the SAGE department at IMT Lille Douai, the effect of relative humidity at 50% and 90% on the response of carbonyls by this technique has been tested. The experience relies on a dynamic system that generates stable and adjustable diluted gaseous flows of carbonyl compounds at different humidity levels (see in Figure II-16). The system is composed of a certified gas standard of carbonyl compounds (Apel Riemer, USA, see more details of their concentrations in Table A.12 in Appendices), different channels to fix the sorbent tubes (DNPH tubes), a water impinger, mass flow controllers with general module controller to adjust the OVOC, the dry and humid dilution air flows and a pump connected to the sorbent tubes (see in Figure II-16).

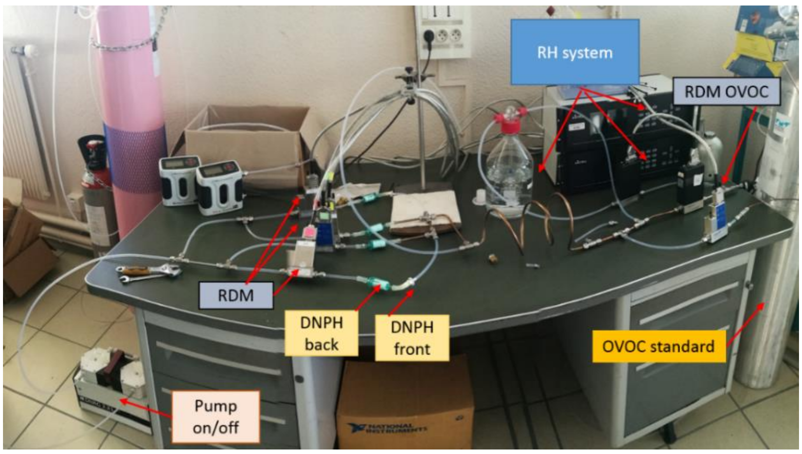

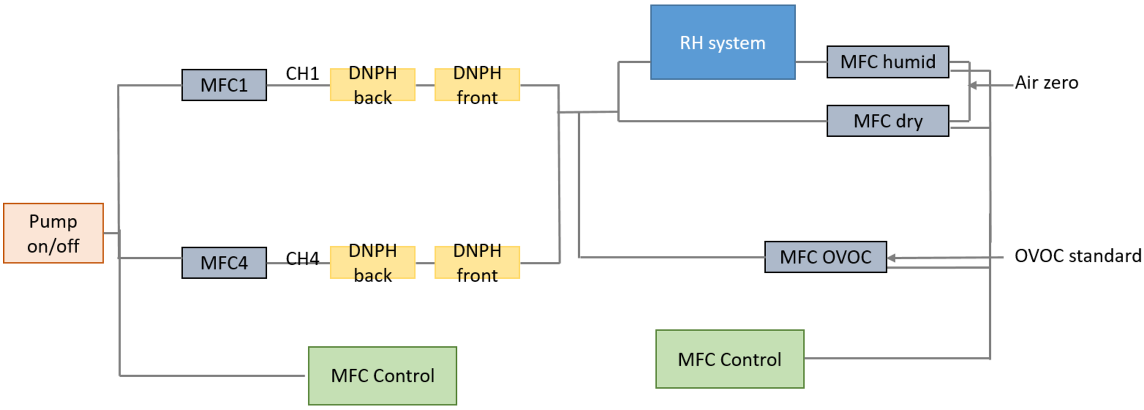

Figure II-16 Laboratory system of adjustable gaseous flow of carbonyl compounds controlled by a supplementary RH system at SAGE IMT Lille Douai and a picture of the combined system.

Two DNPH cartridges (Supelco, FR) are connected at channel 1 and 4 (one front and one back sampling tubes) at a sampling flow rate of 1 L min^{-1} for 2 h. The system is adjusted with flow of gaseous carbonyls at 1, 5 and 20 mL min^{-1}. After 2-h-gas sampling in the system, DNPH cartridges are desorbed with 3 mL of acetonitrile. The cartridge dead volume is taken into account by weighting the eluted acetonitrile. Liquid calibration standards are prepared by diluting carbonyl-DNPH hydrazones (Ampoule SUPELCO 040618-100%) in an acetonitrile solution. Concentrations of individual carbonyls in the calibration standards range from 0.25 to 2.0 g mL^{-1}. The DNPH-carbonyl derivatives are separated and analyzed by high-performance liquid chromatography (HPLC). Twenty µL is injected into a high performance liquid chromatographic system (Waters 2695) coupled to an ultraviolet detector (Waters 2487). Chromatographic separation is achieved on a Pinnacle Ultra C18 250 mm × 4.6 mm × 5µm (Restek, France). The oven temperature is set at 40 °C and the mobile phase is a gradient mixture of acetonitrile, tetrahydrofuran and water with a constant flow of 1.5 mL min^{-1} over 27 min. Acquisition is performed at 365 nm wavelength.

The linearity of DNPH tube responses are reported at the two tested relative humidity levels in Figure II-17. On the one hand the linearity of the response is verified at both RH levels. On the other hand, the response of carbonyls is equivalent at both HR levels The calibration of gaseous carbonyl compounds by DNPH-HPLC is almost independent of the relative humidity (see in Figure II-17). The deployment of DNPH tubes are an alternative in particular for light carbonyls (such as MACR and MVK), especially in cloudy conditions.

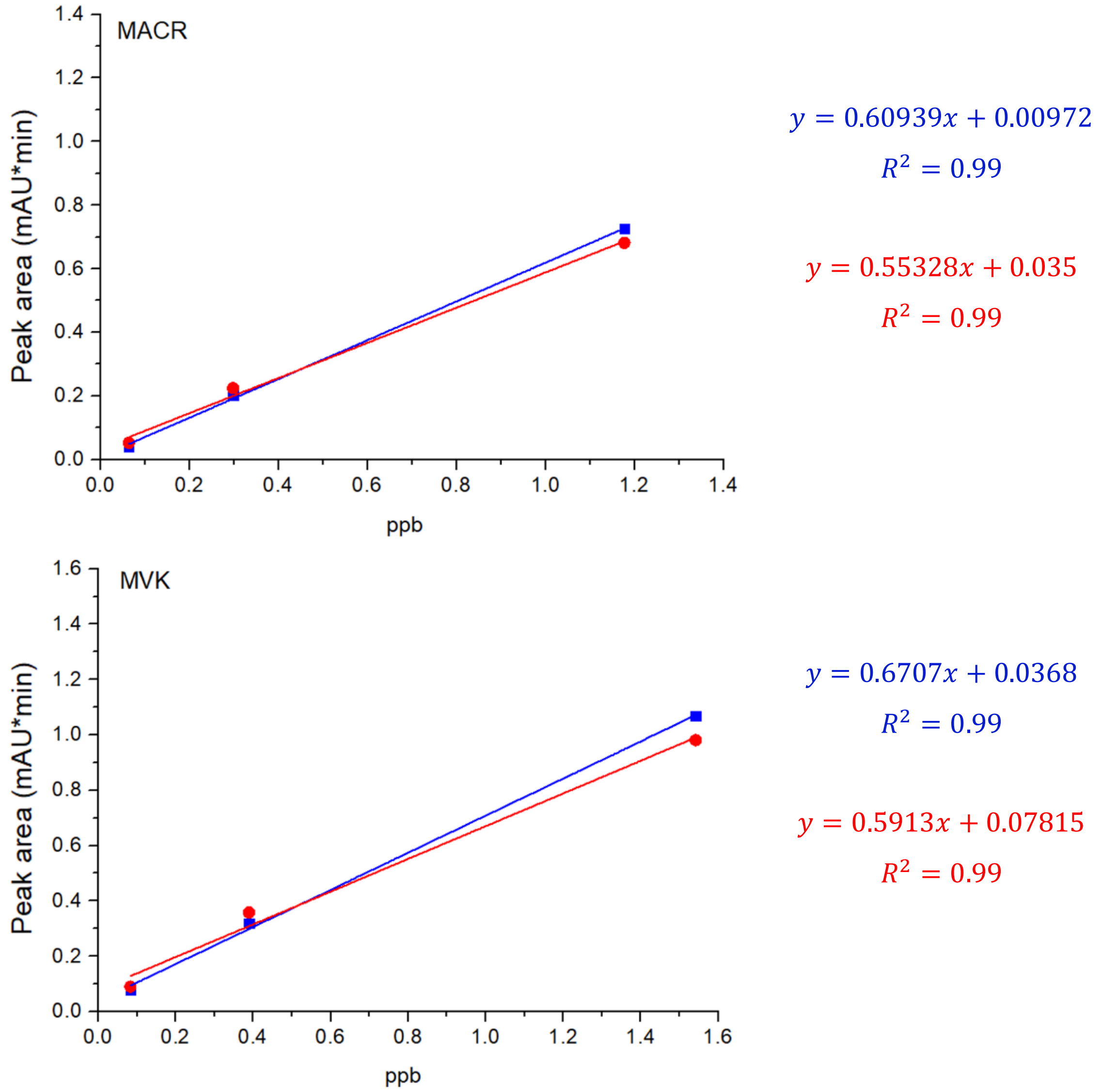

Figure II-17 The calibration curves at 50 and 90% RH for MVK and MACR using DNPH tubes analysed by HPLC.

II.3.8 Preliminary analysis of alcohol and carboxylic acid functions using derivatization

For alcohols and acids, we defined the analytical conditions for their separation and identification as described in Section II.2.1. A preliminary evaluation of the linearity by an external calibration for methanol and propionic acid is shown in Figure II-18. The others are presented in Figure A.6 in Appendices. The method shows a very good linearity with an R^2 usually higher than 0.98. The use of an internal standard (tridecane) remains highly relevant for pretreatment steps and will have to be considered as well for future optimization tests. Future laboratory tests will also include the (i) definition of the procedure of Tenax TA tube pre-coating with MTBSTFA, (ii) the study of the influence of relative humidity and ozone (iii) the evaluation of the breakthrough volume (iv) the evaluation of the performances (sensitivity, linearity, repeatability).

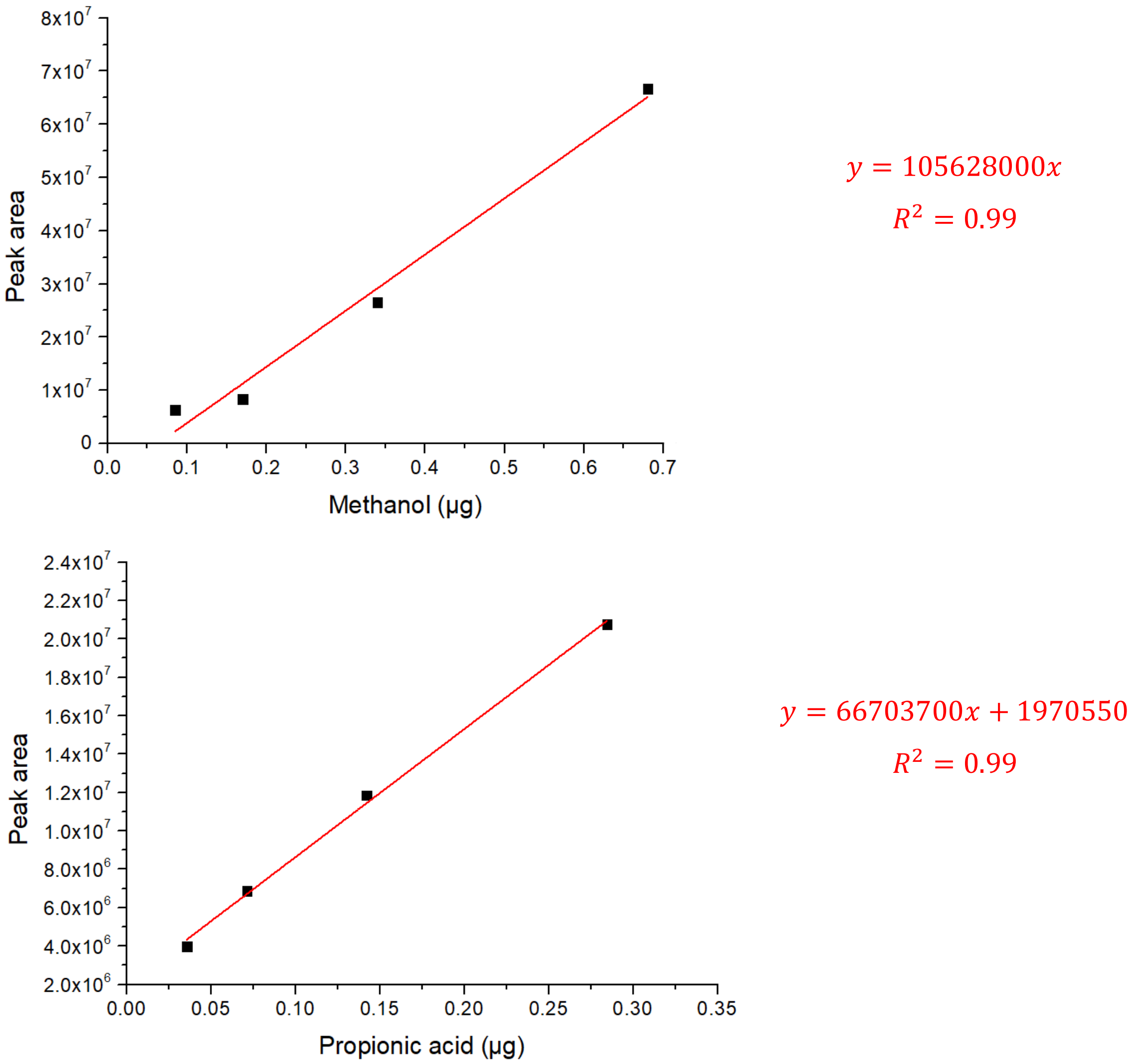

Figure II-18 External calibration curves for methanol and pyruvic acid on MTBSFA pre-coated tubes. "Peak area" refers to chromatogram with their characteristic ions m/z, in area units.

II.3.9 Conclusion for measurement of gaseous carbonyls and perspectives

While laboratory tests have shown the potentiality of the on-sorbent pre-coated PFBHA tube method, especially for carbonyls, the breakthrough volume appeared to be a critical issue in contrast with other published studies in the literature. Additional tests at the laboratory in controlled conditions and, in particular, by generating known concentrations levels of OVOC are still needed. Indeed, working in ambient conditions during which the OVOC are sometimes not detected has been a limitation to the number of experimental tests. Future tests will also focus on simultaneous gaseous sampling with PFBHA tubes in parallel. In addition, ozone (O_3) is known to disturb VOC/OVOC sampling on sorbent tubes. Reactions with O_3 may alter the quantities of the VOC/OVOC and may also contribute to the formation of artifact products (positive artifact) which may mistakenly be interpreted as atmospheric constituents (Helmig, 1997; Mermet et al., 2019). In the VOC sampling onto solid adsorbents and onto derivatization cartridges, artifacts may not only be formed by reactions of reactive air constituents with the previously adsorbed compounds but also from reactions with the solid adsorbent bed (such as the polymer Tenax) or the derivatization agent (DNPH, PFBHA, *etc.*). Some studies showed that in the sampling of aldehydes on DNPH cartridges, either the formed products or the derivatization agent itself may be depleted during the sampling. The investigation of interferences from reactions during sampling is an important issue of method development. Therefore, for the future tests, ozone removal techniques during VOC sampling should be considered. Different tests can be arranged with different each scrubber to quantify (1) the ozone removal efficiency, (2) losses of OVOC in the absence of ozone, and (3) potential ozone-induced losses of OVOC in the scrubber.

II.4 Extraction and analysis of VOC and OVOC in the cloud droplet phase

II.4.1 SBSE: a well-adapted extraction technique for VOC and OVOC in the cloud water and compatible with TD-GC-MS

VOC concentration levels found in natural water samples are typically in the order of ppt (ng L^{-1}) to ppb (µgL^{-1}) (Dewulf and Van Langenhove, 1999). Unless large volume injection is applied, the injection volume into a capillary GC column is normally limited to microliter(s) (Huybrechts et al., 2003). Taking into account the sensitivity of most detectors, high preconcentration factors are usually necessary during sample preparation for trace analysis of VOC in water. Solvent extraction has been used for long time, but current challenges within the scope of “green” analytical chemistry favor the development of “solvent-minimized” and “solvent-free” sample preparation methods, such as solid-phase micro-extraction (SPME), stir-bar sorptive extraction (SBSE), single-drop micro-extraction (SDME), liquid-phase microextraction (LPME), membrane-assisted solvent extraction (MASE), micro-porous membrane liquid-liquid extraction (MMLLE), membrane extraction with sorbent interface (MESI) or supported liquid membrane extraction (SLME) have substituted the more solvent consumer techniques such as liquid-liquid extraction (LLE) or solid-phase extraction (SPE) (Tobiszewski et al., 2009). These new techniques miniaturize sample preparation and, thus, reduce organic solvent consumption. Besides, a higher sensitivity, a reduced potential of analyte loss and a reduction of the sample amount are needed for many applications’ analysis, especially for environmental analysis.

SBSE was first introduced by Baltussen et al. (1999) as a new and improved sample preparation technique. SBSE has been successfully used for environmental analysis, biological fluids, food analysis biomedical and pharmaceutical applications (Lancas et al., 2009; Zhang et al., 2005; Soini et al., 2005; Novotny et al., 2007). In particular, VOC have been already detected and analyzed by SBSE for different environmental media like river water, seawater, soil, food and flavor (Alves et al., 2005; Coelho et al., 2009; Tredoux et al., 2008), but not yet in cloud waters. Like SPME, SBSE is a solventless sample preparation techniques based upon sorptive extraction. The working principles rely on analyte absorption (partitioning) on an absorption phase such as polydimethylsiloxane (PDMS) from the sample. PDMS is the most widely used sorptive extraction phase. Indeed, inorganic adsorbents interact too strongly with trapped compounds and require very high desorption temperature, which leads to degradation reactions. Additionally, PDMS is a well-known stationary phase in gas chromatography (GC), is thermally stable over a wide range of temperatures (220–320 °C) and has interesting diffusion properties (David and Sandra, 2003, 2007; Kawaguchi et al., 2007; Baltussen et al., 1999). An example of an SBSE kit is illustrated in Figure II-19.

Figure II-19 A Twister Kit of SBSE.

While SPME techniques have some limitations such as the fragile nature of the fiber and the limited extraction capacity due to the small PDMS volume (0.5 µL) coated on fiber (Ouyang et al., 2011), the SBSE technique has typically a higher absorption capacity and higher analytical recovery due to higher PDMS volumes compared with SPME (Seethapathy et al., 2012). At present only PDMS-coated stir-bars are commercially available and this represents one of the main SBSE drawbacks, since, due to the non-polarity of the PDMS polymer, polar compounds are poorly extracted. Therefore, for OVOC, derivatization should be considered such as *in situ* and in-tube derivatization and multi-shot mode (Kawaguchi et al., 2007) (see more details in following Section II.4.2).

II.4.2 SBSE steps

II.4.2.1 Extraction step

During the extraction step, the PDMS-coated stir-bar is put in contact with the solutes by immersion or by headspace sampling (Figure II-20). This extraction step can be carried out under steady state conditions or in the absence of them.

In the immersion mode (Figure II-20 a), which is usually abbreviated simply as SBSE, the PDMS-coated stir-bar is added into a headspace vial or a container that contains the liquid sample and the sample is stirred under controlled physical and chemical conditions. After extraction, the stir-bar is removed, rinsed with distilled water in order to remove other components, dipped on a clean paper tissue to remove water, and submitted to desorption. The rinsing step is extremely important when analytes are thermally desorbed in order to avoid the formation of non-volatile material that can clog the desorption unit. Besides, rinsing does not cause solute loss since, as PDMS is applied, the solutes are sorbed in the polymer phase (Kawaguchi et al., 2006).

The use of SBSE was extended to sample VOC in the vapor phase (headspace mode Figure II-20 b) by Bicchi et al. (2000) and is known as headspace solvent extraction (HSSE). In HSSE, sampling is performed by suspending the coated stir-bar in the headspace vial and the polymer is in static contact with the vapor phase of a solid or liquid matrix. The sample is usually stirred in order to favor the presence of the solutes in the vapor phase. After headspace sampling it is also recommended to rinse the coated stir-bar with distilled water and to dip it on a clean paper tissue. Despite the selectivity of this approach, not many works using HSSE are found in the literature (Bicchi et al., 2000, 2002). Working with the HSSE mode preserves the polymer from the absorption of non-volatile species and increases the lifetime of the stir-bar. Even though HSSE seems suitable for very volatile compounds, SBSE with immersion mode is more suitable for cloud application due to the very low concentration for VOC/OVOC detected in cloud.

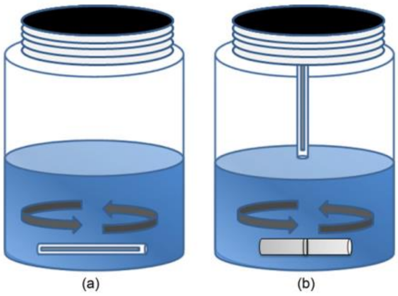

Figure II-20 Extraction step with modes in SBSE: immersion (a) and headspace (b) (from Prieto et al., 2009).

II.4.2.2 Desorption step

After the extraction, the solutes can be introduced quantitatively into the analytical system by thermal desorption (TD) (Baltussen et al., 1999) or liquid desorption (LD) (Niehus et al., 2002). In the former, a PDMS-coated stir bar is placed inside an empty tube of TD. In some cases, rinsing the stir bar lightly with distilled water is recommended in order to remove adsorbed materials or other sample components. This step prevents the formation of non-volatile materials during the TD step. Rinsing does not cause solute loss because the adsorbed solute is present in the PDMS phase. Finally, the solute is thermally desorbed. The desorption temperature is application-dependent and primarily determined by the volatility of the solute; it is typically between 150 and 300 °C. Desorption is accomplished within 5–15 min under 10–50 ml min^{-1} helium flow. As an alternative to TD, the analyst can use LD. Sampling can also be performed in the headspace of a liquid or a solid sample, the so-called head space sorptive extraction (HSSE) method and LD is used (Popp et al., 2001, 2004; De Villiers et al., 2004). For LaMP, desorption step by TD is obviously more adapted, because of the system TD-GC-MS is already present in the lab.

II.4.2.3 SBSE with derivatization

Derivatization of polar and thermally labile compounds is one of the most used alternatives to implement SBSE for compounds like OVOC. Different derivatization strategies can be employed *in situ* and on-stir-bar (Prieto et al., 2010). *in situ* derivatization is the simplest approach (see in Figure II-21 a). Derivatization occurs in the aqueous sample before, or simultaneously, with the extraction step. Thus, the desired derivatives are formed first and then extracted into the PDMS phase. It improves both the affinity of the analyte for the PDMS phase and the subsequent GC separation. However, the major limitation of the approach using direct derivatization in the sample is that it is not applicable to moisture-sensitive reactions. On-stir-bar derivatization (see in Figure II-21 b) can be performed either by preloading the stir-bar with the derivatization agent, so the reaction takes place as soon as analytes are incorporated in the PDMS phase (simultaneous extraction and derivatization) or by first concentrating the analytes in the PDMS phase and then exposing the stir-bar to the vapor of the derivatization agent (extraction followed by derivatization).

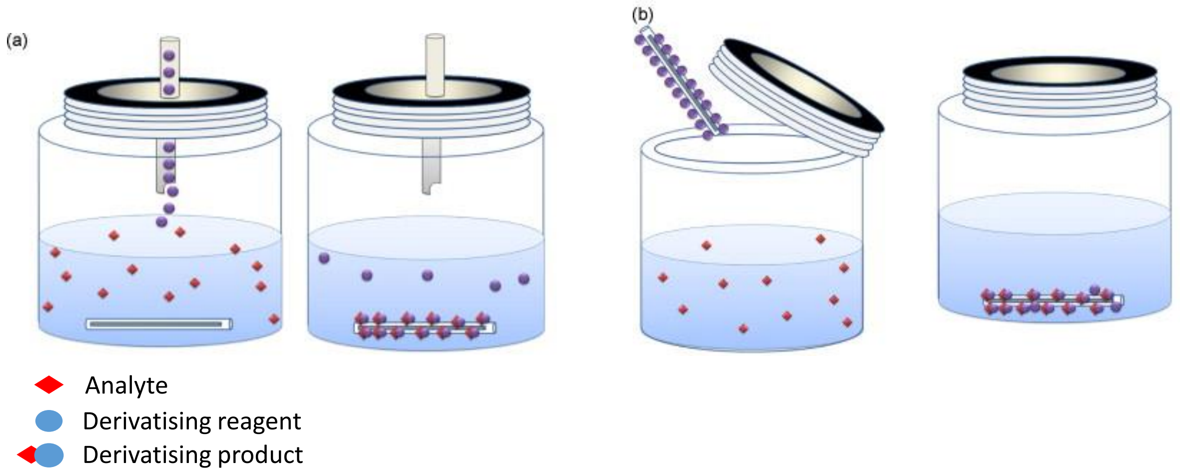

Figure II-21 Different derivatization modes in SBSE: in situ (a), on-stir-bar with the derivatization reagent preloaded before exposure to the sample (b) and in-tube derivatization (from Prieto et al.,2009).

As we know, silylation can be used to derivatise a wide range of functional groups, such as aromatic and aliphatic alcohols, carboxylic acids, amines and amides. N-(tert-butyldimethylsilyl)-N-methyltrifluoroacetamide (MTBSTFA) has been applied for in-extract derivatization of phenolic compounds and acidic pharmaceuticals and herbicides (Quintana et al., 2007). Furthermore, aldehydes and ketones can be converted into oximes by reaction with (2,3,4,5,6-pentafluorobenzyl)hydroxylamine (PFBHA), either directly in the sample (*in situ*) or on the stir-bar previously loaded with PFBHA (on-stir-bar), using the HSSE mode. A comparison between these two modes revealed that the extraction efficiency of aldehydes from beer was slightly higher by *in situ* derivatization (Ochiai et al., 2005; Stopforth et al., 2007). That is the reason why we have decided to apply the simplest approach, *in situ* derivatization, by applying firstly the derivatization in liquid sample and then extraction for derivative products by SBSE.

II.4.3 Optimization of SBSE conditions for VOC extraction

II.4.3.1 SBSE theory

Sorptive extraction is, by nature, an equilibrium technique, and for water samples, the extraction of solute from the aqueous phase into the extraction phase is controlled by the partitioning coefficient of the solute between the silicone phase and the aqueous phase. Recent studies show that the partitioning coefficients between PDMS stationary phases and solvent water ($K_{PDMS/W}$) can be approximated to the octanol-water partitioning coefficient ($K_{o/w}$) of analyte that is described by the following equation:

$$K_{O/W} \approx K_{PDMS/W} = \frac{C_{PDMS}}{C_W} = \frac{m_{PDMS}}{m_W} \times \frac{V_W}{V_{PDMS}} \qquad \text{(Eq.1)}$$

where C_W is the concentration of analyte in the aqueous sample (g L^{-1}); C_{PDMS} is the concentration of analyte in the extractant (g L^{-1}); m_W is the mass of analyte remaining in the aqueous sample (g); m_{PDMS} is the mass of analyte in the extractant phase (g); V_{PDMS} is the volume of the extractant (L); and V_W is the sample volume (L). β is the phase ratio of the extraction system and is defined as:

$$\beta = \frac{sample\ volume}{PDMS\ volume} = \frac{V_W}{V_{PDMS}} \qquad \text{(Eq.2)}$$

The total mass of analyte is defined as $m_{tot} = m_{PDMS} + m_W$; then Eq.1 can be rewritten as :

$$\frac{K_{PDMS/W}}{\beta} = \frac{m_{PDMS}}{m_W} = \frac{m_{PDMS}}{m_{tot} - m_{PDMS}} \qquad \text{(Eq.3)}$$

Finally, extraction efficiency E is defined by Eq.4:

$$E = \frac{m_{PDMS}}{m_{tot}} = \frac{K_{o/w}}{K_{o/w} + \beta} \qquad \text{(Eq.4)}$$

The extraction efficiency E is usually a percentage and corresponds to the recovery of analyte in the sample. Only two terms affect the recovery of an analyte: β and $K_{o/w}$. Very large partitioning constants lead to 100% recovery. Very large phase ratios (small volume of extractant relative to the sample volume) lead to low recovery.

For the SBSE technique, extraction time, stirring rate, pH solution value, ionic strength, and desorption time, sample volume, extraction phase volume and desorption can affect the equilibrium and extraction efficiency. The theoretical extraction efficiency can be calculated for different aqueous sample volumes and stationary PDMS phase volumes to choose the optimal conditions (Figure II-22). Each compound has a constant $\log K_{o/w}$. As shown in Figure II-22, the greater the volume of PDMS being applied and the smaller volume of the sample being tested, the higher the extraction percentage is. To accomplish optimal extraction efficiency, the factors above have been tested and optimized using standard samples.

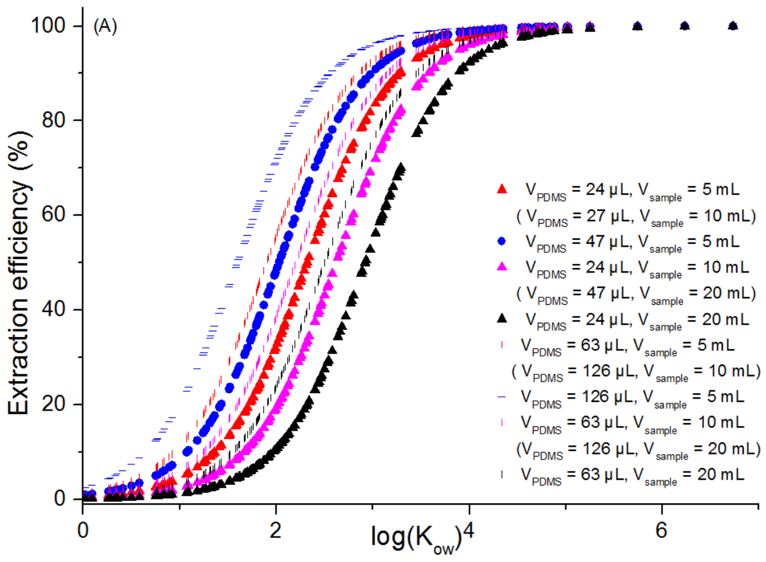

Figure II-22 Example of theoretical extraction efficiency for 5, 10 and 20 mL sample volumes and 24, 47, 63, 126 µL PDMS volumes.

II.4.3.2 SBSE optimization

Tens of anthropogenic and biogenic compounds of our target compounds from pure commercial standards (Megamix standards and Terpenes standards, 200 µg mL^{-1} for each compound in methanol, RESTEK, France) have been studied. The complete data set is provided in Table A.1 in Appendices.

The design of the entire test protocol is based on several previous studies (Ochiai et al., 2001; Kawaguchi et al., 2005; David and Sandra, 2007). One polymer-coated stir bar was introduced into the diluted standard in Milli-Q water by immersion (see in Figure II-20).

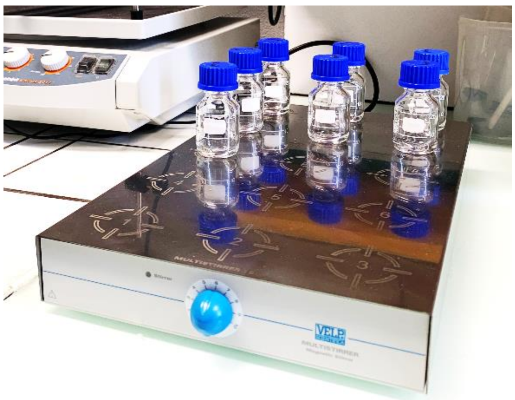

Figure II-23 Test of SBSE optimization.

The sample is stirred on a magnetic stirring plate for at least 2 h (Figure II-23). After extraction the stir bar was removed from the sample solution, rinsed with distilled water in order to remove salts, sugars, proteins or other sample components and dipped on a clean paper tissue to remove water. As discussed in previous section, this rinsing step is extremely important to avoid the formation of non-volatile material that can clog the desorption unit. Rinsing does not cause solute loss since the solutes are sorbed in the polymer phase (David and Sandra, 2007). A second polymer-coated stir bar was then placed into the sample after adding sodium chloride (NaCl) and stirred for at least 2 h. NaCl is often added to a sample matrix to enhance the extraction efficiency as it contributes to the salting-out effect in SBSE which can increases the recoveries of polar compounds (León et al., 2003; Ochiai et al., 2006). After extraction, the same protocol was applied. The SBSE samples were then transferred into an empty cartridge following analysis *via* TD-GC-MS as described in CHAPTER III. Several tests were performed to optimize the method for analysis cloud samples: the effect of PDMS volume, extraction time, sample volume and ionic strength were studied.

The range of cloud water concentrations of VOC are expected to vary between 0-100 µg L^{-1} (Aneja, 1993). All tests were performed for an intermediate aqueous concentration of VOC of 20 µg L^{-1} by introducing 0.5 µL of standard solution to 5 mL Milli-Q water.

II.4.3.2.1 Extraction time

Five extractions were carried out at extraction times varying between 1 to 19 h with the 24 µL PDMS stir bar on 5 mL Milli-Q water with 20 µg L^{-1} standards. Generally, extraction during two hours was the most efficient for these compounds with extraction efficiency around 10 to 80% as shown in Figure II-24. However, the variation of extraction efficiency between 1 to 19 h lies from 3 to 12%. This fluctuation is within the measurement uncertainty range. Since 2 h is convenient for laboratory conditions, this extraction time was chosen.

II.4.3.2.2 Sample volume

A decrease of extraction efficiencies with increasing sample volume is observed for all compounds (Figure II-24). It is in agreement with the SBSE partitioning theory which predicts a decrease in extraction efficiency at a constant stir bar PDMS volume (Figure II-22). As a consequence, a 5 mL sample volume is appropriate and increases the extraction efficiency for most of the studied compounds. This small volume is also convenient since sampled cloud water volumes are usually rather low.

II.4.3.2.3 PDMS volume

The effect of the PDMS volume of commercial Twisters or PDMS stir bar (24, 63, 47 and 126 µL) on the extraction efficiency was investigated. Extraction experiments were carried out during 2 h on 5 mL Milli-Q water with 20 µg L^{-1} standards. The extraction efficiency as a function of the PDMS volume is reported in Figure II-24 for selected VOC. As expected, compounds with a log $K_{O/W}$ lower than 2.5 show the lowest extraction efficiency (*e.g.*, benzene, toluene, dichloromethane, 1,1,2-trichloroethane) with values below 45%. On the opposite, compounds with a log $K_{O/W}$ higher than 3.5 show greatest extraction efficiencies (*e.g.*, xylenes, 1,3,5-trimethylbenzene, 1,2,3-trichlorobenzene) with values higher than 70%. For all compounds, the stir bar with the highest PDMS volume (126 µL) provided the best extraction efficiency and was chosen for cloud water extraction (Figure II-24). Benzene (log $K_{O/W}$

= 1.99) and 1,1,2-trichloroethane (log $K_{O/W}$ = 2.4) are the most sensitive to PDMS volume change with an increase of their extraction efficiency by +200% with PDMS volume. Indeed, the SBSE partitioning theory predicts the most significant changes of extraction efficiency for log $K_{O/W}$ values between 2.0 and 3.5 Figure II-22).

II.4.3.2.4 Ionic strength

NaCl is often added to a sample matrix to enhance the extraction efficiency (León et al., 2003; Ochiai et al., 2006) as it contributes to the salting-out effect in SBSE which increases the recoveries of polar compounds (*i.e.*, for the compounds with log $K_{O/W}$ < 3 or log $K_{O/W}$ ≈3).

The effect of ionic strength on the extraction efficiency was first investigated (Figure II-24 and Figure II-25) with 2 g of NaCl added to the 5 mL volume. The extraction efficiency increased almost for all polar compounds (log $K_{O/W}$ < 3.18). Meanwhile, the extraction efficiency decreased for non-polar compounds (log $K_{O/W}$ > 3.18). The extraction efficiency of SBSE for all target VOC increased with the increase of NaCl concentration from 30 to 40% and then remained stable or decreased with further increase of NaCl concentration up to 60%. This phenomenon can be explained by two processes that occur during the extraction process. Initially, the extraction efficiency for VOC compounds increases with the enhancement of NaCl concentration due to the salting out effect, which drives more VOC into the PMDS layer. The further addition of NaCl increases the solution viscosity, which may potentially decrease the extraction efficiency (Quintana et al., 2007; Pang et al., 2011). Consequently, 40% of NaCl in the sample solution is chosen as the optimal ionic strength. In the presence of 40% NaCl, the extraction efficiency of benzene, toluene, o-xylene, styrene and 1,1,2-trichloroethane is enhanced up to 20% with intermediate log $K_{O/W}$ between 1.99 and 3.09 .

All results described above confirm the judicious choice to carry out a "sequential SBSE" (Ochiai et al., 2006) which takes place in two stages: a first extraction without salt which will extract the non-polar compounds followed by a second extraction after salt addition, which allows extracting the polar compounds remaining in solution.

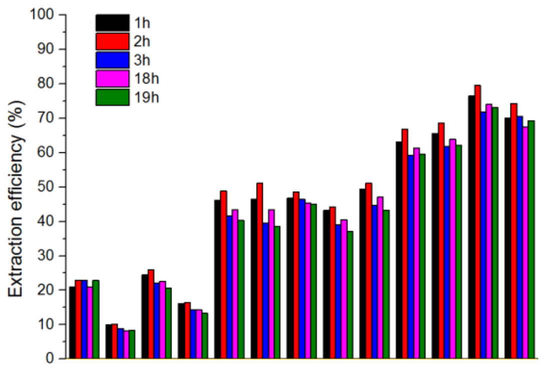

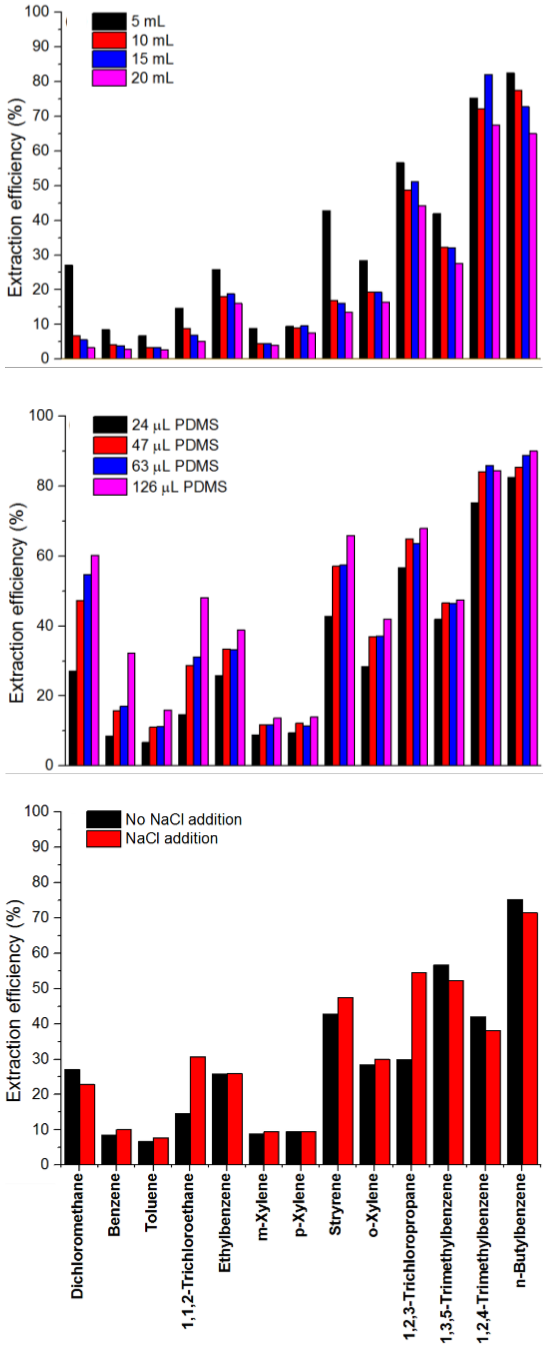

Figure II-24 Effects of extraction time, sample volume, PDMS volume and NaCl effect on the extraction efficiency E (%) for a selection of VOC：dichloromethane, benzene, toluene, 1,1,2-trichloroethane, ethylbenzene, m-xylene, p-xylene, styrene, o-xylene, 1,3,5-trimethylbenzene, 1,2,4-trimethylbenzene, 1,2,3-trichlorobenzene and n-butylbenzene.

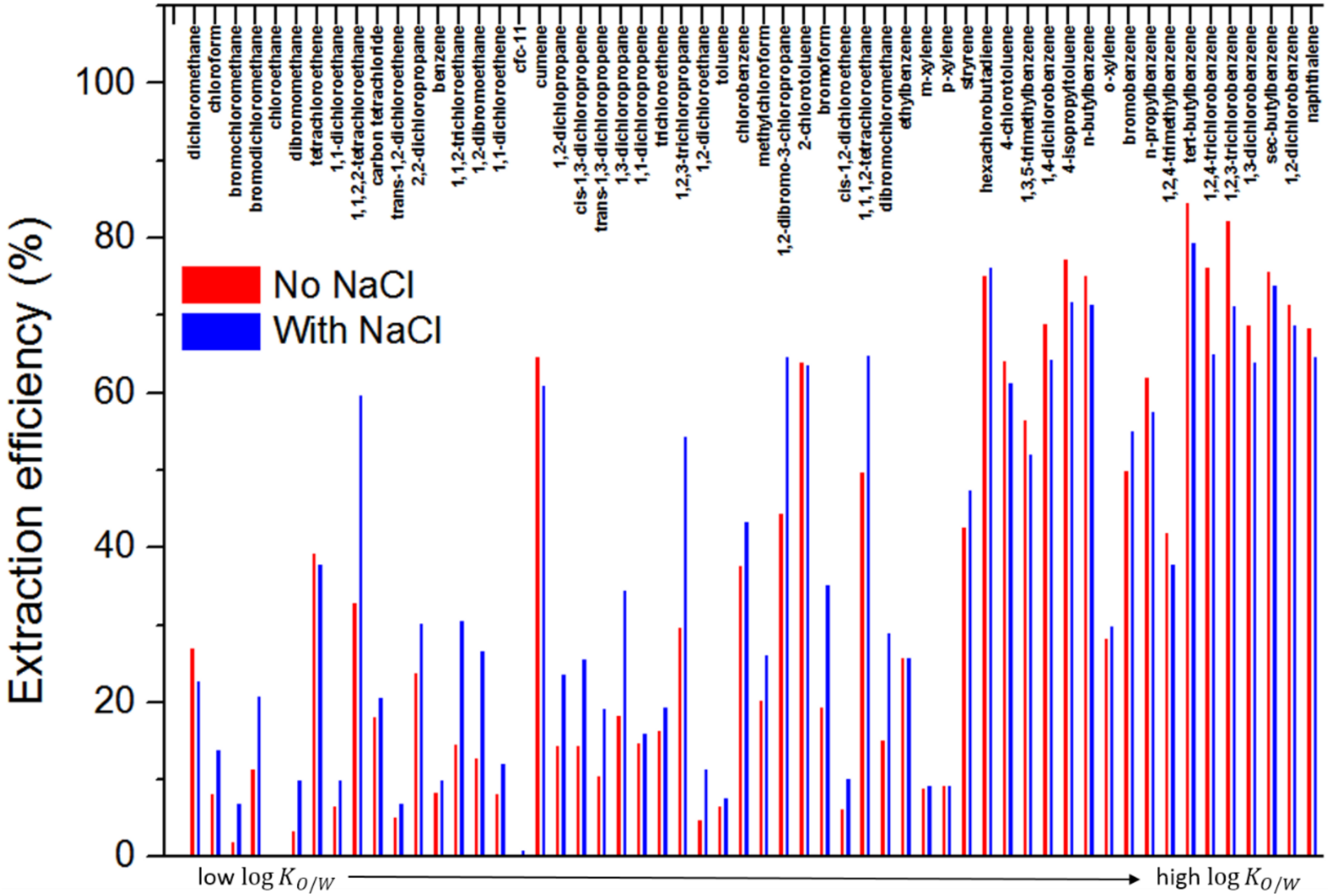

Figure II-25 Effects of NaCl addition on the extraction efficiency E (%) for a all standards of VOC, classified ranging from low log $K_{o/w}$ = 1.18 to high log $_{Ko/w}$ = 4.72.

II.4.3.2.5 Final protocol for VOC extraction from cloud water

The following protocol has been chosen for the extraction of VOC from cloud water samples: 5 mL of cloud water is introduced in a glass bottle (10 mL size); then, a first 126 µL stir bar is placed into the bottle under magnetic stirring at 80 rpm. The extraction takes 2 h at ambient temperature (between 20 and 22 °C) with the objective to get the maximum extraction of non-polar compounds. This stir bar is rinsed with Milli-Q water and dried with an absorbent paper. A second extraction is additionally performed using a second 126 µL stir bar after 2 g NaCl salt addition. This allows extracting remaining polar compounds from the sample. This second bar is also rinsed with Milli-Q water and dried with an absorbent paper. Finally, stir bars are placed in a desorption tube (empty cartridge) and analyzed by TD-GC-MS. Extraction efficiencies of VOC vary between 22.4% for isoprene and 96.8% for m+p-xylenes (see in Table II-6). A comparison of the experimental extraction efficiencies for styrene (log $K_{O/W}$ = 2.89), ethylbenzene (log $K_{O/W}$ = 3.03), m+p-xylenes (log $K_{O/W}$ = 3.09) and naphthalene (log $K_{O/W}$ = 3.17) showed a good consistency with the theoretical extraction efficiencies (88.6 - 96.7%) (see in Figure II-26). For other compounds with log $K_{O/W}$ < 3, the experimental extraction efficiency is lower than the theory. This protocol is also applied for BLANC test with two stir bars by SBSE for the same liquid volume 5 mL of Milli-Q water. There is no VOC detected from standard list. Detection limits were estimated (see in Section II.6) demonstrating the ability of the SBSE technique to quantify low concentrations (1.0−8.7 ng L^{-1}).

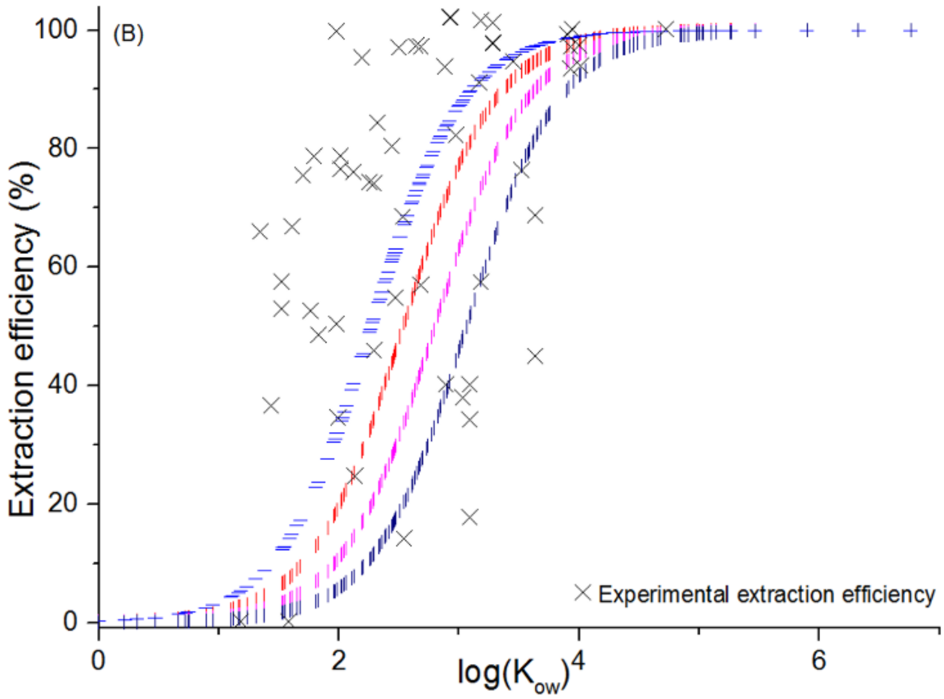

Figure II-26 Example of theoretical extraction efficiency for 5, 10 and 20 mL sample volumes and 63, 126 µL PDMS volumes and comparison between experimental and theoretical extraction efficiency with experimental conditions based on 63 µL PDMS volume and 5 mL sample volume.

Table II-6 Extraction efficiency (E) of SBSE for a selection of VOC (%).

Compounds	**E (%)**
Benzene	34.9
Toluene	52.5
Ethylbenzene	90.9
m+p-xylene	96.8
o-xylene	94.0
Styrene	94.7
Cumene (isopropylbenzene)	100.0
n-Propylbenzene	100.0
1.3.5-Trimethylbenzene	100.0
Tert-butylbenzene	100.0
1.2.4-Trimethylbenzene	100.0
Sec-butylbenzene	100.0
4-Isopropyltoluene (p-cymene)	100.0
n-Butylbenzene	100.0
Naphtalene	88.7
Isoprene	22.4
α-pinene	100.0
β-pinene	100.0
Limonene	100.0
Nopinone	100.0

II.4.3.2.6 Linearity of the coupled SBSE-GC-MS method

The linearity of the coupled SBSE-GC-MS method for the VOC quantification in real cloud water samples was evaluated by establishing a calibration curve for target VOC. A series of VOC liquid standards of 60, 100, 140 ng were added separately in 5 mL Milli-Q water in the 10 mL-bottle. The optimized extraction protocol by SBSE described in the previous section is applied to each sample. An internal C_{13}-alkane standard (tridecane) which is not expected to be present in cloud water samples is also added in each bottle with the same amount (15.2 µg L^{-1}). The internal calibration makes the quantification free from extraction problem or changes in extraction efficiency due the aging of PDMS phase. Future analysis can be also compared and verified by the internal standard. The external and internal calibration curves for toluene and isoprene are reported on Figure II-27. The coupled SBSE-GC-MS method shows a very good linearity for all target compounds with an R^2 usually higher than 0.95. The chromatogram of selected VOC extracted by SBSE is shown in Figure II-28. For future atmospheric applications, the concentrations of VOC in cloud liquid samplers will be directly deduced from theses curves without any *a priori* knowledge of their extraction efficiency.

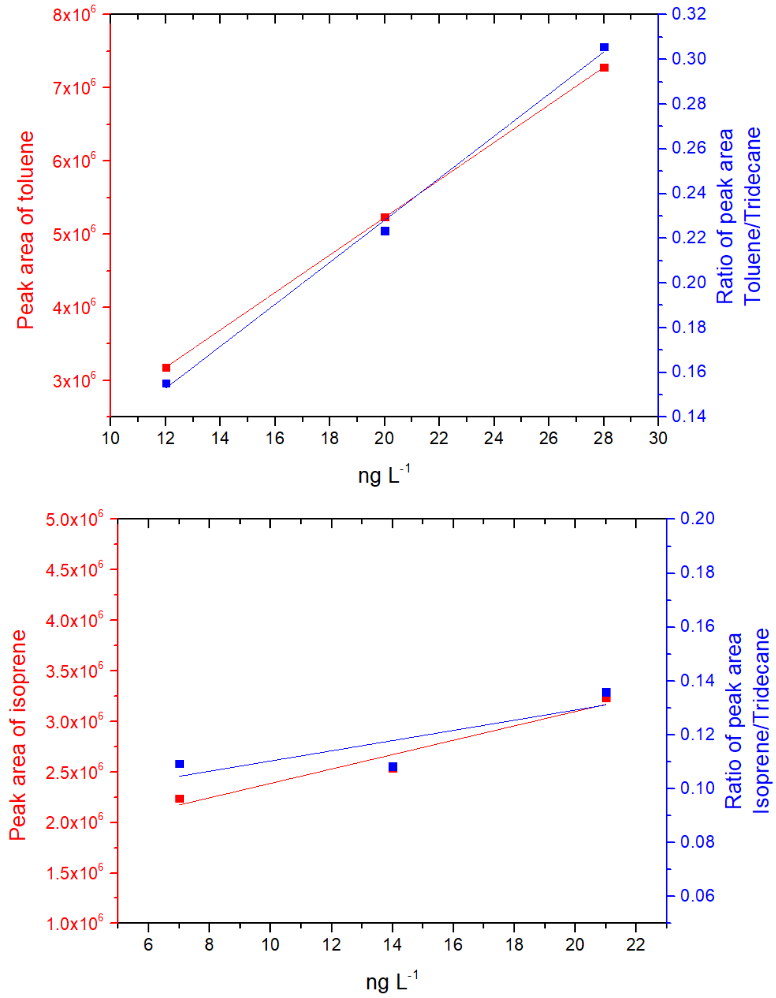

$$y = 256267.88x + 106631.5$$
$$R^2 = 0.99$$

$$y = 0.0094x + 0.04$$
$$R^2 = 0.99$$

$$y = 71180.14x + 1675430$$
$$R^2 = 0.97$$

$$y = 0.00189x + 0.0914$$
$$R^2 = 0.85$$

Figure II-27 Calibration curves for toluene and isoprene for external (red) and internal (blue) calibration. "Peak area" refers to the total ion chromatogram obtained in the electron ionization mode, in area units.

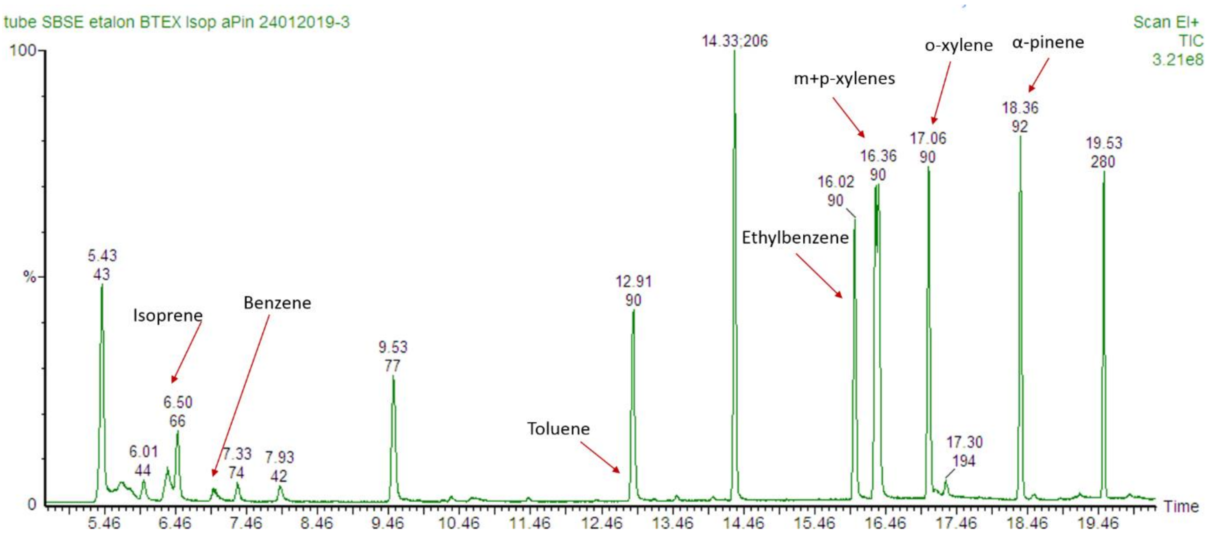

Figure II-28 Chromatogram of VOC (from total SIM ion chromatogram) extracted by SBSE. Peak identification is noted with corresponding compound by red arrow.

II.4.4 Optimization of SBSE conditions for the analysis and extraction of OVOC

The optimization tests of OVOC SBSE is based on the optimized protocol for VOC described in the previous section. The liquid sample is firstly treated by derivatization with PFBHA (PFBHA solution at 0.05 mM) for carbonyl compounds and MTBSTFA (pure MTBSTFA liquid, 4.6 M) for alcohols and carboxylic acids. Then tests were conducted, namely the effect of the extraction time duration and ionic strength to optimize extraction efficiency. The PDMS volume of 126 µL and a sample volume of 5 mL have been fixed after VOC SBSE Carbonyl functions derivatization in liquid phase samples

II.4.4.1 Carbonyl functions derivatization in liquid phase samples

II.4.4.1.1 Carbonyl functions derivatization and SBSE procedures

The same in liquid derivatization protocols as the one described in Section II.2.1 are applied. The derivatization is left 24 h for the complete derivatization of carbonyls by PFBHA. 1 µL of the derivatized solution is then transformed into 5 mL of MilliQ water in a 10-mL glass bottle. The 126 µL PDMS volume stir bar of SBSE is introduced for extraction at 80 r.p.m.

II.4.4.1.2 Test on the influence of the extraction time and ionic strength

The extraction time is tested separately for 1 to 6 h with and without the addition of NaCl (see in Figure II-29), respectively. After extraction the stir bar is removed from the standard solution and dried by a tissue paper to clean the solution adhering to its surface. Stir bas is then placed in an empty cartridge and analyzed by TD-GC-MS.

The results of the tests are illustrated in Figure II-29 for MVK and butanal as examples. The absence of NaCl greatly improves the extraction efficiency for all compounds After 6 h the maximum extraction efficiency is achieved for most of the compounds (MACR, acetone, MVK, butanal, pentanal, GA and HA). Some additional tests at longer time duration have been performed up to 24 h. While some improvements have been observed for formaldehyde and acetaldehyde, this duration is long and hardly compatible with the analysis of a high number of cloud samples without excluding the degradation of oximes beyond 24 h of derivatization . Therefore a 6 h-time duration is the best compromise.

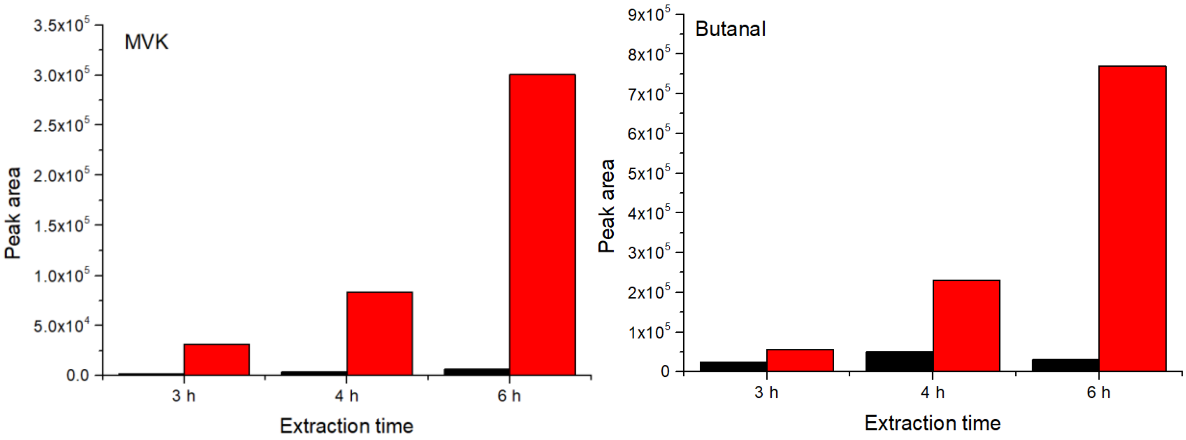

Figure II-29 Effects of extraction time (3 h, 4 h and 6 h) and NaCl effect (with the presence of NaCl in black and without the presence of NaCl in red) on the extraction for MVK and butanal. "Peak Area" refers to the m/z 181 extracted ion chromatogram obtained in the electron ionization mode, in area units.

II.4.4.1.3 Linearity of the coupled SBSE-GC-MS for carbonyl functions

Three to five standard solutions of carbonyl compounds 0.2 µM - 10 mM were diluted from the primary-C=O standard solution (see in Section II.2.1). Diluted C=O standards are separately added into the PFBHA solution for a total volume of 5 mL. 1 µL of each mixture solution is then transferred into 5 mL of MilliQ water in a 10-mL glass bottle. The Extraction by SBSE stir bar is conducted with the 126 µL PDMS volume stir bar at a speed of 80 r.p.m. for 6 h without NaCl addition before analysis by TD-GC-MS. As for VOC, the introduction of tridecane as an internal standard is tested (see in Section II.4.3.2.6). The external and internal calibration curves for MACR and pentanal are reported on Figure II-30 as an example. The coupled SBSE-TD-GC-MS method shows a very good linearity for all target compounds with an R^2 usually higher than 0.97. The chromatogram of selected carbonyl compounds, derivatized with PFBHA (extracted by m/z 181 from total SIM ion chromatogram) and extracted by SBSE, is shown Figure II-31.

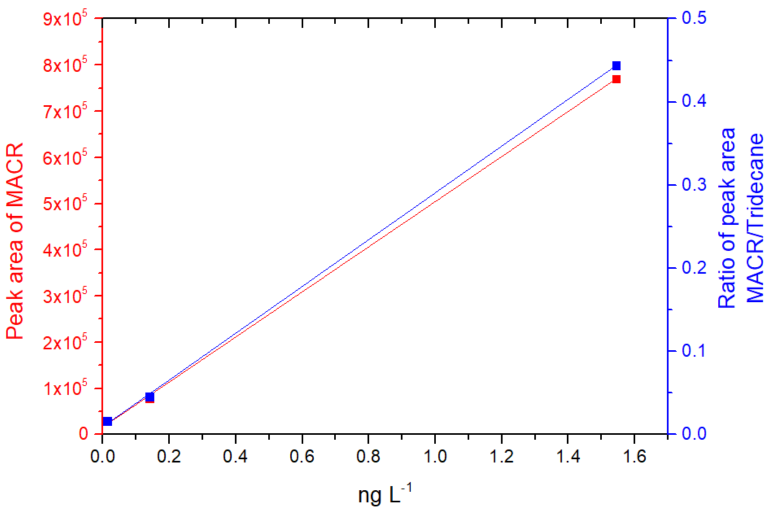

$$y = 488223.69x + 16383.75$$
$$R^2 = 0.99$$

$$y = 0.2814x + 0.00963$$
$$R^2 = 0.99$$

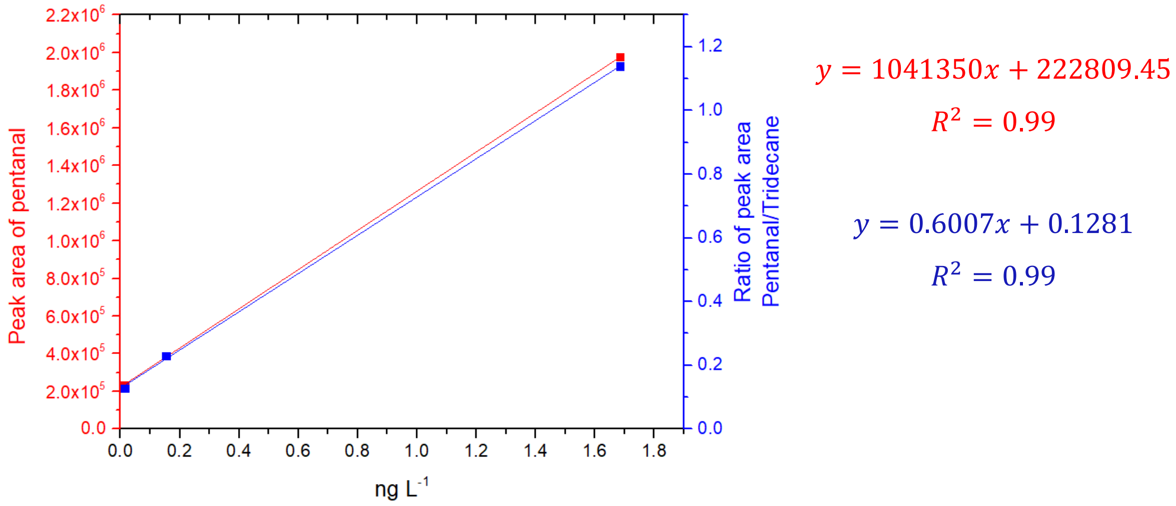

Figure II-30 The external (red) and internal (blue) calibration curves for MACR and pentanal. "Peak Area" refers to the m/z 181 extracted ion chromatogram obtained in the electron ionization mode, in area units.

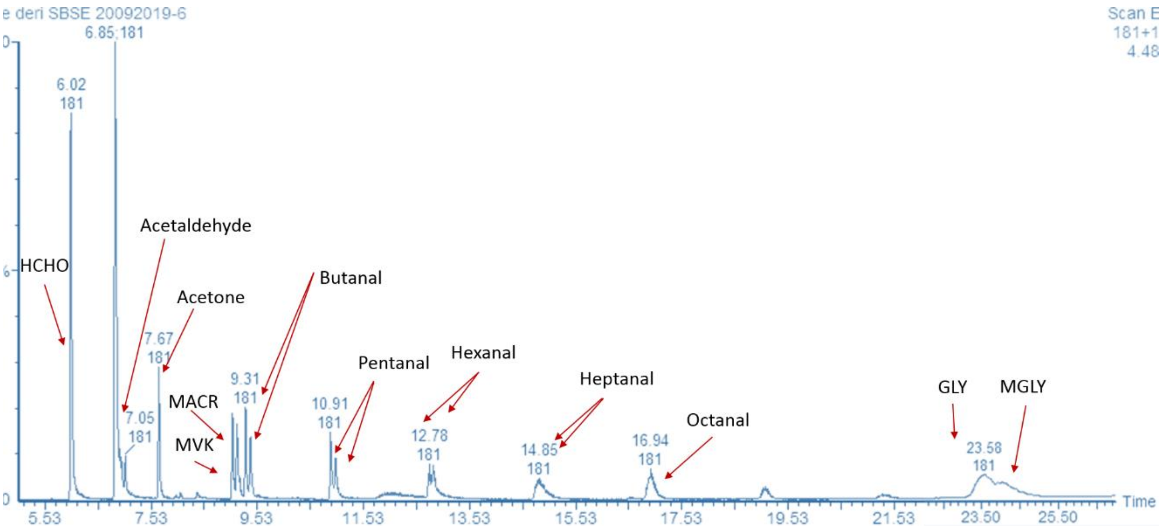

Figure II-31 Chromatogram of carbonyl compounds, derivatized with PFBHA (extracted by m/z 181 from total SIM ion chromatogram) and extracted by SBSE. Peak identification is noted with corresponding compound by red arrow. HCHO: formaldehyde; MACR: methacrolein; MVK: methyl vinyl ketone; GLY: glyoxal; MGLY: methylglyoxal.

II.5 Detection limits for OVOC by Tenax® tube and SBSE

Both detection limits of SBSE and Tenax® tube of OVOC are evaluated from calibration curves. A series of diluted carbonyl compound solutions from 0.1 µM- 10 µM is used. Diluted C=O standard solutions are separately added to PFBHA solution for a total mixture solution volume of 5 mL following the same protocol as described previously. One µL of each mixture solution was then transferred into the clean Tenax® tube. For SBSE part, the same 1 µL of each mixture solution is transferred into 5 mL of MilliQ water in a new glass bottle of 10 mL size. Extraction of SBSE is conducted with the 126 µL PDMS volume stir bar at speed of 80 rpm for 6 hours without NaCl addition following the same optimized protocol as described previously (see in Section II.4.3.2.5). Finally, analysis is performed by TD-GC-MS. The detection limits are reported in Table II-7. Detection limits (corresponding to 3 times the noise) are given in absolute mass per sample tube and in concentration for SBSE. They range from 0.44 to 4.68 ng per tube and from 1.45 10^{-3} to 1.29 mM.

Table II-7: GC-MS detection limits for the analyzed OVOC.

Compounds	Detection limit by SBSE (nM)	Detection limit by Tenax® tube (ng)
MVK	9.86 10^{-2}	3.45
MACR	9.70 10^{-2}	3.40
Butanal	0.91	3.26
Pentanal	0.75	3.22
Hexanal	0.65	3.26
Hrdoxyacetone	1.16	4.32
Heptanal	0.60	3.40
Octanal	0.51	3.28
Formaldehyde	1.45 10^{-3}	0.44
Acetone	5.45 10^{-3}	3.16
Glyoxal	0.70	2.04
Methylglyoxal	1.29	4.68

Calibration curves for on-sorbent-tube derivatization, in-solution derivatization and derivatization-SBSE are all summarized in Table A.13 in Appendices, including calibration curve slopes, good correlation coefficients (most of them ranging from 0.90 to 0.99). The response linearity was evaluated from a specific 181 m/z ion extraction for each compound and was statistically validated.

II.6 VOC measurement uncertainty

The measurement of VOC involves different steps, each step being a potential source of error, it seems essential to evaluate the uncertainty associated with each measure. As explained above, the concentration of compound *i* is a function not only of the mass of compound *i* trapped on the cartridge but also the sampling volume. As a result, the associated uncertainty will depend on uncertainties related to these two grandeurs (AFNOR (2008) and EURACHEM (2000)). The VOC concentration uncertainty $u(C_i)$ of a compound i is expressed according to the equation:

$$\frac{u^2(C_i)}{{C_i}^2} = \frac{u^2(m_{i,mes})}{m_{i,mes}^2} + \frac{u^2(V)}{V^2} \qquad \text{(Eq.5)}$$

where $u(V)$ is the variance associated with the sampling volume V and $u(m_{i,mes})$ the variance associated with the mass $m_{i,mes}$ trapped on Tenax® TA or PDMS stir bar of compound i. This equation allows calculating the relative standard uncertainty of VOC concentration in both gas and aqueous phases.

- Uncertainty on V :

For air sampling on Tenax® TA tubes, the flow rate D (100 mL min^{-1}) and the sampling time t (180 min) allow estimating the sampling volume uncertainty defined by:

$$u^2(V) = D^2 \times u^2(t) + t^2 \times u^2(D) \qquad \text{(Eq.6)}$$

where $u(t)$ is the variance associated with the sampling time and $u(D)$ is the variance associated with the flow rate.

$$u^2(D) = \left(\frac{3\% \times 100}{\sqrt{3}}\right)^2 = 3 \qquad \text{(Eq.7)}$$

$$u^2(t) = \left(\frac{2}{\sqrt{3}}\right)^2 = 1.33 \qquad \text{(Eq.8)}$$

$$u^2(V) = 332.42 \qquad \text{(Eq.9)}$$

$$\frac{u^2(V)}{V^2} = \frac{332.42}{100 \times 180} \times 100\% = 1.85\% \qquad \text{(Eq.10)}$$

For cloud sample, the variance of sampling volume V is associated with collected cloud water volume. 5 mL of cloud water is taken by micropipette from initial sample container. The variance of sample volume is 0.5% (Micropipette Eppendorf ref 033326, 10000 µL, France).

- Uncertainty on $m_{i,mes}$:

Uncertainty on the mass of compound *i* trapped on Tenax® TA or extracted by SBSE and measured by TD-GC-MS involves many error terms. Indeed, according to Hoerger et al. (2015), the mass of compound *i* deduced from the calibration curve is associated with the linearity of the calibration curve, the selectivity of the peaks on the chromatograms, the mass of compound *i* in the standard and the reproducibility of the measurement. The variance of $m_{i,mes}$ is defined as:

$$\frac{u^2(m_{i,mes})}{m_{i,mes}^2} = \frac{u^2(m_{i,linearity})}{m_{i,linearity}^2} + \frac{u^2(X_{i,selectivity})}{X_{i,selectivity}^2} + \frac{u^2(m_{i,std})}{m_{i,std}^2} \qquad \text{(Eq.11)}$$

For air and cloud water measurements, the uncertainty on $m_{i,mes}$ is calculated with the same calibration curve.

✓ Linearity term $\frac{u^2(m_{i,linearity})}{m_{i,linearity}^2}$:

The standard uncertainty of linearity is determined by the maximum difference between the line of least squares and experimental points. The standard uncertainty for a compound *i* is defined as:

$$\frac{u^2(m_{i,linearity})}{m_{i,linearity}^2} = \frac{1}{3} \times (R_{i,linearity})^2 \qquad \text{(Eq.12)}$$

$$R_{i,linearity} = \frac{m_{i,cal} - m_{i,exp}}{m_{i,exp}} \quad \text{(Eq.13)}$$

with $R_{i,linearity}$ the maximum linearity difference, $m_{i,cal}$ the calculated mass depending on calibration range and $m_{i,exp}$ the experimental mass. The relative standard uncertainties for linearity for compounds taken from cartridge range from 1.9% (ethylbenzene) to 17.4% (isoprene).

- ✓ Selectivity term $\frac{u^2(X_{i,selectivity})}{X^2_{i,selectivity}}$:

The uncertainty about selectivity depends on how to identify and isolate the peaks on the chromatogram compared with interfering peaks. According to Hoerger et al. (2015), the chromatographic separation is optimized if the resolution between two successive peaks is greater than 1. The expression of the resolution R (s^{-1}) is given by equation:

$$R = \frac{\Delta t_r}{0.85 \times h_B \times h_L} \quad \text{(Eq.14)}$$

where Δt_r is the difference between the retention time of the selected compound and the interfering compound, h_B the width of the peak at half height for the selected compound (s) and h_L the width of the peak at half height for the interfering (s). When R is greater than or equal to 1, the peaks are then considered to be well separated. In our case, peaks are well separated with R=1. Therefore, $\frac{u^2(X_{i,selectivity})}{X^2_{i,selectivity}}$ is equal to 0.

- ✓ Standard term $\frac{u^2(m_{i,std})}{m^2_{i,std}}$:

The uncertainty on the standard is based on the propagation of variances. For a compound X, the term $u^2(m_{i,std})$ can be noted as $u^2(m_X)$, which depends on different equipment used during the preparation of standards and their injection into the system analysis, namely the balance and the syringe.

$$u^2(m_X) = u^2_{accuracy}(m_X) + u^2_{repeatability}(m_X) \quad \text{(Eq.15)}$$

An uncertainty on the standards related to the accuracy of the syringe can be determined. For that, the uncertainty indicated by the manufacturer is used. This amounts to 1% of the volume taken. The uncertainty related to the accuracy of the syringe is then determined by equation:

$$u^2_{accuracy} = \frac{0.01 \times m_{X,a}}{\sqrt{3}} \quad \text{(Eq.16)}$$

with $m_{X,a}$ mass of compound x in the standard a (in g). The uncertainty related to the accuracy of standards represents 0.57% of the mass m_X.

The repeatability of the measurement of the standards takes into account possible evaporation that can occur between two additions of compounds in the bottle during their preparation. The variance of the repeatability $u_{repeatability}(m_X)$ corresponds to the standard deviation between these 10 measurements with peak area of chromatography for a compound and is given as:

$$u_{repeatability}(m_X) = \frac{standard\ deviation}{mean} \qquad \text{(Eq.17)}$$

and repeatability of the measurement ranges between 2.4 and 3.2% depending on the compounds.

After summing up all the variances for $m_{i,mes}$, the $\frac{u^2(m_{i,mes})}{m_{i,mes}^2}$ is between 0.7% and 1.59%.

- Uncertainty on C_i:

The uncertainty is calculated by applying Eq.5. The uncertainty ranges are 8.5-12.6% and 5.06-12.6% for air and liquid measurements, respectively (see in Table II-8). The uncertainty on $m_{i,mes}$ contributes the most to the total uncertainty and the standard term and linearity term are identified as the most important sources of uncertainty on $m_{i,mes}$. For gas sampling by Tenax® cartridges, the standard term accounts for 44.2 to 97.8%. For cloud extracted by PDMS stir bar, the linearity term accounts for 3.4 to 95.6% depending on the compounds.

- Detection limit DL_i :

The detection limit (DL) is the smallest concentration that can be detected for a compound. The peak of a compound *i* must be distinguished from the background noise ("bgn") of a chromatogram so that it is considered as detectable. The detection limits are determined according to the equation:

$$DL_i = \frac{3 \times H_{bgn} \times C_i}{H_i} \qquad \text{(Eq.18)}$$

with DL_i the detection limit of the compound i in ppb, H_{bgn} the height of the background noise in mm, C_i is the concentration of compound i in ppb and H_i the height of the peak of compound i in mm. Detection limits for the analyzed VOC are shown for GC-MS system (detectable masses) and for the whole method (atmospheric gaseous and aqueous concentrations) in Table II-9.

Table II-8 Extended (2 σ) calculated uncertainties of VOC concentrations in air and cloud waters.

Compound	Uncertainty (%) for air samples	Uncertainty (%) for cloud water samples
Benzene	19.6	11.8
Toluene	17.4	10.2
Ethylbenzene	17.4	16.0
m+p-xylene	18.2	17.8
o-xylene	17.0	16.2
Styrene	17.0	16.6
Cumene (isopropylbenzene)	20.2	20.1
n-propylbenzene	25.2	25.2
1,3,5-trimethylbenzene	23.0	23.0
1,2,4-trimethylbenzene	20.4	20.6
Naphtalene	20.4	18.8
Isoprene	22.2	20.4
α-pinene	19.4	19.4
β-pinene	20.8	20.8
Limonene	17.8	18.0
Nopinone	17.2	19.6

Table II-9: Detection limits for the analyzed VOC "" refers to the calculation for a sampling of 18 L of air (100 ml min^{-1} for 3h of sampling).*

Compounds	Detectable mass (ng) (gaseous samples)	Atmospheric gaseous concentration* (ppt)	Detectable mass (ng) (aqueous samples)	Atmospheric aqueous concentration (ng L^{-1})
Benzene	0.65	10.3	0.019	3.7
Toluene	0.13	1.7	0.005	1.0
Ethylbenzene	0.34	3.9	0.018	3.6
m+p-xylene	0.11	1.3	0.005	1.0
o-xylene	0.25	2.9	0.014	2.8
Styrene	0.46	5.4	0.026	5.2
Isopropylbenzene	0.39	4.0	0.020	4.0
n-propylbenzene	0.74	7.6	0.038	7.6
1,3,5-trimethylbenzene	0.19	2.0	0.010	1.9
1,2,4-trimethylbenzene	0.22	2.3	0.011	2.2
Naphtalene	0.89	8.6	0.039	7.7
Isoprene	0.67	12.2	0.014	2.8
α-pinene	0.95	8.6	0.044	8.7
β-pinene	0.33	3.0	0.015	2.9
Limonene	0.13	1.2	0.006	1.1
Nopinone	0.60	5.4	0.027	5.4

II.7 Summary of the analytical developments

Experimental investigations described in this chapter have included:

- the optimization of gaseous OVOC identification and quantification onto Tenax TA sorbent tubes precoated with two derivatization agents coupled to TD-GC-MS analysis;
- the optimization of dissolved OVOC/VOC identification and quantification by Stir Bar Sorbtive Extraction (SBSE) coupled to TD-GC-MS analysis.

After the optimization of the analytical TD-GC-MS conditions, various tests have been performed at the laboratory (influence of environmental factors like relative humidity, derivatization duration, extraction time duration, volumes of the sample and of PDMS stir bar, ionic strength). The protocols have been established for Tenax TA tube pre-coating and SBSE extraction for VOC and carbonyls. At the end, the method performances have been evaluated (*i.e.*, linearity, repeatability, sensitivity, extraction efficiency). These achievements are indicated by the white squares in Figure II-32.

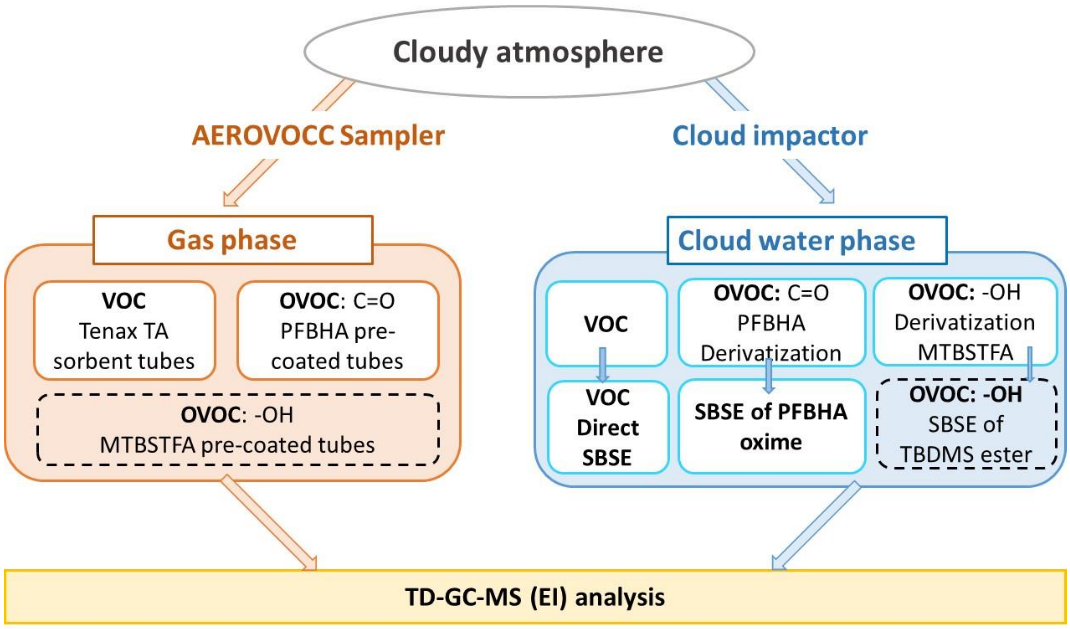

Figure II-32 Observational strategy overview.

While the optimized GC-MS analytical conditions allow the separation and identification of carbonyl and hydroxyl VOC by TD-GC-MS analysis, there are still some tests to carry out for their measurements in both gas and cloud water phases (dotted lines squares in Figure II-32). The breakthrough volume is a critical issue for light OVOC sampling on PFBHA pre-coated Tenax TA tubes and tests under controlled conditions are still needed to evaluate the potentiality of the method for atmospheric applications. However, the use of commercial 2,4-dinitrophenylhydrazine tubes could be an alternative for carbonyls in cloudy conditions. Gaseous samples pre-coated with MTBSTFA require the definition of protocols for the coating of Tenax TA sorbent tubes with MTBSTFA and derivatization conditions.

The extraction by SBSE of derivative MTBSTFA and corresponding calibration have to be evaluated to complete the investigation of cloud water phase (noted in Figure II-32). Finally, laboratory tests have shown the reliability of the optimized method for VOC of interest in both atmospheric gas and cloud water phases.

All the optimized protocols described in this chapter have been applied to the atmospheric measurements of VOC and carbonyls in both gas and cloud water phases for two contrasted environments: the puy de Dôme station and La Réunion Island. Part of these data have been used for the study of air/water partitioning. A newly developed gas sampler (AEROVOCC) have been developed at LaMP for field measurement. Associated results are presented in CHAPTER III.

CHAPTER III Multiphasic VOC sampling in the cloudy atmosphere: towards air-water partitioning

III.1 Measurement sites and multiphasic sampling

The results described in this chapter rely on the VOC/OVOC measurements performed at two contrasted measurement sites. In this first section, we present the measurement sites, the associated instrumental instrumentation and its recent evolution.

III.1.1 Presentation of the puy de Dôme station

The puy de Dôme station is a part of the global instrumented site "CO-PDD" (Cézeaux-Aulnat-Opme-Puy De Dôme), which allows the monitoring over long period of the various components of the atmosphere (greenhouse gases, reactive trace gases, aerosols, atmospheric waters (water vapor, clouds, precipitation). For the last twenty-five years, this site has evolved from a meteorological station to a full instrumented platform for atmospheric research. CO-PDD is nationally labelled by CNRS, the French national center for scientific research, and recognized as a global GAW (Global Atmospheric Watch, station PUY). It is also part of the European and national research infrastructure ACTRIS (Aerosol Cloud and Trace gases Research Infrastructure) and ICOS for greenhouse gases (Integrated Carbon Observing System). CO-PDD is composed of *in situ* and remote sensing observations from different connected sites (Cézeaux-Aulnat, Opme and puy de Dôme) at different altitudes (see in Figure III-1): the puy de Dôme station (PUY, 45.77°N, 2.96°E, 1465m a.s.l.) far from immediate pollution sources, Opme (45.71°N, 3.09°E, 660 m a.s.l.) in a rural area, and Cézeaux (45.76°N, 3.11°E, 410 m a.s.l.) and Aulnat sites (45.79°N, 3.15°E, 330 m a.s.l.) located in a suburban area, near the city of Clermont-Ferrand. The sites are 10 to 15 km apart. This multi-site platform allows documenting the variability of particulate and gaseous atmospheric composition, but also the optical, biochemical and physical properties of clouds and precipitations.

PUY is the highest point of "Chaîne des Puys", that represents an orographic barrier to the prevailing oceanic westerly winds (Hervo et al., 2014). The height of the mixing layer varies widely between day and night, and as a function of the meteorological context (season, day/night…) between 700 m and 2200 m a.s.l. (Farah et al., 2018). The altitude of PUY localizes it below or above the atmospheric mixing layer, depending on the season. PUY is in free tropospheric conditions 50% of the time in winter, but it is in the mixing layer in summer especially during daytime. In addition, dynamical exchanges between these two atmospheric compartments can occur and significantly influence the lifetime and transport of aerosol injected in the free troposphere (Freney, 2016). PUY is in cloudy condition for 30% of the time, the cloud occurrence varies from 20% in summer to 60% in winter during the year by a systematic analysis of webcam PUY images (Baray et al., 2019). During cloudy event, the summit of the puy de Dôme is often in the free troposphere. A high variety of cloud situations is encountered at the PUY station (orographic, frontal, convective clouds, warm and/or cold clouds, masses of polluted air or not...); this makes this site a strategic location for aerosol and clouds studies. Specifically, long-term measurements are performed and processes linking gases, aerosols, clouds and precipitation are studied in the frame of the impact of anthropogenic changes on climate (cloud, radiation) and meteorology (precipitation). Innovative research investigations are also conducted such as on new particle formation or on the bio-physico-chemistry of clouds.

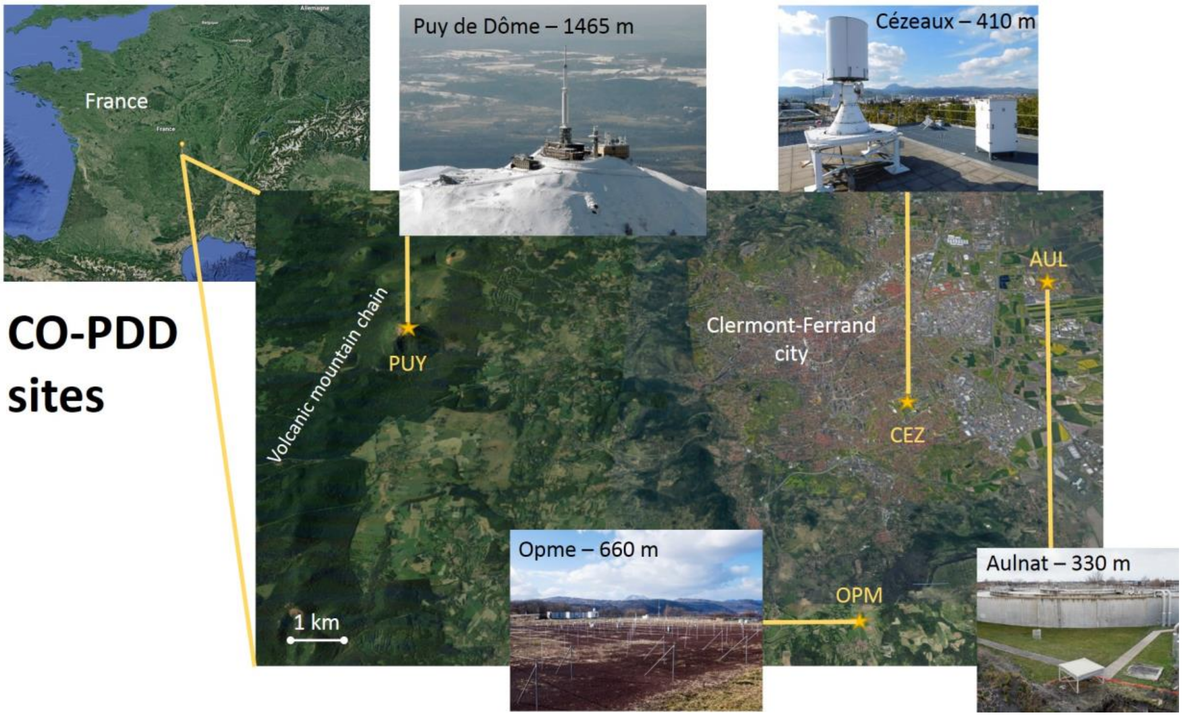

Figure III-1 Overview maps showing the location of CO-PDD sites as well as photography of the different sites and altitudes. This picture is extracted from Baray et al. (2019).

In the frame of my thesis, the puy de Dôme station was a reference site for cloud sampling and gas sampling. I have taken in charge the analysis of VOC/OVOC. Moreover, I had access to the gaseous VOC data for the air partitioning study described in Section III.2 and Section III.3.

III.1.2 Presentation of the Maïdo observatory

Réunion Island (21◦ S, 55◦ E) is a volcanic island located in the southwestern part of the Indian Ocean. It is particularly well located to study stratospheric tropical waves and largescale dynamics of air masses. Due to its location, Réunion Island is seasonally exposed to biomass burning plumes, which can significantly affect the free tropospheric concentrations of ozone (Clain et al., 2009) and other pollutants like carbon monoxide and several volatile organic compounds (Duflot et al., 2010; Vigouroux et al., 2012). Moreover, it is affected by the dynamical influence of the subtropical jet stream and the tropical convection which are key processes for the understanding of the tropical transition layer.

Réunion Island is affected by southeasterly trade winds near the ground, and westerlies in the free troposphere. The eastern/western parts of the island are respectively wet and dry. Clouds develop daily on the summits of the island, with a well-established diurnal cycle (formation in the late morning, dissipation at the beginning of the night). Maïdo mount is a summit on the western part of the island.

During the night and at the beginning of the morning, air masses at the Maïdo mount are separated from local and regional sources of pollution, due to the strengthening of the large-scale subtropical subsidence at night. A recent numerical study allowed identification of processes of pollution transport and dispersion, including vortices in the wake of the island, causing counterflow circulation and trapping of polluted air masses near the northwestern coast and protecting the observatory from volcanic plumes in case of eruption (Lesouëf et al., 2011).

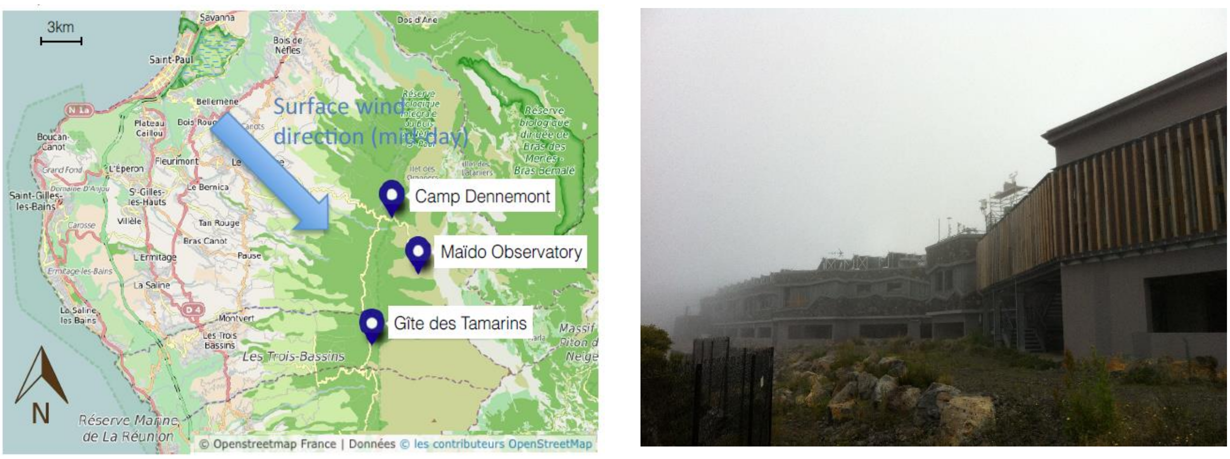

Figure III-2 Localization of Maïdo observatory and a picture of the building.

On La Réunion Island, major potential sources of SOA are present, especially biogenic sources, which are favored by the tropical forest, marine sources and anthropogenic sources from the coastline. This SOA formation is potentially enhanced by the elevated temperature and actinic flux. Moreover, the slope of the mountain allows the formation of clouds that are also medium contributing to SOA formation *via* the aqueous phase reactivity. In this frame, the ANR project “BIOMAIDO” have been established with the objective to characterize the influence of clouds on the organic matter emitted by various sources (ocean, vegetation, human activities) and under different phases (gases, aerosol particles). A field campaign was performed during March 2019 where many instruments were deployed for documenting the chemistry of atmospheric components (especially organic compounds) during their transport along the slope of the mountain. Many devices for characterizing cloud microphysical properties and the atmospheric transport were implemented (tethered balloon equipped with microphysical probes, radar, lidar…). During this campaign, cloud waters were collected below the Maïdo observatory on the mountain slope and gaseous VOC/OVOC were sampled simultaneously. The available devices inside the consortium (tethered balloon, radar, lidar, cloud collector) for cloud observation were adapted to the particular context of La Réunion Island. The Maïdo observatory maintains a complementary set of devices to characterize the physical-chemistry of the atmosphere.

In the frame of my thesis, I took in charge the analysis of the gaseous VOC/OVOC samples at the laboratory. These results are presented in Section III.4

III.1.3 Multiphasic sampling

This section has the objective to present the historic developments that have been conducted in the past to sample the various atmospheric matrices. Initially the sampling and analysis of chemicals was carried out and developed independently in the gaseous and the aqueous phases. During specific field campaigns (2012 and 2013), the objectives were to characterize at the same time VOC in the various phases of the clouds. Results demonstrated the necessity to develop a new instrumental set-up for sampling simultaneously the various cloud phases. This development has been realized recently in the frame of my PhD thesis.

Since 2001, cloud water sampling is regularly performed at PUY using a dynamic one-stage cloud water impactor (Brantner et al., 1994), with a cut off diameter of approximately 7 µm (Figure III-3). The cloudy air is pumped into the collector and cloud droplets impact onto a collection plate. The water then falls down into the collection vessel. Afterwards, the collected cloud water is transferred into a sterilized bottle and the analysis are performed in the lab. A new cloud water collector has been developed to increase the efficiency of collection since 2014 (see in Figure III-4). Cloud droplets impact on three collection plates that are vertically positioned. Impacted cloud droplets fall down into a sterilized bottle placed below. Cloud water samples during 2015-2019 were conducted with this new cloud water collector that is around 3 times more efficient (around 150 mL of water in average, depending on the droplet radius and the liquid water content).

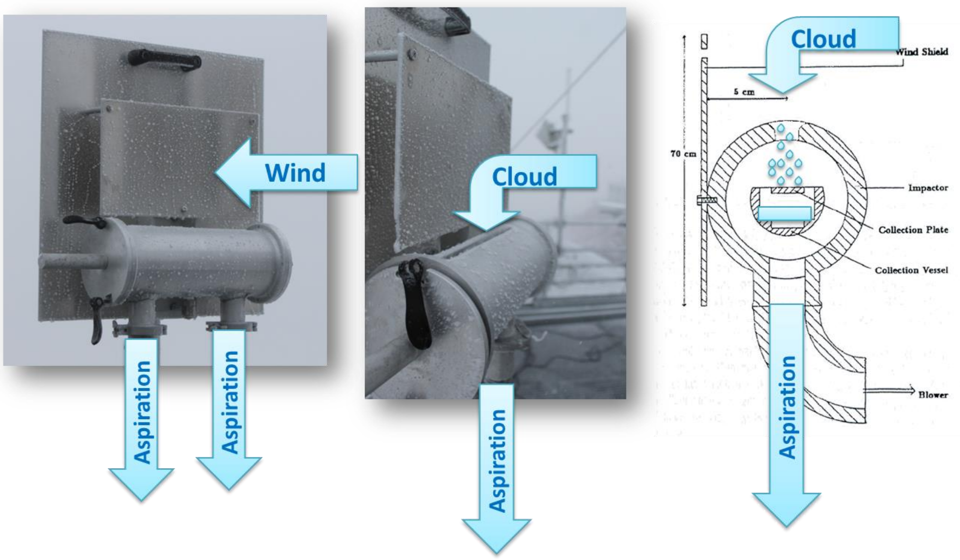

Figure III-3 One-stage cloud water impactors of LaMP.

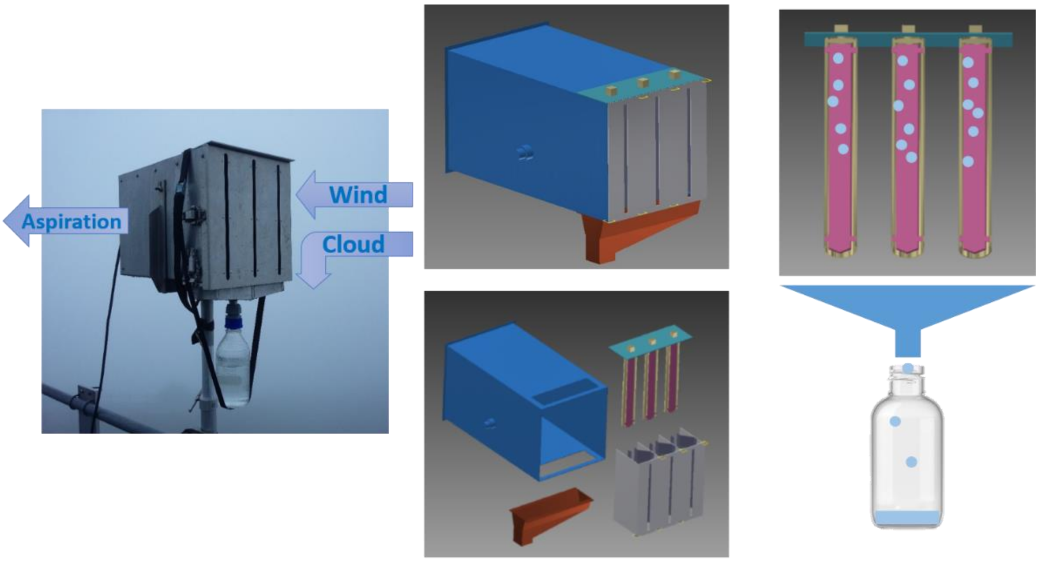

Figure III-4 The new cloud water collector of LaMP.

Air sampling has been conducted since 2010 at PUY station using Tenax® TA cartridges with a total sample number of 659. Before sampling, Tenax® TA cartridges need a pre-conditioning step in order to prevent any contamination from the sorbent. The sampling was carried out by using SASS with a controlled flow rate of 100 mL min^{-1} for duration of 40-180 min dependent on the target species. Between 2011 and 2014, several simultaneous samplings of cloud water and gas were carried out at PUY station in order to investigate the partitioning of VOC in air/cloud droplet phases.

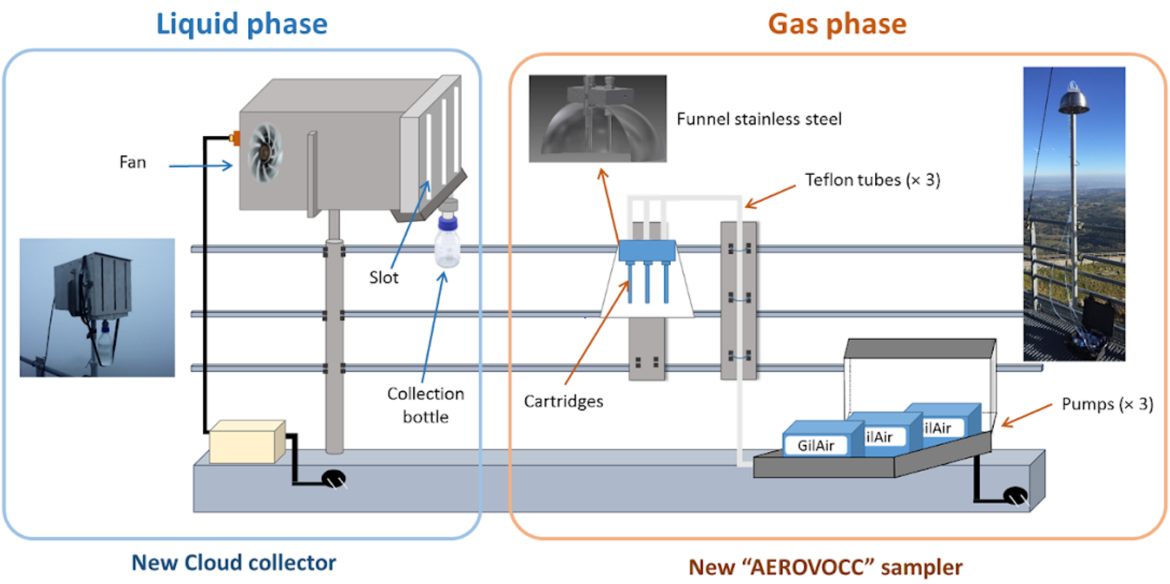

Figure III-5 New system for simultaneous sampling in both gas and liquid phases.

A new system was developed in 2018 for sampling gaseous VOC/OVOC in parallel to cloud collector. This system allows to explore VOC and more specifically OVOC in both gas and liquid phases under cloudy condition (see in Figure III-5). This newly developed gas sampler called AEROVOCC (AEROsol Volatile Organic Compounds Cloud) benefited from the technical support of the IAD Pole at LaMP and the STD at OPGC. AEROVOCC can collect gaseous VOC/OVOC (–C=O and –OH functional groups) simultaneously by deploying three types of sorbent tubes: Tenax® TA sorbent tube, PFBHA pre-coated sorbent tube and MTBSTFA pre-coated sorbent tubes (see in CHAPTER II). Those cartridges are connected with a Gilan pump with a controlled flow rate of 100 mL min^{-1} for a sampling duration between 40 and 180 min. Cloud sampling is performed with simultaneously the new cloud collector presented above. Several samplings have been conducted at PUY station (in October 2018 and in February of 2019).

As explained before, an intensive field campaign at La Réunion Island was conducted in March and April in 2019 as part of the BIO-MAIDO Project. The AEROVOCC system was deployed with the cloud collector. Some technical adaptions have been made since they needed to be installed on a 10 m mast in the field. Meteorological probes (T, P, wind speed and direction) and a CDP (Cloud Droplet Probe) for microphysical cloud parameters (droplet distribution, LWC) from the CNRM laboratory (Toulouse, France) was also installed on the mast. Figure III-6 presents the system installed on the slope of the mountain at La Réunion Island.

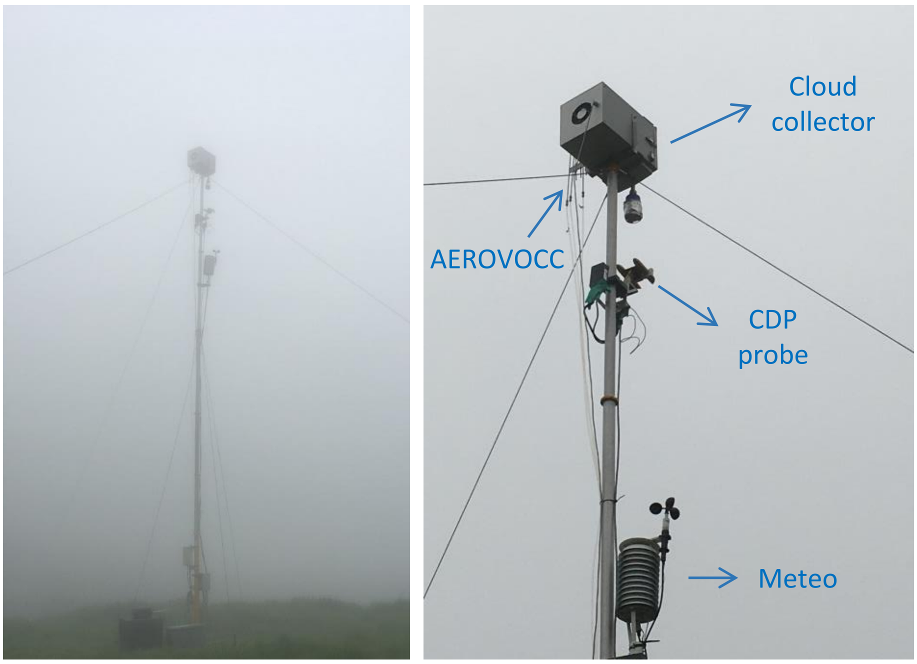

Figure III-6 Presentation of the instruments deployed during the BIOMAIDO field campaign in 2019 for collecting gaseous compounds and cloud droplets.

III.2 Distribution and seasonal variation of gaseous VOC at PUY

III.2.1 VOC distribution at PUY

Gaseous VOC measurements have been conducted at PUY since 2010 including June and July of 2010, March and April of 2011, January, February, June and July of 2012 and 2013 at PUY station. The distribution of concentration values between 2010 and 2013 for some major anthropogenic and biogenic compounds are reported in Figure III-7. The median concentrations are rather low and lie between 0.04 and 0.15 ppb. The systematic presence of isoprene and pinenes which have the lowest residential time point out their probable local origin. Note that the distribution of the compounds is quite scattered with average values usually equal or above the 75th percentile. One reason might be the alternation between the boundary layer (BL) and the free troposphere (FT) (see below for further discussion).

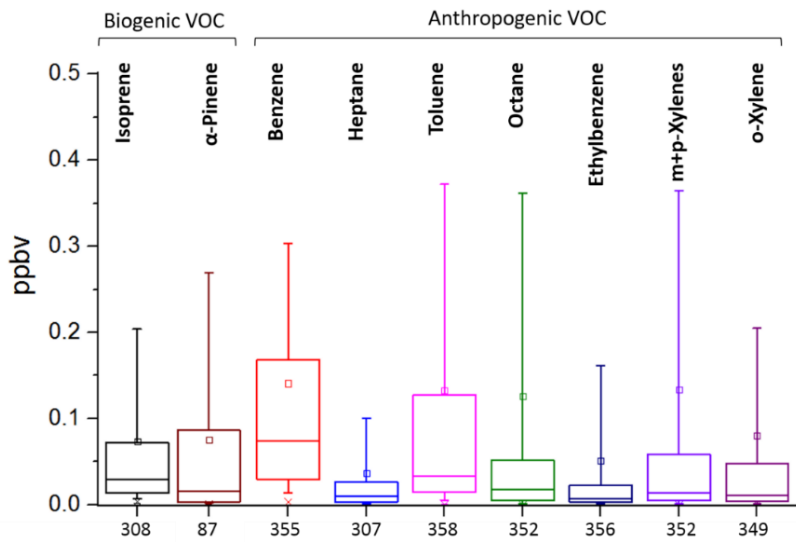

Figure III-7 Distribution of major gaseous VOC concentrations (ppbv) during 2010-2013 at PUY station. The number of samples analyzed is indicated under each box plot. The bottom and top of box plots are the 25th and 75th percentiles, respectively. The full line and the open square symbol represent the median and mean values, respectively. The "-" represents 10th and 90th percentiles.

III.2.2 Seasonal variation of VOC at PUY

The seasonal variation of VOC at PUY station is shown in Figure III-8 from the data collected in June-July and January-February 2012 and 2013. While the median concentrations are still low, all VOC concentrations show a clear seasonal cycle with higher summertime concentrations (0.05-0.17 ppbv) compared to the wintertime ones (0.001-0.07 ppbv). The distribution is more scattered in summer than in winter. The distribution is controlled by primary emissions, dynamics and chemistry. The distribution of isoprene and pinenes seem to be mainly controlled by their local biogenic emissions which are usually favored in summer due to the higher temperatures and/or solar radiation as described in CHAPTER I in Section I.2.1.4. Note that α-pinene is only detected in summer with a high median concentration of about 0.13 ppb. On the opposite, the distribution of anthropogenic VOC like aromatics show an opposite trend to the seasonal cycle of their emissions in northern mid latitudes which are usually higher in winter due to combustion heating. The cyclic alternation of the BL/FT in summer is expected to bring higher loads of anthropogenic VOC compared to the wintertime period. This effect has been investigated in the following section.

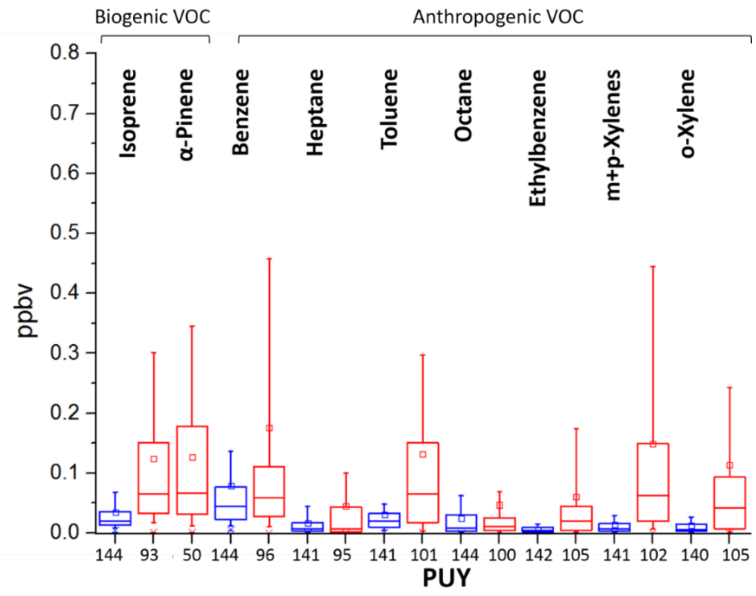

Figure III-8 Distribution of VOC concentrations (ppbv) in summer (red boxplots) and in winter (blue boxplots) 2012 and 2013 at PUY station. The number of samples analyzed is indicated under each box plot. The bottom and top of box plots are the 25th and 75th percentiles, respectively. The full line and the open square symbol represent the median and mean values, respectively. The "-" represents 10th and 90th percentiles.

III.2.3 Investigation of the influence of the FT/BL alternation on the VOC distribution at PUY

There is no direct measurements of the boundary layer height at the PUY station. In the frame of Antoine Farah's PhD (2018), an indirect evaluation of the boundary layer height was performed by using different criteria: the analysis of LIDAR profiles, the radon concentrations, the ratio of NOx to CO concentrations and the European Center for Medium-Range Weather Forecasts (ECMWF) model outputs. This indirect evaluation helps in distinguishing periods where the PUY station is estimated within the BL or FT. Results from Farah et al. (2018) show that the PUY station is located in the BL with frequencies ranging from 50% during the winter, up to 97% during the summer. For July 2015, Figure III-9 shows that the top of puy de Dôme is most of the time located in the boundary layer.

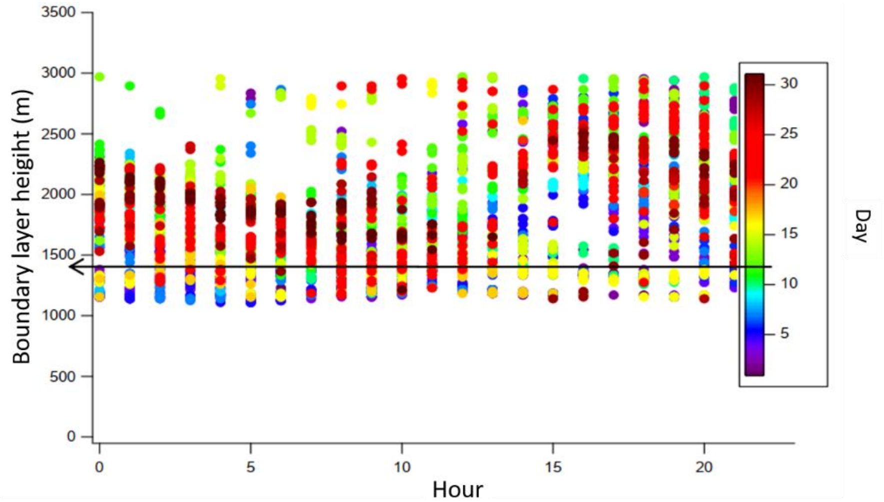

Figure III-9 Evolution of the boundary layer height as a function of the time (shown with local time in hour) during the July of 2015.

On this basis, the concentrations of VOC in July of 2015 was segregated between BL and FT periods for July 2015 (see in Figure III-10). The distribution in the BL is more scattered than in the FT; higher concentrations of all VOC are observed in the BL than in the FT. This suggests that the BL air masses are more freshly loaded in VOC precursors emitted by primary sources at the surface. The lower levels in the FT are more representative of the clean atmosphere after VOC photochemical depletion.

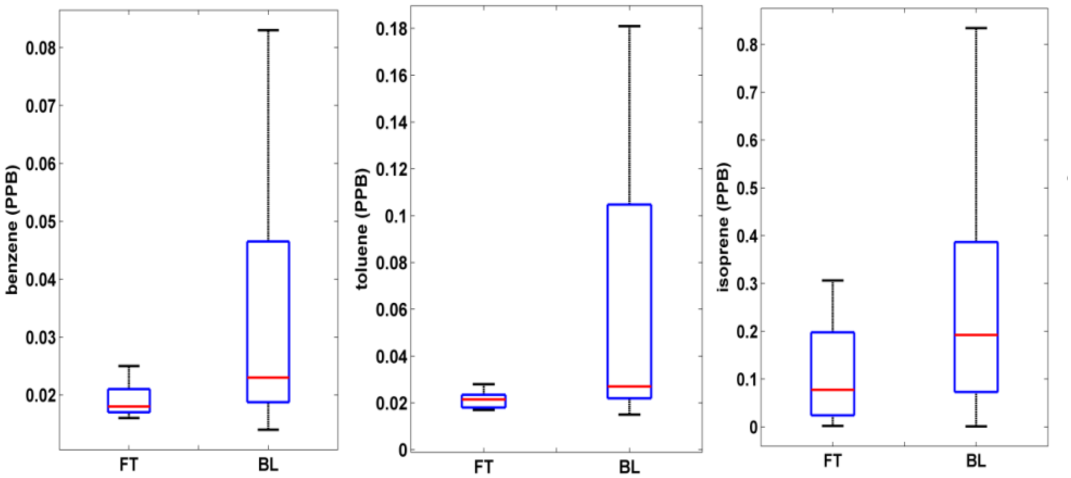

Figure III-10 Distribution of a selection of VOC in the free troposphere (FT) and in the boundary layer (BL) (from the thesis of A. Farah, 2018).

Figure III-11 reports the temporal evolution of isoprene concentration levels with the height of the BL in July 2015 and ambient temperature. Temperature is known to control the biogenic emissions of isoprene as described in CHAPTER I (see in Figure I-3). Isoprene concentrations show their typical diurnal cycle with maxima concentrations in the middle of the day and low concentrations at night and before 9:00 AM. However, the increase of isoprene is delayed compared to the one of temperature known to be one of the main driver controlling its biogenic emissions along with solar radiation. This delay is well marked on July 11th and July 12th. Isoprene is expected to be locally emitted by the trees at lower altitudes and reaches the puy de Dôme summit later in the day along with the development of the height mixing layer isoprene at night by ozone and nitrates.

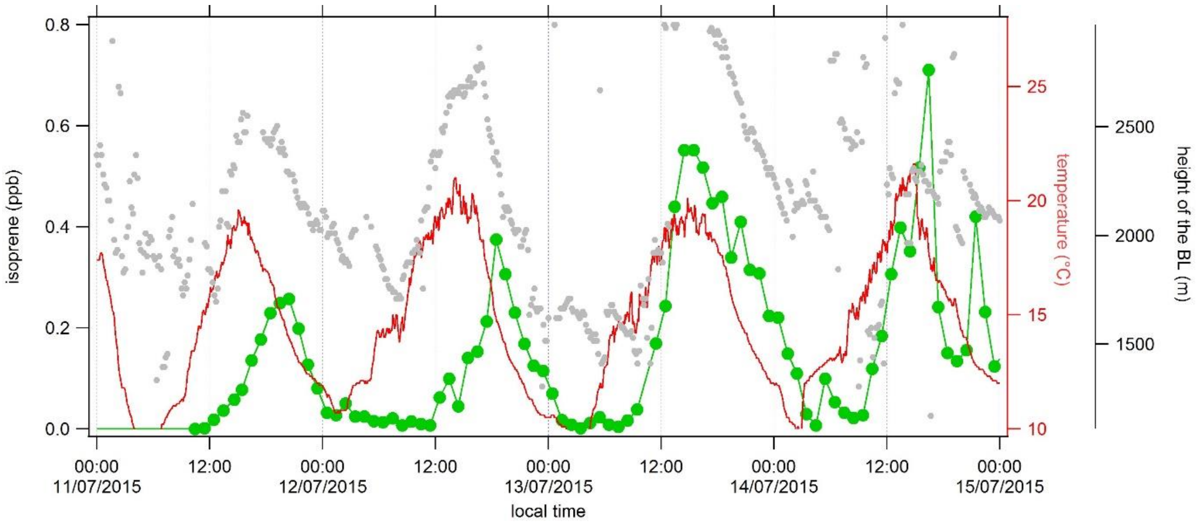

Figure III-11 Diurnal evolution of isoprene concentration (in green) at PUY in July 2015 along with ambient temperature (in red) and boundary layer (BL) height (in grey).

Figure III-12 reports the scatterplot between toluene and benzene concentrations during winter and summer for the whole period of measurements. The ratio toluene-to-benzene is a useful indicator of air mass aging, toluene being 5 times more reactive than benzene relative to the oxidation by $HO^{\bullet}$ radicals. The wintertime and summertime urban toluene-to-benzene emission ratios (ER) are also reported (Borbon et al., 2013; Shnitzhofer et al., 2008). These values correspond to fresh air masses representative of the urban emission mixing before photochemical processes occur. As the air mass ages, the toluene-to-benzene ratios are expected to decrease to values below the urban emission ratio ones. In summer, the scatterplot at PUY sometimes lies along the urban ER line (in red) indicating the influence of fresh air masses probably favored by an efficient vertical mixing height and weak photochemistry. However, the scatterplot spread below the urban ER most of the time, due to photochemical aging. In winter, the scatterplot is always below the urban ER indicating the dominant presence of clean air masses at PUY for free tropospheric conditions. The toluene-to-benzene scatterplot highlights the diversity of air mass ages sampled at PUY from clean to polluted conditions.

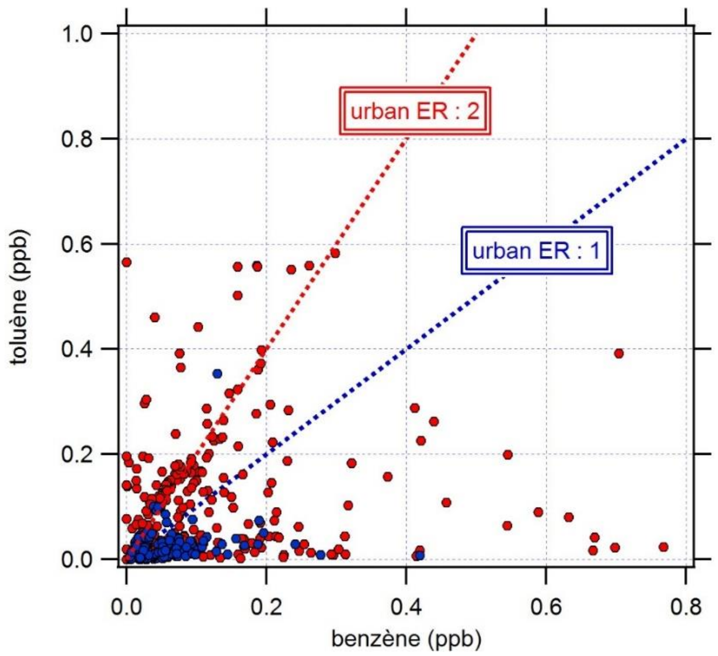

Figure III-12 Scatterplot of toluene to benzene concentrations in winter (blue dots) and in summer (red dots) from VOC data collected between 2010 and 2015 at PUY station. The urban emission ratios (ER) are the ones provided by Schnitzhofer et al. (2008) in a highway tunnel in Europe.

To conclude, the observed scattered distribution of VOC at PUY (see Figure III-7 and Figure III-8) seems to be strongly affected by the summertime alternation of the BL/FT height.

III.2.4 Comparison of VOC concentrations at PUY with other GAW sites

Gaseous VOC measurements are also conducted at two other Global Atmosphere Watch (GAW) program sites in Europe at high and low altitudes: (1) Mt. Cimone (2165 m a.s.l.) (CMN), the highest peak of the Northern Apennines influenced by two distinct climatic regions (continental Europe and Mediterranean Basin) and (2) Hohenpeißenberg station (HPB) (980 m a.s.l.), located at pre-Alpine hill and sticking out 300 m above the surrounding forest/grassland and representative of rural central European environment (see in Figure III-13). VOC concentrations at these two sites are continuously measured by on-line GC-FID. The VOC data have been extracted from the EBAS database (http://ebas.nilu.no/Default.aspx) for the period 2010-2013 (from January to December). The levels and the seasonal variations between the three stations have been compared.

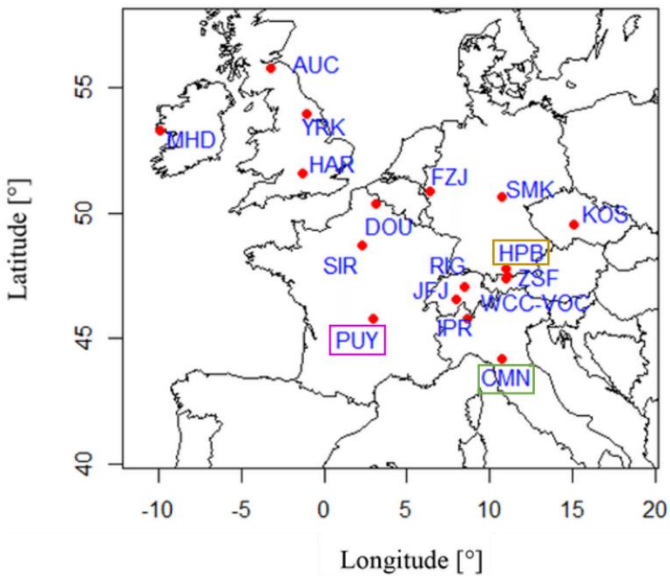

Figure III-13 Location of other Global Atmosphere Watch program sites: Mt. Cimone station (CMN) in green frame, Hohenpeißenberg station (HPB) in yellow frame and PUY station in pink frame.

The concentrations of VOC at PUY are usually higher and much more variable than the ones at CMN station and at HPB station (see in Figure III-14). However, the concentrations are in the same range of order (see in Figure III-14 and Table A.9 in Appendices) especially when looking at the medians between PUY and HPB. At midday, HBP is considered to be in a vertically fully developed mixed-layer (Leuchner et al., 2015). The lowest concentration levels are reported at Mt. Cimone which can be considered as representative of free tropospheric conditions and often under the influence of the Mediterranean basin/south Europe air masses (Bonasoni et al., 2000; Henne et al., 2010).

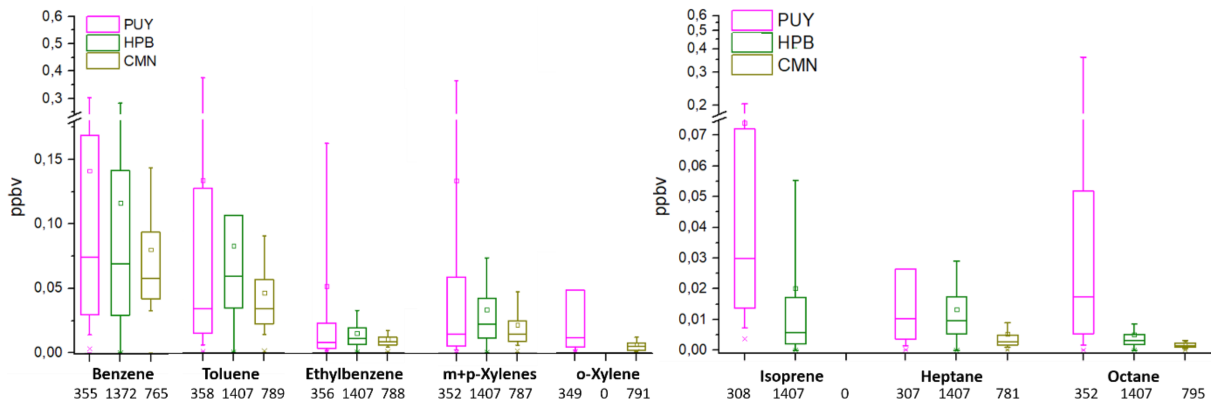

Figure III-14 Distribution of VOC concentrations (ppbv) for 2010-2013 measured at PUY station (pink boxplots), HPB station HPB station (green boxplots) and CMN (yellow boxplots). The number of samples analyzed is indicated under each box plot. The bottom and top of box plots are the 25th and 75th percentiles, respectively. The full line and the open square symbol represent the median and mean values, respectively. The "-" represents 10th and 90th percentiles.

The seasonal comparison for summer and winter 2012 and 2013 of these three stations show remarkable differences (see in Figure III-15 and Figure III-16). On the one hand, the seasonal variation of isoprene is consistent at PUY and HPB stations in line with the seasonal cycle of its well-known biogenic emissions which are light and temperature dependent as already discussed in the previous sections (Figure I-3). This cycle also points out the influence of the BL at both sites regarding the significant reported levels of several tens of ppt. On the other hand, the seasonal variation of anthropogenic VOC at PUY shows an opposite trend to the ones at the two other stations. Indeed, the highest levels are observed in winter at both HPB and CMN stations, a typical feature of northern mid latitude atmosphere. This seasonal cycle is usually explained by the longer residence time of VOC in winter due to weaker photochemistry and higher emission rates with increasing combustion activities. Again, the opposite seasonal cycle observed at PUY, highlights the influence of the BL/FT alternation in favor of higher loading in summer: 50% of the time in the FT in winter *versus* 97% of the time in the BL in summer. By segregating BL and FT, vertical dynamics are a key factor controlling the VOC distribution at PUY station.

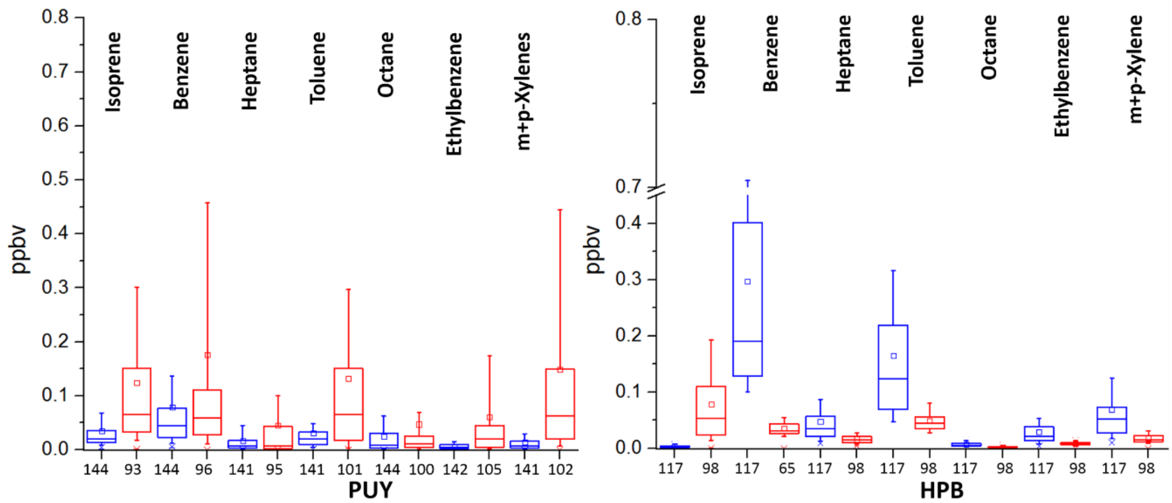

Figure III-15 Seasonal distribution of VOC concentrations (ppbv) in summer June and July (red boxplots) and in winter January and February (blue boxplots) 2012 and 2013 at PUY (A) and HPB (B) for VOC. The number of samples analyzed is indicated under each box plot. The bottom and top of box plots are the 25th and 75th percentiles, respectively. The full line and the open square symbol represent the median and mean values, respectively. The "-" represents 10th and 90th percentiles.

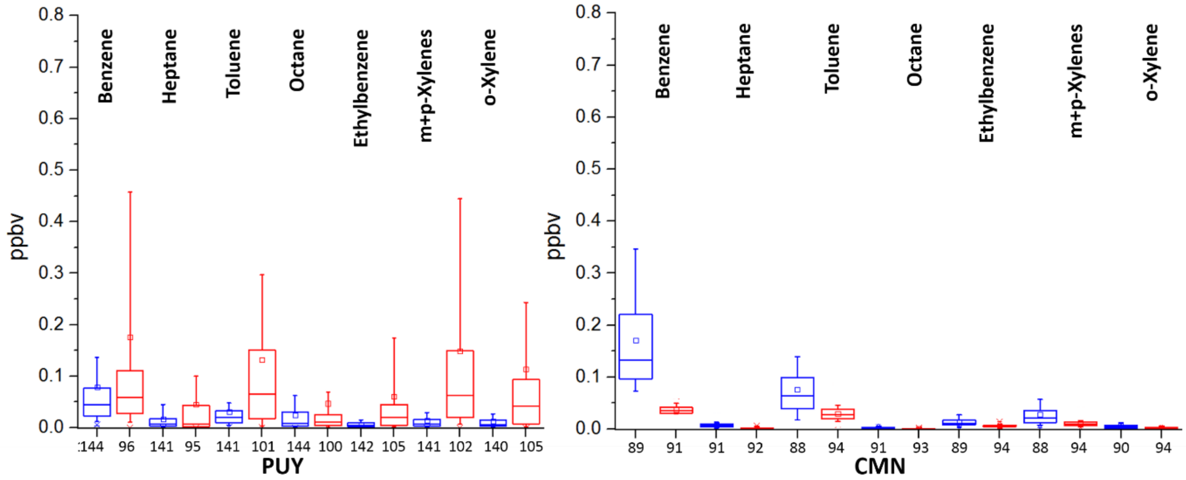

Figure III-16 Seasonal distribution of VOC concentrations (ppbv) in summer June and July (red boxplots) and in winter January and February (blue boxplots) 2012 and 2013 at PUY (A) and CMN (B) for VOC.

Table III-1 Comparison of VOC concentrations (min-max, mean value) in gaseous at PUY, HPB and CMN stations (pptv) during 2012 and 2013 (/: below detection limit).

	PUY					
	Winter			Summer		
pptv	Min	Max	Mean	Min	Max	Mean
Isoprene	2.1	535.2	35.0	1.5	1391.8	124.6
a-pinene	/	/	/	1.5	457.0	127.3
Benzene	0.5	815.2	79.2	0.1	3287.9	176.5
Ethylbenzene	0.1	38.4	7.0	0.0	762.7	61.1
	HPB					
	Winter			Summer		
pptv	Min	Max	Mean	Min	Max	Mean
Isoprene	/	31.8	4.3	0.7	391.1	78.5
Benzene	/	999.6	297.0	/	105.6	36.2
Ethylbenzene	/	276.4	29.7	/	24.4	9.0
m+p-Xylenes	/	1089.4	68.9	/	60.1	18.4
	CMN					
	Winter			Summer		
pptv	Min	Max	Winter	Min	Max	Summer
Benzene	39.4	702.2	171.4	21.6	63.8	37.6
Ethylbenzene	2.3	56.2	13.7	2.2	14.5	6.8
m+p-Xylenes	2.4	164.7	28.3	3.3	50.0	11.4

III.3 Evaluation of air/droplet partitioning for VOC at PUY

In this section, a first evaluation of the air/droplet partitioning of VOC are presented based on specific field campaigns organized at the puy de Dôme station. A selection of anthropogenic and biogenic compounds have been analyzed in this frame. They include benzene, toluene, ethylbenzene and xylenes

(BTEX) as well as biogenic species like isoprene and other terpenes. These compounds are usually detected in the gas phase but are not expected to be present in the aqueous phase due to their low solubility. Indeed, previous works have highlighted the accumulation of hydrophobic compounds in the aqueous phase of fogs (Valsaraj, 1988a, 1988b , 1993) and the objective was to investigate this point at the puy de Dôme station for cloud under remote condition. Beyond the health impact for some of them, like benzene, these compounds are also well-known to contribute to the formation of secondary pollutants like ozone and SOA (Hu et al., 2008; Fu et al., 2009). A description of the sampling is first proposed; then gaseous and aqueous concentrations are discussed and finally the partitioning of those species are evaluated and discussed. This work is under revision in the journal Atmospheric Research (minor revision).

III.3.1 Cloud and gaseous sampling

Between 2011 and 2014, several simultaneous samplings of cloud water and gas were performed. Table III-2 summarizes sampling dates and durations for clouds sampled during this period. Among one single cloud event, up to 3 different samples were collected, equaling a total of 16 samples.

Table III-2 Cloud sampling dates and durations. C stands for "Cloud events" and S stands for "Samples" collected during one single cloud event.

Cloud samples	Sampling date	Sampling beginning time	Sampling ending time	Sampling duration (min)
C1	06/25/2012	15:34	19:00	206
C2	09/13/2012	09:50	11:50	120
C3	10/10/2012	08:45	10:40	115
C4	05/22/2013	09:40	12:55	195
C5 S1	03/22/2014	07:35	11:00	205
C5 S2	03/22/2014	11:00	14:00	180
C6 S1	03/25/2014	11:05	13:00	115
C6 S2	03/25/2014	13:15	15:05	110
C6 S3	03/25/2014	19:22	20:30	78
C7 S1	03/26/2014	07:40	09:10	90
C7 S2	03/26/2014	09:20	11:00	100
C8 S1	04/04/2014	19:45	21:45	120
C8 S2	04/04/2014	21:45	00:00	135
C9 S1	04/05/2014	1:30	04:05	155
C9 S2	04/05/2014	04:05	07:00	175
C9 S3	04/05/2014	07:00	09:40	160

Table III-3 presents gas sampling that has been performed in parallel to cloud sampling. Among the 16 cloud samples, 5 gaseous samples were simultaneously collected. The volume in L of air sampled for the cloud sampling and the air sampling are indicated. The resulting volumes of collected water are also indicated in mL as well as the times where the sample have been performed.

Table III-3 Among the 16 cloud samples (presented in previous table), five cloud samples present simultaneous air samples. Sampling times (beginning and ending) are indicated for air samples (orange lines) and cloud samples (blue lines). For each air sample, 18L of air has been pumped into the cartridge and is indicated in grey lines. For cloud samples, the volume of air that have been pumped is also indicated and the obtained cloud water volume is indicated as well.

Volume of cloud water	90 mL	100 mL	130 mL	70 mL	100 mL	Cloud sampling
Volume of air	273300 L	180000 L	206600 L	233300 L	166600 L	
	07H35 – 11H00	21H45 – 00H00	01H30 – 04H05	04H05 – 07H00	07H00 – 09H40	
	07H30 – 11H00	22H00 – 01H00	01H00 – 04H00	04H00 – 07H00	07H00 – 10H00	Air sampling
Volume of air	18 L	18 L	18 L	18 L	18 L	
	C5 S1 22/03/2014	C8 S2 04/04/2014	C9 S1 05/04/2014	C9 S2 05/04/2014	C9 S3 05/04/2014	

III.3.2 History of the air masses: classification of sampled clouds

16 cloud samples corresponding to 9 cloud events sampled between 2011 and 2014 at different seasons were classified by the same approach described in Deguillaume et al. (2014) using principal component analysis (PCA) with hierarchical clustering analysis (HCA). This classification is based on the chemical properties of the aqueous phase and is also confronted to backward trajectories that give information on the air mass history.

Routine analysis has been effected on these cloud samples. pH is determined immediately after sampling. Main inorganic cations (Na^+, NH_4^+, K^+, Mg^{2+}, Ca^{2+}) and anions (Cl^-, NO_3^-, SO_4^{2-}, PO_4^{3-}) as well as short chain carboxylic acids (formate, acetate, succinate, oxalate) are measured by ion chromatography (IC). An analyzer measuring the total organic carbon concentration allows to evaluate the organic matter amount in cloud water. All chemical properties of the 9 cloud waters collected are summarized in Table III-4. Liquid water content (LWC) is also given in the same table, which is averaged over the sampling period.

Table III-4 Chemical and physical properties of the 16 cloud waters collected at the PUY station. Liquid water content (LWC) is averaged over the sampling period. Note that ND means "not determined" in samples, BDL means "below detection limit", Mar means "marine" and Cont means "continental".

Cloud sample	**Cat.**	**LWC (g/m^3)**	**pH**	**TOC mgC/L**	**SO_4^{2-} µmol/L**	**NO_3^- µmol/L**	**Cl^- µmol/L**	**Acetate µmol/L**	**Formate µmol/L**	**Oxalate µmol/L**	**Succinate µmol/L**	**Na^+ µmol/L**	**NH_4^+ µmol/L**	**Mg^{2+} µmol/L**	**K^+ µmol/L**	**Ca^{2+} µmol/L**
C1	Mar	ND	5.52	ND	1.15	3.02	0.93	BDL	18.23	3.32	BDL	5.99	77.85	2.22	4.02	4.33
C2	Mar	ND	5.89	ND	0.49	1.01	1.03	3.23	3.24	1.04	BDL	8.81	16.82	1.35	5.53	4.51
C3	Mar	ND	6.22	ND	5.33	10.95	26.73	4.00	13.58	0.74	BDL	21.22	39.31	8.33	7.57	2.34
C4	Mar	ND	4.90	ND	43.39	43.16	9.58	11.94	14.86	3.19	BDL	6.03	90.83	5.16	2.40	14.06
C5 S1	Mar	0.38	6.67	2.90	34.77	24.68	65.73	13.33	48.28	4.13	0.14	20.92	87.56	12.38	2.33	4.72
C5 S2	Mar	0.21	6.65	5.39	37.13	23.73	133.79	20.40	43.84	5.42	0.21	36.76	108.75	8.67	4.94	6.64
C6 S1	Mar	ND	6.6	3.42	49.17	19.03	228.45	13.77	30.58	3.17	0.13	56.79	73.24	10.34	9.12	7.13
C6 S2	Mar	0.08	6.4	6.02	32.60	18.98	153.78	13.97	65.11	3.31	0.16	38.84	79.56	12.48	6.43	6.92
C6 S3	Mar	0.19	6.1	8.66	14.79	21.29	72.96	12.49	64.99	3.75	0.19	20.78	50.22	13.57	4.04	9.43
C7 S1	Cont	0.47	5.5	6.52	56.42	219.64	25.17	26.19	38.32	5.91	0.75	9.64	252.35	7.23	2.92	7.91
C7 S2	Cont	0.11	5.4	8.60	45.42	205.61	26.46	15.82	34.94	5.27	0.71	8.33	206.03	8.98	2.37	15.64
C8 S1	Mar	0.35	6.24	1.52	13.54	19.98	19.42	9.58	23.59	3.37	0.43	5.03	39.62	5.37	7.78	BDL
C8 S2	Mar	0.35	6.53	1.71	18.19	37.35	18.22	7.17	24.16	3.79	0.28	3.9	71.44	4.33	7.09	BDL
C9 S1	Mar	0.34	6.60	2.60	26.02	72.62	29.36	14.26	32.49	4.43	0.29	6.88	124.07	4.43	7.41	0.00
C9 S2	Mar	0.34	6.88	3.87	39.77	131.85	48.67	25.42	48.80	6.87	0.39	12.60	192.77	4.27	4.79	0.00
C9 S3	Mar	0.35	6.80	4.53	67.47	133.11	76.08	30.41	63.37	7.42	0.48	18.02	212.73	5.30	4.25	2.03

Principal Component Analysis (PCA) is performed with XlStat, an add-in package of Microsoft Excel (Addinsoft. XLSTAT 2016: Data Analysis and Statistical Solution for Microsoft Excel.; Paris (France), 2016.). The dataset is autoscaled by the software and Pearson correlation coefficient is used. The PCA loadings are calculated as linear combinations of the variables (pH, concentration of Cl^- , NO_3^- , SO_4^{2-}, Na^+ and NH_4^+) and the number of factorial axes retained for the analysis is of two on the basis of the cumulated variability. The combined plot of scores and loadings allows us to identify groups of samples with similar behavior and the existing correlation among the original variables. Hierarchic Cluster Analysis (HCA), using Euclidean square distance and Ward method, was used on reduced and centered data to assign samples to the classes defined by Deguillaume et al. (2014) “marine”, “highly marine”, “continental” and “polluted”. Back trajectory plots are calculated to confirm the statistical classification.

To do this, the air mass origin for each cloud event is calculated using 72 h back-trajectories obtained by the NOAA HYSPLIT (Hybrid Single Particle Lagrangian Integrated Trajectory Model) Trajectory Model using GDAS (Global Data Assimilation System) (1 degree, global, 2006–present) archive and default settings (Draxler and Rolph, 2012). All the backward trajectories are plotted below: the direction of air mass before arriving at the summit of the puy de Dôme Mountain is drawn in red and blue for all samples (calculated at the beginning of the cloud sampling and at the end of cloud sampling, respectively). Black line corresponds to terrain height (see in Figures A.10 in Appendices).

Among all cloud events, the majority was classified as “marine” clouds, except for one cloud event sampled on March 26th, 2014 classified as “continental”. This is explained by higher concentrations of NH_4^+ and NO_3^- that are typical of continental emissions. Cloud events classified as marine show air mass back-trajectories coming from different sectors: west, northwest/north, and south/southwest. The “continental” cloud event is characterized by a back-trajectory coming from the west/northwest sector (see more details in Figures A.10 and Table III-4).

III.3.3 Quantification of VOC in gas and liquid phases

The concentrations of compounds detected in cloud waters are summarized in Table A.11 in Appendices (in ng mL^{-1}). The distributions of VOC concentration values are reported in Figure III-17. The median concentrations are rather low and lie between 0.01 and 2.4 ng mL^{-1}. In average, the total concentration of these chemical compounds represent ~ 0.5 ng mL^{-1}, corresponding to less than 0.1 µmol L^{-1}. These compounds represent in mass a small fraction of the organic carbon in cloud water (less than 0.1% of the measured dissolved organic carbon (DOC)). As a comparison, carboxylic acids measured systematically at the PUY station represent ~ 10% of the measured DOC for cloud classified as marine (Deguillaume et al., 2014). Toluene was the most abundant anthropic compounds in all the samples; cloud event C9 presents the higher concentration observed in this work, reaching 5.77 ng mL^{-1} (by a factor 3 in average).

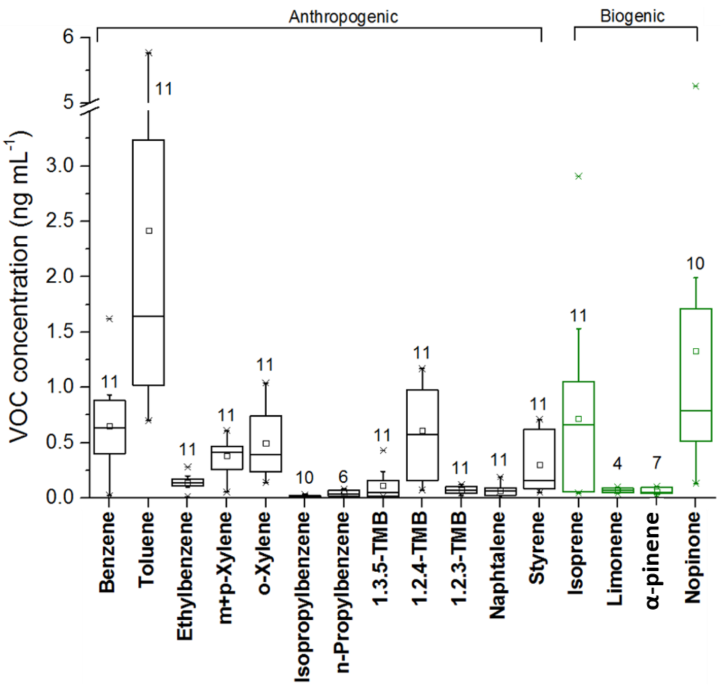

Figure III-17 Distribution of VOC concentrations (ng mL^{-1}) in cloud waters sampled at PUY station for VOC from anthropogenic sources (black boxplots) and from biogenic origin (green boxplots). The number of samples analyzed is indicated above each box plot. The bottom and top of box plots are the 25th and 75th percentiles, respectively. The full line and the open square symbol represent the median and mean values, respectively. The ends of whiskers are 10th and 90th percentiles. The asterisks are maximum and minimum values. Note that 1,3,5-TMB, 1,2,4-TMB, 1,2,3-TMB stand for 1,3,5-trimethylbenzene, 1,2,4-trimethylbenzene and 1,2,3- trimethylbenzene.

Few studies have already reported the presence of hydrophobic VOC from anthropogenic origin in cloud water or fog droplets. Measurements performed at the remote Gibbs peak (Mt. Mitchell State Park, 2006 m a.s.l., USA) have shown average concentrations of ethylbenzene, o-xylene, toluene and trimethyl-benzenes ~ 0.17, 0.45, 0.60 and 0.34 ng mL^{-1} (Aneja, 1993) by GC-MS and GC coupled with Flame Ionization Detector (FID) and Electron Capture Detector (ECD). Other organic compounds like alkanes and polycylic aromatic hydrocarbons (PAH) were also detected in urban fogwater in Dubendörf (Swizerland) (Leuenberger et al., 1988; Capel et al., 1990; Li et al., 2011). At Dubendörf, ethylbenzene, xylenes, trimethylbenzenes were also detected in rain and snow with concentration ranges of 0.015-0.44, 0.02-0.30 and 0.020-0.21 ng mL^{-1}, respectively (Czuczwa et al., 1988). The values at PUY are in the same range of order than the ones reported in those studies (see in Table III-5). Among the selected compounds, nopinone has been already detected in cloud waters sampled at the PUY station (Lebedev et al., 2018) by GC×GC-TOF-MS. In that study, phenols (*i.e.*, phenol, benzyl alcohol, p-cresole, 4-ethylphenol, 3,4-dimethylphenol, 4-nitrophenol) have been quantified in cloud water and present mass concentrations in the same range (0.03 to 0.74 ng mL^{-1}) than compounds detected in this work. Non-targeted analysis by FT-ICR MS in clouds sampled at the same site in previous studies showed the presence of oxidation products of nopinone (Bianco et al., 2018). Additionally, this product was also observed in clouds sampled at the Storm Peak laboratory (Colorado, USA) (Zhao et al., 2013).

Table III-5 Comparison of VOC concentrations (min-max, mean value) in cloud aqueous phases measured at PUY with similar measurements performed at other sampling sites (/: below detection limit.).

Sampling site / Conc. Range (ng mL^{-1})	PUY station	Gibbs Peak	EAWAG
	Mt. puy de Dôme 1465 m a.s.l. France	**Mt. Mitchell State Park 2006 m a.s.l. United States**	**Dübendorf 400 m a.s.l. Switzerland**
	Remote site Cloud	**Remote site Cloud**	**Urban area Rain**
Ethyl-benzene	0.01-0.28 (0.12)	(0.17)	0.02-0.05 (0.04)
o-xylene	0.14-1.04 (0.50)	(0.45)	0.02-0.13 (0.03)
Toluene	0.70-5.77 (2.42)	(0.60)	/
Trimethyl-benzenes	/	(0.34)	/
1,3,5-TMB	0.02-0.43 (0.11)	/	/
1,2,4-TMB	0.07-1.17 (0.61)	/	0.02-0.04 (0.03)
1,2,3-TMB	0.02-0.12 (0.07)	/	/
Naphtalene	0.02-0.19 (0.07)	/	0.02-0.04 (0.03)

Detected VOC were mostly primary aromatics (benzene, toluene, ethylbenzene, xylenes) and terpenoïds (isoprene, limonene, α-pinene and nopinone). These compounds are known to be present in the gas phase. These families of compounds are released into the atmosphere by either anthropogenic or biogenic sources. Aromatics are usually related to fossil fuel combustion and evaporation emissions as well as solvent use related activities (Borbon et al., 2018). Terpenoïds are released by terrestrial vegetation. On the one hand isoprene is emitted by deciduous trees and is light and temperature dependent. Terpenes are emitted by conifers (Fuentes et al., 2000). Nopinone is a secondary product of biogenic compounds oxidation (Cahill et al., 2006). Those compounds have been detected in the gaseous samples that have been collected in parallel with cloud samples. The range of concentrations of VOC detected both in cloud and air samples are presented in Figure III-18. Toluene, benzene, isoprene and nopinone which are the most abundant in the gas phase also show the highest concentrations in cloud droplets. Samples were collected during spring 2014 when biogenic emissions begin to increase, which may explain the large presence of biogenic compounds in the multiphasic samples. Nopinone is a secondary products resulting from the oxidation of for example β-pinene by the hydroxyl radicals ($HO^•$) (Aschmann et al., 1998; Fry et al., 2009); this last compound is surely consumed, possibly explaining its absence in the collected samples.

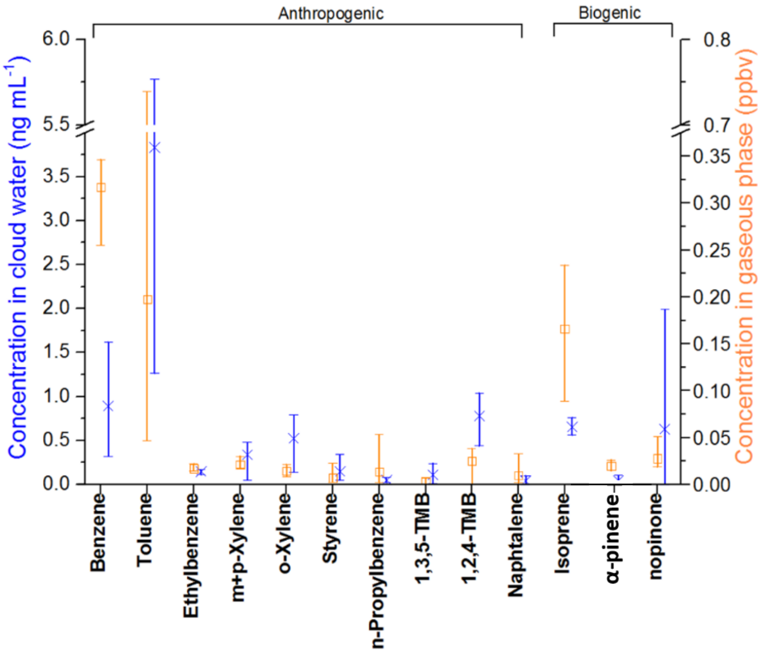

Figure III-18 Concentration variability of VOC in gas phase in ppbv (in orange) and in cloud water samples in ng mL-1 (in blue) during parallel sampling periods of 2014 at PUY station (clouds number C5 S1, C8 S2, C9 S1, C9 S2 and C9 S3). The top and bottom of line are maximum and minimum values. The square and asterisk symbols represent the mean values of VOC in gas phase and in cloud water samples, respectively.

Gaseous VOC measurements were also conducted in other Global Atmosphere Watch (GAW) program sites such as: (1) Mt. Cimone (2165 m a.s.l.) (CMN), the highest peak of the Northern Apennines influenced by two distinct climatic regions (continental Europe and Mediterranean Basin) and (2) Hohenpeißenberg station (HPB) (980 m a.s.l.), located at pre-Alpine hill and sticking out 300 m above the surrounding forest/grassland and representative of rural central European environment. Gaseous VOC concentrations at these two sites by GC-FID online measurements have been extracted from the EBAS database (http://ebas.nilu.no/Default.aspx) averaged over the period of March and April 2014 where the cloud samples have been collected. Mount Cimone during this period can be considered as representative of free tropospheric conditions and often under the influence of the Mediterranean basin/south Europe air masses (Bonasoni et al., 2000; Henne et al., 2010). This confirms the fact that VOC concentrations monitored at CMN are in the same range of order as what is observed at the PUY station for the cloud samples from marine origin. Concentrations monitored at the HPB station are also similar to the ones from the PUY station; this is explained by the remoteness of the HPB (see in Table III-6).

III.3.4 Calculation of the partitioning coefficient "*q*"

As described in CHAPTER I in Section I.5.3, to determinate the deviation from thermodynamic equilibrium, the partitioning of chemical compounds between the gas and aqueous phases can be represented by a partitioning coefficient q, defined by Audiffren et al. (1998) and used in other studies such as in van Pinxteren et al. (2005) and Rose et al. (2018) which is defined as:

$$q = \frac{C_{aq}}{LWC \times H_{eff} \times R \times T \times C_{gas}} \qquad \text{(Eq.1)}$$

Where C_{aq} and C_{gas} are, respectively, the gaseous and aqueous concentrations of compound of interest in molec cm^{-3}, the LWC liquid water content of the cloud event in vol / vol. H_{eff} is the effective Henry's law constant in M atm^{-1} and R = 0.08206 atm M^{-1} K^{-1}.

This factor q indicates whether X is at the Henry's law equilibrium (q = 1), undersaturated in the aqueous phase (q < 1) or supersaturated in the aqueous phase (q > 1).

The q factors for the selected VOC characterized in this study are estimated using gaseous and aqueous measurements of these compounds, considering the temperature during the sampling and the mean LWC. H_{eff} are also used in this study and are extracted from the database presented in Sander (2015); calculations are presented in Table III-7.

The partitioning between the gas and aqueous phases cannot be described by a thermodynamic equilibrium assumption (Ervens, 2015). The factor q can evolve with time, since cloud microphysical properties, mass transfer and chemical reactivity modify the partitioning of the species in the gas and aqueous phases. Figure III-19 shows that hydrophobic VOC measured in this study are all largely supersaturated by a factor of 1-3000 compared to Henry's law equilibrium (q = 1).

Table III-6 Comparison of VOC concentrations (min-max, mean value) in gaseous phases measured at PUY with similar measurements performed at other sampling sites (/: below detection limit).

Sampling site / Conc. Range (ppb)	PUY station	Observatorium Hohenpeißenberg	Po Valley Observatory
	Mt. puy de Dôme 1465 m a.s.l. France	**Hohenpeißenberg 977 m a.s.l Germany**	**Mt Cimone 2165 m a.s.l. Italy**
	Remote site Air	**Remote site Air**	**Remote site Air**
Benzene	0.26-0.35 (0.32)	0.06-0.30 (0.13)	0.13-0.19 (0.16)
Toluene	0.05-0.74 (0.20)	0.02-0.33 (0.81)	0.02-0.08 (0.05)
Ethylbenzene	0.02-0.03 (0.02)	0.01-0.04 (0.02)	0.00-0.01 (0.01)
(m+p)-Xylene	0.02-0.03 (0.02)	0.01-0.12 (0.03)	0.00-0.02 (0.01)
o-Xylene	0.01-0.02 (0.01)	/	0.00-0.01 (0.01)
Isoprene	0.09-0.23 (0.17)	0.01-0.08 (0.01)	/

Table III-7 Summary of all parameters: average measured LWC, experimental concentrations of detected VOC in air ("gas") and aqueous ("aq") phases, Henry's law constant at 298.15K, average in situ temperatures measured during each cloud events, partitioning factors q calculated for each cloud events.

VOC	Cloud event/sample	LWC vol/vol	C_{gas} exp molec cm^{-3}_{air}	C_{gas} exp ppbv	C_{aq} exp molec cm^{-3}_{air}	C_{aq} exp ng mL^{-1}	Henry's law constant M atm^{-1} at 298.15 K	$-\Delta H/R$ K	Henry's law constant $Matm^{-1}$ at T_{exp}	T_{exp} K	Partitioning factor q
Benzene	C5 S1	0.38	8.85×10^{9}	0.34	9.37×10^{5}	0.32	1.82×10^{-1}	4.20×10^{3}	6.25×10^{-1}	274.15	1.98×10^{1}
	C8 S2	0.35	6.73×10^{9}	0.26	4.37×10^{6}	1.62	1.82×10^{-1}	4.20×10^{3}	5.88×10^{-1}	275.25	1.40×10^{2}
	C9 S1	0.34	8.38×10^{9}	0.32	2.31×10^{6}	0.88	1.82×10^{-1}	4.20×10^{3}	5.78×10^{-1}	275.55	6.19×10^{1}
	C9 S2	0.34	8.67×10^{9}	0.33	2.44×10^{6}	0.93	1.82×10^{-1}	4.20×10^{3}	5.78×10^{-1}	275.55	6.32×10^{1}
	C9 S3	0.35	9.14×10^{9}	0.35	1.89×10^{6}	0.7	1.82×10^{-1}	4.20×10^{3}	5.44×10^{-1}	276.65	4.78×10^{1}
Toluene	C5 S1	0.38	1.48×10^{9}	0.06	3.13×10^{6}	1.26	1.52×10^{-1}	4.30×10^{3}	5.37×10^{-1}	274.15	4.61×10^{2}
	C8 S2	0.35	2.16×10^{9}	0.08	7.23×10^{6}	3.16	1.52×10^{-1}	4.30×10^{3}	5.05×10^{-1}	275.25	8.41×10^{2}
	C9 S1	0.34	1.95×10^{10}	0.74	7.21×10^{6}	3.24	1.52×10^{-1}	4.30×10^{3}	4.96×10^{-1}	275.55	9.69×10^{1}
	C9 S2	0.34	1.66×10^{9}	0.063	1.28×10^{7}	5.77	1.52×10^{-1}	4.30×10^{3}	4.96×10^{-1}	275.55	2.03×10^{3}
	C9 S3	0.35	1.23×10^{9}	0.047	1.30×10^{7}	5.70	1.52×10^{-1}	4.30×10^{3}	4.66×10^{-1}	276.65	2.85×10^{3}
Ethylbenzene	C5 S1	0.38	4.17×10^{8}	0.016	3.45×10^{5}	0.16	1.32×10^{-1}	4.40×10^{3}	4.80×10^{-1}	274.15	2.01×10^{2}
	C8 S2	0.35	5.89×10^{8}	0.022	2.58×10^{5}	0.13	1.32×10^{-1}	4.40×10^{3}	4.51×10^{-1}	275.25	1.23×10^{2}
	C9 S1	0.34	4.58×10^{8}	0.017	2.12×10^{5}	0.11	1.32×10^{-1}	4.40×10^{3}	4.43×10^{-1}	275.55	1.36×10^{2}
	C9 S2	0.34	4.11×10^{8}	0.016	2.89×10^{5}	0.15	1.32×10^{-1}	4.40×10^{3}	4.43×10^{-1}	275.55	2.06×10^{2}
	C9 S3	0.35	3.93×10^{8}	0.015	3.37×10^{5}	0.17	1.32×10^{-1}	4.40×10^{3}	4.16×10^{-1}	276.65	2.60×10^{2}
m+p-Xylenes	C5 S1	0.38	4.68×10^{8}	0.018	1.03×10^{6}	0.48	1.42×10^{-1}	4.20×10^{3}	4.87×10^{-1}	274.15	5.30×10^{2}
	C8 S2	0.35	7.99×10^{8}	0.030	5.56×10^{5}	0.28	1.42×10^{-1}	4.20×10^{3}	4.58×10^{-1}	275.25	1.92×10^{2}
	C9 S1	0.34	5.67×10^{8}	0.021	9.64×10^{4}	0.05	1.42×10^{-1}	4.20×10^{3}	4.51×10^{-1}	275.55	4.90×10^{1}
	C9 S2	0.34	5.00×10^{8}	0.019	8.09×105	0.42	1.42×10-1	4.20×10^{3}	4.51×10^{-1}	275.55	4.67×10^{2}
	C9 S3	0.35	4.69×10^{8}	0.018	8.93×10^{5}	0.45	1.42×10^{-1}	4.20×10^{3}	4.24×10^{-1}	276.65	5.64×10^{2}

VOC	Cloud event/sample	LWC vol/vol	C_{gas} exp molec cm^{-3}_{air}	C_{gas} exp ppbv	C_{aq} exp molec cm^{-3}_{air}	C_{aq} exp ng mL^{-1}	Henry's law constant M atm^{-1} at 298.15 K	-ΔH/R K	Henry's law constant $Matm^{-1}$ at T_{exp}	T_{exp} K	Partitioning factor q
o-Xylene	C5 S1	0.38	2.31×10^{8}	0.009	1.27×10^{6}	0.59	1.42×10^{-1}	4.20×10^{3}	4.87×10^{-1}	274.15	1.32×10^{3}
	C8 S2	0.35	5.76×10^{8}	0.022	7.14×10^{5}	0.36	1.42×10^{-1}	4.20×10^{3}	4.58×10^{-1}	275.25	3.42×10^{2}
	C9 S1	0.34	4.10×10^{8}	0.016	2.70×10^{5}	0.14	1.42×10^{-1}	4.20×10^{3}	4.51×10^{-1}	275.55	1.90×10^{2}
	C9 S2	0.34	3.42×10^{8}	0.013	1.43×10^{6}	0.74	1.42×10^{-1}	4.20×10^{3}	4.51×10^{-1}	275.55	1.20×10^{3}
	C9 S3	0.35	3.24×10^{8}	0.012	1.57×10^{6}	0.79	1.42×10^{-1}	4.20×10^{3}	4.24×10^{-1}	276.65	1.43×10^{3}
Styrene	C5 S1	0.38	5.95×10^{8}	0.023	7.46×10^{5}	0.34	3.34×10^{-1}	4.20×10^{3}	1.15	274.15	1.28×10^{2}
	C8 S2	0.35	1.26×10^{8}	0.005	3.24×10^{5}	0.16	3.34×10^{-1}	4.20×10^{3}	1.08	275.25	3.00×10^{2}
	C9 S1	0.34	7.11×10^{7}	0.003	9.82×10^{4}	0.05	3.34×10^{-1}	4.20×10^{3}	1.06	275.55	1.69×10^{2}
	C9 S2	0.34	7.22×10^{7}	0.002	1.96×10^{5}	0.1	3.34×10^{-1}	4.20×10^{3}	1.06	275.55	3.34×10^{2}
	C9 S3	0.35	8.79×10^{7}	0.003	1.62×10^{5}	0.08	3.34×10^{-1}	4.20×10^{3}	9.98×10^{-1}	276.65	2.32×10^{2}
n-Propylbenzene	C5 S1	0.38	1.41×10^{9}	0.05	1.52×10^{5}	0.08	1.11×10^{-1}	4.70×10^{3}	4.41×10^{-1}	274.15	2.86×10^{1}
	C8 S2	0.35	1.58×10^{8}	0.006	7.01×10^{4}	0.04	1.11×10^{-1}	4.70×10^{3}	4.12×10^{-1}	275.25	1.36×10^{2}
	C9 S1	0.34	8.84×10^{7}	0.003	3.41×10^{4}	0.02	1.11×10^{-1}	4.70×10^{3}	4.04×10^{-1}	275.55	1.24×10^{2}
	C9 S2	0.34	7.50×10^{7}	0.002	8.51×10^{4}	0.05	1.11×10^{-1}	4.70×10^{3}	4.04×10^{-1}	275.55	3.65×10^{2}
	C9 S3	0.35	6.00×10^{7}	0.002	1.05×10^{5}	0.06	1.11×10^{-1}	4.70×10^{3}	3.78×10^{-1}	276.65	5.84×10^{2}
1,3,5-Trimethylbenzene	C5 S1	0.38	/	/	4.57×10^{5}	0.24	1.32×10^{-1}	3.00×10^{3}	3.19×10^{-1}	274.15	/
	C8 S2	0.35	1.95×10^{8}	0.007	2.80×10^{5}	0.16	1.32×10^{-1}	3.00×10^{3}	3.05×10^{-1}	275.25	5.96×10^{2}
	C9 S1	0.34	9.55×10^{7}	0.004	1.70×10^{5}	0.1	1.32×10^{-1}	3.00×10^{3}	3.01×10^{-1}	275.55	7.70×10^{2}
	C9 S2	0.34	7.28×10^{7}	0.003	5.11×10^{4}	0.03	1.32×10^{-1}	3.00×10^{3}	3.01×10^{-1}	275.55	3.03×10^{2}
	C9 S3	0.35	6.50×10^{7}	0.002	1.75×10^{4}	0.01	1.32×10^{-1}	3.00×10^{3}	2.89×10^{-1}	276.65	1.18×10^{2}
1,2,4-Trimethylbenzene	C5 S1	0.38	/	/	1.67×10^{6}	0.88	1.72×10^{-1}	3.60×10^{3}	4.95×10^{-1}	274.15	/
	C8 S2	0.35	1.01×10^{9}	0.04	9.99×10^{5}	0.57	1.72×10^{-1}	3.60×10^{3}	4.70×10^{-1}	275.25	2.67×10^{2}
	C9 S1	0.34	7.32×10^{8}	0.03	7.49×10^{5}	0.44	1.72×10^{-1}	3.60×10^{3}	4.63×10^{-1}	275.55	2.87×10^{2}
	C9 S2	0.34	8.59×10^{8}	0.03	1.77×10^{6}	1.04	1.72×10^{-1}	3.60×10^{3}	4.63×10^{-1}	275.55	5.79×10^{2}
	C9 S3	0.35	7.51×10^{8}	0.03	1.68×10^{6}	0.96	1.72×10^{-1}	3.60×10^{3}	4.40×10^{-1}	276.65	6.42×10^{2}

VOC	Cloud event/sample	LWC vol/vol	C_{gas} exp molec cm^{-3}_{air}	C_{gas} exp ppbv	C_{aq} exp molec cm^{-3}_{air}	C_{aq} exp ng mL^{-1}	Henry's law constant M atm^{-1} at 298.15 K	-ΔH/R K	Henry's law constant $Matm^{-1}$ at T_{exp}	T_{exp} K	Partitioning factor q
Naphtalene	C5 S1	0.38	5.01×10^{7}	0.0019	3.57×10^{4}	0.02	2.23	5.20×10^{3}	1.03×10^{1}	274.15	8.11
	C8 S2	0.35	8.60×10^{8}	0.033	8.22×10^{4}	0.05	2.23	5.20×10^{3}	9.52	275.25	1.27
	C9 S1	0.34	1.86×10^{8}	0.007	/	/	2.23	5.20×10^{3}	9.32	275.55	/
	C9 S2	0.34	1.19×10^{8}	0.004	3.19×10^{4}	0.02	2.23	5.20×10^{3}	9.32	275.55	3.76
	C9 S3	0.35	9.09×10^{7}	0.003	1.64×10^{5}	0.1	2.23	5.20×10^{3}	8.65	276.65	2.63×10^{1}
Isoprene	C5 S1	0.38	2.35×10^{9}	0.088	2.56×10^{6}	0.76	1.42×10^{-1}	4.20×10^{3}	4.87×10^{-1}	274.15	2.62×10^{2}
	C8 S2	0.35	4.22×10^{9}	0.16	2.20×10^{6}	0.71	1.42×10^{-1}	4.20×10^{3}	4.58×10^{-1}	275.25	1.44×10^{2}
	C9 S1	0.34	4.81×10^{9}	0.18	1.98×10^{6}	0.66	1.42×10^{-1}	4.20×10^{3}	4.51×10^{-1}	275.55	1.19×10^{2}
	C9 S2	0.34	4.35×10^{9}	0.16	1.71×10^{6}	0.57	1.42×10^{-1}	4.20×10^{3}	4.51×10^{-1}	275.55	1.14×10^{2}
	C9 S3	0.35	6.17×10^{9}	0.23	1.73×10^{6}	0.56	1.42×10^{-1}	4.20×10^{3}	4.24×10^{-1}	276.65	8.33×10^{1}
a-pinene	C5 S1	0.38	4.02×10^{8}	0.015	/	/	4.76×10^{-3}	4.40×10^{3}	1.73×10^{-2}	274.15	/
	C8 S2	0.35	4.72×10^{8}	0.018	/	/	4.76×10^{-3}	4.40×10^{3}	1.63×10^{-2}	275.25	/
	C9 S1	0.34	5.38×10^{8}	0.02	1.13×10^{4}	0.0073	4.76×10^{-3}	4.40×10^{3}	1.60×10^{-2}	275.55	1.71×10^{2}
	C9 S2	0.34	4.87×10^{8}	0.018	1.48×10^{5}	0.096	4.76×10^{-3}	4.40×10^{3}	1.60×10^{-2}	275.55	2.48×10^{3}
	C9 S3	0.35	6.90×10^{8}	0.026	1.56×10^{5}	0.104	4.76×10^{-3}	4.40×10^{3}	1.50×10^{-2}	276.65	1.90×10^{3}
Nopinone	C5 S1	0.38	1.34×10^{9}	0.05	3.29×10^{6}	1.99	1.95×10^{2}	1.18×10^{4}	6.21×10^{3}	274.15	4.62×10^{-2}
	C8 S2	0.35	5.02×10^{8}	0.019	7.43×10^{5}	0.502	1.95×10^{2}	1.18×10^{4}	5.23×10^{3}	275.25	3.58×10^{-2}
	C9 S1	0.34	5.73×10^{8}	0.022	7.84×10^{5}	0.514	1.95×10^{2}	1.18×10^{4}	4.99×10^{3}	275.55	3.56×10^{-2}
	C9 S2	0.34	5.18×10^{8}	0.02	/	/	1.95×10^{2}	1.18×10^{4}	4.99×10^{3}	275.55	/
	C9 S3	0.35	7.35×10^{8}	0.03	1.93×10^{5}	0.13	1.95×10^{2}	1.18×10^{4}	4.21×10^{3}	276.65	7.83×10^{-3}

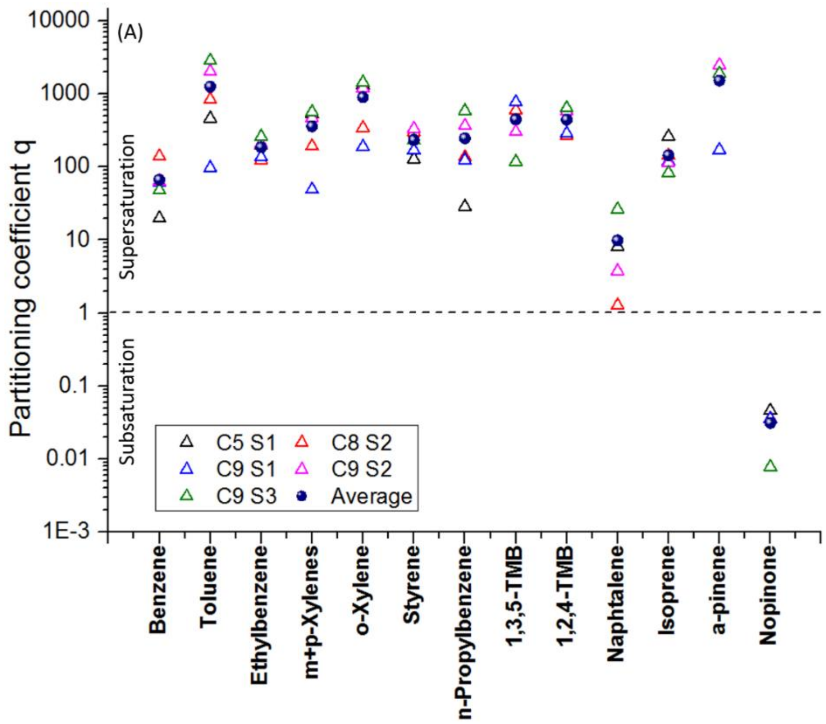

Figure III-19 q factors calculated for each cloud sample and for each chemical compound (blue circles correspond to mean values).

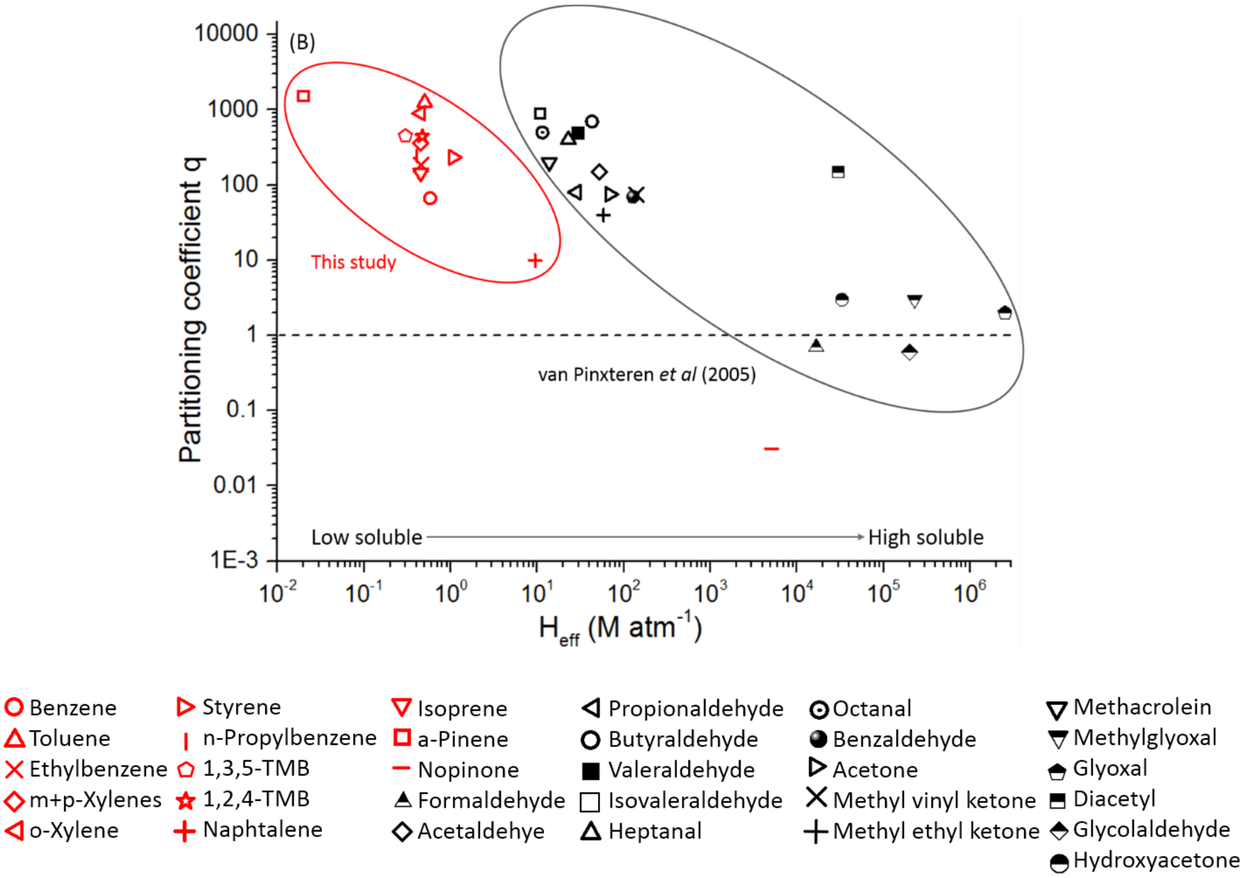

Figure III-20 Mean q factors calculated in this study are compared with the study from van Pinxteren et al. (2005); chemical compounds are classified as a function of their effective Henry's law constants.

III.3.5 Discussions about the deviations from the Henry's law equilibrium

Previous studies investigated the partitioning of small carboxylic acids and carbonyls that have been commonly measured in cloud aqueous phase, such as formic, acetic, oxalic acids and formaldehyde (Winiwarter et al., 1988; Voisin et al., 2000). In these works, the calculated partitioning coefficients are in agreement with the ones that are expected considering Henry's law equilibrium. Some deviations have been observed for formic and acetic acids that are found undersaturated in certain case (Facchini et al., 1992). For cloud waters with pH < 3, these compounds are inversely found slightly supersaturated (Winiwarter et al., 1994). Solubility of carboxylic acids and carbonyls is a function of temperature and pH (for the acids) and observed deviations commonly increases with increasing pH. Several explanations have been in the past proposed to the observed deviations (Facchini et al., 1992; Winiwarter et al., 1994; Voisin et al., 2000) and are discussed below.

Sampling artefacts can lead to bias in measured aqueous concentrations. In the air, cloud droplets are in equilibrium with the interstitial air. By grouping all of them in a bulk sample, this equilibrium is perturbed with respect to the original conditions (Perdue and Beck, 1988; Pandis and Seinfeld, 1991; Keene et al., 1995). The pH values of bulk water is also different from individual droplets and may modify the Henry's law values of acids (Ervens et al., 2003). Outgassing of organic molecules could also occur from the sample and effects resulting from temperature differences from the field to the lab have to be considered and may change the partitioning. Actually those points have been discussed but it is still impossible due to technical limitation to evaluate this possible sampling artefacts.

Deviations can be due to kinetic transport limitations through the air/water surface; gas phase diffusion and transfer of molecules at the gas/liquid interface (phase/phase transition and diffusion from the surface) are critical steps to consider. Notably, parameters such as droplet lifetime and accommodation coefficient α are difficult to estimate and the experimental measurements are scarce as highlighted in CHAPTER I in Section I.5 (Davidovits et al., 2006). This mass transfer is also perturbed by the presence and potential accumulation of hydrophobic compounds on the droplet surfaces (Capel et al., 1990; Gill et al., 1983).

In the present study, we investigate the partitioning of more hydrophobic molecules from both biogenic and anthropogenic origins. In van Pinxteren et al. (2005), carbonyl compounds have been measured both in the gaseous and aqueous phases and they have shown that larger and less soluble compounds (valeraldehyde, methyl ethylketone, methyl vinyl ketone, heptanal, octanal, and benzaldehyde) are supersaturated by a factor of 100 to 1000 in clouds sampled during the FEBUKO (Field investigations of budgets and conversions of particle phase organics in tropospheric cloud processes) campaign at Mount Schmücke in Germany. Those results have been compared to measured values of the present study (Figure III-20).

q factor is plotted for both studies as a function of the effective Henry's law constant. In both studies, we observe that the q factor is higher when the Henry's law constant is small. Similar observations are reported for different hydrophobic compounds such as certain pesticides, PAHs, polychlorinated biphenyls (PCBs), and alkanes in fog water (Glotfelty et al., 1987; Valsaraj et al., 1993). A possible explanation for this could be that hydrophobic compounds are associated with dissolved or colloidal organic matter. This tendency of colloids to bind hydrophobic compounds has been already observed in both soil-water and sediment-water media (Kile and Chiou, 1989; Capel et al., 1990; Schomburg et al., 1991). Another reason could be the effect of air/water interface presenting very high specific area available for adsorption of hydrophobic compounds (Djikaev, 2003). The hydrophobicity of those compounds are correlated with the $K_{O/W}$. Therefore, phase partitioning could not be predicted by Henry's law values but using $K_{O/W}$. Thus, to investigate that point, a new figure has been drawn linking the $K_{O/W}$ coefficient with an "Enrichment factor" E (Figure III-21) that considers the effect of both adsorption of hydrophobic compounds at the air/water interface and their association to the colloids in cloud water media. This parameter has been initially proposed by Valsaraj et al. (1993) and is calculated as following:

$$E = 1 + \frac{3}{r}K_a + \rho_s^* K_{oc} \qquad \text{(Eq.2)}$$

with r: cloud droplet radius; K_a: is the partition constant for hydrophobic organic carbon between the air-water interface and water. The term of $\frac{3}{r}K_a$ is relative to the air-water interfacial adsorption. The term $\rho_s^* K_{oc}$ results from the adsorption on filterable solids and the sorption on non-filterable dissolved organic carbon in cloud water as described in previous works (Valsaraj, 1988a,b; Thoma et al., 1991; Morel and Gschwend, 1987) and calculated as following:

$$\rho_s^* = \rho_s\, f_{oc} + \rho_{col} \qquad \text{(Eq.3)}$$

$$K_{oc} \approx K_{col} \qquad \text{(Eq.4)}$$

ρ_s^* : concentration of all non-dissolved organic carbon in cloud droplets (mgC L^{-1});

ρ_s : concentration of all non-dissolved organic carbon that has been filtered (mgC L^{-1});

f_{oc} : fraction of all non-dissolved organic carbon that has been filtered;

ρ_{col} : concentration of all non-dissolved organic carbon under the form of colloids (non-filtered) (mgC L^{-1}).

K_{oc} is the partition constant ($cm^3\ g^{-1}$) for hydrophobic organic carbon between the organic carbon fraction in filterable solids and cloud water; K_{col} is the partition constant ($cm^3\ g^{-1}$) between the colloidal dissolved organic carbon and cloud water. We assume that K_{oc} and K_{col} are closed as proposed by Thoma et al. (1991) and Morel and Gschwend (1987).

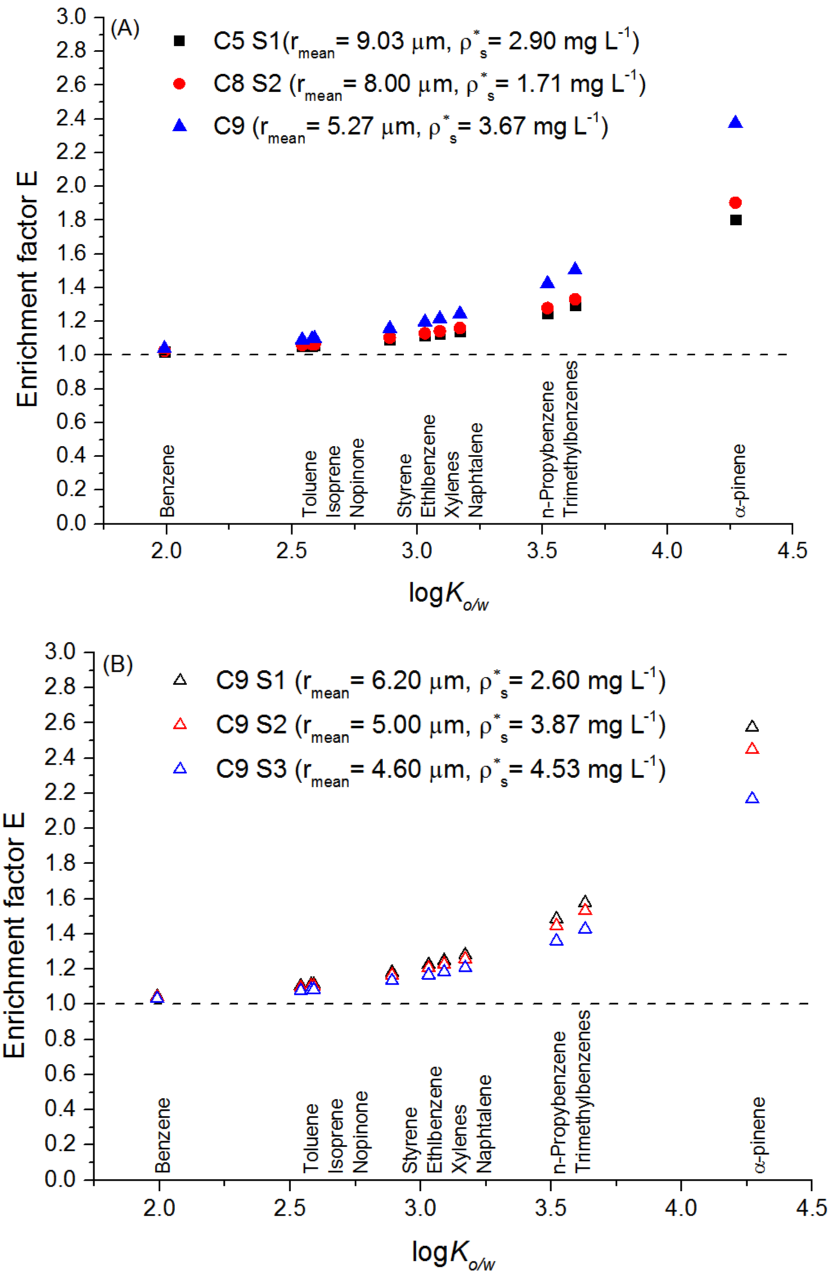

Figure III-21 (A) Enrichment factors E for each chemical compound and for each cloud sample presenting different mean droplet radius r_{mean} and concentrations of non-dissolved organic carbon (ρ_s^*). For C9 cloud event, is presented the E coefficient averaged for the 3 samples (mean radius and mean non-dissolved organic carbon); (B) Enrichment factors E for each chemical compound of samples from cloud event C9 with mean droplet radius r_{mean} for samples and different concentrations of non-soluble organic compounds.

To estimate the "enrichment factor" E, several parameters are needed. Some of them are available such as the radius r. Cloud droplet radius for the studied cloud samples ranges from 4 to 10 µm with a mean value around 6 µm and have been considered for the calculation (Table III-8).

In the same way, ρ_s^* need to be estimated. For that, DOC measurements for the various cloud events are available (see in Table III-8). Based on long term cloud measurements at PUY, DOC commonly ranges from 1 to 20 mgC L^{-1} depending on the air mass origins. The values of DOC are quite close to the TOC values for the cloud sampled at PUY (Marinoni et al., 2004; Deguillaume et al., 2014) demonstrating that a small fraction of the organic matter is non-soluble. The same result has been observed by Reyes-Rodriguez et al. (2009) where DOC and TOC concentrations respectively ranged from 0.15 to 0.66 mgC L^{-1} and from 0.13 to 0.65 mgC L^{-1}: a significant fraction of TOC was composed of water-soluble organics (DOC/TOC = 0.79). Fog measurements have highlighted similar conclusion with DOC constituting about 80% of the total organic carbon in the aqueous phase (Raja et al., 2008; Straub et al., 2012). For the calculation, we consider a value for ρ_S^* based on DOC measurements where we recalculate a TOC value (DOC/TOC = 90%) and we consider that 10% of TOC is insoluble. This is a rough assumption that has been evaluated afterwards.

Table III-8 Cloud droplet radius r (µm) (with min, max and mean values over the collection period) and DOC concentrations (mgC L^{-1}) for each cloud events.

	C5 S1	**C8 S2**	**C9 S1**	**C9 S2**	**C9 S3**
r_{min} (µm)	6.3	6.3	5.2	4.8	4.3
r_{max} (µm)	10.0	10.0	7.6	6.4	5.2
r_{mean} (µm)	9.0	8.0	6.2	5.0	4.6
DOC (mgC L^{-1})	2.9	1.7	2.6	3.9	4.5

Schomburg et al. (1991) determined the K_{oc} values for some of the neutral hydrophobic compounds such as pesticides in fog water. $log\ K_{oc}$ shows a linear relationship with $logK_{o/w}$ as in Figure III-22 with a slope of 0.82.

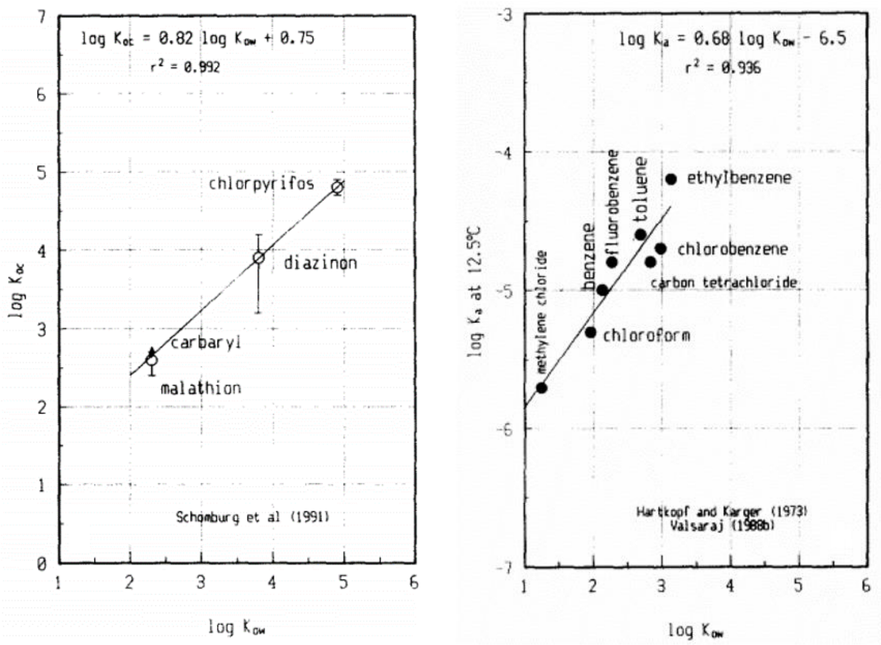

Figure III-22 K_{oc} as a function of $K_{o/w}$ (left); air-water interfacial binding constant K_a as a function of $K_{o/w}$ (right) (from Valsaraj et al., 1993).

Thus K_{oc} and $K_{o/w}$, are related following this empirical equation:

$$K_{oc} = 5.6 \times K_{o/w}^{0.82} \tag{Eq.5}$$

For some neutral hydrophobic organic compounds, there are few values for adsorption from the vapor phase onto pure water surfaces at 12.5 °C (Hartkopf and Karger, 1973). Values of the adsorption constant, $K_a' = C_a/C_v$ were reported, where C_a is the adsorbed concentration at the air-water interface (molec cm^{-2}) and C_v is the vapor concentration (molec cm^{-3}). Hartkopf and Karger (1973) conducted the simultaneous measurement of the Henry's constant, at the same temperature for which, $K_a{}'$ values were obtained by the gas chromatography method. The adsorption constant K_a, between the air-water interface and the bulk aqueous phase at 12.5 °C, was established by using the $K_a{}'$ value along with the Henry's constant (Valsaraj, 1988a, b; Mackay et al., 1991). A linear proportionality between logK_a and log$K_{o/w}$ was observed as in Figure III-22,

$$K_a = 3 \times 10^{-7} \times K_{o/w}^{0.68} \tag{Eq.6}$$

where K_a is in cm.

We should note that values of K_a for fogwater surfaces may be different from those for more pure liquid sample surfaces or even pure water surface since the surface free energy of a fogwater surface will be less than that of a pure water surface (Capel et al., 1990). However, the difference in surface free energies is small. Therefore, K_a obtained from Figure III-22 can be used as an approximate value.

Experimental data on the adsorption of neutral and highly hydrophobic compounds such as those of concern here are lacking. The validity of extrapolating K_a values from compound of less hydrophobic nature (log $K_{o/w}$< 3) to those that have greater log$K_{o/w}$ values remains to be protest experimentally. Efforts should be directed towards this end as was recommended in the review by Mackay et al. (1991) on air-water interracial exchange of hydrophobic pollutants.

Finally, by combining all the empirical relationships (Eq.5 and Eq.6), we obtain:

$$E = 1 + 3 \times 10^{-7} \times \frac{3}{r} \times K_{o/w}^{0.68} + 5.6 \times \rho_s^* \times K_{o/w}^{0.82} \tag{Eq.7}$$

A brief analysis of the effect of the various parameters of Eq.7 can be done. By fixing the value of r and ρ_s^*, we obtain a surface plot of E *versus* K_{oc} and K_a. as shown in Figure III-23 (for r = 10 µm and ρ_s^* = 20 mgC L^{-1} without coloration; for r = 1 µm and ρ_s^* = 200 mgC L^{-1}, r = 1 µm and ρ_s^* = 20 mgC L^{-1} with coloration in red and blue, respectively).

For r = 10 µm and ρ_s^* = 20 mgC L^{-1} (the surface plot without coloration in Figure III-23), we can see that:

- when $K_{oc} \approx 10^6$ cm^3 g^{-1} and for negligible value of K_a ($\approx 10^{-5}$ cm), the maximum value of E is about 20. The E value remains independent of K_a for all values of $K_a \leq 10^{-4}$ cm. Beyond a K_a about 10^{-4} cm, the value of E is proportional to K_a and reaches a value of 3 10^5 for K_a = 1 cm;
- when K_{oc} is small ($\leq 10^4$), the E value increases proportionally to K_a for all values of K_{oc}. Thus, the air-water interfacial adsorption on fog droplets becomes important leading to an enrichment. When the average droplet radius increases, the term $3K_a/\mathrm{r}$ becomes smaller and K_{oc} becomes increasingly important.

Table III-9 Parameters used for the calculation of the enrichment factors E: Octanol-water partition coefficients ($K_{o/w}$); cloud droplet radius r (µm) (min, max and mean values) and DOC concentrations (mgC L^{-1}) for each cloud cloud events.

	$K_{o/w}$	$\log K_{o/w}$	$K_{o/w}^{0.68}$	$K_{o/w}^{0.82}$
Benzene	97.7	1.9	22.5	42.8
Toluene	346.7	2.5	53.3	121.0
Ethylbenzene	1071.5	3.0	114.9	305.2
m+p-Xylenes	1230.2	3.0	126.2	341.8
o-Xylene	1230.2	3.0	126.2	341.8
Styrene	776.2	2.8	92.3	234.3
n-Propylbenzene	3311.3	3.5	247.5	769.8
1,3,5-Trimethylbenzene	4265.8	3.6	294.0	947.5
1,2,4-Trimethylbenzene	4265.8	3.6	294.0	947.5
Naphtalene	1479.1	3.1	143.0	397.5
Isoprene	380.1	2.5	56.8	130.5
α-pinene	18620.8	4.2	800.9	3172.4
Nopinone	389.0	2.5	57.7	132.9

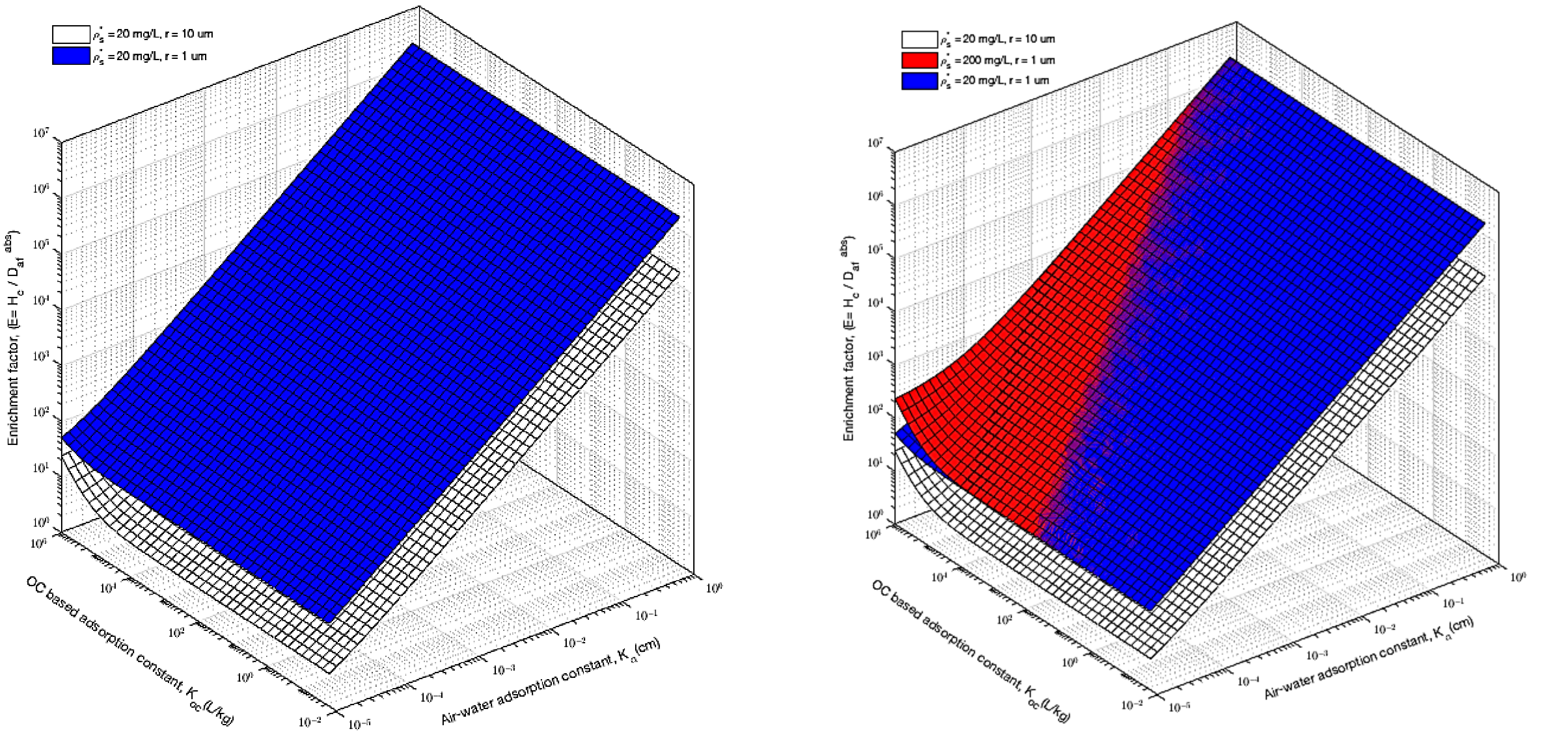

Figure III-23 Enrichment factor as a function of K_{oc} and K_a. Note that for r=10 µm and ρ_S^*=20 mgC L^{-1} without coloration; for r=1 µm and ρ_S^*=200 mgC L^{-1}, r=1 µm and ρ_S^*=20 mgC L^{-1} with coloration in red and blue, respectively.

Predictions from the above equation are shown in Figure III-21. The calculation predicts a small enrichment for compounds in cloud samples, except for α-pinene which has a high $K_{o/w}$ value. Enrichment factors E of each cloud sample increase when cloud droplet radius decrease. When the cloud droplet radius is constant, enrichment factors E do not vary significantly as a function of ρ_s^* non-soluble organic carbon. More important mass fraction of total organic compound were considered is the calculation of the enrichment factor E. The factor E is not influenced even by having a fraction of TOC around 100%. It is clear that the contribution to the enrichment factor from surface adsorption is much more important than that from dissolved or colloidal organic matter. This is explained by the fact that the concentration of colloids and non-soluble organic carbon in cloud water samples at PUY are much less important (around a factor of 100 less concentrated) than what is observed for fog event in the study from Valsaraj et al. (1993). The contribution of adsorption calculated for the cloud samples is also less important in the present study since the mean cloud droplet radius (~6−10 µm) is more important than the one measured for fog droplets (~1 µm).

These results underline the fact that the partitioning of hydrophobic compounds in clouds are poorly understood. Further laboratory and field investigations are needed to understand the interfacial processes and to better parametrize cloud chemistry models. These numerical tools commonly consider the mass transfer as a kinetical process (see CHAPTER I Section I.5.2) following for example the parametrization of Schwartz (1986). It proposes a transfer coefficient depending on gaseous diffusion and interfacial transport constrained by the accommodation coefficient α (Davidovits et al., 2006; 2011) and the droplet radius. Of course, cloud chemistry models also consider the solubility of chemical compounds based on the available or estimated Henry's law constants (Mouchel-Vallon et al., 2017). Finally, models simulate the partitioning of organic and inorganic compounds that are perturbed by microphysical processes, mass transfer and gaseous and aqueous chemical reactivity (Mouchel-Vallon et al., 2013; Ervens, 2015; Rose et al., 2018; Hoffmann et al., 2018). As explained in CHAPTER I, those models predict, for targeted small organic compounds, small deviations from the Henry's law equilibrium that can be explained by the LWC, droplet radius and pH variations. It seems clear that, for hydrophobic compounds, those models will not be able to simulate the strong observed supersaturation of those species in the aqueous phase. For those compounds, additional processes (mainly at the air/water interface) should be considered in cloud chemistry models since phase partitioning cannot be predicted considering only the solubility of organic compounds.

III.4 Preliminary result of VOC and OVOC characterization during the BIOMAIDO campaign

III.4.1 Presentation of the field campaign

As presented in Section III.1.2, the environmental context of La Réunion Island is favorable to study the atmospheric organic matter multiphasic transformations since (i) VOC and organic aerosols are emitted by several natural and anthropogenic sources, (ii) since cloud formation often occurs along the slope of the mountain, (iii) since temperature and solar irradiation are optimal for chemical and biological transformations. In this frame, a field campaign was conducted in March and April 2019 during 5 weeks. Several sites along the mountain slope were instrumented to document the various atmospheric compartments (gas, aerosol, cloud) chemically, physically and also biologically (see in Figure III-24): “Gite Petite-France” (965 m a.s.l.): chemical characterization of the air mass (gases, aerosols); “Domaine des Orchidées Sauvages” (1465 m a.s.l.): balloon and remote sensing measurements for boundary layer evolution and cloud life cycle; “Hôtel du Maïdo” (1500 m a.s.l.): 24 m instrumented mast and container for OVOC flow and concentration measurements; “piste Omega” (1760 m a.s.l.): cloud droplet collector installed at the top of a 10 m mast for cloud bio-physico-chemical characterization; “Observatoire du Maïdo” (2165 m a.s.l.): chemical characterization of the air mass (gases, aerosols).

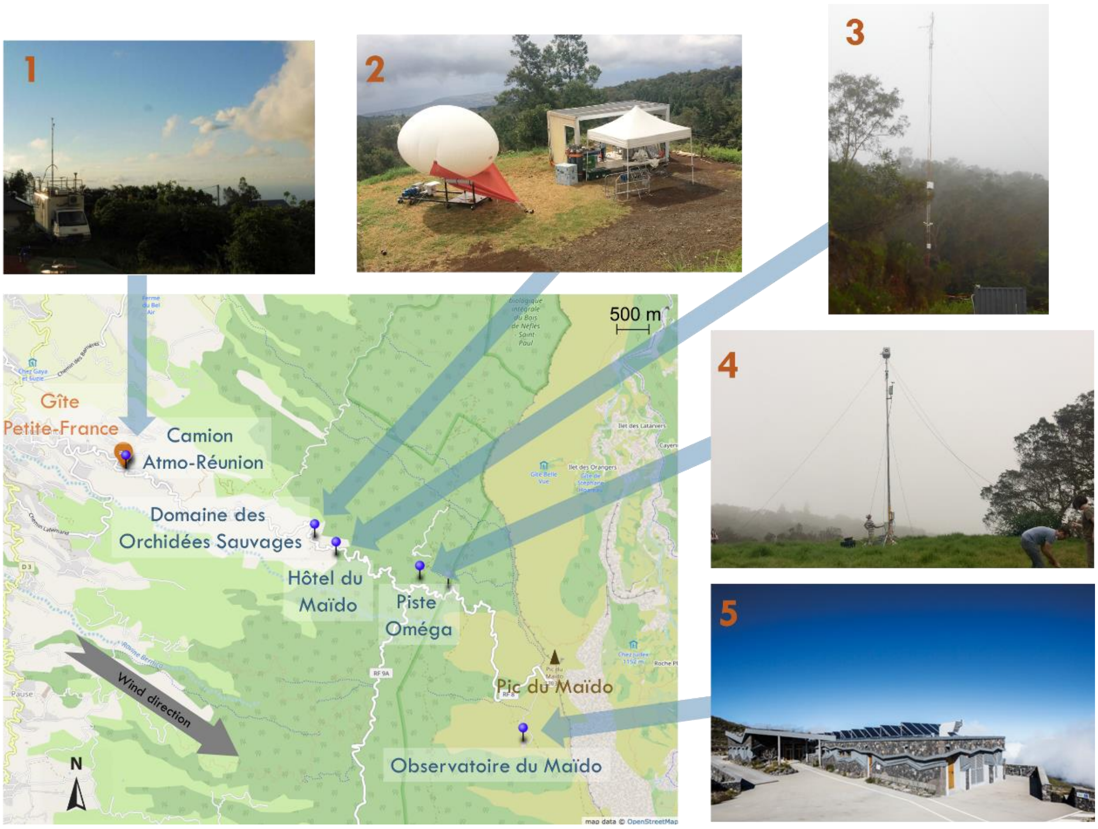

Figure III-24 Summarize of the various instrumented sites allowing the sample atmospheric compartments along the mountain slope during the BIOMAIDO campaign.

Several French laboratories were involved in this project: Laboratoire d'Aérologie (LA, Toulouse), Laboratoire de Météorologie Physique (LaMP, Clermont-Ferrand), Institut de Chimie de Clermont-Ferrand (ICCF, Clermont-Ferrand), Laboratoire de l'Atmosphère et des Cyclones (LACy, Saint-Denis), Institut des Géosciences de l'Environnement (IGE, Grenoble), Centre National de Recherches Météorologiques (CNRM, Toulouse), Laboratoire de Recherche en Géoscience et Energie (LaRGE, Pointre à Pitre).

During the campaign, the mobile mast for cloud characterization was deployed during 13 days for a total of 14 samples. The average volume of cloud water was around 110 mL for each event. During the cloud water collection, gaseous samplings of VOC and OVOC were conducted simultaneously during a total of 10 cloud events (noted as "R" see in Table III-10).

Table III-10 The identification of gas and cloud event samplings during BIOMAIDO in 2019, with sampling date, number of cloud event, measurement type of gas, sampling time (local time) and sampling volume of air. Each line in the table corresponds to a cartridge analyzed afterwards.

Sampling date	Cloud event	Type of measurement	Starting time of sampling (local time)	Ending time of sampling (local time)	Sampling volume of air (L)
14 Mar 2019	R1	VOC	14:50	15:30	4
		VOC	15:35	16:15	4
15 Mar 2019	R2	VOC	13:45	14:25	4
		VOC	15:13	15:53	4
18 Mar 2019	R3	VOC	14:30	15:10	4
		VOC	16:01	16:41	4
		OVOC	16:01	16:41	4
19 Mar 2019	R4	VOC	13:48	14:28	4
		OVOC	13:48	14:28	4
		OVOC	13:48	14:28	4
20 Mar 2019	R5	OVOC	/	/	4
22 Mar 2019	R6	VOC	11:30	12:10	4
		OVOC	11:30	12:10	4
28 Mar 2019	R8	VOC	11:25	12:05	4
		VOC	11:45	12:25	4
29 Mar 2019	Rcat	VOC	11:50	12:30	4
		OVOC	11:50	12:30	6
30 Mar 2019	R9	VOC	14:25	15:44	4
		VOC	15:50	17:00	4
		OVOC	15:50	17:00	8
01 Apr 2019	R10	VOC	14:30	15:28	4
		VOC	15:38	16:40	4
		OVOC	15:38	16:40	6
02 Apr 2019	R11	VOC	12:39	14:15	10
		VOC	12:39	14:15	10
		VOC	14:51	15:35	4
03 Apr 2019	R12	VOC	15:18	16:10	5
04 Apr 2019	R13	VOC	12:24	13:25	6
		VOC	12:24	13:25	6
		VOC	14:08	15:21	7

Cartridges were analyzed by the same analytical procedure described in CHAPTER II and preliminary results are presented below. One should keep in mind that the sampling air volumes are most of the time around 4L or higher. The breakthrough volumes might be overpassed for the lighter OVOC (<C5). The discussed values should be seen as “semi-quantitative”.

III.4.2 VOC atmospheric concentration during cloud events

During the whole field campaign, we paid attention to the quality of the field blank. In Figure III-25, two non-exposed tubes during field measurement have been analyzed, namely sealed and non-sealed field campaign blanks. The values of the non-sealed tube blank is higher than the sealed one indicating a potential contamination by passive sampling. Except for BTEX, the field blanks are usually lower than 20 ppt. One should note that toluene shows the highest signal either in the field blank and the blank system. The mixing ratios of VOC and OVOC was calculated by the consideration of the blank effect and shown in Figure III-26 and Figure III-27.

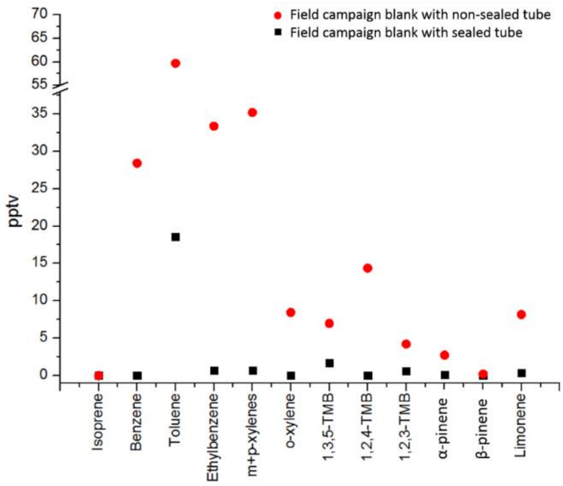

Figure III-25 Field campaign blanks with sealed and non-sealed tubes. One field campaign blank tube is kept sealed during the whole field campaign "'Field campaign blank with sealed tube" (red dots). The other field campaign blank is connected to the AEROVOCC device during the sampling without any air flow "Field campaign blank with sealed tube" (black dots).

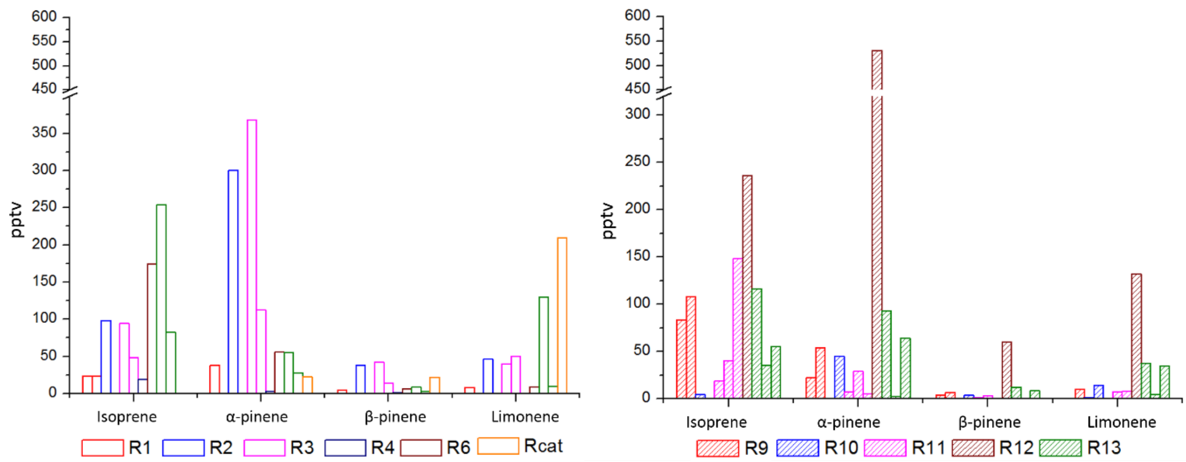

Figure III-26 Gaseous mixing ratios of biogenic VOC measured during the cloud events (indicated with "R").

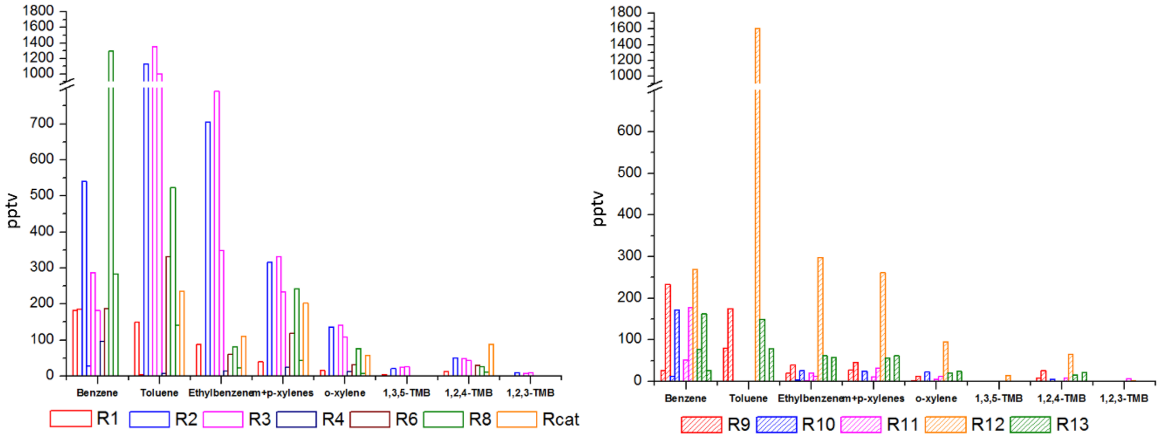

Figure III-27 Gaseous mixing ratios of anthropogenic VOC measured during the cloud events (indicated with "R").

The measurements indicate that the dominant VOC species are isoprene, α-pinene, β-pinene and limonene from natural sources and benzene, toluene, ethylbenzene and xylenes from anthropogenic sources. Isoprene and α-pinene are found generally highly concentrated during all these cloud events, which can be explained by the presence of the nearby "tamarin forest" that is an endogenic forest recognized as a main emitter of isoprene. During cloud event R12, the levels of both biogenic and anthropogenic VOC are the highest. For instance, the levels for toluene (1.8 ppb) are close to the ones encountered in urban areas. These values will be crosschecked with other geophysical parameters.

Table III-11 VOC concentrations (min-max, mean value) during the cloud events of BIOMAIDO field campaign.

Observed compounds	**Concentration range (pptv)**		
	Min value	**Max value**	**Mean value**
AVOC			
Benzene	5.5	1271.8	196.5
Toluene	3.5	1793.1	365.3
Ethylbenzene	14.3	790.2	128.9
m+p-xylenes	13.8	332.2	97.9
o-xylene	2.4	141.7	37.9
1,3,5-TMB	0.6	25.9	9.1
1,2,4-TMB	1.1	85.3	24.4
1,2,3-TMB	0.3	9.6	4.3
BVOC			
α-pinene	2.5	528.2	82.4
β-pinene	0.2	59.9	10.8
Limonene	0.04	206.5	33.9
Isoprene	0.03	267.5	78.9

Isoprene ranges from 0.03 to 267.5 ppt with a mean value of 78.9 for all cloud events. α-pinene presents values between 2.5 and 528.2 ppt with a mean value of 82.4 ppt. BTEX concentrations were found in the same order of magnitude as BVOC, except for several max values. This observation is mainly linked to air mass history. The air evolves along the slope of the mountain and can be enriched in anthropogenic compounds coming for example from road traffic. Further analysis of the data campaign should be carried out to confirm this statement.

There are few studies focused on measurement of VOC and OVOC at tropical sites. A recent study by Duflot et al. (2019) investigated the isoprene concentration over several sites at La Réunion Island. The concentration of isoprene ranges from 0.01 to 300 ppt with a mean value of 95 ppt, which shows the same order of magnitude than what we observed (see in Table III-11). At Amazonia forest, the concentration level of isoprene (<500 ppt) is found higher probably due to the higher emission by the vegetation (Yannez-Serano et al., 2015). They have also observed pinenes and limonene. The sum of concentration level of these compounds is less than 600 ppt, which is almost twice as high as the sum of pinenes and limonene concentration during BIOMAIDO.

Mixing ratios of gaseous OVOC are also determined by applying the method that I have developed at LaMP. Again, one has to keep in mind that these values are semi-quantitative due to the breakthrough volume issue discussed in Section II.3 of CHAPTER II. Formaldehyde and acetone were found highly concentrated in our samples with mixing ratios in the order of ppb. Other carbonyl compounds are also observed (see in Figure III-28) but in the order of ppb. Some of them originate from photochemical oxidation of biogenic compounds, particularly isoprene (*i.e.*, MVK as first oxidation products and MGLY and GLY as secondary oxidation products). C4 to C8 carbonyls (from butanal to octanal) result from primary sources (plant emission, wood burning, vehicles…).

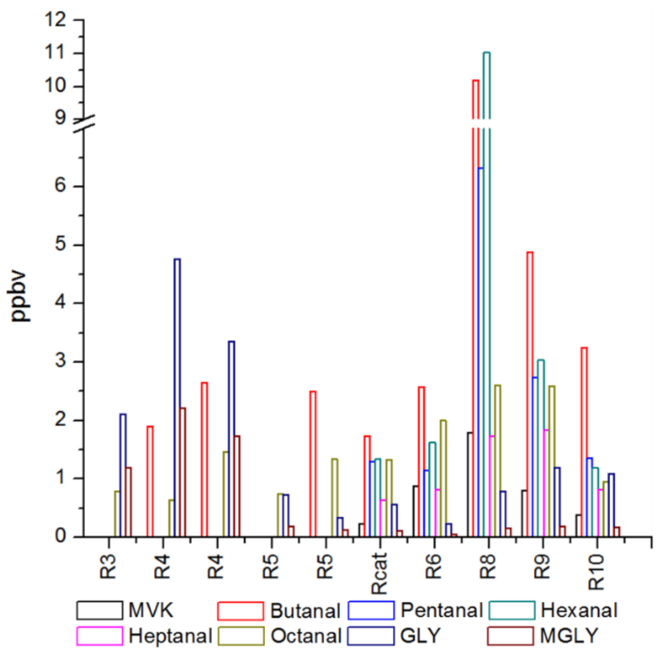

Figure III-28 Distribution of OVOC mixing ratios (ppbv) during BIOMAIDO for the various cloud events (MVK: methyl vinyl ketone; MGLY: methylglyoxal; GLY: glyoxal).

MGLY and GLY are highly soluble with effective Henry's law constants superior to 10^5 M atm^{-1}. We expect that they transfer efficiently in the cloud aqueous phase where they are highly reactive towards the $HO^{\bullet}$ radicals. We can notice that cloud events R3-R4 present significant levels of those compounds in comparison to other cloud events. This can be explained by several parameters. Cloud microphysical properties (mainly LWC) (data not yet available) could explain this difference: a lower LWC for those cloud events can lead to a less efficient scavenging of those compounds by cloud water. Another reason is due to possible sampling artefacts (continuous or interrupted operation).

Finally, the aging of the air mass for these cloud events could be more important than for other clouds (*i.e.*, R6, R8, R9, and R10). Of course, all these explanations are speculative and additional measurements should deny or confirm them.

Summary conclusion and perspectives

This thesis had the objective to quantify VOC and OVOC in the cloud system in order to investigate their air/cloud droplet partitioning. To fulfill this objective, analytical developments both in the field and in the laboratory have been first conducted.

In the laboratory, new analytical procedures have been implemented to quantify VOC and OVOC in both gaseous and liquid phases by Thermal Desorption-Gas Chromatography-Mass Spectrometry (TD-GC-MS). This includes (i) the optimization of gaseous OVOC identification and quantification onto Tenax TA sorbent tubes pre-coated with two derivatization agents coupled to TD-GC-MS analysis (ii) the optimization of dissolved VOC/OVOC identification and quantification by Stir Bar Sorptive Extraction (SBSE) coupled to TD-GC-MS analysis. Various tests have been performed looking at the influence of environmental factors like relative humidity and analytical conditions such as derivatization duration, extraction time duration, volumes of the sample and of PDMS stir bar, ionic strength. The performances of the methods have been evaluated (*i.e.*, linearity, repeatability, sensitivity, extraction efficiency), demonstrating the potentiality of the optimized protocols for both rather hydrophobic anthropogenic and biogenic VOC and highly soluble carbonyl compounds in both gas and cloud water phases. However, the breakthrough volume for light OVOCs stays an issue.

All the optimized protocols have been applied to the atmospheric measurements of the chemical compounds in both gas and cloud water phases in two contrasted environments: the puy de Dôme station and La Réunion Island in the frame of the BIOMAIDO ANR project. In this frame, a newly gas sampler (AEROVOCC) has been developed at LaMP for field measurements. Part of these data (only those determined at the puy de Dôme station) have been used to investigate air/water partitioning.

First, the temporal variability and speciation of VOC measured at the puy de Dôme station have been investigated. The concentration levels are representative of remote mountain sites with the influence of biogenic and anthropogenic VOC transported from their sources to the puy de Dôme station. The seasonal variations have been discussed regarding their main controlling factors. The dynamic of the boundary layer height is a key parameter for understanding the variability of the measured concentrations and air mass aging. Second, the air/droplet partitioning of hydrophobic anthropogenic and biogenic VOC has been evaluated based on specific field campaigns at the puy de Dôme station. These results emphasize the fact that the partitioning of VOC in clouds are poorly understood since a strong supersaturation in the aqueous phase, with respect to the Henry's law equilibrium, is observed for all the studied cloud events. Finally, preliminary results on the detection and quantification of VOC and OVOC in the frame of the intensive field campaign of the BIOMAIDO project at La Réunion Island have been presented and discussed. Measurements show the presence of significant concentrations of VOC species from biogenic origin (isoprene, α-pinene, β-pinene and limonene) associated to anthropogenic VOC such as benzene, toluene, ethylbenzene and xylenes of anthropogenic sources. The latter are surely emitted by local emissions from the road traffic. Concentrations of OVOC from the gas samples have been also determined by deploying the pre-coated Tenax TA sorbent tubes.

While this thesis contributed to the reinforcement of the analytical capabilities of LaMP in quantifying the multiphasic composition of VOC/OVOC in the cloudy atmosphere, further laboratory studies need to be conducted for OVOC quantification.

- For carbonyl compounds, laboratory tests have shown the good performances of the method. However, the breakthrough volume seems to be a critical issue in contrast with other published studies in the literature. Future tests will focus on simultaneous gaseous sampling with PFBHA tubes in series (even more than two back tubes) and in controlled conditions are needed.
- For alcohols and acids, future tests will include (i) of the methodology for Tenax TA tube pre-coated with MTBSTFA, (ii) the study of the influence of relative humidity and ozone and (iii) the evaluation of the performances (sensitivity, linearity, repeatability) for both gaseous (on-sorbent-tube) and liquid phase (SBSE).
- Ambient ozone due to its high oxidant capacity can potentially create positive or negative artifacts during VOC/OVOC sampling. Future test will be arranged for different ozone scrubber to quantify (i) the ozone removal efficiency, (ii) losses of VOC/OVOC in the absence of ozone, and (iii) potential ozone-induced losses of VOC/OVOC in the scrubber.

Although gaseous samples of the field campaign at La Réunion Island has been analyzed during my PhD, there are still more work need to be complemented by the characterization of the same compounds in the cloud aqueous phase by SBSE extraction followed by TD-GC-MS analysis. This will allow to perform similar study on the air/liquid partitioning of VOC than the one performed at the puy de Dôme station. Observations at both sites will be compared and the effect of environmental conditions will be analyzed in details (aging of the air mass, pH of the cloud water, sources, meteorological parameters such as the temperature, solar irradiation…). For this, several additional tools could help for measurement interpretation: back trajectories will be calculated with for example the HYSPLIT or LACYTRAJ model; air and cloud samples can be studied/classified by statistical studies (*i.e.*, PCA/HCA analysis) based on their physical-chemical properties; Positive Matrix Factorization (PMF) can help for identifying and elaborating source profiles of observed VOC. This will be achieved in the frame of the ANR BIOMAIDO project.

For the puy de Dôme station, simultaneous air/cloud sampling need to be conducted over longer period and for various conditions in order to better characterize this multiphasic medium and analyses this potential interfacial processes highlighted during my PhD thesis. This will allow to validate and develop the new cloud chemistry model CLEPS recently developed at LaMP.

References

Akagi, S.K., Yokelson, R.J., Wiedinmyer, C., Alvarado, M.J., Reid, J.S., Karl, T., Crounse, J.D., Wennberg, P.O., 2011. Emission factors for open and domestic biomass burning for use in atmospheric models. Atmospheric Chemistry and Physics. 11, 4039–4072.

Alam, M.S., Rickard, A.R., Camredon, M., Wyche, K.P., Carr, T., Hornsby, K.E., Monks, P.S., Bloss, W.J., 2013. Radical Product Yields from the Ozonolysis of Short Chain Alkenes under Atmospheric Boundary Layer Conditions. The Journal of Physical Chemistry A. 117, 12468–12483.

Alves, R.F., Nascimento, A.M.D., Nogueira, J.M.F., 2005. Characterization of the aroma profile of Madeira wine by sorptive extraction techniques. Analytica Chimica Acta. 546, 11–21.

Amato, P., M. Joly, L. Besaury, A. Oudart, N. Taib, A.I. Moné, L. Deguillaume, A.-M. Delort, D. Debroas., 2017 Active microorganisms thrive among extremely diverse communities in cloud water. PLOS ONE. 12(8), e0182869.

Amato, P., L. Besaury, M. Joly, B. Penaud, L. Deguillaume, A.-M. Delort., 2019. Metatranscriptomic exploration of microbial functioning in clouds, Scientific Reports. 9, 4383.

An, W.J., Pathak, R.K., Lee, B.H., Pandis, S.N., 2007. Aerosol volatility measurement using an improved thermodenuder: application to secondary organic aerosol. Journal of Aerosol Science. 38, 305e314.

Anderson, L.G., Lanning, J.A., Barrell, R., Miyagishima, J., Jones, R.H., Wolfe, P., 1996. Sources and sinks of formaldehyde and acetaldehyde: An analysis of Denver's ambient concentration data. Atmospheric Environment. 30, 2113–2123.

Andreae, M.O., 2019. Emission of trace gases and aerosols from biomass burning–an updated assessment. Atmospheric Chemistry and Physics. 19, 8523–8546.

Andreae, M.O., Merlet, P., 2001. Emission of trace gases and aerosols from biomass burning. Global Biogeochemical Cycles. 15, 955–966.

Aneja, V.P., 1993. Organic compounds in cloud water and their deposition at a remote continental site. Air & Waste. 43, 1239–1244.

Anglada, J.M., Aplincourt, P., Bofill, J.M., Cremer, D., 2002. Atmospheric Formation of OH Radicals and H_2O_2 from Alkene Ozonolysis under Humid Conditions. ChemPhysChem. 3, 215–221.

Apte, J.S., Brauer, M., Cohen, A.J., Ezzati, M., Pope, C.A., 2018. Ambient $PM_{2.5}$ reduces global and regional life expectancy. Environmental Science & Technology Letters. 5, 546–551.

Ariya, P.A., Sander, R., Crutzen, P.J., 2000. Significance of HO_x and peroxides production due to alkene ozonolysis during fall and winter: A modeling study. Journal of Geophysical Resarch. 105, 17721–17738.

Arroo, R., 2007. Eberhard Breitmaier. Terpenes-flavors, fragrances, pharmaca, pheromones. Wiley-VCH, 2006, 214 pp ISBN 3-527-31786-4. Applied Organometallic Chemistry. 21, 377–377.

Aschmann, S.M., Reisseil, A., Atkinson, R., Arey, J., 1998. Products of the gas phase reactions of the OH radical with α- and β-pinene in the presence of NO. Journal of Geophysical Research: Atmospheres. 103, 25553–25561.

Atkinson, R., 2000. Atmospheric chemistry of VOCs and NOx. Atmospheric Environment. 34, 2063–2101.

Atkinson, R., 1997. Gas-phase tropospheric chemistry of volatile organic compounds: 1. alkanes and alkenes. Journal of Physical and Chemical Reference Data. 26, 215–290.

Atkinson, R., Arey, J., 2003. Atmospheric degradation of volatile organic compounds. Chemical Reviews. 103, 4605–4638.

Atkinson, R. 1988. Atmospheric transformations of automotive emissions. Pp. 99-132 in Air Pollution, the Automobile, and Public Health, A.Y. Watson, R.R. Bates, and D. Kennedy, eds. Washington DC: National Academy Press.

Atkinson, R. 1990. Gas-phase tropospheric chemistry of organic compounds: A review. Atmospheric Environment. 24A:1—41.

Atkinson, R. 1991. Kinetics and mechanisms of the gas-phase reactions of the NO_3 radical with organic compounds. Journal of physical and chemical reference data. 20:-459—507.

Audiffren, N., Renard, M., Buisson, E., Chaumerliac, N., 1998. Deviations from the Henry's law equilibrium during cloud events: a numerical approach of the mass transfer between phases and its specific numerical effects. Atmospheric Research. 49, 139–161.

Aumont, B., Szopa, S., Madronich, S., 2005. Modelling the evolution of organic carbon during its gas-phase tropospheric oxidation: development of an explicit model based on a self generating approach. Atmospheric Chemistry and Physics. 5, 2497–2517.

Bachy, A., Aubinet, M., Schoon, N., Amelynck, C., Bodson, B., Moureaux, C., Heinesch, B., 2016. Are BVOC exchanges in agricultural ecosystems overestimated? Insights from fluxes measured in a maize field over a whole growing season. Atmospheric Chemistry and Physics. 16, 5343–5356.

Badol, C., Locoge, N., Galloo, J.-C., 2008. Using a source-receptor approach to characterise VOC behaviour in a French urban area influenced by industrial emissions. Science of The Total Environment. 389, 429–440.

Baltussen, E., Cramers, C., Sandra, P., 2002. Sorptive sample preparation – a review. Analytical and Bioanalytical Chemistry. 373, 3–22.

Baltussen, E., Sandra, P., David, F., Cramers, C., 1999. Stir bar sorptive extraction (SBSE), a novel extraction technique for aqueous samples: Theory and principles. Journal of Microcolumn Separations. 11, 737–747.

Barth, M.C., 2006. The importance of cloud drop representation on cloud photochemistry. Atmospheric Research. 82, 294–309.

Baray, J.L., Bah, A., Cacault, P., Sellegri, K., Pichon, J.-M., Deguillaume, L., Montoux; N., Noel, V., Seze, G., Gabarrot, F., Payen, G., Duflot, V., 2019. Cloud occurrence at puy de Dôme deduced from an automatic webcam images analysis: Method, validation and comparisons with larger scale cloud fraction, sumitted to Atmosphere.

Baray, J.L., L. Deguillaume, A. Colomb, K. Sellegri, E. Freney, C. Rose, J. Van Baelen, J.-M. Pichon, D. Picard, P. Fréville, L. Bouvier, M. Ribeiro, P. Amato, S. Banson, A. Bianco, A. Borbon, L. Bourcier, Y. Bras, M. Brigante, P. Cacault, A. Chauvigné, T. Charbouillot, N. Chaumerliac, A.-M. Delort, M. Delmotte, R. Dupuy, A. Farah, G. Febvre, A. Flossmann, C. Gourbeyre, C. Hervier, M. Hervo, N. Huret, M. Joly, V. Kazan, M. Lopez, G. Mailhot, A. Marinoni, O. Masson, N. Montoux, M. Parazols, F. Peyrin, Y. Pointin, M. Ramonet, M. Rocco, M. Sancelme, S. Sauvage, M. Schmidt, E. Tison, M. Vaïtilingom, P. Villani, M. Wang, C. Yver-Kwok, P. Laj., 2019. Cézeaux-Aulnat-Opme-Puy De Dôme: a multi-site for the long term survey of the tropospheric composition and climate change, submitted to Atmospheric Measurement Techniques.

Baudic, A., Gros, V., Sauvage, S., Locoge, N., Sanchez, O., Sarda-Estève, R., Kalogridis, C., Petit, J.-E., Bonnaire, N., Baisnée, D., Favez, O., Albinet, A., Sciare, J., Bonsang, B., 2016. Seasonal variability and source apportionment of volatile organic compounds (VOCs) in the Paris megacity (France). Atmospheric Chemistry and Physics. 16, 11961–11989.

Behnke, K., Ehlting, B., Teuber, M., Bauerfeind, M., Louis, S., Hänsch, R., Polle, A., Bohlmann, J., Schnitzler, J.-P., 2007. Transgenic, non-isoprene emitting poplars don’t like it hot: Thermotolerance in isoprene emission knock-down mutants of poplar. The Plant Journal. 51, 485–499.

Bianco, A., Deguillaume, L., Chaumerliac, N., Vaïtilingom, M., Wang, M., Delort, A.-M., Bridoux, M.C., 2019. Effect of endogenous microbiota on the molecular composition of cloud water: a study by Fourier-transform ion cyclotron resonance mass spectrometry (FT-ICR MS). Scientific Reports. 9, 7663.

Bianco, A., Deguillaume, L., Vaïtilingom, M., Nicol, E., Baray, J.-L., Chaumerliac, N., Bridoux, M., 2018. Molecular characterization of cloud water samples collected at the puy de Dôme (France) by Fourier Transform Ion Cyclotron Resonance Mass Spectrometry. Environmental Science & Technology. 52, 10275–10285.

Bianco, A., Passananti, M., Perroux, H., Voyard, G., Mouchel-Vallon, C., Chaumerliac, N., Mailhot, G., Deguillaume, L., Brigante, M., 2015. A better understanding of hydroxyl radical photochemical sources in cloud waters collected at the puy de Dôme station – experimental versus modelled formation rates. Atmospheric Chemistry and Physics. 15, 9191–9202.

Bianco, A., Vaïtilingom, M., Bridoux, M., Chaumerliac, N., Pichon, J.-M., Piro, J.L., Deguillaume, L., 2017. Trace metals in cloud water sampled at the puy de Dôme station. Atmosphere. 8, 225.

Bianco, A., Voyard, G., Deguillaume, L., Mailhot, G., Brigante, M., 2016. Improving the characterization of dissolved organic carbon in cloud water: Amino acids and their impact on the oxidant capacity. Scientific Reports. 6, 37420.

Bicchi, C., Cordero, C., Iori, C., Rubiolo, P., Sandra, P. 2000. Headspace sorptive extraction (HSSE) in the headspace analysis of aromatic and medicinal plants. Journal of High Resolution Chromatography. 23(9), 539-546.

Bicchi, C., Iori, C., Rubiolo, P., Sandra, P. 2002. Headspace sorptive extraction (HSSE), stir bar sorptive extraction (SBSE), and solid phase microextraction (SPME) applied to the analysis of roasted Arabica coffee and coffee brew. Journal of agricultural and food chemistry. 50(3), 449-459.

Bonasoni, P., Stohl, A., Cristofanelli, P., Calzolari, F., Colombo, T., Evangelisti, F., 2000. Background ozone variations at Mt. Cimone Station. Atmospheric Environment. 34, 5183–5189.

Bonsang, B., Polle, C., Lambert, G., 1992. Evidence for marine production of isoprene. Geophysical Research Letters. 19, 1129–1132.

Borbon, A., Boynard, A., Salameh, T., Baudic, A., Gros, V., Gauduin, J., Perrussel, O., Pallares, C., 2018. Is traffic still an important emitter of monoaromatic organic compounds in European urban areas? Environmental Science & Technology. 52, 513–521.

Borbon, A., Fontaine, H., Locoge, N., Veillerot, M., Galloo, J.C., 2003. Developing receptor-oriented methods for non-methane hydrocarbon characterisation in urban air. Part II: source apportionment. Atmospheric Environment. 37, 4065–4076.

Borbon, A., Gilman, J.B., Kuster, W.C., Grand, N., Chevaillier, S., Colomb, A., Dolgorouky, C., Gros, V., Lopez, M., Sarda-Esteve, R., Holloway, J., Stutz, J., Petetin, H., McKeen, S., Beekmann, M., Warneke, C., Parrish, D.D., de Gouw, J.A., 2013. Emission ratios of anthropogenic volatile organic compounds in northern mid-latitude megacities: Observations versus emission inventories in Los Angeles and Paris. Journal of Geophysical Research Atmospheres. 118, 2041–2057.

Borbon, A., Locoge, N., Veillerot, M., Galloo, J., Guillermo, R., 2002. Characterisation of NMHCs in a French urban atmosphere: overview of the main sources. The Science of The Total Environment. 292, 177–191.

Boynard, A., Borbon, A., Leonardis, T., Barletta, B., Meinardi, S., Blake, D.R., Locoge, N., 2014. Spatial and seasonal variability of measured anthropogenic non-methane hydrocarbons in urban atmospheres: Implication on emission ratios. Atmospheric Environment. 82, 258–267.

Brantner, B., Fierlinger, H., Puxbaum, H., Berner, A., 1994. Cloudwater chemistry in the subcooled droplet regime at Mount Sonnblick (3106 m a.s.l., Salzburg, Austria). Water, Air, and Soil Pollution. 74, 363–384.

Breus, I.P., Mishchenko, A.A., Shinkarev, A.A., Neklyudov, S.A., Breus, V.A., 2014. Effect of organic matter on the sorption activity of heavy loamy soils for volatile organic compounds under low moisture conditions. Eurasian Soil Science. 47, 1216–1226.

Broadgate, W.J., Malin, G., Küpper, F.C., Thompson, A., Liss, P.S., 2004. Isoprene and other non-methane hydrocarbons from seaweeds: a source of reactive hydrocarbons to the atmosphere. Marine Chemistry. 88, 61–73.

Burnett, R., Chen, H., Szyszkowicz, M., Fann, N., Hubbell, B., Pope, C.A., Apte, J.S., Brauer, M., Cohen, A., Weichenthal, S., Coggins, J., Di, Q., Brunekreef, B., Frostad, J., Lim, S.S., Kan, H., Walker, K.D., Thurston, G.D., Hayes, R.B., Lim, C.C., Turner, M.C., Jerrett, M., Krewski, D., Gapstur, S.M., Diver, W.R., Ostro, B., Goldberg, D., Crouse, D.L., Martin, R.V., Peters, P., Pinault, L., Tjepkema, M., van Donkelaar, A., Villeneuve, P.J., Miller, A.B., Yin, P., Zhou, M., Wang, L., Janssen, N.A.H., Marra, M., Atkinson, R.W., Tsang, H., Quoc Thach, T., Cannon, J.B., Allen, R.T., Hart, J.E., Laden, F., Cesaroni, G., Forastiere, F., Weinmayr, G., Jaensch, A., Nagel, G., Concin, H., Spadaro, J.V., 2018. Global estimates of mortality associated with long-term exposure to outdoor fine particulate matter. Proceedings of the National Academy of Sciences. 115, 9592–9597.

Cahill, T.M., Seaman, V.Y., Charles, M.J., Holzinger, R., Goldstein, A.H., 2006. Secondary organic aerosols formed from oxidation of biogenic volatile organic compounds in the Sierra Nevada Mountains of California. Journal of Geophysical Research. 111.13D.

Cai, C., Geng, F., Tie, X., Yu, Q., An, J., 2010. Characteristics and source apportionment of VOCs measured in Shanghai, China. Atmospheric Environment. 44, 5005–5014.

Cancilla, D.A., Que Hee, S.S., 1992. O-(2,3,4,5,6-Pentafluorophenyl)methylhydroxylamine hydrochloride: a versatile reagent for the determination of carbonyl-containing compounds. Journal of Chromatography A. 627, 1–16.

Capel, P.D., Gunde, R., Zuercher, F., Giger, W., 1990. Carbon speciation and surface tension of fog. Environmental Science & Technology. 24, 722–727.

Carlton, A.G., Wiedinmyer, C., Kroll, J.H., 2009. A review of Secondary Organic Aerosol (SOA) formation from isoprene. Atmospheric Chemistry and Physics 9, 4987–5005.

Carter, M. C. and Foster, C. D., 2004. Prescribed burning and productivity in southern pine forests: a review, Forest Ecol. Manag. 191, 93– 109.

Chaumerliac, N., Leriche, M., Audiffren, N., 2000. Modeling of scavenging processes in clouds: some remaining questions about the partitioning of gases among gas and liquid phases. Atmospheric Research. 53, 29–43.

Cheize, M., Sarthou, G., Croot, P.L., Bucciarelli, E., Baudoux, A.-C., Baker, A.R., 2012. Iron organic speciation determination in rainwater using cathodic stripping voltammetry. Analytica Chimica Acta. 736, 45–54.

Chen, C.-L., Li, L., Tang, P., Cocker, D.R., 2018. SOA formation from photooxidation of naphthalene and methylnaphthalenes with m -xylene and surrogate mixtures. Atmospheric Environment 180, 256–264.

Chen, X., Millet, D.B., Singh, H.B., Wisthaler, A., Apel, E.C., Atlas, E.L., Blake, D.R., Bourgeois, I., Brown, S.S., Crounse, J.D., de Gouw, J.A., Flocke, F.M., Fried, A., Heikes, B.G., Hornbrook, R.S., Mikoviny, T., Min, K.-E., Müller, M., Neuman, J.A., OSullivan, D.W., Peischl, J., Pfister, G.G., Richter, D., Roberts, J.M., Ryerson, T.B., Shertz, S.R., Thompson, C.R., Treadaway, V., Veres, P.R., Walega, J., Warneke, C., Washenfelder, R.A., Weibring, P., Yuan, B., 2019. On the sources and sinks of atmospheric VOCs: an integrated analysis of recent aircraft campaigns over North America. Atmospheric Chemistry and Physics. 19, 9097–9123.

Chi, Y., Feng, Y., Wen, S., Lu, H., Yu, Z., Zhang,W., Sheng, G., and Fu, J., 2007. Determination of carbonyl compounds in the atmosphere by DNPH derivatisation and LC-ESI-MS/MS detection, Talanta, 72, 539–545.

Chung, S.H., 2002. Global distribution and climate forcing of carbonaceous aerosols. Journal of Geophysical Research 107.33D

Clain, G., Baray, J. L., Delmas, R., Diab, R., Leclair de Bellevue, J., Keckhut, P., Posny, F., Metzger, J. M., and Cammas, J. P., 2009. Tropospheric ozone climatology at two Southern Hemisphere tropical/subtropical sites, (Reunion Island and Irene, South Africa) from ozonesondes, LIDAR, and in situ aircraft measurements, Atmospheric Chemistry and Physics. 9, 1723–1734.

Cocheo, V., Sacco, P., Boaretto, C., De Saeger, E., Ballesta, P.P., Skov, H., Goelen, E., Gonzalez, N., Caracena, A.B., 2000. Urban benzene and population exposure. Nature. 404, 141-142.

Coelho, E., Coimbra, M.A., Nogueira, J.M.F., Rocha, S.M., 2009. Quantification approach for assessment of sparkling wine volatiles from different soils, ripening stages, and varieties by stir bar sorptive extraction with liquid desorption. Analytica Chimica Acta. 635, 214–221.

Cohen, A.J., Brauer, M., Burnett, R., Anderson, H.R., Frostad, J., Estep, K., Balakrishnan, K., Brunekreef, B., Dandona, L., Dandona, R., Feigin, V., Freedman, G., Hubbell, B., Jobling, A., Kan, H., Knibbs, L., Liu, Y., Martin, R., Morawska, L., Pope, C.A., Shin, H., Straif, K., Shaddick, G., Thomas, M., van Dingenen, R., van Donkelaar, A., Vos, T., Murray, C.J.L., Forouzanfar, M.H., 2017. Estimates and 25-year trends of the global burden of disease attributable to ambient air pollution: an analysis of data from the Global Burden of Diseases Study 2015. The Lancet 389, 1907–1918.

Colmán, E. G., Blanco, M. B., Barnes, I., Teruel, M. A., 2015. Ozonolysis of a series of C7–C9 unsaturated biogenic aldehydes: reactivity study at atmospheric pressure. RSC Advances. 5(39), 30500-30506.

Cordes, E. H., Jencks, W. P., 1962. On the mechanism of Schiff base formation and hydrolysis. Journal of the American Chemical Society, 84(5), 832-837.

Czuczwa, J., Leuenberger, C., Giger, W., 1988. Seasonal and temporal changes of organic compounds in rain and snow. Atmospheric Environment. (19) 22, 907–916.

David, F., Sandra, P., 2007. Stir bar sorptive extraction for trace analysis. Journal of Chromatography A. 1152, 54–69.

Davidovits, P., Kolb, C.E., Williams, L.R., Jayne, J.T., Worsnop, D.R., 2011. Update 1 of: Mass accommodation and chemical reactions at gas−liquid interfaces. Chemical Reviews. 111.

Davidovits, P., Kolb, C.E., Williams, L.R., Jayne, J.T., Worsnop, D.R., 2006. Mass accommodation and chemical reactions at gas−liquid interfaces. Chemical Reviews. 106, 1323–1354.

de Gouw, J.A., Gilman, J.B., Borbon, A., Warneke, C., Kuster, W.C., Goldan, P.D., Holloway, J.S., Peischl, J., Ryerson, T.B., Parrish, D.D., Gentner, D.R., Goldstein, A.H., Harley, R.A., 2012. Increasing atmospheric burden of ethanol in the United States: increasing atmospheric burden of ethanol. Geophysical Research Letters. 39.12D

de Laat, A.T.J., de Gouw, J.A., Lelieveld, J., Hansel, A., 2001. Model analysis of trace gas measurements and pollution impact during INDOEX. Journal of Geophysical Research. 106, 28469–28480.

Deguillaume, L., Charbouillot, T., Joly, M., Vaïtilingom, M., Parazols, M., Marinoni, A., Amato, P., Delort, A.-M., Vinatier, V., Flossmann, A., Chaumerliac, N., Pichon, J.M., Houdier, S., Laj, P., Sellegri, K., Colomb, A., Brigante, M., Mailhot, G., 2014. Classification of clouds sampled at the puy de Dôme (France) based on 10 yr of monitoring of their physicochemical properties. Atmospheric Chemistry and Physics. 14, 1485–1506.

Deguillaume, L., Leriche, M., Desboeufs, K., Mailhot, G., George, C., Chaumerliac, N., 2005. Transition Metals in Atmospheric Liquid Phases: Sources, Reactivity, and Sensitive Parameters. Chemical Reviews. 105, 3388–3431.

de Villiers, A., Vanhoenacker, G., Lynen, F., Sandra, P., 2004. Stir bar sorptive extraction-liquid desorption applied to the analysis of hop-derived bitter acids in beer by micellar electrokinetic chromatography. Electrophoresis. 25(4-5), 664-669.

Dewick, P.M., 2002. The biosynthesis of C5–C25 terpenoid compounds. Natural Product Reports. 19, 181–222.

Dewulf, J., Van Langenhove, H., 1999. Anthropogenic volatile organic compounds in ambient air and natural waters: a review on recent developments of analytical methodology, performance and interpretation of field measurements. Journal of Chromatography A. 843, 163–177.

Djikaev, Y.S., 2003. Effect of adsorption on the uptake of organic trace gas by cloud droplets. Journal of Geophysical Research. 108.D22.

Doherty, R.E., 2000. A history of the production and use of carbon tetrachloride, tetrachloroethylene, trichloroethylene and 1,1,1-trichloroethane in the United States: Part 1--Historical Background; Carbon Tetrachloride and Tetrachloroethylene. Environmental Forensics. 1, 69–81.

Dominutti, P.A., Nogueira, T., Borbon, A., Andrade, M. de F., Fornaro, A., 2016. One-year of NMHCs hourly observations in São Paulo megacity: meteorological and traffic emissions effects in a large ethanol burning context. Atmospheric Environment. 142, 371–382.

Donahue, N. M., Chuang, W., Schervish, M., 2019. Gas-phase organic oxidation chemistry and atmospheric particles. Advances In Atmospheric Chemistry-Volume 2: Organic Oxidation And Multiphase Chemistry. 2, 199.

Doussin, J.-F., Monod, A., 2013. Structure–activity relationship for the estimation of OH-oxidation rate constants of carbonyl compounds in the aqueous phase. Atmospheric Chemistry and Physics. 13, 11625–11641.

Draxler, R.R., Rolph G.D., 2012. Evaluation of the transfer coefficient matrix (TCM) approach to model the atmospheric radionuclide air concentrations from Fukushima. Journal of Geophysical Research. 117, p. D05107 dx.

Duflot, V., Dils, B., Baray, J. L., De Mazière, M., Attié, J. L., Vanhaelewyn, G., Senten, C., Vigouroux, C., Clain, G., Delmas, R., 2010. Analysis of the origin of distribution of CO in the subtropical southern Indian Ocean, Journal of Geophysical Research. 115, D22106.

Duflot, V., Tulet, P., Flores, O., Barthe, C., Colomb, A., Deguillaume, L., Vaïtilingom, M., Perring,A., Huffman, A., Hernandez, M.T., Sellegri, K., Robinson, E., O Connor, D.J., Gomez, O.M., Burnet, F., Bourrianne, T., Strasberg, D., Rocco, M., Bertram, A.K., Chazette, P., Totems, J., Fourne, J., Stamenoff, P., Metzger, J.M., Chabasset, M., Rousseau, C., Bourrianne, E., Sancelme1, M., Delort, A.M., Wegener, R.E., Chou,C., and Elizondo, P., 2019. Preliminary results from the FARCE 2015 campaign: multidisciplinary study of the forest–gas–aerosol–cloud system on the tropical island of La Réunion. Atmospheric Chemistry and Physics. 19(16), 10591-10618.

Dumanoglu, Y., Kara, M., Altiok, H., Odabasi, M., Elbir, T., 2014. Spatial and seasonal variation and source apportionment of volatile organic compounds (VOCs) in a heavily industrialized region. Atmospheric Environment. 98, 168–178.

Ehrenhauser, F.S., Khadapkar, K., Wang, Y., Hutchings, J.W., Delhomme, O., Kommalapati, R.R., Herckes, P., Wornat, M.J., Valsaraj, K.T., 2012. Processing of atmospheric polycyclic aromatic hydrocarbons by fog in an urban environment. Journal of Environmental Monitoring. 14, 2566.

Ellis, S.R., Hughes, J.R., Mitchell, T.W., Panhuis, M., Blanksby, S.J., 2012. Using ambient ozone for assignment of double bond position in unsaturated lipids. The Analyst. 137, 1100–1110.

Epstein, S.A., Blair, S.L., Nizkorodov, S.A., 2014. Direct photolysis of α-pinene ozonolysis secondary organic aerosol: effect on particle mass and peroxide content. Environmental Science & Technology. 48, 11251–11258.

Ervens, B., 2015. Modeling the processing of aerosol and trace gases in clouds and fogs. Chemical Reviews. 115, 4157–4198.

Ervens, B., Gligorovski, S., Herrmann, H., 2003. Temperature-dependent rate constants for hydroxyl radical reactions with organic compounds in aqueous solutions. Physical Chemistry Chemical Physics. 5, 1811–1824.

Ervens, B., Wang, Y., Eagar, J., Leaitch, W.R., Macdonald, A.M., Valsaraj, K.T., Herckes, P., 2013. Dissolved organic carbon (DOC) and select aldehydes in cloud and fog water: the role of the aqueous phase in impacting trace gas budgets. Atmospheric Chemistry and Physics. 13, 5117–5135.

Facchini, M.C., Fuzzi, S., Kessel, M., Wobrock, W., Jaeschke, W., Arends, B.G., Möls, J.J., Berner, A., Solly, I., Kruisz, C., Reischl, G., Pahl, S., Hallberg, A., Ogren, J.A., Fierlinger-Oberlinninger, H., Marzorati, A., Schell, D., 1992. The chemistry of sulfur and nitrogen species in a fog system A multiphase approach. Tellus B. 44, 505–521.

Fall, R., Karl, T., Hansel, A., Jordan, A., Lindinger, W., 1999. Volatile organic compounds emitted after leaf wounding: On-line analysis by proton-transfer-reaction mass spectrometry. Journal of Geophysical Research. 104, 15963–15974.

Farah, A., Freney, E., Chauvigné, A., Baray, J.-L., Rose, C., Picard, D., Colomb, A., Hadad, D., Abboud, M., Farah, W., Sellegri, K., 2018.Seasonal variation of aerosol size distribution data at the puy de Dôme station with emphasis on the boundary layer/free troposphere segregation." Atmosphere. 9.7. 244.

Fernández-Martínez, G., López-Mahía, P., Muniategui-Lorenzo, S., Prada-Rodríguez, D., Fernández-Fernández, E., 2001. Distribution of volatile organic compounds during the combustion process in coal-fired power stations. Atmospheric Environment. 35, 5823–5831.

Finlayson-Pitts, B.J., Pitts, J.N., 2000. Particles in the troposphere, in: chemistry of the upper and lower atmosphere. Elsevier, pp. 349–435.

Folkers, M., Mentel, Th.F., Wahner, A., 2003. Influence of an organic coating on the reactivity of aqueous aerosols probed by the heterogeneous hydrolysis of N_2O_5: organic coatings and aerosol reactivity. Geophysical Research Letters. 30.12.

Freney, E., Sellegri, K., Eija, A., Rose, C., Chauvigne, A., Baray, J.L., Colomb, A., Hervo, M., Montoux, N., Bouvier, L., Picard, D., 2012. Experimental evidence of the feeding of the free troposphere with aerosol particles from the mixing layer, Aerosol and Air Quality Research. 16(3), 702–716.

Fry, J. L., Draper, D. C., Barsanti, K. C., Smith, J. N., Ortega, J., Winkler, P. M., Lee, L., 2014. Secondary organic aerosol formation and organic nitrate yield from NO_3 oxidation of biogenic hydrocarbons. Environmental Science & Technology. 48(20), 11944-11953.

Fry, J.L., Kiendler-Scharr, A., Rollins, A.W., Wooldridge, P.J., Brown, S.S., Fuchs, H., Dubé, W., Mensah, A., dal Maso, M., Tillmann, R., Dorn, H.-P., Brauers, T., Cohen, R.C., 2009. Organic nitrate and secondary organic aerosol yield from NO_3 oxidation of β-pinene evaluated using a gas-phase kinetics/aerosol partitioning model. Atmospheric Chemistry and Physics. 9, 1431–1449.

Fu, P., Kawamura, K., Chen, J., Barrie, L.A., 2009. Isoprene, monoterpene, and sesquiterpene oxidation products in the high arctic aerosols during late winter to early summer. Environmental Science & Technology. 43, 4022–4028.

Fuentes, J.D., Gu, L., Lerdau, M., Atkinson, R., Baldocchi, D., Bottenheim, J.W., Ciccioli, P., Lamb, B., Geron, C., Guenther, A., Sharkey, T.D., Stockwell, W., 2000. Biogenic hydrocarbons in the atmospheric boundary layer: a review. Bulletin of the American Meteorological Society. 81, 1537–1575.

Gallego, E., Roca, F.J., Perales, J.F., Guardino, X., 2010. Comparative study of the adsorption performance of a multi-sorbent bed (Carbotrap, Carbopack X, Carboxen 569) and a Tenax TA adsorbent tube for the analysis of volatile organic compounds (VOCs). Talanta 81, 916–924.

Gentner, D.R., Harley, R.A., Miller, A.M., Goldstein, A.H., 2009. Diurnal and seasonal variability of gasoline-related volatile organic compound emissions in Riverside, California. Environmental Science & Technology. 43, 4247–4252.

George, I.J., Abbatt, J.P.D., 2010. Chemical evolution of secondary organic aerosol from OH-initiated heterogeneous oxidation. Atmospheric Chemistry and Physics. 10, 5551–5563.

Geron, C., Guenther, A., Sharkey, T., Arnts, R.R., 2000. Temporal variability in basal isoprene emission factor. Tree Physiology. 20, 799–805.

Gfeller, A., Laloux, M., Barsics, F., Kati, D.E., Haubruge, E., du Jardin, P., Verheggen, F.J., Lognay, G., Wathelet, J.-P., Fauconnier, M.-L., 2013. Characterization of volatile organic compounds emitted by barley (Hordeum vulgare L.) roots and their attractiveness to wireworms. J Chem Ecol. 39, 1129–1139.

Gill, P.S., Graedel, T.E., Weschler, C.J., 1983. Organic films on atmospheric aerosol particles, fog droplets, cloud droplets, raindrops, and snowflakes. Reviews of Geophysics. 21, 903.

Glotfelty, D.E., Seiber, J.N., Liljedahl, A., 1987. Pesticides in fog. Nature. 325, 602–605.

Goldstein, A.H., Galbally, I.E., 2007. Known and unexplored organic constituents in the Earth's Atmosphere. Environmental Science & Technology. 41, 1514–1521.

Goldstein, A.H., Schade, G.W., 2000. Quantifying biogenic and anthropogenic contributions to acetone mixing ratios in a rural environment. Atmospheric Environment. 34, 4997–5006.

Graus, M., Schnitzler, J.-P., Hansel, A., Cojocariu, C., Rennenberg, H., Wisthaler, A., Kreuzwieser, J., 2004. Transient release of oxygenated volatile organic compounds during light-dark transitions in grey poplar leaves. Plant Physiology. 135, 1967–1975.

Gray, C.M., Monson, R.K., Fierer, N., 2010. Emissions of volatile organic compounds during the decomposition of plant litter. Journal of Geophysical Research. 115, G03015.

Greenberg, J.P., Asensio, D., Turnipseed, A., Guenther, A.B., Karl, T., Gochis, D., 2012. Contribution of leaf and needle litter to whole ecosystem BVOC fluxes. Atmospheric Environment. 59, 302–311.

Gros, V., Gaimoz, C., Herrmann, F., Custer, T., Williams, J., Bonsang, B., Sauvage, S., Locoge, N., d'Argouges, O., Sarda-Estève, R., Sciare, J., 2011. Volatile organic compounds sources in Paris in spring 2007. Part I: qualitative analysis. Environmental Chemistry. 8, 74.

Guenther, A., Hewitt, C.N., Erickson, D., Fall, R., Geron, C., Graedel, T., Harley, P., Klinger, L., Lerdau, M., Mckay, W.A., Pierce, T., Scholes, B., Steinbrecher, R., Tallamraju, R., Taylor, J., Zimmerman, P., 1995. A global model of natural volatile organic compound emissions. Journal of Geophysical Research. 100, 8873.

Guenther, A., Karl, T., Harley, P., Wiedinmyer, C., Palmer, P.I., Geron, C., 2006. Estimates of global terrestrial isoprene emissions using MEGAN (Model of Emissions of Gases and Aerosols from Nature). Atmospheric Chemistry and Physics. 6, 3181–3210.

Guenther, A.B., Jiang, X., Heald, C.L., Sakulyanontvittaya, T., Duhl, T., Emmons, L.K., Wang, X., 2012. The model of emissions of gases and aerosols from nature version 2.1 (MEGAN2.1): an extended and updated framework for modeling biogenic emissions. Geoscientific Model Development. 5, 1471–1492.

Guenther, A.B., Zimmerman, P.R., Harley, P.C., Monson, R.K., Fall, R., 1993. Isoprene and monoterpene emission rate variability: Model evaluations and sensitivity analyses. Journal of Geophysical Research. 98, 12609.

Hallquist, M., Wenger, J.C., Baltensperger, U., Rudich, Y., Simpson, D., Claeys, M., Dommen, J., Donahue, N.M., George, C., Goldstein, A.H., Hamilton, J.F., Herrmann, H., Hoffmann, T., Iinuma, Y., Jang, M., Jenkin, M.E., Jimenez, J.L., Kiendler-Scharr, A., Maenhaut, W., McFiggans, G., Mentel, Th.F., Monod, A., Prévôt, A.S.H., Seinfeld, J.H., Surratt, J.D., Szmigielski, R., Wildt, J., 2009. The formation, properties and impact of secondary organic aerosol: current and emerging issues. Atmospheric Chemistry and Physics. 9, 5155–5236.

Hansel, A., Jordan, A., Holzinger, R., Prazeller, P., Vogel, W., and Lindinger, W., 1995. Proton transfer reaction mass spectrometry: online trace gas analysis at the ppb level, International Journal of Mass Spectrometry and Ion Processes. 149–150, 609–619.

Hansel, A., Jordan, A., Warneke, C., Holzinger, R., Wisthaler, A., and Lindinger, W., 1999. Proton-transfer-reaction mass spectrometry (PTR-MS): on-line monitoring of volatile organic compounds at volume mixing ratios of a few pptv, Plasma Sources Science & Technology. 8, 332–336.

Hanson, D.T., Swanson, S., Graham, L.E., Sharkey, T.D., 1999. Evolutionary significance of isopreneemission from mosses. American Journal of Botany. 86, 634–639.

Harley, P.C., Monson, R.K., Lerdau, M.T., 1999. Ecological and evolutionary aspects of isoprene emission from plants. Oecologia. 118, 109–123.

Harley, R.A., Hannigan, M.P., Cass, G.R., 1992. Respeciation of organic gas emissions and the detection of excess unburned gasoline in the atmosphere. Environmental Science & Technology. 26, 2395–2408.

Hartkopf A. and Karger B. L., 1973. Study of the interfacial properties of water by gas chromatography. Accounts of Chemical Research. Res. 6, 209-216

Hatanaka, A., 1993. The biogeneration of green odour by green leaves. Phytochemistry. 34, 1201–1218.

Hatch, L.E., Yokelson, R.J., Stockwell, C.E., Veres, P.R., Simpson, I.J., Blake, D.R., Orlando, J.J., Barsanti, K.C., 2017. Multi-instrument comparison and compilation of non-methane organic gas emissions from biomass burning and implications for smoke-derived secondary organic aerosol precursors. Atmospheric Chemistry and Physics. 17, 1471–1489.

Heald, C.L., Coe, H., Jimenez, J.L., Weber, R.J., Bahreini, R., Middlebrook, A.M., Russell, L.M., Jolleys, M., Fu, T.-M., Allan, J.D., Bower, K.N., Capes, G., Crosier, J., Morgan, W.T., Robinson, N.H., Williams, P.I., Cubison, M.J., DeCarlo, P.F., Dunlea, E.J., 2011. Exploring the vertical profile of atmospheric organic aerosol: comparing 17 aircraft field campaigns with a global model. Atmospheric Chemistry and Physics. 11, 12673–12696.

Hellen, H., Hakola, H., Laurila, T., 2003. Determination of source contributions of NMHCs in Helsinki (60o N, 25o E) using chemical mass balance and the Unmix multivariate receptor models. Atmospheric Environment. 37, 1413–1424.

Helmig, D., 1997. Ozone removal techniques in the sampling of atmospheric volatile organic trace gases. Atmospheric Environment. 31(21), 3635-3651.

Henne, W.M., Boucrot, E., Meinecke, M., Evergren, E., Vallis, Y., Mittal, R., McMahon, H.T., 2010. FCHo Proteins are nucleators of clathrin-mediated endocytosis. Science. 328, 1281–1284.

Henry, K.M., Donahue, N.M., 2012. Photochemical aging of α-pinene secondary organic aerosol: effects of OH radical sources and photolysis. The Journal of Physical Chemistry A. 116, 5932–5940.

Henze, D.K., Seinfeld, J.H., 2006. Global secondary organic aerosol from isoprene oxidation. Geophysical Research Letters. 33.9.

Herckes, P., Leenheer, J.A., Collett, J.L., 2007. Comprehensive characterization of atmospheric organic matter in Fresno, California fog water. Environmental Science & Technology. 41, 393–399.

Heringa, M. F., DeCarlo, P. F., Chirico, R., Tritscher, T., Dommen, J., Weingartner, E Baltensperger, U., 2011. Investigations of primary and secondary particulate matter of different wood combustion appliances with a high-resolution time-of-flight aerosol mass spectrometer. Atmospheric Chemistry and Physics. 11(12), 5945-5957.

Herrmann, H., Schaefer, T., Tilgner, A., Styler, S.A., Weller, C., Teich, M., Otto, T., 2015. Tropospheric aqueous-phase chemistry: kinetics, mechanisms, and its coupling to a changing gas phase. Chemical Reviews. 115, 4259–4334.

Herrmann, H., Wolke, R., Müller, K., Brüggemann, E., Gnauk, T., Barzaghi, P., Mertes, S., Lehmann, K., Massling, A., Birmili, W., Wiedensohler, A., Wieprecht, W., Acker, K., Jaeschke, W., Kramberger, H., Svrcina, B., Bächmann, K., Collett, J.L., Galgon, D., Schwirn, K., Nowak, A., van Pinxteren, D., Plewka, A., Chemnitzer, R., Rüd, C., Hofmann, D., Tilgner, A., Diehl, K., Heinold, B., Hinneburg, D., Knoth, O., Sehili, A.M., Simmel, M., Wurzler, S., Majdik, Z., Mauersberger, G., Müller, F., 2005. FEBUKO and MODMEP: Field measurements and modelling of aerosol and cloud multiphase processes. Atmospheric Environment. 39, 4169–4183.

Hervo, M., Sellegri, K., Pichon, J. M., Roger, J. C. and Laj, P., 2014. Long term measurements of optical properties and their hygroscopic enhancement, Atmospheric Chemistry and Physics. 2014, 27731–27767.

Ho, S. S. H. and Yu, J. Z., 2004. Determination of airborne carbonyls: comparison of a thermal desorption/GC method with the standard DNPH/HPLC method, Environmental Science & Technology. 38, 862–870.

Ho, S.S.H., Wang, L., Chow, J.C., Watson, J.G., Xue, Y., Huang, Y., Qu, L., Li, B., Dai, W., Li, L., Cao, J., 2018. Optimization and evaluation of multi-bed adsorbent tube method in collection of volatile organic compounds. Atmospheric Research. 202, 187–195.

Hodzic, A., Kasibhatla, P.S., Jo, D.S., Cappa, C.D., Jimenez, J.L., Madronich, S., Park, R.J., 2016. Rethinking the global secondary organic aerosol (SOA) budget: stronger production, faster removal, shorter lifetime. Atmospheric Chemistry and Physics. 16, 7917–7941.

Hodzic, A., Madronich, S., Kasibhatla, P.S., Tyndall, G., Aumont, B., Jimenez, J.L., Lee-Taylor, J., Orlando, J., 2015. Organic photolysis reactions in tropospheric aerosols: effect on secondary organic aerosol formation and lifetime. Atmospheric Chemistry and Physics. 15, 9253–9269.

Hoerger, C.C., Claude, A., Plass-Duelmer, C., Reimann, S., Eckart, E., Steinbrecher, R., Aalto, J., Arduini, J., Bonnaire, N., Cape, J.N., Colomb, A., Connolly, R., Diskova, J., Dumitrean, P., Ehlers, C., Gros, V., Hakola, H., Hill, M., Hopkins, J.R., Jäger, J., Junek, R., Kajos, M.K., Klemp, D., Leuchner, M., Lewis, A.C., Locoge, N., Maione, M., Martin, D., Michl, K., Nemitz, E., ODoherty, S., Pérez Ballesta, P., Ruuskanen, T.M., Sauvage, S., Schmidbauer, N., Spain, T.G., Straube, E., Vana, M., Vollmer, M.K., Wegener, R., Wenger, A., 2015. ACTRIS non-methane hydrocarbon intercomparison experiment in Europe to support WMO GAW and EMEP observation networks. Atmospheric Measurement Techniques. 8, 2715–2736.

Hoffmann, E.H., Tilgner, A., Wolke, R., Böge, O., Walter, A., Herrmann, H., 2018. Oxidation of substituted aromatic hydrocarbons in the tropospheric aqueous phase: kinetic mechanism development and modelling. Physical Chemistry Chemical Physics. 20, 10960–10977.

Holopainen, J.K., Gershenzon, J., 2010. Multiple stress factors and the emission of plant VOCs. Trends in Plant Science. 15, 176–184.

Holopainen, J.K., Kivimäenpää, M., Nizkorodov, S.A., 2017. Plant-derived secondary organic material in the air and ecosystems. Trends in Plant Science. 22, 744–753.

Hörtnagl, L., Bamberger, I., Graus, M., Ruuskanen, T.M., Schnitzhofer, R., Müller, M., Hansel, A., Wohlfahrt, G., 2011. Biotic, abiotic, and management controls on methanol exchange above a temperate mountain grassland. Journal of Geophysical Research. 116.G3.

Houdier, S., Barret, M., Dominé, F., Charbouillot, T., Deguillaume, L., Voisin, D., 2011. Sensitive determination of glyoxal, methylglyoxal and hydroxyacetaldehyde in environmental water samples by using dansylacetamidooxyamine derivatization and liquid chromatography/fluorescence. Analytica Chimica Acta. 704, 162–173.

Holzinger, R., Acton, W. J. F., Bloss, W. J., Breitenlechner, M., Crilley, L. R., Dusanter, S. Kramer, L. J., 2019. Validity and limitations of simple reaction kinetics to calculate concentrations of organic compounds from ion counts in PTR-MS. Atmospheric Measurement Techniques.446, 5194.

Hoshi J Y, Amano S, Sasaki Y, Korenaga T, 2008. Investigation and estimation of emission sources of 54 volatile organic compounds in ambient air in Tokyo. Atmospheric Environment. 42(10): 2383–2393.

Hu, D., Bian, Q., Li, T.W.Y., Lau, A.K.H., Yu, J.Z., 2008. Contributions of isoprene, monoterpenes, β -caryophyllene, and toluene to secondary organic aerosols in Hong Kong during the summer of 2006. Journal of Geophysical Research. 113.D22 .

Huang, G., Brook, R., Crippa, M., Janssens-Maenhout, G., Schieberle, C., Dore, C., Guizzardi, D., Muntean, M., Schaaf, E., Friedrich, R., 2017. Speciation of anthropogenic emissions of non-methane volatile organic compounds: a global gridded data set for 1970–2012. Atmospheric Chemistry and Physics. 17, 7683–7701.

Husárová, S., Vaïtilingom, M., Deguillaume, L., Traikia, M., Vinatier, V., Sancelme, M., Amato, P., Matulová, M., Delort, A.-M., 2011. Biotransformation of methanol and formaldehyde by bacteria isolated from clouds. Comparison with radical chemistry. Atmospheric Environment. 45, 6093–6102.

Hutchings, J.W., Ervens, B., Straub, D., Herckes, P., 2010. *N* -Nitrosodimethylamine occurrence, formation and cycling in clouds and fogs. Environmental Science & Technology. 44, 8128–8133.

Hutchings, J. W., Robinson, M. S., McIlwraith, H., Kingston, J. T., Herckes, P., 2009. The chemistry of intercepted clouds in Northern Arizona during the North American monsoon season. Water, air, and soil pollution. 199(1-4), 191-202.

Huybrechts, T., Dewulf, J., Van Langenhove, H., 2003. State-of-the-art of gas chromatography-based methods for analysis of anthropogenic volatile organic compounds in estuarine waters, illustrated with the river Scheldt as an example. Journal of Chromatography A. 1000, 283–297.

Iribarne, J.V., Cho, H.R., 1989. Models of cloud chemistry. Tellus B. 41B, 2–23.

Jackson, R.B., Mooney, H.A., Schulze, E.-D., 1997. A global budget for fine root biomass, surface area, and nutrient contents. Proceedings of the National Academy of Sciences. 94, 7362–7366.

Jacob, D., 2000. Heterogeneous chemistry and tropospheric ozone. Atmospheric Environment. 34, 2131–2159.

Jacob, D.J., 2005. Global budget of methanol: Constraints from atmospheric observations. Journal of Geophysical Research. 110.D8.

Jacob, D.J., Field, B.D., Jin, E.M., Bey, I., Li, Q., Logan, J.A., Yantosca, R.M., Singh, H.B., 2002. Atmospheric budget of acetone: atmospheric budget of acetone. Journal of Geophysical Research Atmospheres. 107, 5-17.

Jardine, K.J., Sommer, E.D., Saleska, S.R., Huxman, T.E., Harley, P.C., Abrell, L., 2010. Gas phase measurements of pyruvic acid and its volatile metabolites. Environmental Science & Technology. 44, 2454–2460.

Johnson, D., Marston, G., 2008. The gas-phase ozonolysis of unsaturated volatile organic compounds in the troposphere. Chemical Society Reviews. 37, 699.

Johnston, F.H., Henderson, S.B., Chen, Y., Randerson, J.T., Marlier, M., DeFries, R.S., Kinney, P., Bowman, D.M.J.S., Brauer, M., 2012. Estimated global mortality attributable to smoke from landscape fires. Environmental Health Perspectives. 120, 695–701.

Jonsson, A. M., Hallquist, M., and Saathoff, H., 2007. Volatility of secondary organic aerosols from the ozone initiated oxidation of α-pinene and limonene, Journal of Aerosol Science. 38, 843–852.

Jonsson, A. M., Hallquist, M., and Ljungström, E., 2008. The effect of temperature and water on secondary organic aerosol formation from ozonolysis of limonene, 13-carene and α-pinene, Atmospheric Chemistry and Physics. 8, 6541–6549.

Kanakidou, M., Seinfeld, J.H., Pandis, S.N., Barnes, I., Dentener, F.J., Facchini, M.C., Van Dingenen, R., Ervens, B., Nenes, A., Nielsen, C.J., Swietlicki, E., Putaud, J.P., Balkanski, Y., Fuzzi, S., Horth, J., Moortgat, G.K., Winterhalter, R., Myhre, C.E.L., Tsigaridis, K., Vignati, E., Stephanou, E.G., Wilson, J., 2005. Organic aerosol and global climate modelling: a review. Atmospheric Chemistry and Physics. 5, 1053–1123.

Karagulian, F., Scott Lea, A., Dilbeck, C.W., Finlayson-Pitts, B.J., 2008. A new mechanism for ozonolysis of unsaturated organics on solids: phosphocholines on NaCl as a model for sea salt particles. Physical Chemistry Chemical Physics. 10, 528–541. D

Kawaguchi, M., Ito, R., Sakui, N., Okanouchi, N., Saito, K., Seto, Y., Nakazawa, H., 2007. Stir-bar-sorptive extraction, with in-situ deconjugation, and thermal desorption with in-tube silylation, followed by gas chromatography-mass spectrometry for measurement of urinary 4-nonylphenol and 4-tert-octylphenol glucuronides. Analytical and Bioanalytical Chemistry. 388, 391–398.

Kawaguchi, M., Sakui, N., Okanouchi, N., Ito, R., Saito, K., Nakazawa, H., 2005. Stir bar sorptive extraction and trace analysis of alkylphenols in water samples by thermal desorption with in tube silylation and gas chromatography–mass spectrometry. Journal of Chromatography A. 1062, 23–29.

Keene, W.C., Mosher, B.W., Jacob, D.J., Munger, J.W., Talbot, R.W., Artz, R.S., Maben, J.R., Daube, B.C., Galloway, J.N., 1995. Carboxylic acids in clouds at a high-elevation forested site in central Virginia. Journal of Geophysical Research: Atmospheres. 100, 9345–9357.

Kesselmeier, J., Staudt, M., 1999. Biogenic volatile organic compounds (VOC): an overview on emission, Physiology and Ecology. Journal of Atmospheric Chemistry. 33, 23–88.

Kile, D.E., Chiou, C.T., 1989. Water solubility enhancements of DDT and trichlorobenzene by some surfactants below and above the critical micelle concentration. Environmental Science & Technology. 23, 832–838.

Kirkman, L. K., Jack, S. B., 2017. Ecological restoration and management of longleaf pine forests. CRC Press.

Knorr, W., Dentener, F., Lamarque, J.-F., Jiang, L., Arneth, A., 2017. Wildfire air pollution hazard during the 21st century. Atmospheric Chemistry and Physics. 17, 9223–9236.

Knote, C., Hodzic, A., Jimenez, J.L., Volkamer, R., Orlando, J.J., Baidar, S., Brioude, J., Fast, J., Gentner, D.R., Goldstein, A.H., Hayes, P.L., Knighton, W.B., Oetjen, H., Setyan, A., Stark, H., Thalman, R., Tyndall, G., Washenfelder, R., Waxman, E., Zhang, Q., 2014. Simulation of semi-explicit mechanisms of SOA formation from glyoxal in aerosol in a 3-D model. Atmospheric Chemistry and Physics. 14, 6213–6239.

Kögel-Knabner, I., 2002. The macromolecular organic composition of plant and microbial residues as inputs to soil organic matter. Soil Biology and Biochemistry. 34(2), 139-162.

Kroll, J. H., Ng, N. L., Murphy, S. M., Flagan, R. C., and Seinfeld, J. H., 2006. Secondary organic aerosol formation from isoprene photooxidation, Environmental Science & Technology. 40, 1869–1877.

Kroll, J.H., Seinfeld, J.H., 2008. Chemistry of secondary organic aerosol: Formation and evolution of low-volatility organics in the atmosphere. Atmospheric Environment. 42, 3593–3624.

Lancas, F.M., Queiroz, M.E.C., Grossi, P., Olivares, I.R.B., 2009. Recent developments and applications of stir bar sorptive extraction. Journal of Separation Science. 32, 813–824.

Lanz, V.A., Hueglin, C., Buchmann, B., Hill, M., Locher, R., Staehelin, J., Reimann, S., 2008. Receptor modeling of C_2-C_7 hydrocarbon sources at an urban background site in Zurich, Switzerland: changes between 1993-1994 and 2005-2006. Atmospheric Chemistry and Physics. 8, 2313–2332.

Lathière, J., Hewitt, C.N., Beerling, D.J., 2010. Sensitivity of isoprene emissions from the terrestrial biosphere to 20th century changes in atmospheric CO_2 concentration, climate, and land use: twentieth century biogenic isoprene emissions. Global Biogeochemical Cycles. 24.1.

Lee, B. H., Pierce, J. R., Engelhart, G. J., Pandis, S. N., 2011. Volatility of secondary organic aerosol from the ozonolysis of monoterpenes. Atmospheric Environment. 45(14), 2443-2452.

Lebedev, A.T., Polyakova, O.V., Mazur, D.M., Artaev, V.B., Canet, I., Lallement, A., Vaïtilingom, M., Deguillaume, L., Delort, A.-M., 2018. Detection of semi-volatile compounds in cloud waters by GC×GC-TOF-MS. Evidence of phenols and phthalates as priority pollutants. Environmental Pollution. 241, 616–625.

Leff, J. W. and Fierer, N., 2008. Volatile organic compound (VOC) emissions from soil and litter samples. Soil Biology and Biochemistry. 40(7) :1629–1636.

Legreid, G., Lööv, J.B., Staehelin, J., Hueglin, C., Hill, M., Buchmann, B., Prevot, A.S.H., Reimann, S., 2007. Oxygenated volatile organic compounds (OVOCs) at an urban background site in Zürich (Europe): Seasonal variation and source allocation. Atmospheric Environment. 41, 8409–8423.

Lelieveld, J., Klingmüller, K., Pozzer, A., Burnett, R.T., Haines, A., Ramanathan, V., 2019. Effects of fossil fuel and total anthropogenic emission removal on public health and climate. Proceedings of the National Academy of Sciences. 116, 7192–7197.

León, V.M., Álvarez, B., Cobollo, M.A., Muñoz, S., Valor, I., 2003. Analysis of 35 priority semivolatile compounds in water by stir bar sorptive extraction–thermal desorption–gas chromatography–mass spectrometry. Journal of Chromatography A. 999, 91–101.

Leriche, M., Deguillaume, L., Chaumerliac, N., 2003. Modeling study of strong acids formation and partitioning in a polluted cloud during wintertime. Journal of Geophysical Research: Atmospheres. 108(D14).

Lesouëf, D., Gheusi, F., Delmas, R., and Escobar, J., 2011. Numerical simulations of local circulations and pollution transport over Reunion Island, Annales Geophysicae. 29, 53–69.

Leuchner, M., Gubo, S., Schunk, C., Wastl, C., Kirchner, M., Menzel, A., Plass-Dülmer, C., 2015. Can positive matrix factorization help to understand patterns of organic trace gases at the continental Global Atmosphere Watch site Hohenpeissenberg? Atmospheric Chemistry and Physics. 15, 1221–1236.

Leuchner, M., Rappengluck, B., 2010. VOC source-receptor relationships in Houston during TexAQS-II. Atmospheric Environment. 44, 4056–4067.

Leuenberger, C., Czuczwa, J., Heyerdahl, E., Giger, W., 1988. Aliphatic and polycyclic aromatic hydrocarbons in urban rain, snow and fog. Atmospheric Environment. 22, 695–705.

Li, J., Hao, Y., Simayi, M., Shi, Y., Xi, Z., Xie, S., 2019. Verification of anthropogenic VOC emission inventory through ambient measurements and satellite retrievals. Atmospheric Chemistry and Physics. 19, 5905–5921.

Li, Q., Sritharathikhun, P., Motomizu, S., 2007. Development of novel reagent for Hantzsch reaction for the determination of formaldehyde by spectrophotometry and fluorometry. Analytical sciences : the international journal of the Japan Society for Analytical Chemistry. 23, 413–7.

Li, S.-M., Macdonald, A.M., Leithead, A., Leaitch, W.R., Gong, W., Anlauf, K.G., Toom-Sauntry, D., Hayden, K., Bottenheim, J., Wang, D., 2008. Investigation of carbonyls in cloudwater during ICARTT. Journal of Geophysical Research. 113. D17.

Li, T., Wang, Z., Wang, Yaru, Wu, C., Liang, Y., Xia, M., Yu, C., Yun, H., Wang, W., Wang, Yan, Guo, J., Herrmann, H., Wang, T., 2019. Chemical characteristics of cloud water and the impacts on aerosol properties at a subtropical mountain site in Hong Kong. Atmospheric Chemistry and Physics Discussions 1–24.

Li, X., Li, P., Yan, L., Chen, J., Cheng, T., Xu, S., 2011. Characterization of polycyclic aromatic hydrocarbons in fog–rain events. Journal of Environmental Monitoring. 13, 2988.

Liakakou, E., Vrekoussis, M., Bonsang, B., Donousis, Ch., Kanakidou, M., Mihalopoulos, N., 2007. Isoprene above the Eastern Mediterranean: Seasonal variation and contribution to the oxidation capacity of the atmosphere. Atmospheric Environment. 41, 1002–1010.

Lim, H.-J., Carlton, A.G., Turpin, B.J., 2005. Isoprene forms secondary organic aerosol through cloud processing: model simulations. Environmental Science & Technology. 39, 4441–4446.

Lin, C., Owen, S., Penuelas, J., 2007. Volatile organic compounds in the roots and rhizosphere of Pinus spp. Soil Biology and Biochemistry. 39, 951–960.

Liu, B., Gumpertz, M.L., Hu, S., Ristaino, J.B., 2007. Long-term effects of organic and synthetic soil fertility amendments on soil microbial communities and the development of southern blight. Soil Biology and Biochemistry. 39, 2302–2316.

Liu, Y., Shao, M., Lu, S., Chang, C.-C., Wang, J.-L., Fu, L., 2008. Source apportionment of ambient volatile organic compounds in the Pearl River Delta, China: Part II. Atmospheric Environment. 42, 6261–6274.

Logan, J.A., 1985. Tropospheric ozone: Seasonal behavior, trends, and anthropogenic influence. Journal of Geophysical Research: Atmospheres. 90, 10463–10482.

Loreto, F., Barta, C., Brilli, F., Nogues, I., 2006. On the induction of volatile organic compound emissions by plants as consequence of wounding or fluctuations of light and temperature. Plant Cell Environment. 29, 1820–1828.

Loreto, F., Forster, A., Durr, M., Csiky, O., Seufert, G., 1998. On the monoterpene emission under heat stress and on the increased thermotolerance of leaves of Quercus ilex L. fumigated with selected monoterpenes. Plant Cell Environment. 21, 101–107.

Lu, T., Lansing, J., Zhang, W., Bechle, M.J., Hankey, S., 2019. Land use regression models for 60 volatile organic compounds: comparing google point of interest (POI) and city permit data. Science of The Total Environment. 677, 131–141.

Ludley, Katherine.E., Jickells, S.M., Chamberlain, P.M., Whitaker, J., Robinson, C.H., 2009. Distribution of monoterpenes between organic resources in upper soil horizons under monocultures of Picea abies, Picea sitchensis and Pinus sylvestris. Soil Biology and Biochemistry. 41, 1050–1059.

Mackay D., 1991. Multimedia environmental models. The Fuoacity Approach, pp. 99-101. Lewis, Chelsea, MI.

Mahmoud, S.S., Croteau, R.B., 2002. Strategies for transgenic manipulation of monoterpene biosynthesis in plants. Trends in Plant Science. 7, 366–373.

Marécal, V., Pirre, M., Rivière, E.D., Pouvesle, N., Crowley, J.N., Freitas, S.R., Longo, K.M., 2010. Modelling the reversible uptake of chemical species in the gas phase by ice particles formed in a convective cloud. Atmospheric Chemistry and Physics 10, 4977–5000.

Marinoni, A., Laj, P., Sellegri, K., Mailhot, G., 2004. Cloud chemistry at the puy de Dôme: variability and relationships with environmental factors. Atmospheric Chemistry and Physics. 4(3), 715-728.

Matsunaga, A., Ziemann, P.J., 2010. Gas-wall partitioning of organic compounds in a teflon film chamber and potential effects on reaction product and aerosol yield measurements. Aerosol Science and Technology. 44, 881–892.

Mermet, K., Sauvage, S., Dusanter, S., Salameh, T., Léonardis, T., Flaud, P.-M., Perraudin, É., Villenave, É., and Locoge, N., 2019. Optimization of a gas chromatographic unit for measuring BVOCs in ambient air, Atmospheric Measurement Techniques in Discussion. 633.

McDonald, B.C., de Gouw, J.A., Gilman, J.B., Jathar, S.H., Akherati, A., Cappa, C.D., Jimenez, J.L., Lee-Taylor, J., Hayes, P.L., McKeen, S.A., Cui, Y.Y., Kim, S.-W., Gentner, D.R., Isaacman-VanWertz, G., Goldstein, A.H., Harley, R.A., Frost, G.J., Roberts, J.M., Ryerson, T.B., Trainer, M., 2018. Volatile chemical products emerging as largest petrochemical source of urban organic emissions. Science. 359, 760–764.

McDonald, B.C., Gentner, D.R., Goldstein, A.H., Harley, R.A., 2013. Long-term trends in motor vehicle emissions in U.S. urban areas. Environmental Science & Technology. 47, 10022–10031.

McDonald, B.C., Goldstein, A.H., Harley, R.A., 2015. Long-term trends in California mobile source emissions and ambient concentrations of black carbon and organic aerosol. Environmental Science & Technology. 49, 5178–5188.

Michoud, V., Sciare, J., Sauvage, S., Dusanter, S., Léonardis, T., Gros, V., Kalogridis, C., Zannoni, N., Féron, A., Petit, J.-E., Crenn, V., Baisnée, D., Sarda-Estève, R., Bonnaire, N., Marchand, N., DeWitt, H.L., Pey, J., Colomb, A., Gheusi, F., Szidat, S., Stavroulas, I., Borbon, A., Locoge, N., 2017. Organic carbon at a remote site of the western Mediterranean Basin: sources and chemistry during the ChArMEx SOP2 field experiment. Atmospheric Chemistry and Physics. 17, 8837–8865.

Millet, D.B., Guenther, A., Siegel, D.A., Nelson, N.B., Singh, H.B., de Gouw, J.A., Warneke, C., Williams, J., Eerdekens, G., Sinha, V., Karl, T., Flocke, F., Apel, E., Riemer, D.D., Palmer, P.I., Barkley, M., 2010. Global atmospheric budget of acetaldehyde: 3-D model analysis and constraints from in-situ and satellite observations. Atmospheric Chemistry and Physics. 10, 3405–3425.

Montero, L., Duane, M., Manfredi, U., Astorga, C., Martini, G., Carriero, M., Krasenbrink, A. and Larsen, B.-R., 2010. Hydrocarbon emission fingerprints from contemporary vehicle/engine technologies with conventional and new fuels, Atmospheric Environment. 44, 2167–2175.

Morel F. M. M. Gschwend P. M., 1987. The role of colloids in the partitioning of solutes in natural waters. In Aquatic Surface Chemistry (edited by Stumm W.), pp. 405-422. Wiley, New York.

Morozov, G., Breus, V., Nekludov, S., Breus, I., 2014. Sorption of volatile organic compounds and their mixtures on montmorillonite at different humidity. Colloids and Surfaces A: Physicochemical and Engineering Aspects. 454, 159–171.

Morrissey, F.A., Grismer, M.E., 1999. Kinetics of volatile organic compound sorption/desorption on clay minerals. Journal of Contaminant Hydrology. 36, 291–312.

Moschonas, N., Glavas, S., 1996. C3–C10 hydrocarbons in the atmosphere of Athens, Greece. Atmospheric Environment. 30, 2769–2772.

Mouchel-Vallon, C., Deguillaume, L., Monod, A., Perroux, H., Rose, C., Ghigo, G., Long, Y., Leriche, M., Aumont, B., Patryl, L., Armand, P., Chaumerliac, N., 2017. CLEPS 1.0: A new protocol for cloud aqueous phase oxidation of VOC mechanisms. Geoscientific Model Development. 10, 1339–1362.

Mouchel-Vallon, C., Bräuer, P., Camredon, M., Valorso, R., Madronich, S., Herrmann, H., Aumont, B., 2013. Explicit modeling of volatile organic compounds partitioning in the atmospheric aqueous phase. Atmospheric Chemistry and Physics. 13, 1023–1037.

Müller, J.-F., 1992. Geographical distribution and seasonal variation of surface emissions and deposition velocities of atmospheric trace gases. Journal of Geophysical Research. 97, 3787.

Munger, J.W., Jacob, D.J., Daube, B.C., Horowitz, L.W., Keene, W.C., Heikes, B.G., 1995. Formaldehyde, glyoxal, and methylglyoxal in air and cloudwater at a rural mountain site in central Virginia. Journal of Geophysical Research: Atmospheres. 100.D5: 9325-9333.

Neeman, E. M., Avilés-Moreno, J. R., Huet, T. R., 2017. The quasi-unchanged gas-phase molecular structures of the atmospheric aerosol precursor β-pinene and its oxidation product nopinone. Physical Chemistry Chemical Physics. 19(21), 13819-13827.

Nelson, P.F., Tibbett, A.R., Day, S.J., 2008. Effects of vehicle type and fuel quality on real world toxic emissions from diesel vehicles. Atmospheric Environment. 42, 5291–5303.

Ng, N.L., Kroll, J.H., Chan, A.W.H., Chhabra, P.S., Flagan, R.C., Seinfeld, J.H., 2007. Secondary organic aerosol formation from *m*-xylene, toluene, and benzene. Atmospheric Chemistry and Physics. 7, 3909–3922.

Nguyen, H.T., Kim, K.-H., Kim, M.-Y., 2009. Volatile organic compounds at an urban monitoring station in Korea. Journal of Hazardous Materials. 161, 163–174.

Nguyen, T.B., Crounse, J.D., Schwantes, R.H., Teng, A.P., Bates, K.H., Zhang, X., St. Clair, J.M., Brune, W.H., Tyndall, G.S., Keutsch, F.N., Seinfeld, J.H., Wennberg, P.O., 2014. Overview of the Focused Isoprene eXperiment at the California Institute of Technology (FIXCIT):

mechanistic chamber studies on the oxidation of biogenic compounds. Atmospheric Chemistry and Physics. 14, 13531–13549.

Niedojadlo, A., Becker, K.H., Kurtenbach, R., Wiesen, P., 2007. The contribution of traffic and solvent use to the total NMVOC emission in a German city derived from measurements and CMB modelling. Atmospheric Environment. 41, 7108–7126.

Niehus, B., Popp, P., Bauer, C., Peklo, G., Zwanziger, H. W., 2002. Comparison of stir bar sorptive extraction and solid phase extraction as enrichment techniques in combination with column liquid chromatography for the determination of polycyclic aromatic hydrocarbons in water samples. International Journal of Environmental & Analytical Chemistry. 82(10), 669-676.

Niinemets, Ü., Loreto, F., Reichstein, M., 2004. Physiological and physicochemical controls on foliar volatile organic compound emissions. Trends in Plant Science. 9, 180–186.

Nollet, L. M., 2005. Chromatographic analysis of the environment: mass spectrometry based approaches. CRC Press.

Novotny, M.V., Soini, H.A., Koyama, S., Wiesler, D., Bruce, K.E., Penn, D.J., 2007. Chemical identification of MHC-influenced volatile compounds in mouse urine. I: quantitative proportions of major chemosignals. Journal of Chemical Ecology. 33, 417–434.

Nozière, B., Kalberer, M., Claeys, M., Allan, J., D'Anna, B., Decesari, S., Finessi, E., Glasius, M., Grgić, I., Hamilton, J.F., Hoffmann, T., Iinuma, Y., Jaoui, M., Kahnt, A., Kampf, C.J., Kourtchev, I., Maenhaut, W., Marsden, N., Saarikoski, S., Schnelle-Kreis, J., Surratt, J.D., Szidat, S., Szmigielski, R., Wisthaler, A., 2015. The molecular identification of organic compounds in the atmosphere: state of the art and challenges. Chemical Reviews. 115, 3919–3983.

Ochiai, N., Sasamoto, K., Kanda, H., Nakamura, S., 2006. Fast screening of pesticide multiresidues in aqueous samples by dual stir bar sorptive extraction-thermal desorption-low thermal mass gas chromatography–mass spectrometry. Journal of Chromatography A. 1130, 83–90.

Ochiai, N., Sasamoto, K., Kanda, H., Yamagami, T., David, F., Tienpont, B., Sandra, P., 2005. Optimization of a multi-residue screening method for the determination of 85 pesticides in selected food matrices by stir bar sorptive extraction and thermal desorption GC-MS. Journal of Separation Science. 28, 1083–1092.

Ochiai, N., Sasamoto, K., Takino, M., Yamashita, S., Daishima, S., Heiden, A., Hoffman, A., 2001. Determination of trace amounts of off-flavor compounds in drinking water by stir bar sorptive extraction and thermal desorption GC-MS. The Analyst. 126, 1652–1657.

Oltmans, S.J., Levy, H., 1994. Surface ozone measurements from a global network. Atmospheric Environment. 28, 9–24.

Ou, J., Guo, H., Zheng, J., Cheung, K., Louie, P.K.K., Ling, Z., Wang, D., 2015. Concentrations and sources of non-methane hydrocarbons (NMHCs) from 2005 to 2013 in Hong Kong: a multi-year real-time data analysis. Atmospheric Environment. 103, 196–206.

Ouyang, G., Vuckovic, D., Pawliszyn, J., 2011. Nondestructive sampling of living systems using *in vivo* solid-phase microextraction. Chemical Reviews. 111, 2784–2814.

Owen, S.M., Boissard, C., Hewitt, C.N., 2001. Volatile organic compounds (VOCs) emitted from 40 Mediterranean plant species: Atmospheric Environment. 35, 5393–5409.

Pacifico, F., Folberth, G.A., Sitch, S., Haywood, J.M., Rizzo, L.V., Malavelle, F.F., Artaxo, P., 2015. Biomass burning related ozone damage on vegetation over the Amazon forest: a model sensitivity study. Atmospheric Chemistry and Physics. 15, 2791–2804.

Pacolay, B.D., Ham, J.E., Slaven, J.E., Wells, J.R., 2008. Feasibility of detection and quantification of gas-phase carbonyls in indoor environments using PFBHA derivatization and solid-phase microextraction (SPME). Journal of Environmental Monitoring. 10, 853.

Palm, B.B., de Sá, S.S., Day, D.A., Campuzano-Jost, P., Hu, W., Seco, R., Sjostedt, S.J., Park, J.-H., Guenther, A.B., Kim, S., Brito, J., Wurm, F., Artaxo, P., Thalman, R., Wang, J., Yee, L.D., Wernis, R., Isaacman-VanWertz, G., Goldstein, A.H., Liu, Y., Springston, S.R., Souza, R., Newburn, M.K., Alexander, M.L., Martin, S.T., Jimenez, J.L., 2018. Secondary organic aerosol formation from ambient air in an oxidation flow reactor in central Amazonia. Atmospheric Chemistry and Physics 18, 467–493.

Palmer, P.I., 2005. Quantifying global marine isoprene fluxes using MODIS chlorophyll observations. Geophysical Research Letters. 32.9.

Palmer, P.I., Abbot, D.S., Fu, T.-M., Jacob, D.J., Chance, K., Kurosu, T.P., Guenther, A., Wiedinmyer, C., Stanton, J.C., Pilling, M.J., Pressley, S.N., Lamb, B., Sumner, A.L., 2006. Quantifying the seasonal and interannual variability of North American isoprene emissions using satellite observations of the formaldehyde column. Journal of Geophysical Research. 111. (D12).

Pandis, S.N., Seinfeld, J.H., 1991. Should bulk cloudwater or fogwater samples obey Henry’s law? Journal of Geophysical Research. 96, 10791.

Pang, X., Lewis, A.C., Hamilton, J.F., 2011. Determination of airborne carbonyls via pentafluorophenylhydrazine derivatisation by GC–MS and its comparison with HPLC method. Talanta. 85, 406–414.

Pankow, J.F., 1997. Partitioning of semi-volatile organic compounds to the air/water interface. Atmospheric Environment. 31, 927–929.

Parra, M.A., Elustondo, D., Bermejo, R., Santamaría, J.M., 2009. Ambient air levels of volatile organic compounds (VOC) and nitrogen dioxide (NO_2) in a medium size city in Northern Spain. Science of The Total Environment. 407, 999–1009.

Parrish, D.D., Stohl, A., Forster, C., Atlas, E.L., Blake, D.R., Goldan, P.D., Kuster, W.C., de Gouw, J.A., 2007. Effects of mixing on evolution of hydrocarbon ratios in the troposphere: mixing effects on NMHC ratio evolution. Journal of Geophysical Research: Atmospheres. 112.

Passant, N. R., 2002. Speciation of UK emissions of non-methane volatile organic compounds, AEA Technology, Report No. AEAT/ENV/R/0545 Issue 1.

Pathak, R. K., Presto, A. A., Lane, T. E., Stanier, C. O., Donahue, N. M., Pandis, S. N., 2007. Ozonolysis of α-pinene: parameterization of secondary organic aerosol mass fraction, Atmospheric Chemistry and Physics. 7, 3811–3821.

Pathak, R., Donahue, N. M., Pandis, S. N., 2008. Ozonolysis of betapinene: temperature dependence of secondary organic aerosol mass fraction, Environmental Science & Technology. 42, 5081–5086.

Peñuelas, J., Asensio, D., Tholl, D., Wenke, K., Rosenkranz, M., Piechulla, B., Schnitzler, J.P., 2014. Biogenic volatile emissions from the soil: Biogenic volatile emissions from the soil. Plant, Cell & Environment. 37, 1866–1891.

Peñuelas, J., Staudt, M., 2010. BVOCs and global change. Trends in Plant Science. 15, 133–144.

Perdue, E.M., Beck, K.C., 1988. Chemical consequences of mixing atmospheric droplets of varied pH. Journal of Geophysical Research. 93, 691–698.

Plum, C.N., E. Sanhueza, R. Atkinson, W.P.L. Carter, J.N. Pitts, Jr. 1983. OH radical rate constants and photolysis rates of a-dicarbonyls. Environmental Science & Technology. 17:479—484.

Popp, P., Bauer, C., Wennrich, L., 2001. Application of stir bar sorptive extraction in combination with column liquid chromatography for the determination of polycyclic aromatic hydrocarbons in water samples. Analytica Chimica Acta. 436(1), 1-9.

Popp, P., Bauer, C., Paschke, A., Montero, L., 2004. Application of a polysiloxane-based extraction method combined with column liquid chromatography to determine polycyclic aromatic hydrocarbons in environmental samples. Analytica chimica acta. 504(2), 307-312.

Presto, A. A., Huff Hartz, K. E., Donahue, N. M., 2005. Secondary organic aerosol production from ozonolysis: 2. Effect of NOx concentration, Environmental Science & Technology. 39, 7046–7054.

Prieto, A., Basauri, O., Rodil, R., Usobiaga, A., Fernández, L.A., Etxebarria, N., Zuloaga, O., 2010. Stir-bar sorptive extraction: A view on method optimisation, novel applications, limitations and potential solutions. Journal of Chromatography A, Extraction Techniques. 1217, 2642–2666.

Prinn, R., D. Cunnold, R. Rasmussen, P. Simmonds, F. Alyea, A. Crawford, P. Fraser, R. Rosen. 1987. Atmospheric trends in methylcholoroform and the global average for the hydroxyl radical. Science. 238:945—950.

Quintana, J.B., Rodil, R., Muniategui-Lorenzo, S., López-Mahía, P., Prada-Rodríguez, D., 2007. Multiresidue analysis of acidic and polar organic contaminants in water samples by stir-bar sorptive extraction–liquid desorption–gas chromatography–mass spectrometry. Journal of Chromatography A. 1174, 27–39.

Raventos-Duran, T., Camredon, M., Valorso, R., Mouchel-Vallon, C., Aumont, B., 2010. Structure-activity relationships to estimate the effective Henry’s law constants of organics of atmospheric interest. Atmospheric Chemistry and Physics. 10, 7643–7654.

Raja, S., Raghunathan, R., Yu, X.-Y., Lee, T., Chen, J., Kommalapati, R. R., Murugesan, K., Shen, X., Qingzhong, Y., Valsaraj, K. T., Collett Jr, J. L., 2008. Fog chemistry in the Texas-Louisiana Gulf Coast corridor, Atmospheric Environment. 42, 2048–2061, 2008.

Reyes-Rodríguez, G. J., Gioda, A., Mayol-Bracero, O. L., and Collett Jr, J., 2009: Organic carbon, total nitrogen, and water-soluble ions in clouds from a tropical montane cloud forest in Puerto Rico, Atmospheric Environment. 43, 4171–4177.

Ribes, A., Carrera, G., Gallego, E., Roca, X., Berenguer, M. J., Guardino, X., 2007. Development and validation of a method for air-quality and nuisance odors monitoring of volatile organic compounds using multi-sorbent adsorption and gas chromatography/mass spectrometry thermal desorption system. Journal of Chromatography A. 1140(1-2), 44-55.

Ricci, L., Fuzzi, S., Laj, P., Lazzari, A., Orsi, G., Berner, A., Guenther, A., Jaeschke, W., Wendisch, M., Arends, B. G., 1998. Gas-liquid equilibria in polluted fog. Beitrage zur Physik der Atmosphare-Contributions to Atmospheric Physics. 71(1), 159-170.

Rogers, J.D. 1990. Ultraviolet absorption cross sections and atmospheric photodissociation rate constants of formaldehyde. The Journal of Physical Chemistry. 94:4011—4015.

Rose, C., Chaumerliac, N., Deguillaume, L., Perroux, H., Mouchel-Vallon, C., Leriche, M., Patryl, L., Armand, P., 2018. Modeling the partitioning of organic chemical species in cloud phases with CLEPS (1.1). Atmospheric Chemistry and Physics. 18, 2225–2242.

Rossignol, S., Chiappini, L., Perraudin, E., Rio, C., Fable, S., Valorso, R., Doussin, J.-F., 2012. Development of a parallel sampling and analysis method for the elucidation of gas/particle partitioning of oxygenated semi-volatile organics : a limonene ozonolysis study. Atmospheric Measurement Techniques. 5, 1459–1489.

Rothweiler, H., Wäger, P.A., Schlatter, C., 1991. Comparison of Tenax TA and Carbotrap for sampling and analysis of volatile organic compounds in air. Atmospheric Environment. Part B. Urban Atmosphere. 25, 231–235.

Ruiz, J., Bilbao, R., Murillo, M.B., 1998. Adsorption of different VOC onto soil minerals from gas phase: influence of mineral, type of VOC, and air humidity. Environmental Science & Technology. 32, 1079–1084.

Safieddine, S.A., Heald, C.L., Henderson, B.H., 2017. The global nonmethane reactive organic carbon budget: A modeling perspective: global reactive organic carbon budget. Geophysical Research Letters. 44, 3897–3906.

Sander, R., 1999. Modeling atmospheric chemistry: Interactions between gas-phase species and liquid cloud/aerosol particles. Surveys in Geophysics. 20(1), 1-31.

Sander, R., 2015. Compilation of Henry's law constants (version 4.0) for water as solvent. Atmospheric Chemistry and Physics. 15, 4399–4981.

Schade, G.W., Custer, T.G., 2004. OVOC emissions from agricultural soil in northern Germany during the 2003 European heat wave. Atmospheric Environment. 38, 6105–6114.

Schade, G.W., Solomon, S.J., Dellwik, E., Pilegaard, K., Ladstätter-Weissenmayer, A., 2011. Methanol and other VOC fluxes from a Danish beech forest during late springtime. Biogeochemistry. 106, 337–355.

Schall, C., Heumann, K.G., Kirst, G.O., 1997. Biogenic volatile organoiodine and organobromine hydrocarbons in the Atlantic Ocean from 42°N to 72°S. Fresenius' Journal of Analytical Chemistry. 359, 298–305.

Schieweck, A., Gunschera, J., Varol, D., Salthammer, T., 2018. Analytical procedure for the determination of very volatile organic compounds (C3–C6) in indoor air. Analytical and Bioanalytical Chemistry. 410, 3171–3183.

Schomburg, C.J., Glotfelty, D.E., Seiber, J.N., 1991. Pesticide occurrence and distribution in fog collected near Monterey, California. Environmental Science & Technology. 25, 155–160.8

Schöne, L., Herrmann, H., 2014. Kinetic measurements of the reactivity of hydrogen peroxide and ozone towards small atmospherically relevant aldehydes, ketones and organic acids in aqueous solutions. Atmospheric Chemistry and Physics. 14, 4503–4514.

Schummer, C., Delhomme, O., Appenzeller, B.M.R., Wennig, R., Millet, M., 2009. Comparison of MTBSTFA and BSTFA in derivatization reactions of polar compounds prior to GC/MS analysis. Talanta. 77, 1473–1482.

Schurgers, G., Arneth, A., Holzinger, R., Goldstein, A.H., 2009. Process-based modelling of biogenic monoterpene emissions combining production and release from storage. Atmospheric Chemistry and Physics. 9, 3409–3423.

Schwartz, S.E., 1986. Mass-transport considerations pertinent to aqueous phase reactions of gases in liquid-water clouds, in: Chemistry of Multiphase Atmospheric Systems. Springer, pp. 415–471.

Schwantes, R. H., Charan, S. M., Bates, K. H., Huang, Y., Nguyen, T. B., Mai, H., Seinfeld, J. H., 2019. Low-volatility compounds contribute significantly to isoprene secondary organic aerosol (SOA) under high-NO x conditions. Atmospheric Chemistry and Physics. 19(11), 7255-7278.

Seco, R., Peñuelas, J., Filella, I., 2007. Short-chain oxygenated VOCs: Emission and uptake by plants and atmospheric sources, sinks, and concentrations. Atmospheric Environment. 41, 2477–2499.

Seethapathy, S., Gorecki, T., 2012. Applications of polydimethylsiloxane in analytical chemistry: A review. Analytica Chimica Acta. 750, 48-62.

Seila, R.L., Main, H.H., Arriaga, J.L., Martínez V, G., Ramadan, A.B., 2001. Atmospheric volatile organic compound measurements during the 1996 Paso del Norte Ozone Study. Science of The Total Environment. 276, 153–169.

Seinfeld, J.H. and Pandis, S.N., 2016. Atmospheric chemistry and physics: from air pollution to climate change. John Wiley & Sons.

Sellegri, K., Laj, P., Marinoni, A., Dupuy, R., Legrand, M., Preunkert, S., 2003. Contribution of gaseous and particulate species to droplet solute composition at the Puy de Dôme, France. Atmospheric Chemistry and Physics. 3, 1509–1522.

Sharkey, T.D., Singsaas, E.L., Vanderveer, P.J., Geron, C., 1996. Field measurements of isoprene emission from trees in response to temperature and light. Tree Physiology 16, 649–654.

Shaw, S.L., Gantt, B., Meskhidze, N., 2010. Production and emissions of marine isoprene and monoterpenes: a review. Advances in Meteorology. 1–24.

Schnitzhofer, R., Beauchamp, J., Dunkl, J., Wisthaler, A., Weber, A., Hansel, A., 2008. Long-term measurements of CO, NO, NO_2, benzene, toluene and PM_{10} at a motorway location in an Austrian valley. Atmospheric Environment. 42(5), 1012-1024.

Scott, C.E., Rap, A., Spracklen, D.V., Forster, P.M., Carslaw, K.S., Mann, G.W., Pringle, K.J., Kivekäs, N., Kulmala, M., Lihavainen, H., Tunved, P., 2014. The direct and indirect radiative effects of biogenic secondary organic aerosol. Atmospheric Chemistry and Physics 14, 447–470.

Shrivastava, M., Fast, J., Easter, R., Gustafson, W.I., Zaveri, R.A., Jimenez, J.L., Saide, P., Hodzic, A., 2011. Modeling organic aerosols in a megacity: comparison of simple and complex representations of the volatility basis set approach. Atmospheric Chemistry and Physics. 11, 6639–6662.

Singh, H.B., Tabazadeh, A., Evans, M.J., Field, B.D., Jacob, D.J., Sachse, G., Crawford, J.H., Shetter, R., Brune, W.H., 2003. Oxygenated volatile organic chemicals in the oceans: Inferences and implications based on atmospheric observations and air-sea exchange models: oxygenated volatile oragnic chemicals in the ocrans. Geophysical Research Letters. 30.16.

Sinha, V., Williams, J., Meyerhöfer, M., Riebesell, U., Paulino, A.I., Larsen, A., 2007. Air-sea fluxes of methanol, acetone, acetaldehyde, isoprene and DMS from a Norwegian fjord following a phytoplankton bloom in a mesocosm experiment. Atmospheric Chemistry and Physics. 7, 739–755.

Soini, H.A., Bruce, K.E., Wiesler, D., David, F., Sandra, P., Novotny, M.V., 2005. Stir Bar Sorptive Extraction: a new quantitative and comprehensive sampling technique for determination of chemical signal profiles from biological;edia. Journal of Chemical Ecology. 31, 377–392.

Spivakovsky, C.M., Logan, J.A., Montzka, S.A., Balkanski, Y.J., Foreman-Fowler, M., Jones, D.B.A., Horowitz, L.W., Fusco, A.C., Brenninkmeijer, C.A.M., Prather, M.J., Wofsy, S.C., McElroy, M.B., 2000. Three-dimensional climatological distribution of tropospheric OH: Update and evaluation. Journal of Geophysical Research: Atmospheres. 105, 8931–8980.

Spracklen, D.V., Jimenez, J.L., Carslaw, K.S., Worsnop, D.R., Evans, M.J., Mann, G.W., Zhang, Q., Canagaratna, M.R., Allan, J., Coe, H., McFiggans, G., Rap, A., Forster, P., 2011. Aerosol mass spectrometer constraint on the global secondary organic aerosol budget. Atmospheric Chemistry and Physics 11. 12109–12136.

Straub, D. J., Hutchings, J. W., and Herckes, P., 2012. Measurements of fog composition at a rural site, Atmospheric Environment. 47, 195–205, 2012.

Steiner, A. H. and Goldstein, A. L. 2007. Biogenic VOCs, in: volatile organic compounds in the atmosphere (ed. R. Koppmann). Blackwell Publishing Ltd, Oxford , 82–128.

Stirnweis, L., Marcolli, C., Dommen, J., Barmet, P., Frege, C., Platt, S. M., Prévôt, A. S., 2017. Assessing the influence of NOx concentrations and relative humidity on secondary organic aerosol yields from α-pinene photo-oxidation through smog chamber experiments and modelling calculations. Atmospheric Chemistry and Physics. 17(8), 5035-5061.

Stookey, L.L., 1970. Ferrozine-a new spectrophotometric reagent for iron. Analytical Chemistry. 42, 779–781.

Stopforth, A., Burger, B.V., Crouch, A.M., Sandra, P., 2007. The analysis of estrone and 17beta-estradiol by stir bar sorptive extraction-thermal desorption-gas chromatography/mass spectrometry: application to urine samples after oral administration of conjugated equine estrogens. Journal of Chromatography B. 856, 156–164.

Suzuki, T., Ohtaguchi, K., Koide, K., 1992. Application of principal components analysis to calculate Henry's constant from molecular structure. Computers & Chemistry. 16, 41–52.

Takekawa, H., Minoura, H., Yamazaki, S., 2003. Temperature dependence of secondary organic aerosol formation by photo-oxidation of hydrocarbons. Atmospheric Environment. 37, 3413–3424.

Tang, X., Madronich, S., Wallington, T., Calamari, D., 1998. Changes in tropospheric composition and air quality. Journal of Photochemistry and Photobiology B: Biology. 46, 83–95.

Temime, B., Healy, R.M., Wenger, J.C., 2007. A denuder-filter sampling technique for the detection of gas and particle phase carbonyl compounds. Environmental Science & Technology. 41, 6514–6520.

Thoma G. J., Koulermos A. C., Vaisaraj K. T., Reible D. D. and Thibodeaux L. J., 1991. The effects of porewater colloids on the transport of hydrophobic organic compounds from bed sediments. In Organic Substances and Sediments in Water, Vol, I: Humics and Soils (edited by Baker R. A.). Lewis, Chelsea, MI.

Tiiva, P., Faubert, P., Michelsen, A., Holopainen, T., Holopainen, J.K., Rinnan, R., 2008. Climatic warming increases isoprene emission from a subarctic heath. New Phytologist. 180, 853–863.

Tingey, D.T., Manning, M., Grothaus, L.C., Burns, W.F., 1980. Influence of light and temperature on monoterpene emission rates from slash pine. Plant Physiology. 65, 797–801.

Tobiszewski, M., Mechlińska, A., Zygmunt, B., Namieśnik, J., 2009. Green analytical chemistry in sample preparation for determination of trace organic pollutants. TrAC Trends in Analytical Chemistry. 28(8), 943-951.

Tran, S., Bonsang, B., Gros, V., Peeken, I., Sarda-Esteve, R., Bernhardt, A., Belviso, S., 2013. A survey of carbon monoxide and non-methane hydrocarbons in the Arctic Ocean during summer 2010. Biogeosciences. 10, 1909–1935.

Tredoux, A., de Villiers, A., Májek, P., Lynen, F., Crouch, A., Sandra, P., 2008. Stir Bar Sorptive Extraction combined with GC-MS analysis and chemometric methods for the classification of south african wines according to the volatile composition. Journal of Agricultural and Food Chemistry. 56, 4286–4296.

Tsigaridis, K., Daskalakis, N., Kanakidou, M., Adams, P.J., Artaxo, P., Bahadur, R., Balkanski, Y., Bauer, S.E., Bellouin, N., Benedetti, A., Bergman, T., Berntsen, T.K., Beukes, J.P., Bian, H., Carslaw, K.S., Chin, M., Curci, G., Diehl, T., Easter, R.C., Ghan, S.J., Gong, S.L., Hodzic, A., Hoyle, C.R., Iversen, T., Jathar, S., Jimenez, J.L., Kaiser, J.W., Kirkevåg, A., Koch, D., Kokkola, H., Lee, Y.H., Lin, G., Liu, X., Luo, G., Ma, X., Mann, G.W., Mihalopoulos, N., Morcrette, J.-J., Müller, J.-F., Myhre, G., Myriokefalitakis, S., Ng, N.L., ODonnell, D., Penner, J.E., Pozzoli, L., Pringle, K.J., Russell, L.M., Schulz, M., Sciare, J., Seland, Ø., Shindell, D.T., Sillman, S., Skeie, R.B., Spracklen, D., Stavrakou, T., Steenrod, S.D., Takemura, T., Tiitta, P., Tilmes, S., Tost, H., van Noije, T., van Zyl, P.G., von Salzen, K., Yu, F., Wang, Z., Wang, Z., Zaveri, R.A., Zhang, H., Zhang, K., Zhang, Q., Zhang, X., 2014. The AeroCom evaluation and intercomparison of organic aerosol in global models. Atmospheric Chemistry and Physics. 14, 10845–10895.

Tsimpidi, A.P., Karydis, V.A., Zavala, M., Lei, W., Molina, L., Ulbrich, I.M., Jimenez, J.L., Pandis, S.N., 2010. Evaluation of the volatility basis-set approach for the simulation of organic aerosol formation in the Mexico City metropolitan area. Atmospheric Chemistry and Physics. 10, 525–546.

Tu, P., Hall IV, W. A., Johnston, M. V., 2016. Characterization of highly oxidized molecules in fresh and aged biogenic secondary organic aerosol. Analytical chemistry. 88(8), 4495-4501.

Vaïtilingom, M., Attard, E., Gaiani, N., Sancelme, M., Deguillaume, L., Flossmann, A.I., Amato, P., Delort, A.-M., 2012. Long-term features of cloud microbiology at the puy de Dôme (France). Atmospheric Environment. 56, 88–100.

Vaïtilingom, M., Charbouillot, T., Deguillaume, L., Maisonobe, R., Parazols, M., Amato, P., Sancelme, M., Delort, A.-M., 2011. Atmospheric chemistry of carboxylic acids: microbial implication versus photochemistry. Atmospheric Chemistry and Physics. 11, 8721–8733.

Vigouroux, C., Stavrakou, T., Whaley, C., Dils, B., Duflot, V., Hermans, C., Kumps, N., Metzger, J.-M., Scolas, F., Vanhaelewyn, G., Müller, J.-F., Jones, D. B. A., Li, Q., and De Mazière, M., 2012. FTIR time-series of biomass burning products (HCN, C_2H_6, C_2H_2, CH_3OH, and HCOOH) at Reunion Island (21◦ S, 55◦ E) and comparisons with model data, Atmospheric Chemistry and Physics. 12, 10367–10385.

Valsaraj, K.T., 1988a. On the physico-chemical aspects of partitioning of non-polar hydrophobic organics at the air-water interface. Chemosphere. 17, 875–887.

Valsaraj, K.T., 1988b. Binding constants for non-polar hydrophobic organics at the air-water interface: Comparison of experimental and predicted values. Chemosphere. 17, 2049–2053.

Valsaraj, K.T., Thoma, G.J., Reible, D.D., Thibodeaux, L.J., 1993. On the enrichment of hydrophobic organic compounds in fog droplets. Atmospheric Environment. Part A. General Topics. 27, 203–210.

van Pinxteren, D., Plewka, A., Hofmann, D., Müller, K., Kramberger, H., Svrcina, B., Bächmann, K., Jaeschke, W., Mertes, S., Collett, J.L., Herrmann, H., 2005. Schmücke hill cap cloud and valley stations aerosol characterisation during FEBUKO (II): Organic compounds. Atmospheric Environment. 39, 4305–4320.

van Roon, A., Parsons, J.R., Krap, L., Govers, H.A.J., 2005. Fate and transport of monoterpenes through soils. Part II: Calculation of the effect of soil temperature, water saturation and organic carbon content. Chemosphere. 61, 129–138.

Vinatier, V., Wirgot, N., Joly, M., Sancelme, M., Abrantes, M., Deguillaume, L., Delort, A.-M., 2016. Siderophores in cloud waters and potential impact on atmospheric chemistry: production by microorganisms isolated at the puy de Dôme Station. Environmental Science & Technology. 50, 9315–9323.

Vione, D., Maurino, V., Minero, C., Pelizzetti, E., Harrison, M.A.J., Olariu, R.-I., Arsene, C., 2006. Photochemical reactions in the tropospheric aqueous phase and on particulate matter. Chemical Society Reviews.

Voisin, D., Legrand, M., Chaumerliac, N., 2000. Scavenging of acidic gases (HCOOH, CH_3COOH, HNO_3, HCl, and SO_2) and ammonia in mixed liquid-solid water clouds at the puy de Dôme mountain (France). Journal of Geophysical Research: Atmospheres. 105, 6817–6835.

Volkamer, R., San Martini, F., Molina, L.T., Salcedo, D., Jimenez, J.L., Molina, M.J., 2007. A missing sink for gas-phase glyoxal in Mexico City: Formation of secondary organic aerosol. Geophysical Research Letters. 34, L19807.

Volkamer, R., Ziemann, P.J., Molina, M.J., 2009. Secondary organic aerosol formation from acetylene (C_2H_2): seed effect on SOA yields due to organic photochemistry in the aerosol aqueous phase. Atmospheric Chemistry and Physics. 9, 1907–1928.

Wang, B., Shao, M., Lu, S.H., Yuan, B., Zhao, Y., Wang, M., Zhang, S.Q., Wu, D., 2010. Variation of ambient non-methane hydrocarbons in Beijing city in summer 2008. Atmospheric Chemistry and Physics. 10, 5911–5923.

Wang, C., Wang, Z., Qiao, X., Li, Z., Li, F., Chen, M., Wang, Y., Huang, Y., Cui, H., 2013. Antifungal activity of volatile organic compounds from *Streptomyces alboflavus* TD-1. FEMS Microbiol Lett. 341, 45–51.

Wang S. P., Meng F. D., Duan J. C., Wang Y. F., Cui X. Y., Piao S. L., Zhang Z.H., 2014. Asymmetric sensitivity of first flowering date to warming and cooling in alpine plants. Ecology. 95, 3387–3398.

Wang, Y., Ren, X., Ji, D., Zhang, J., Sun, J., Wu, F., 2012. Characterization of volatile organic compounds in the urban area of Beijing from 2000 to 2007. Journal of Environmental Sciences. 24(1), 95 – 101.

Warneke, C., de Gouw, J.A., Holloway, J.S., Peischl, J., Ryerson, T.B., Atlas, E., Blake, D., Trainer, M., Parrish, D.D., 2012. Multiyear trends in volatile organic compounds in Los Angeles, California: Five decades of decreasing emissions: trends in VOCs in Los Angeles. Journal of Geophysical Research. 117.D21 (2012).

Wayne, R.P., Barnes, I., Biggs, P., Burrows, J.P., Canosa-Mas, C.E., Hjorth, J., Le Bras, G., Moortgat, G.K., Perner, D., Poulet, G., Restelli, G., Sidebottom, H., 1991. The nitrate radical: Physics, chemistry, and the atmosphere. Atmospheric Environment. Part A. General Topics. 25, 1–203.

Wheatley, R., 2002. The consequences of volatile organic compound mediated bacterial and fungal interactions. Antonie van Leeuwenhoek. 357–364.

Winiwarter, W., Fierlinger, H., Puxbaum, H., Facchini, M.C., Arends, B.G., Fuzzi, S., Schell, D., Kaminski, U., Pahl, S., Schneider, T., Berner, A., Solly, I., Kruisz, C., 1994. Henry’s law and the behavior of weak acids and bases in fog and cloud. Journal of Atmospheric Chemistry. 19, 173–188.

Winiwarter, W., Puxbaum, H., Fuzzi, S., Facchini, M.C., Orsi, G., Beltz, N., Enderle, K., Jaeschke, W., 1988. Organic acid gas and liquid-phase measurements in Po Valley fall-winter conditions in the presence of fog. Tellus B. 40B, 348–357.

Wirgot, N., Vinatier, V., Deguillaume, L., Sancelme, M., Delort, A.-M., 2017. H_2O_2 modulates the energetic metabolism of the cloud microbiome. Atmospheric Chemistry and Physics. 17.24, 14841-14851.

Wright, G.A., Schiestl, F.P., 2009. The evolution of floral scent: the influence of olfactory learning by insect pollinators on the honest signalling of floral rewards. Functional Ecology. 23, 841–851.

Wu, K., Yang, X., Chen, D., Gu, S., Lu, Y., Jiang, Q, Lu, S., 2018. Estimation of biogenic VOC emissions and their corresponding impact on ozone and secondary organic aerosol formation in China. Atmospheric Research. 231, 104656.

Wu, L. J., Hee, S. S. Q. , 1995. A solid sorbent personal air sampling method for aldehydes. American Industrial Hygiene Association Journal. 56(4), 362-367.

Yáñez-Serrano, A. M., Nölscher, A. C., Williams, J., Wolff, S., Alves, E., Martins, G. A., Bourtsoukidis, E., Brito, J., Jardine, K., Artaxo, P., Kesselmeier, J., 2015. Diel and seasonal changes of biogenic volatile organic compounds within and above an Amazonian rainforest. Atmospheric Chemistry and Physics. 15(6), 3359-3378.

Yokelson, R.J., Christian, T.J., Karl, T.G., Guenther, A., 2008. The tropical forest and fire emissions experiment: laboratory fire measurements and synthesis of campaign data. Atmospheric Chemistry and Physics. 8, 3509–3527.

Yu, J., Jeffries, H. E., Le Lacheur, R. M.,1995. Identifying airborne carbonyl compounds in isoprene atmospheric photooxidation products by their PFBHA oximes using gas chromatography/ion trap mass spectrometry. Environmental Science & Technology. 29(8), 1923-1932.

Yuan, B., Hu, W. W., Shao, M., Wang, M., Chen, W. T., Lu, S. H., Hu, M., 2013. VOC emissions, evolutions and contributions to SOA formation at a receptor site in eastern China. Atmospheric Chemistry and Physics. 13(17), 8815-8832.

Ye, Q., Robinson, E. S., Ding, X., Ye, P., Sullivan, R. C., Donahue, N. M., 2016. Mixing of secondary organic aerosols versus relative humidity. Proceedings of the National Academy of Sciences. 113(45), 12649-12654.

Yue, X., Unger, N., 2018. Fire air pollution reduces global terrestrial productivity. Nature Communications. 9(1), 5413..

Zeng, P., Lyu, X., Guo, H., Cheng, H., Wang, Z., Liu, X., Zhang, W., 2019. Spatial variation of sources and photochemistry of formaldehyde in Wuhan, Central China. Atmospheric Environment. 214, 116826.

Zhang, J.X., Soini, H.A., Bruce, K.E., Wiesler, D., Woodley, S.K., Baum, M.J., Novotny, M.V., 2005. Putative chemosignals of the Ferret (Mustela furo) associated with individual and gender recognition. Chemical Senses. 30, 727–737.

Zhang, X., Cappa, C.D., Jathar, S.H., McVay, R.C., Ensberg, J.J., Kleeman, M.J., Seinfeld, J.H., 2014. Influence of vapor wall loss in laboratory chambers on yields of secondary organic aerosol. Proceedings of the National Academy of Sciences. 111, 5802–5807.

Zhao, Y., Hallar, A.G., Mazzoleni, L.R., 2013. Atmospheric organic matter in clouds: exact masses and molecular formula identification using ultrahigh-resolution FT-ICR mass spectrometry. Atmospheric Chemistry and Physics. 13, 12343–12362.

Zheng, J., Garzon, J.P., Huertas, M.E., Zhang, R., Levy, M., Ma, Y., Huertas, J.I., Jardon, R.T., Ruiz, L.G., Tan, H., Molina, L.T., 2013. Volatile organic compounds in Tijuana during the Cal-Mex 2010 campaign: measurements and source apportionment. Atmospheric Environment. 70, 521–531.

Zwenger, S., and Basu, C., 2008. Plant terpenoids: applications and future potentials. Biotechnology and Molecular Biology Reviews. 3(1), 1.

Zhu, S., Zheng, X., Stevanovic, S., Wang, Lin, Wang, H., Gao, J., Xiang, Z., Ristovski, Z., Liu, J., Yu, M., Wang, Lina, Chen, J., 2018. Investigating particles, VOCs, ROS produced from mosquito-repellent incense emissions and implications in SOA formation and human health. Building and Environment 143, 645–651.

Appendices

A.1 List of compounds in "Megamix" and terpenes standards with logKo/w>3 (apolar compouds) / logKo/w <3 (polar compounds), molar mass, concentration, retention time and characteristic ions.

"Megamix" standards								
	Compounds	Cas #	log $K_{O/W}$	M (g mol^{-1})	Conc. (µg mL^{-1})	Mass of 0.5µL standard (ng)	Retention time (min)	Characteristic ions
1	CFC-12	75-71-8	1.82	120.9	200	100		85; 101
2	Chloromethane	74-87-3	1.09	50.5	200	100		50; 52
3	Vinyl chloride	75-01-4	1.62	62.5	200	100		62; 64
4	Bromomethane	74-83-9	1.18	94.9	200	100		94; 96
5	Chloroethane	75-00-3	1.58	64.5	200	100		64; 66
6	CFC-11	75-69-4	2.13	137.4	200	100		101; 103
7	1,1-Dichloroethene	75-35-4	2.12	96.9	200	100	3.53	96; 61
8	Dichloromethane	75-09-2	1.34	84.9	200	100	3.54	84; 49
9	Trans-1,2-dichloroethene	156-60-5	1.98	96.9	200	100	3.96	96; 61
10	1,1-Dichloroethane	75-34-3	1.76	99	200	100	4.71	63; 98
11	2,2-Dichloropropane	594-20-7	2.92	113	200	100	5.88	77; 41
12	Cis-1,2-Dichloroethene	156-59-2	1.98	96.9	200	100	5.86	61; 96
13	Chloroform	67-66-3	1.52	119.4	200	100	6.69	83; 85
14	Bromochloromethane	74-97-5	1.43	129.4	200	100	6.38	49; 130
15	Methylchloroform	71-55-6	2.68	133.4	200	100	6.93	97; 99
16	1,1-Dichloropropene	563-58-6	2.53	111	200	100	7.27	75; 39
17	Carbon tetrachloride	56-23-5	2.44	153.8	200	100	7.23	117; 119
18	Benzene	71-43-2	1.99	78.1	200	100	7.66	78
19	1,2-Dichloroethane	107-06-2	1.83	99	200	100	7.86	62; 64
20	Trichloroethene	79-01-6	2.47	131.4	200	100	9.25	95; 130
21	1,2-Dichloropropane	78-87-5	2.25	113	200	100	9.84	63; 62
22	Bromodichloromethane	75-27-4	1.61	163.8	200	100	10.56	83; 85
23	Dibromomethane	74-95-3	1.52	173.8	100	100	10.02	174; 93
24	Cis-1,3-Dichloropropene	10061-01-5	2.29	111	200	100	11.65	75; 39
25	Toluene	108-88-3	2.54	92.1	200	100	12.39	91; 92
26	Trans-1,3-Dichloropropene	10061-02-6	2.29	111	200	100	13.18	75; 39
27	1,1,2-Trichloroethane	79-00-5	2.01	133.4	200	100	13.63	97; 83
28	1,3-Dichloropropane	142-28-9	2.32	113	200	100	13.99	76; 41
29	Tetrachloroethene	127-18-4	2.97	165.8	200	100	13.65	166; 164
30	Dibromochloromethane	124-48-1	1.7	208.3	200	100	14.51	129; 127
31	1,2-Dibromoethane	106-93-4	2.01	187.9	200	100	14.69	107; 109
32	Chlorobenzene	108-90-7	2.64	112.6	200	100	16.05	112; 77

33	1,1,1,2-Tetrachloroethane	630-20-6	2.93	168	200	100	16.4	133; 131
34	Ethylbenzene	100-41-4	3.03	106.2	200	100	16.44	91; 106
35	m-xylene	108-38-3	3.09	106.2	200	100	16.84	91; 106
36	p-xylene	106-42-3	3.09	106.2	200	100	16.84	91; 106
37	o-xylene	95-47-6	3.09	106.2	200	100	17.84	91; 106
38	Styrene	100-42-5	2.89	104.2	200	100	17.94	104; 78
39	Cumene (isopropylbenzene)	98-82-8	3.45	120.2	200	100	18.96	105; 120
40	Bromoform	75-25-2	1.79	252.7	200	100	18.33	173; 171
41	1,1,2,2-Tetrachloroethane	79-34-5	2.19	167.9	200	100	19.99	83; 85
42	1,2,3-Trichloropropane	96-18-4	2.5	147.4	200	100	20.02	75; 110
43	n-Propylbenzene	103-65-1	3.52	120.2	200	100	20.16	91; 120
44	Bromobenzene	108-86-1	2.88	157	200	100	19.63	77; 156
45	1,3,5-Trimethylbenzene	108-67-8	3.63	120.2	200	100	20.76	105; 120
46	2-Chlorotoluene	95-49-8	3.18	126.6	200	100	20.26	91; 126
47	4-Chlorotoluene	106-43-4	3.18	126.6	200	100	20.65	91; 126
48	Tert-butylbenzene	98-06-6	3.9	134.2	200	100	21.6	119; 91
49	1,2,4-Trimethylbenzene	95-63-6	3.63	120.2	200	100	21.78	105; 120
50	Sec-butylbenzene	135-98-8	3.94	134.2	200	100	22.26	105; 134
51	4-Isopropyltoluene (p-cymene)	99-87-6	4	134.2	200	100	22.79	119; 134
52	1,3-Dichlorobenzene	541-73-1	3.28	147	200	100	22.43	146; 148
53	1,4-Dichlorobenzene	106-46-7	3.28	147	200	100	22.77	146; 148
54	n-Butylbenzene	104-51-8	4.01	134.2	200	100	23.96	91; 92
55	1,2-Dichlorobenzene	95-50-1	3.28	147	200	100	23.73	146; 148
56	1,2-Dibromo-3-Chloropropane	96-12-8	2.68	236.3	200	100	26.12	157; 75
57	1,2,4-Trichlorobenzene	120-82-1	3.93	181.5	200	100	28.54	180; 182
58	Hexachlorobutadiene	87-68-3	4.72	260.8	200	100	29.1	225; 227
59	Naphtalene	91-20-3	3.17	128.2	200	100	29.24	128
60	1,2,3-trichlorobenzene	87-61-6	3.93	181.5	200	100	29.92	180; 182

Terpenes standards

	Compounds	Cas #	log $K_{O/W}$	M (g mol^{-1})	Conc. (µg/mL)	Diluted concentration (µg mL^{-1})	Mass of 0.5µL standard (ng)	Retention time (min)	Characteristic ions
1	Isoprene	78-79-5	2.58	68.11	680000	200	100	2.69	67; 68
2	α-pinene	80-56-8	4.27	136.23	858000	200	100	18.86	93
3	β-pinene	127-91-3	4.35	136.23	872000	200	100	20.73	41; 93
4	Limonene	138-86-3	4.83	136.23	840000	200	100	22.62	68; 93
5	Nopinone	38651-65-9	2.59	138.21	980000	200	100	28.25	55; 83

A.2 Effects of PDMS volume, extraction time and sample volume on the extraction efficiency E (%) for a selection of VOC.

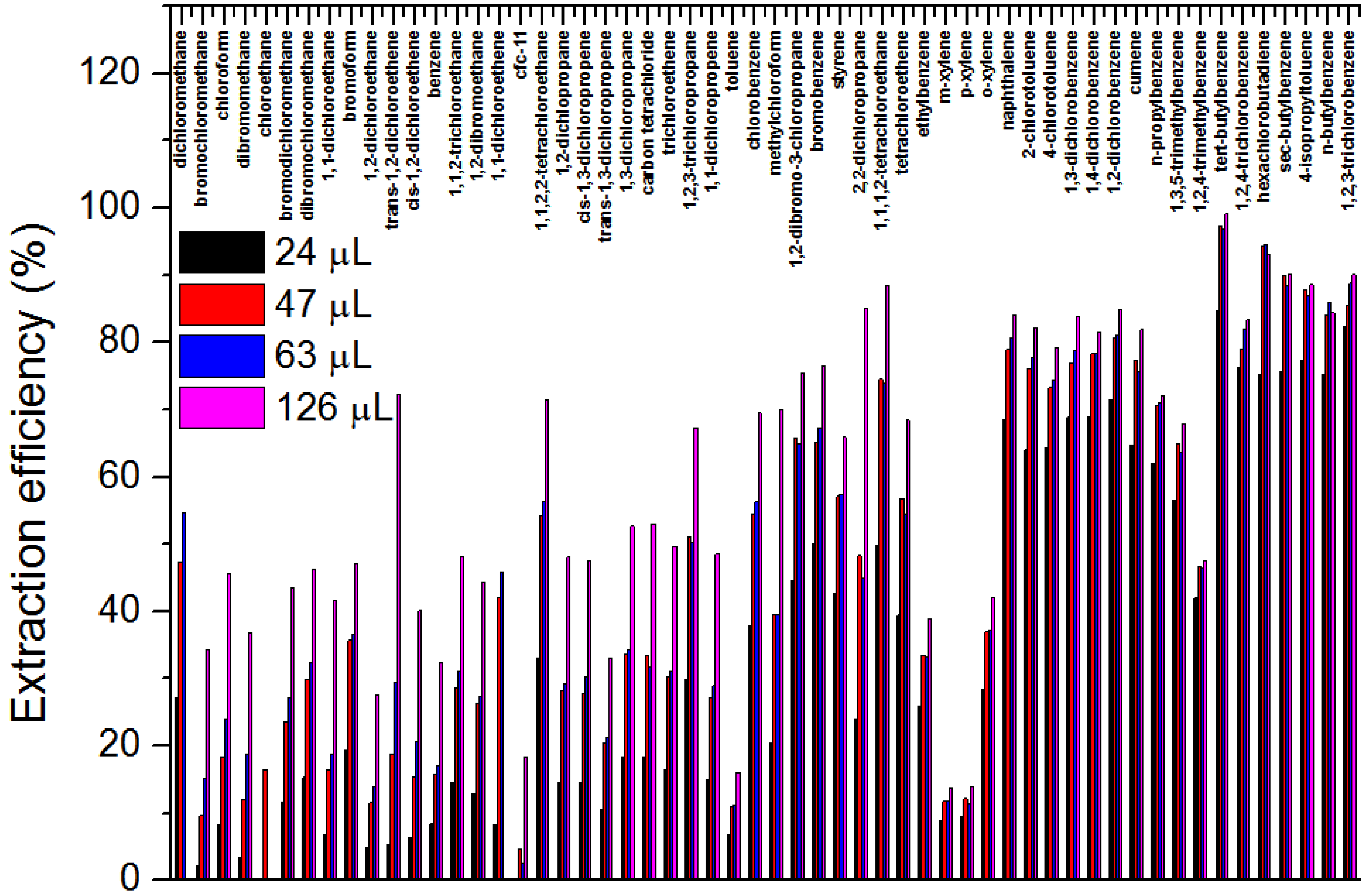

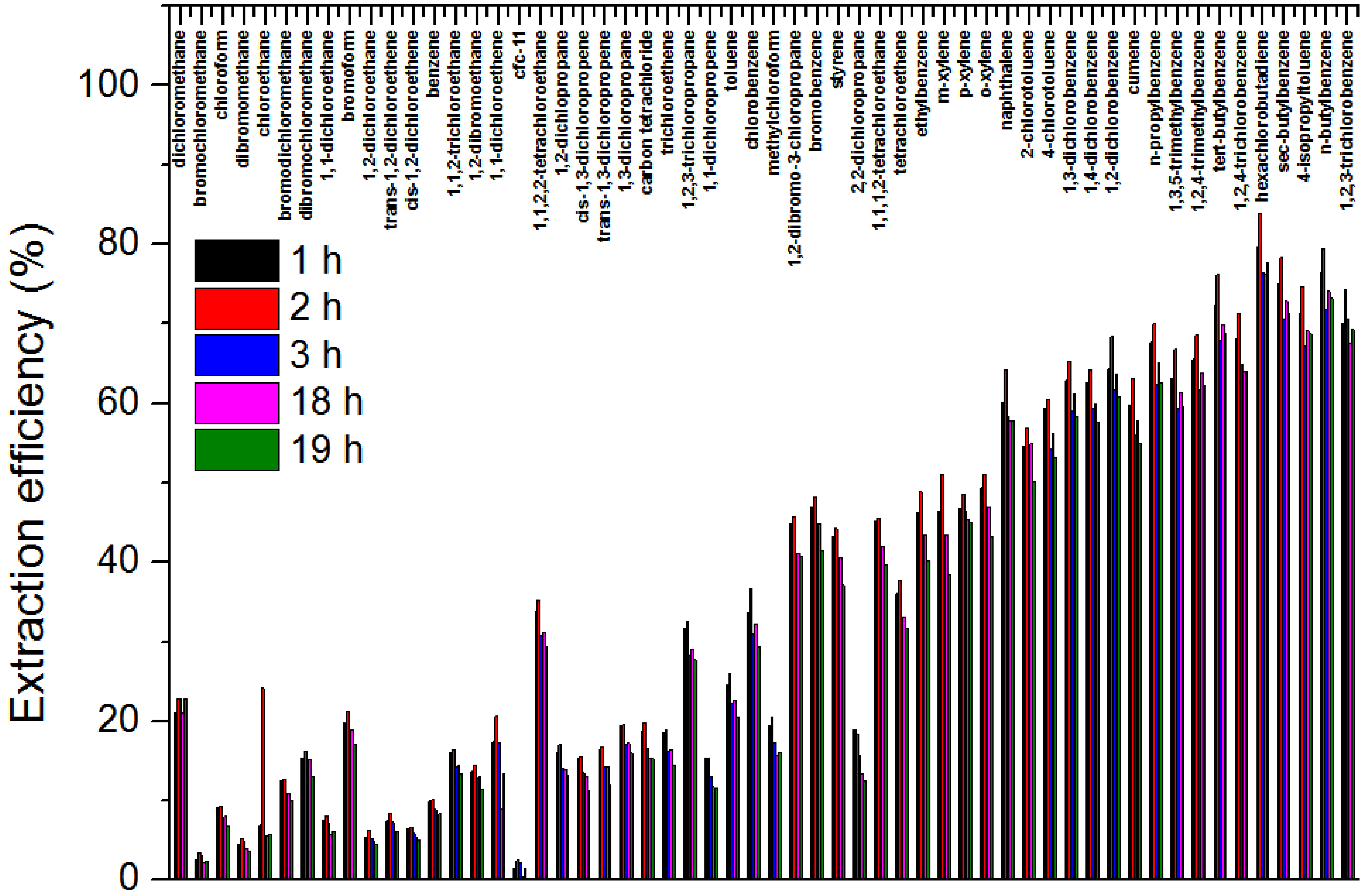
Extraction efficiency (%)
0
20
40
60
80
100
1 h
2 h
3 h
18 h
19 h
dichloromethane
bromochloromethane
chloroform
dibromomethane
chloroethane
bromodichloromethane
dibromochloromethane
1,1-dichloroethane
bromoform
1,2-dichloroethane
trans-1,2-dichloroethene
cis-1,2-dichloroethene
benzene
1,1,2-trichloroethane
1,2-dibromoethane
1,1-dichloroethene
cfc-11
1,1,2,2-tetrachloroethane
1,2-dichlopropane
cis-1,3-dichloropropene
trans-1,3-dichloropropene
1,3-dichloropropane
carbon tetrachloride
trichloroethene
1,2,3-trichloropropane
1,1-dichloropropene
toluene
chlorobenzene
methylchloroform
1,2-dibromo-3-chloropropane
bromobenzene
styrene
2,2-dichloropropane
1,1,1,2-tetrachloroethane
tetrachloroethene
ethylbenzene
m-xylene
p-xylene
o-xylene
naphthalene
2-chlorotoluene
4-chlorotoluene
1,3-dichlorobenzene
1,4-dichlorobenzene
1,2-dichlorobenzene
cumene
n-propylbenzene
1,3,5-trimethylbenzene
1,2,4-trimethylbenzene
tert-butylbenzene
1,2,4-trichlorobenzene
hexachlorobutadiene
sec-butylbenzene
4-isopropyltoluene
n-butylbenzene
1,2,3-trichlorobenzene

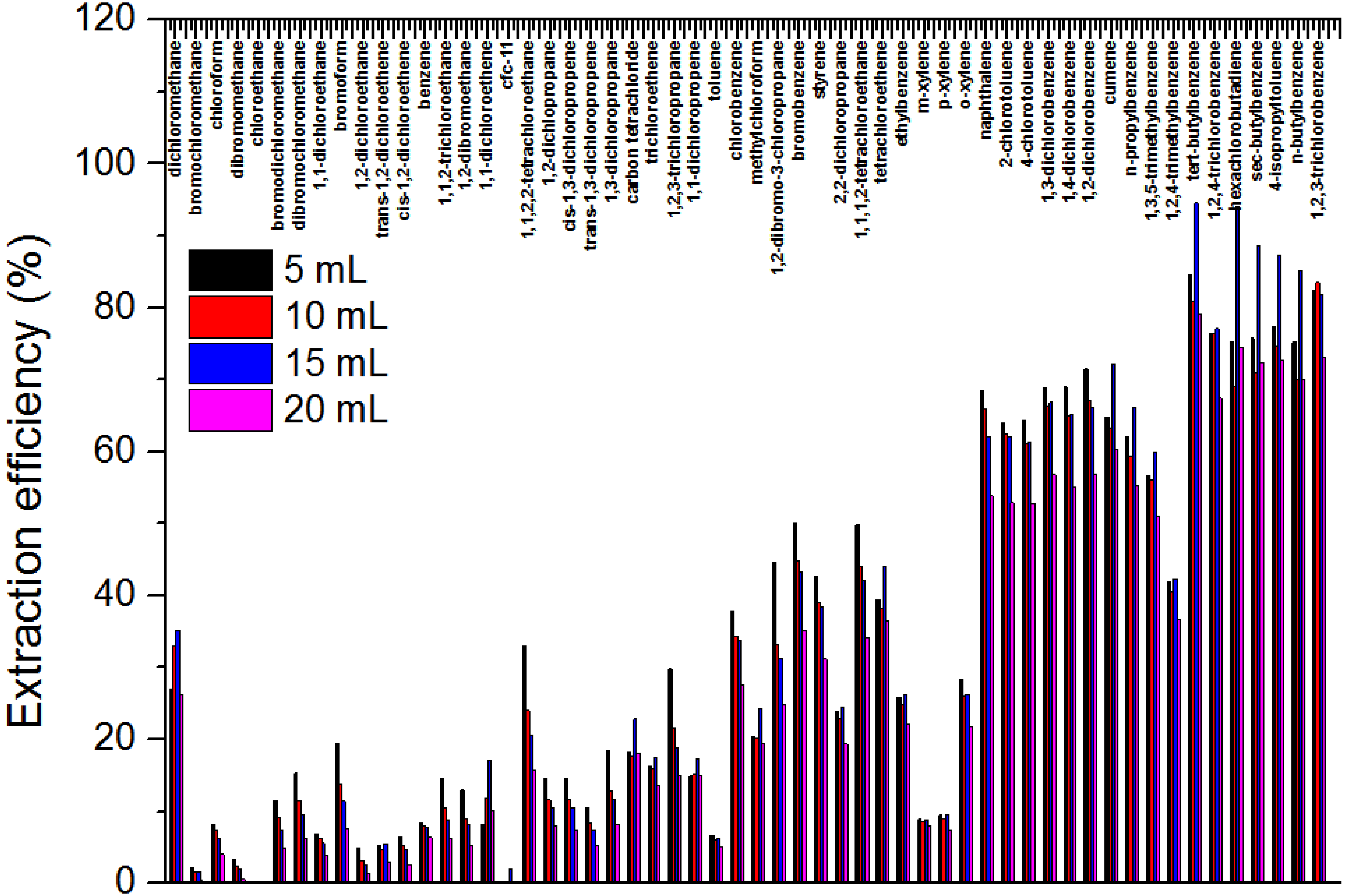

Extraction efficiency (%)
0
20
40
60
80
100
120
5 mL
10 mL
15 mL
20 mL
dichloromethane
bromochloromethane
chloroform
dibromomethane
chloroethane
bromodichloromethane
dibromochloromethane
1,1-dichloroethane
bromoform
1,2-dichloroethane
trans-1,2-dichloroethene
cis-1,2-dichloroethene
benzene
1,1,2-trichloroethane
1,2-dibromoethane
1,1-dichloroethene
cfc-11
1,1,2,2-tetrachloroethane
1,2-dichlopropane
cis-1,3-dichloropropene
trans-1,3-dichloropropene
1,3-dichloropropane
carbon tetrachloride
trichloroethene
1,2,3-trichloropropane
1,1-dichloropropene
toluene
chlorobenzene
methylchloroform
1,2-dibromo-3-chloropropane
bromobenzene
styrene
2,2-dichloropropane
1,1,1,2-tetrachloroethane
tetrachloroethene
ethylbenzene
m-xylene
p-xylene
o-xylene
naphthalene
2-chlorotoluene
4-chlorotoluene
1,3-dichlorobenzene
1,4-dichlorobenzene
1,2-dichlorobenzene
cumene
n-propylbenzene
1,3,5-trimethylbenzene
1,2,4-trimethylbenzene
tert-butylbenzene
1,2,4-trichlorobenzene
hexachlorobutadiene
sec-butylbenzene
4-isopropyltoluene
n-butylbenzene
1,2,3-trichlorobenzene

A.3 The calibration curves of VOC by SBSE for external and internal calibration.

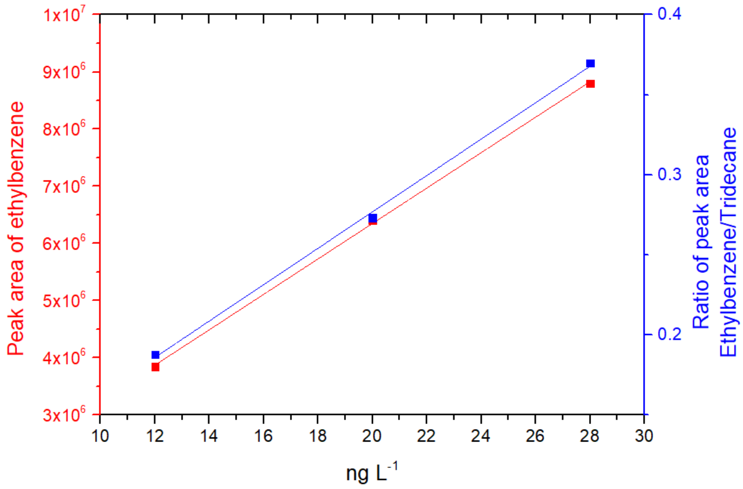

$$y = 309791.25x + 155015.33$$

$$R^2 = 0.99$$

$$y = 0.0114x + 0.0496$$

$$R^2 = 0.99$$

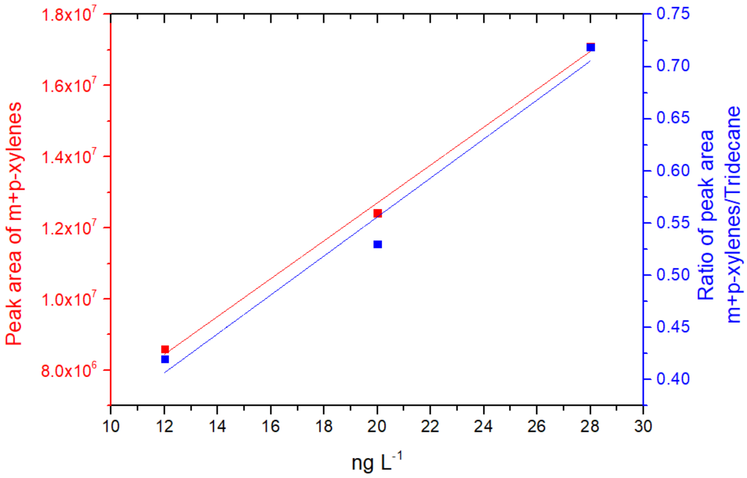

$$y = 531988.31x + 2067620$$

$$R^2 = 0.99$$

$$y = 0.0187x + 0.183$$

$$R^2 = 0.98$$

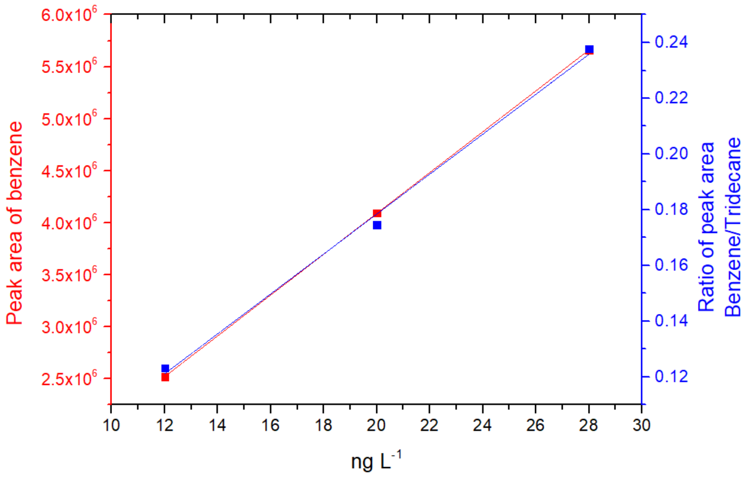

$$y = 196268.44x + 165798.25$$

$$R^2 = 0.99$$

$$y = 0.00716x + 0.0352$$

$$R^2 = 0.99$$

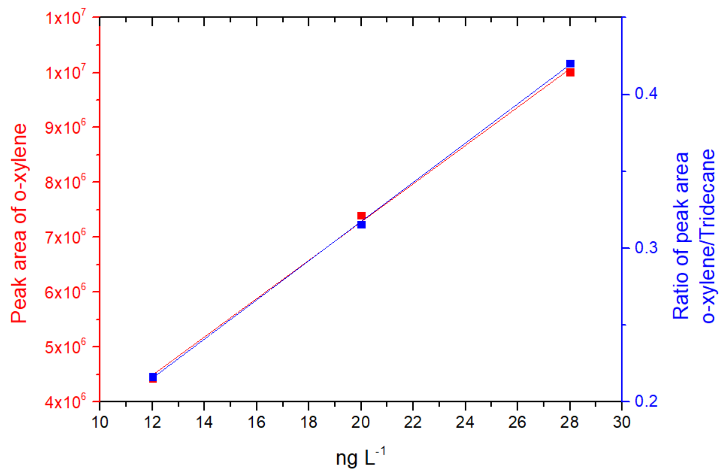

$$y = 348552.83x + 309318.83$$
$$R^2 = 0.99$$
$$y = 0.01274x + 0.0627$$
$$R^2 = 0.99$$

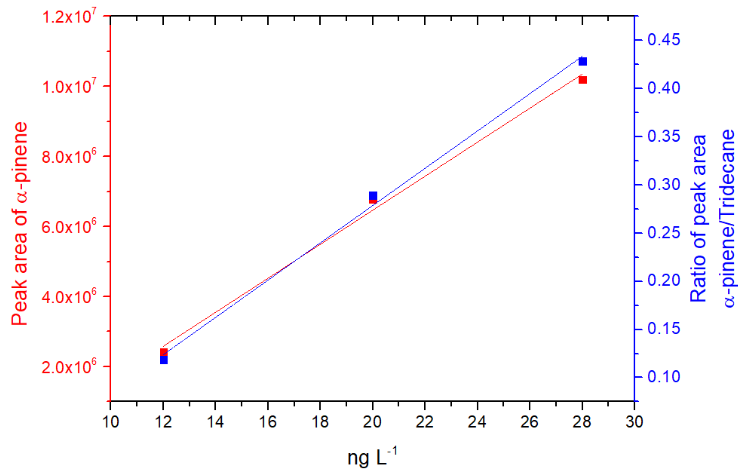

$$y = 485807.88x - 3245510$$
$$R^2 = 0.99$$
$$y = 0.01936x - 0.10848$$
$$R^2 = 0.99$$

A.4 Effects of extraction time (3h, 4h and 6h) and NaCl effect (with the presence of NaCl in black and without the presence of NaCl in red) on the extraction for OVOC.

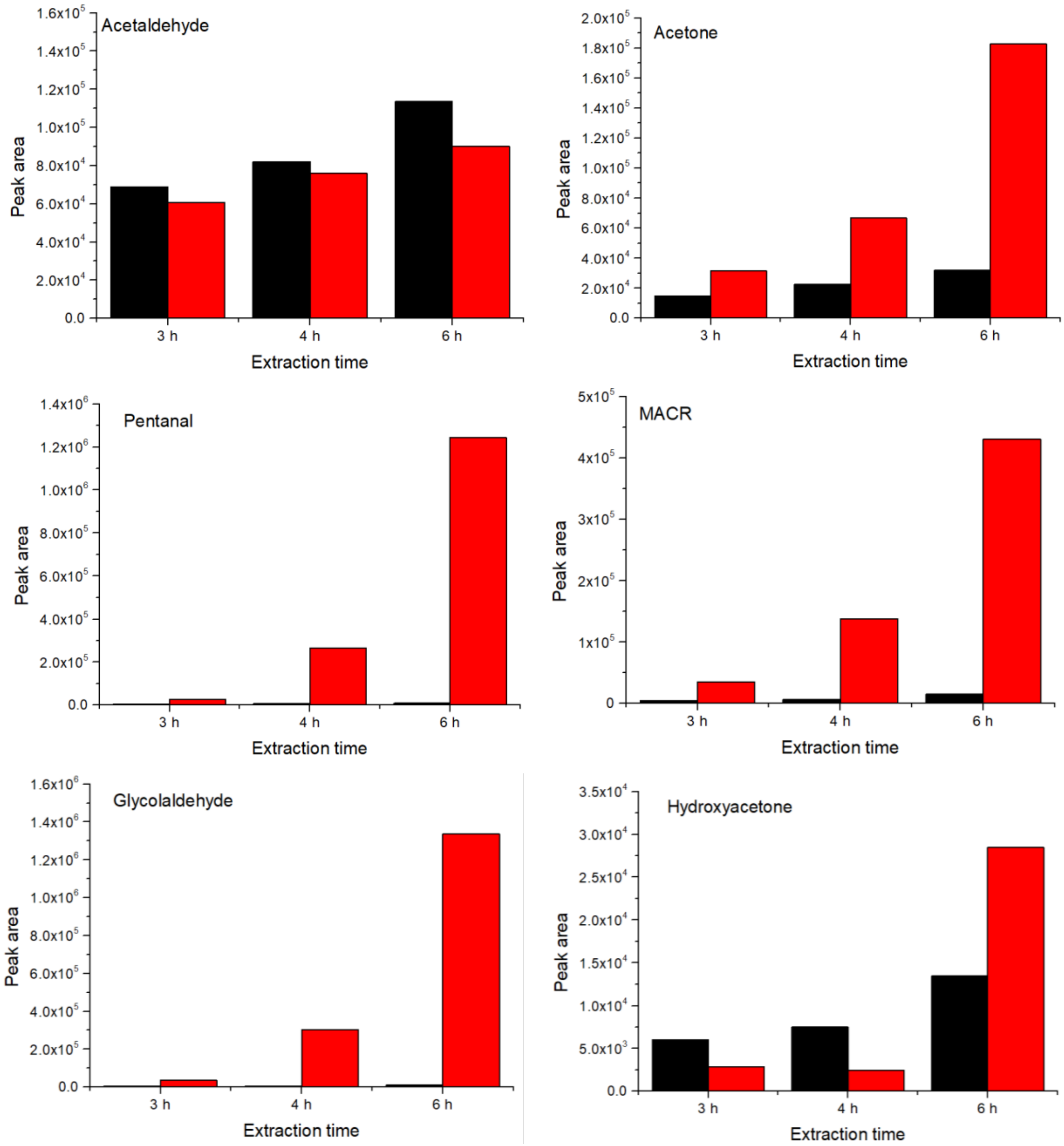

A.5 The calibration curves of OVOC by SBSE for external and internal calibration.

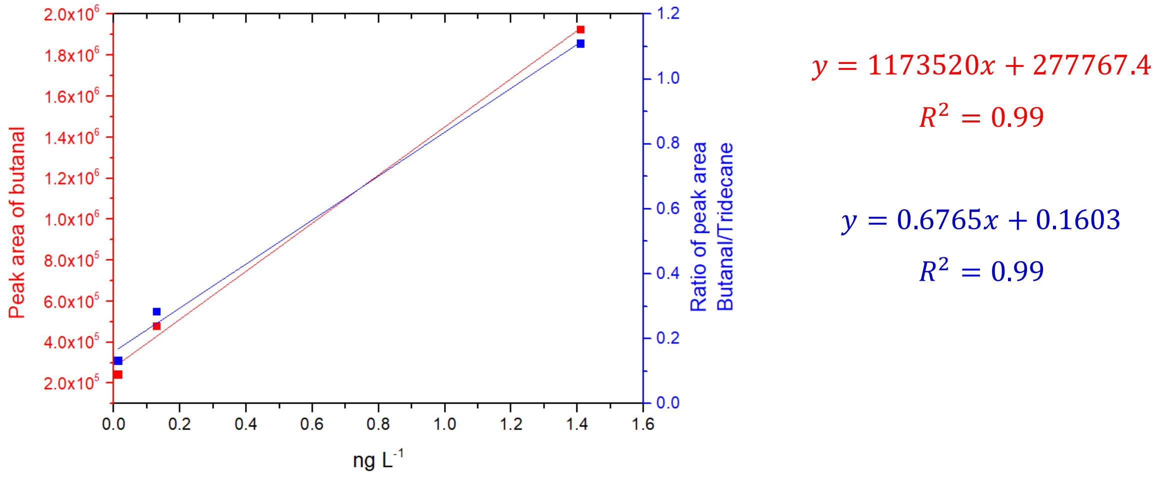

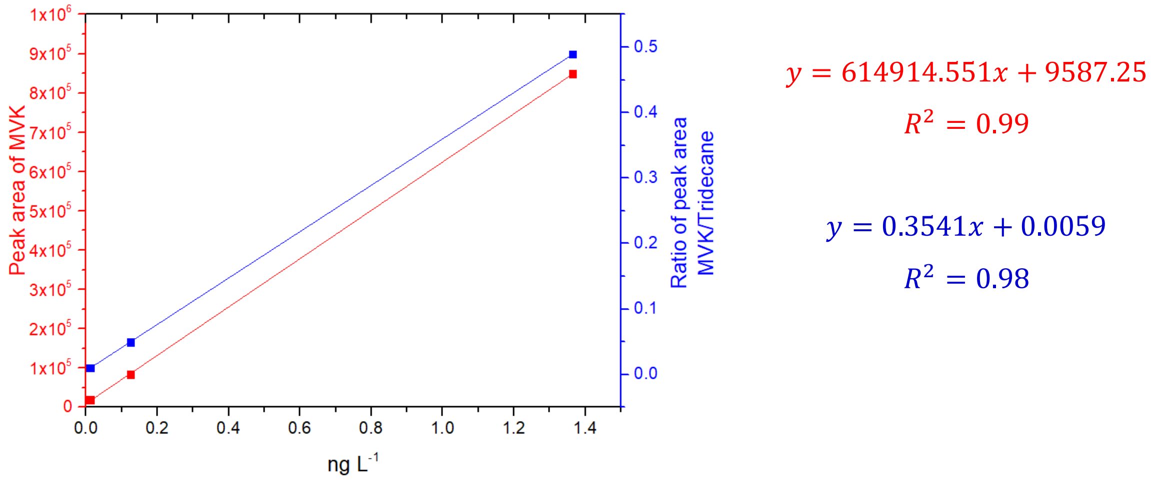

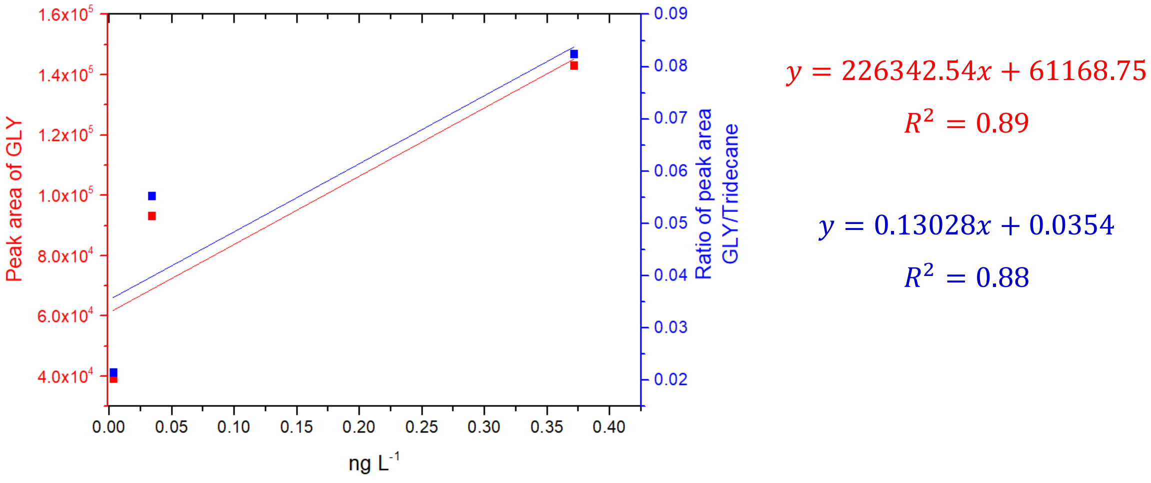

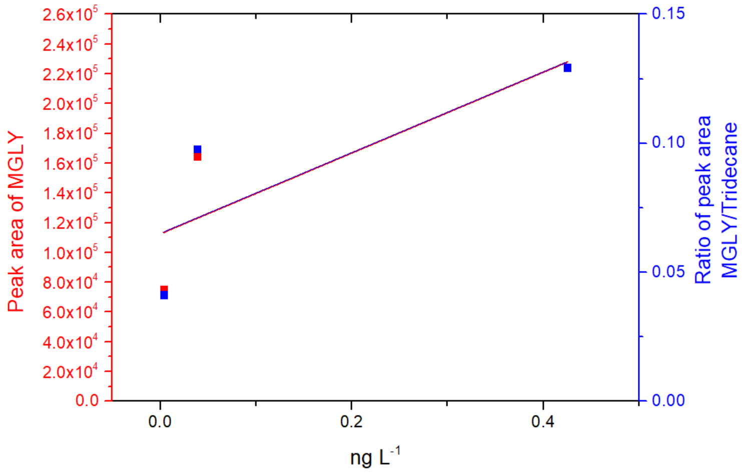

$$y = 271515.368x + 112623$$
$$R^2 = 0.85$$

$$y = 0.15646x + 0.06512$$
$$R^2 = 0.82$$

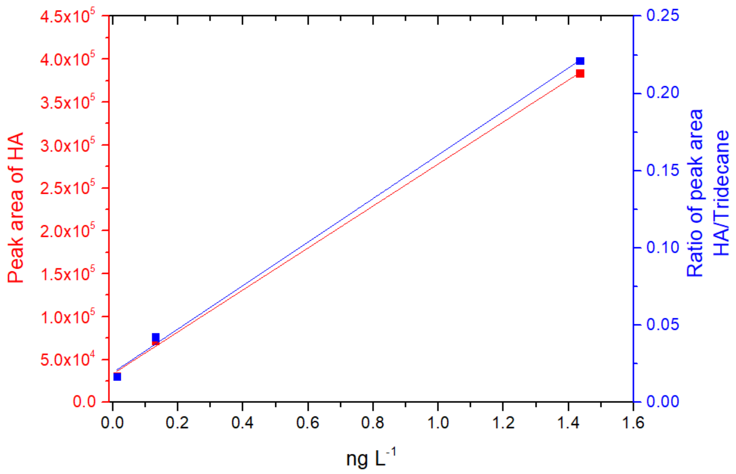

$$y = 244676.743x + 33362.25$$
$$R^2 = 0.99$$

$$y = 0.14098x + 0.01935$$
$$R^2 = 0.99$$

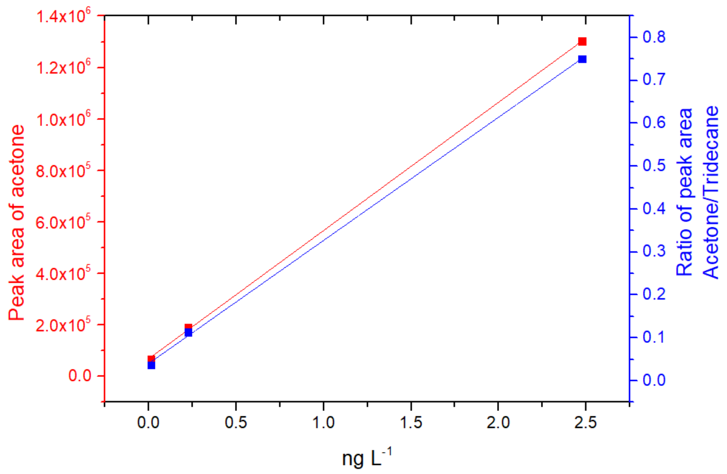

$$y = 498075.9506x + 69609.83$$
$$R^2 = 0.99$$

$$y = 0.2869x + 0.0407$$
$$R^2 = 0.99$$

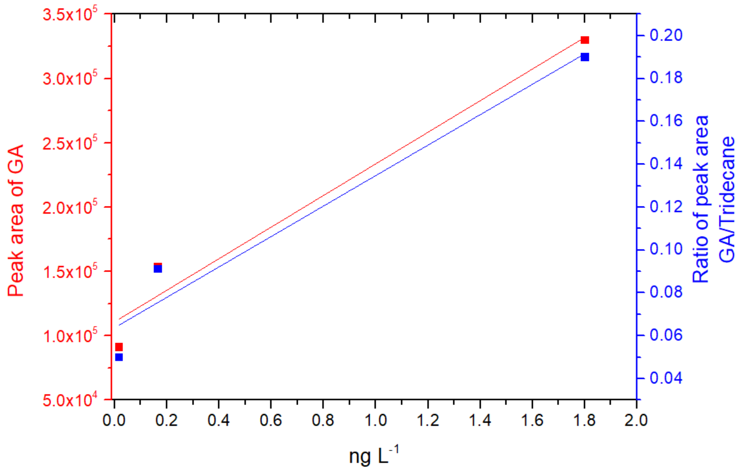

$$y = 122903.5514x + 110856.6$$
$$R^2 = 0.98$$

$$y = 0.07102x + 0.0638$$
$$R^2 = 0.98$$

A.6 The calibration curves for hydroxyl compounds, alcohols and carboxylic acids.

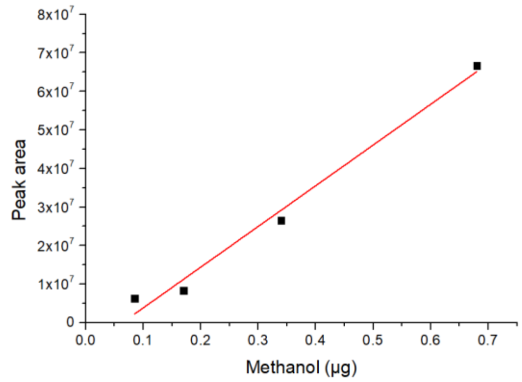

$$y = 105628000x$$
$$R^2 = 0.99$$

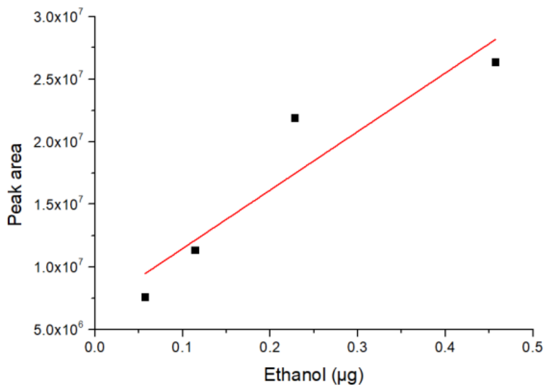

$$y = 46768300x + 6784950$$
$$R^2 = 0.94$$

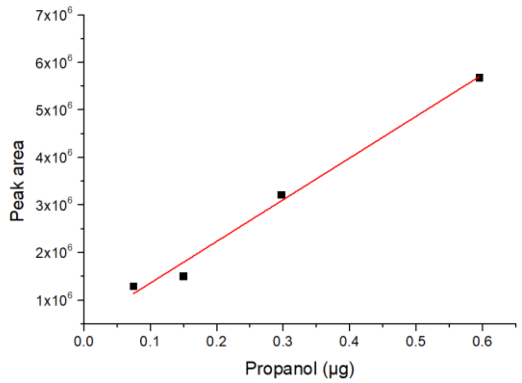

$$y = 8770410x + 483800$$
$$R^2 = 0.99$$

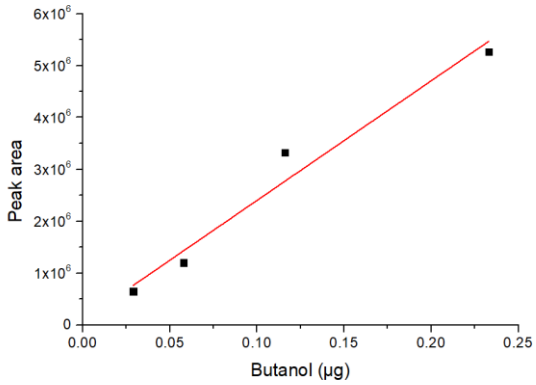

$$y = 23060400x + 94963$$
$$R^2 = 0.98$$

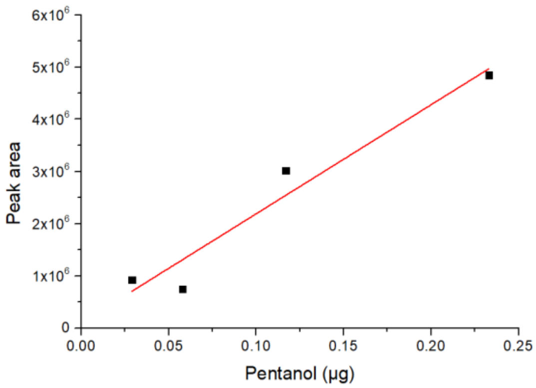

$$y = 20895800x + 100214$$
$$R^2 = 0.97$$

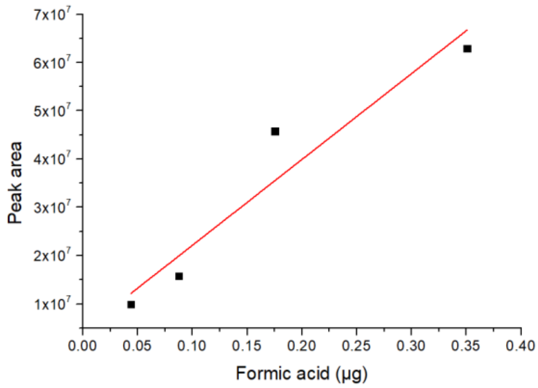

$$y = 177868000x + 4353500$$
$$R^2 = 0.96$$

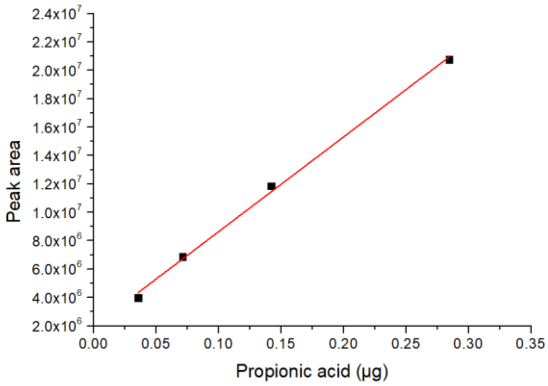

$$y = 66703700x + 1970550$$
$$R^2 = 0.99$$

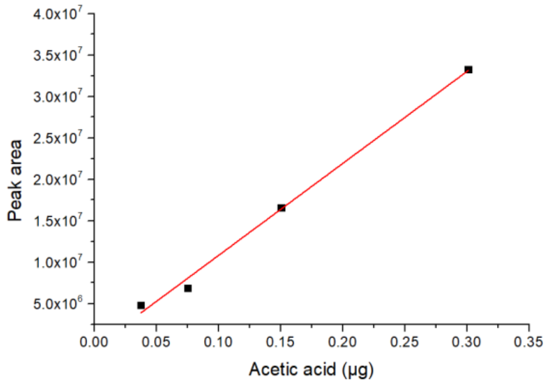

$$y = 111004000x$$
$$R^2 = 0.99$$

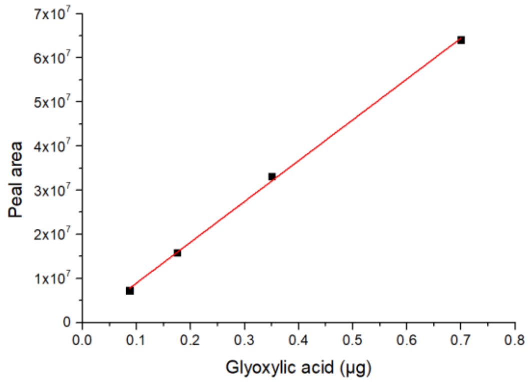

$$y = 92509900x + 633670$$
$$R^2 = 0.97$$

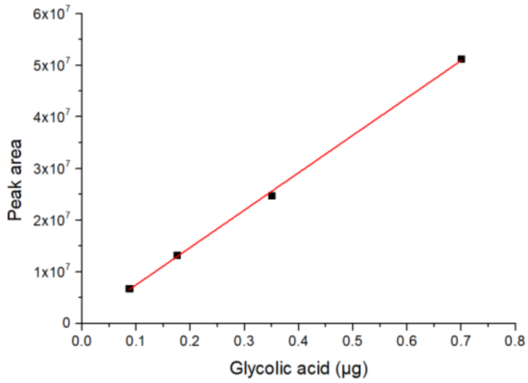

$$y = 72408800x + 232727$$
$$R^2 = 0.99$$

A.7 **The calibration curves for carbonyl compounds derivatization on Tenax® tube pre-coated with PFBHA.**

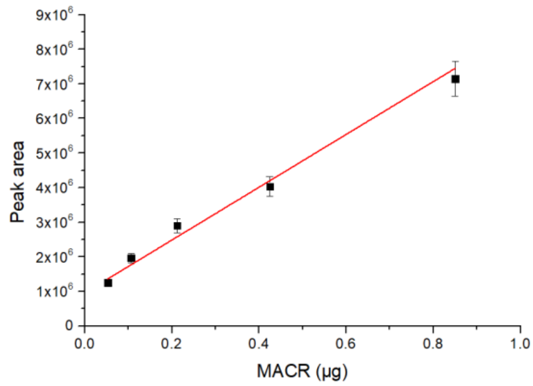

$$y = 7633530x + 959661$$
$$R^2 = 0.99$$

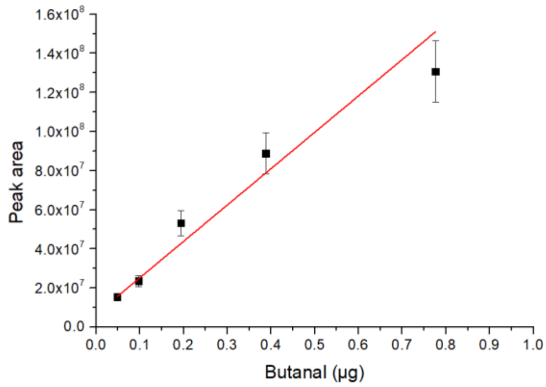

$$y = 186013000x + 6594000$$
$$R^2 = 0.98$$

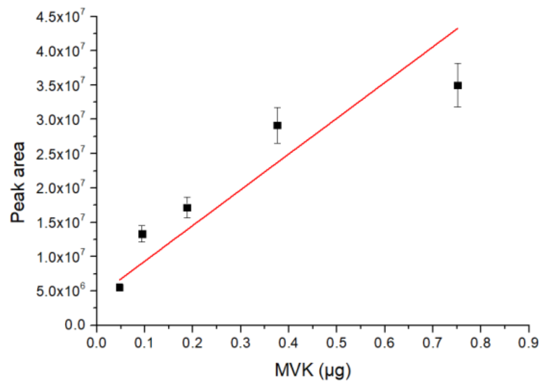

$$y = 52054700x + 4141750$$
$$R^2 = 0.92$$

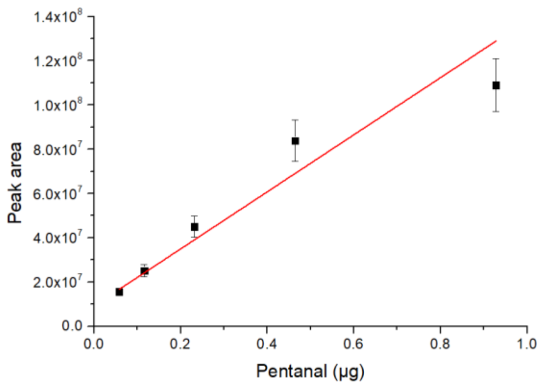

$$y = 128955000x + 9186610$$
$$R^2 = 0.97$$

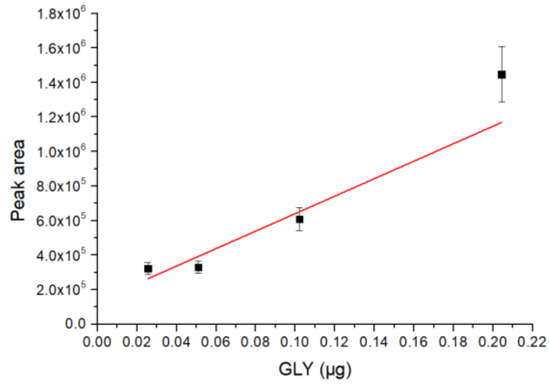

$$y = 5060800x + 134421$$
$$R^2 = 0.92$$

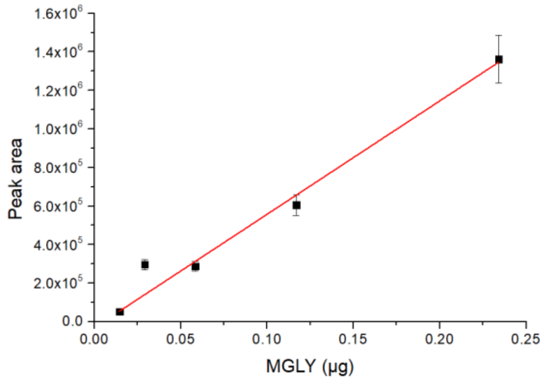

$$y = 5884610x$$
$$R^2 = 0.95$$

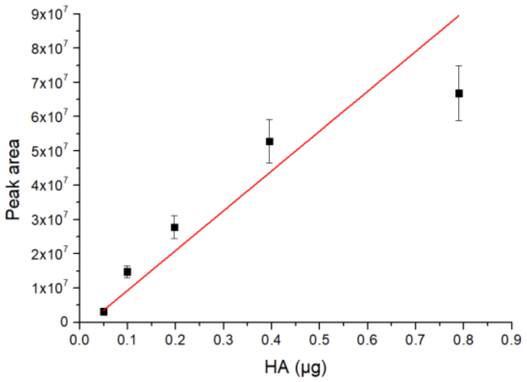

$$y = 116131000x$$
$$R^2 = 0.94$$

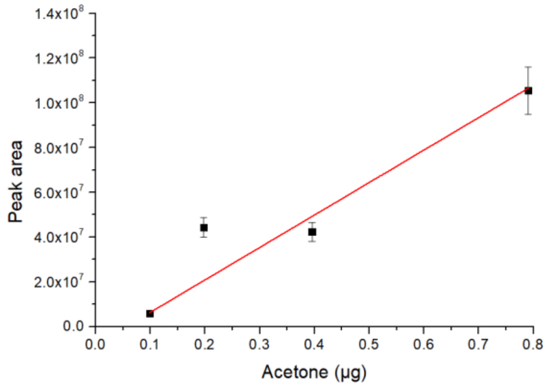

$$y = 145048000x$$
$$R^2 = 0.93$$

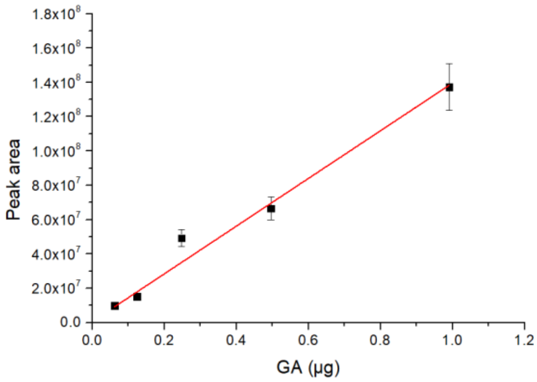

$$y = 138994000x + 633670$$
$$R^2 = 0.97$$

A.8 **Chromatogram of hydroxyl compound standards prepared and derivatized with MTBSTFA (extracted by characteristic ions m/z from total SIM ion chromatogram). Peak identification is noted with corresponding compound by red arrow.**

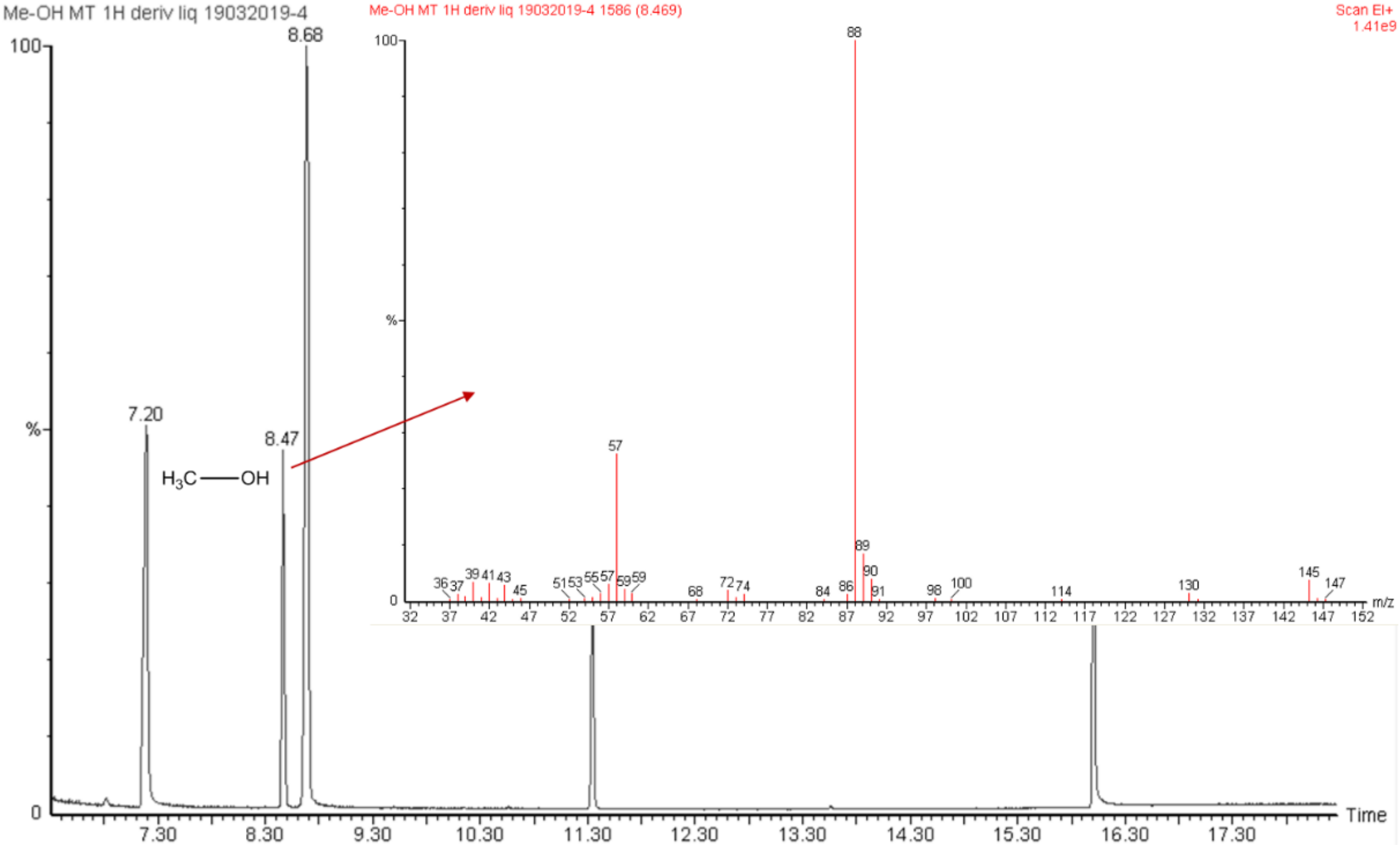

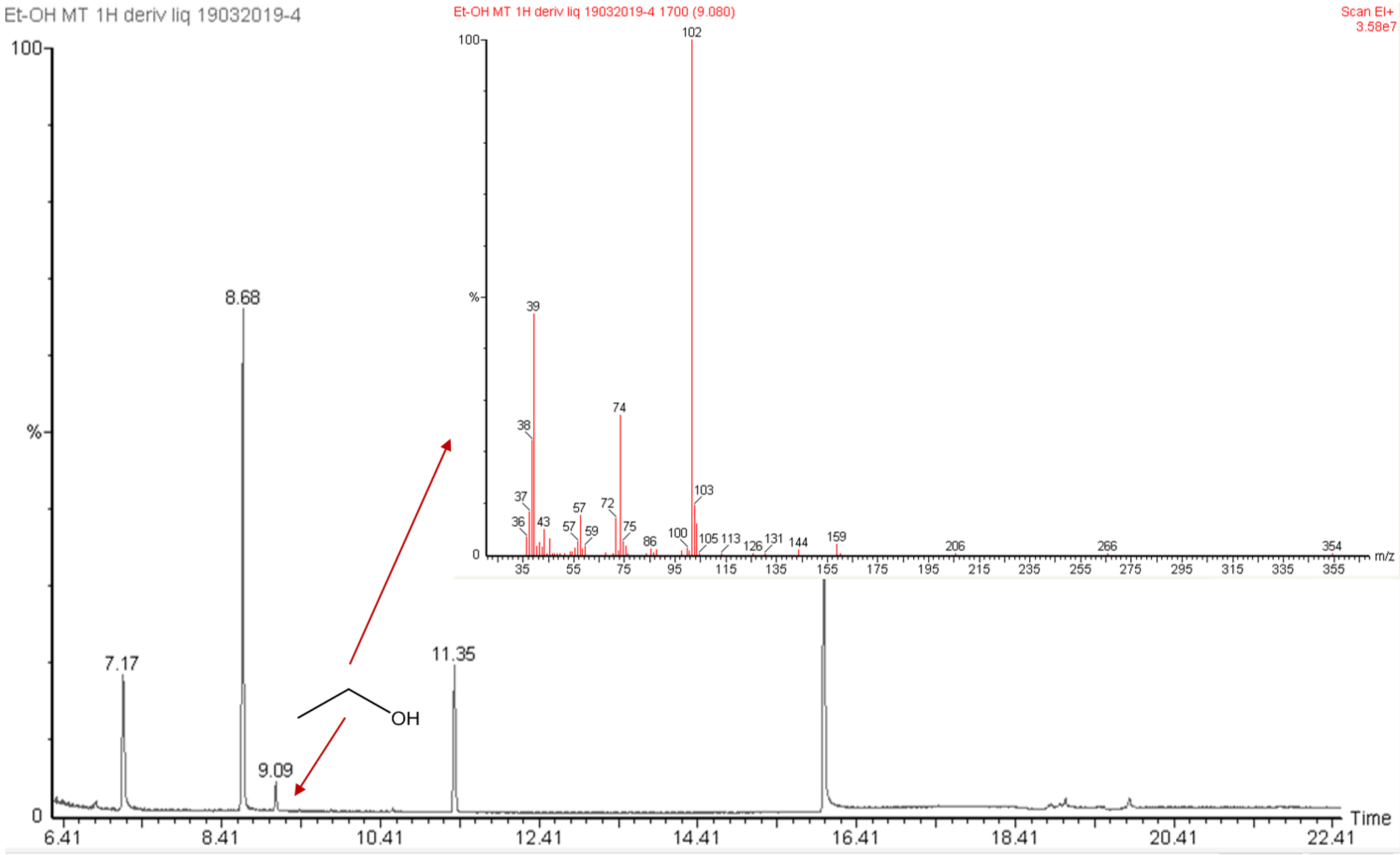

Et-OH MT 1H deriv liq 19032019-4
100
%
0
7.17
8.68
9.09
11.35
OH
Time
6.41
8.41
10.41
12.41
14.41
16.41
18.41
20.41
22.41
Et-OH MT 1H deriv liq 19032019-4 1700 (9.080)
Scan EI+
3.58e7
102
39
38
74
37
36
43
57
57
59
72
75
86
100
103
105
113
126
131
144
159
206
266
354
m/z

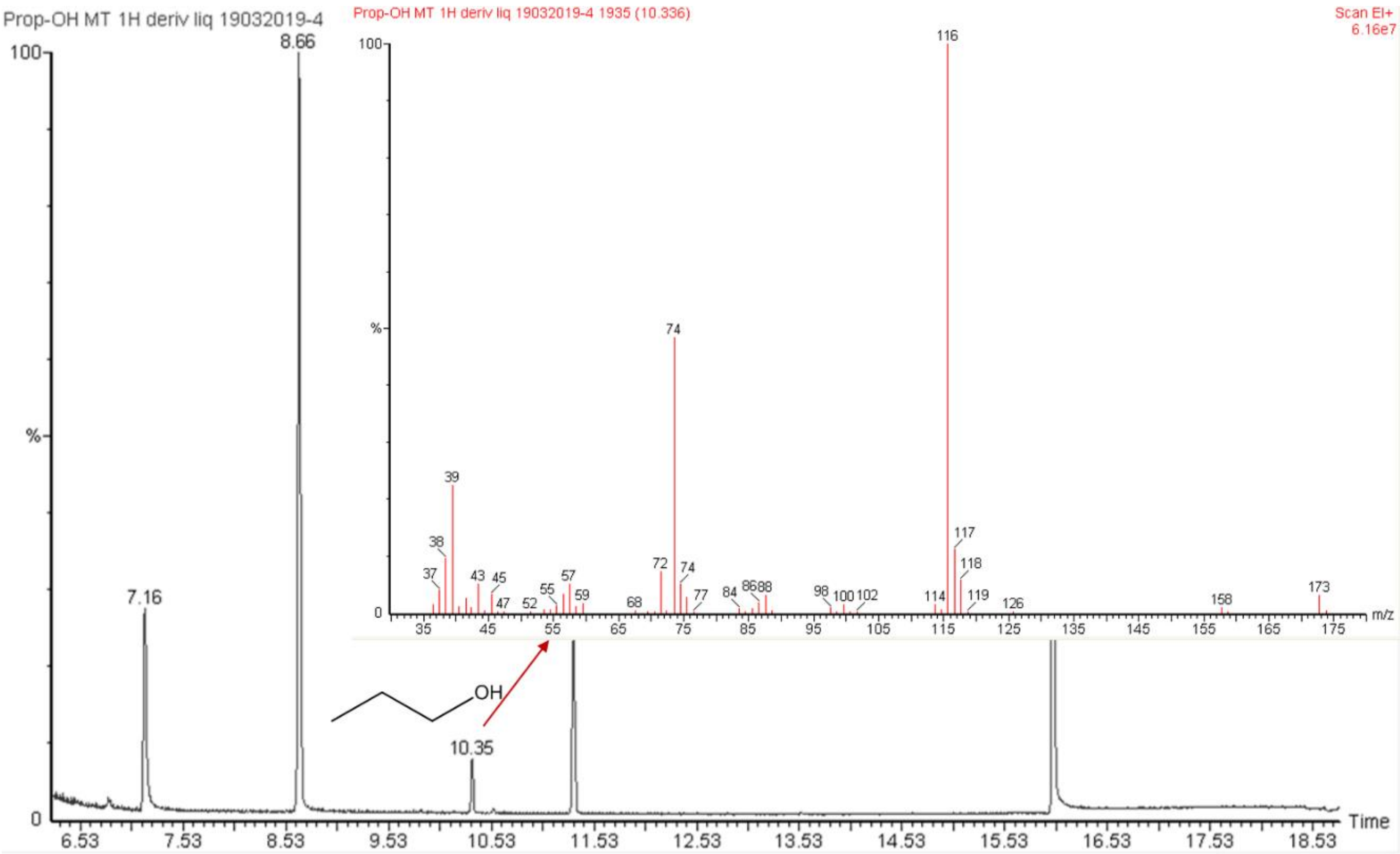

Prop-OH MT 1H deriv liq 19032019-4
8.66
7.16
10.35
OH
Time
Prop-OH MT 1H deriv liq 19032019-4 1935 (10.336)
Scan EI+
6.16e7
116
74
39
117
118
m/z
173
158

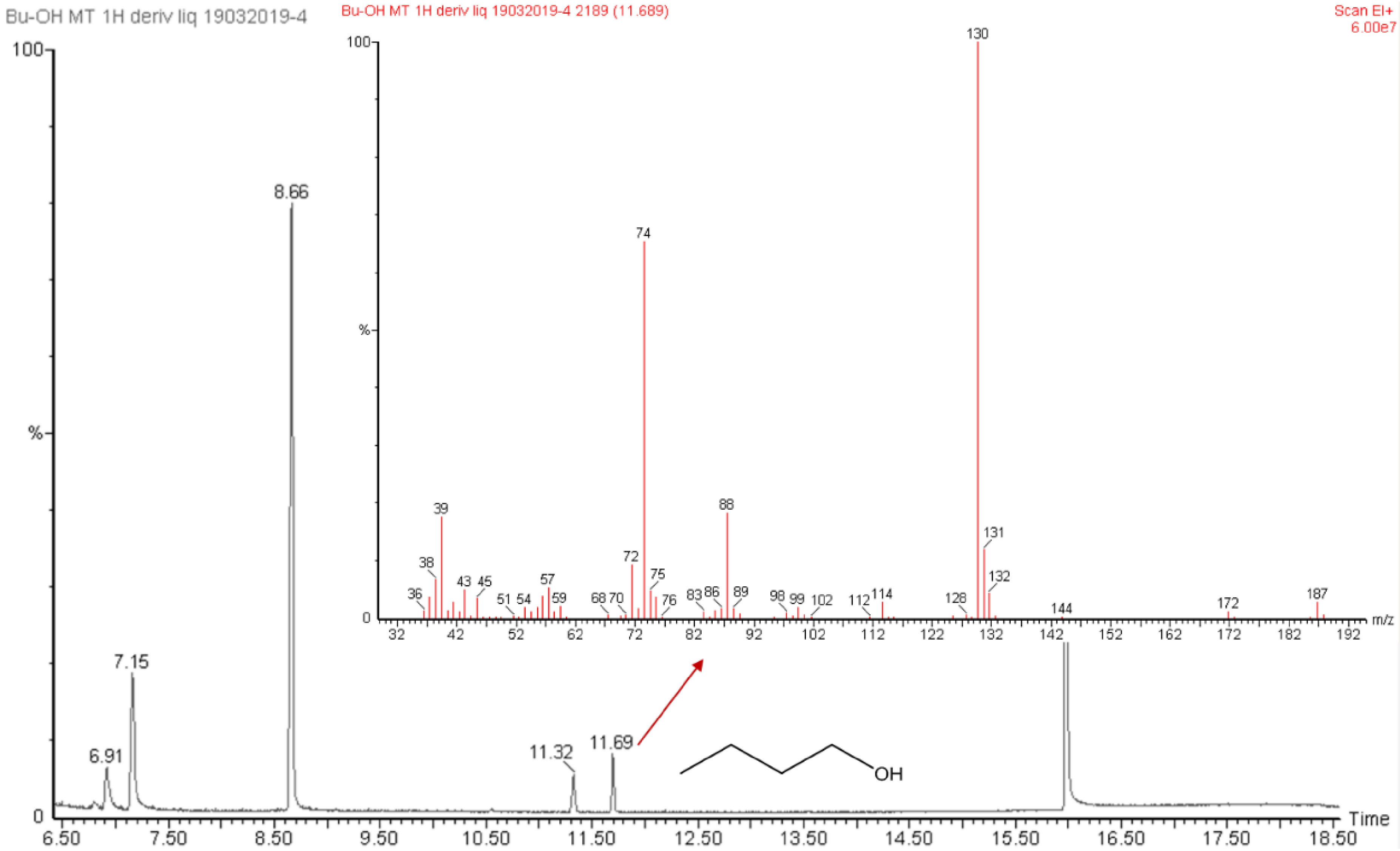
Bu-OH MT 1H deriv liq 19032019-4
Bu-OH MT 1H deriv liq 19032019-4 2189 (11.689)
Scan EI+
6.00e7
130
74
88
39
131
132
72
75
187
172
144
Time
m/z
6.91
7.15
8.66
11.32
11.69
OH

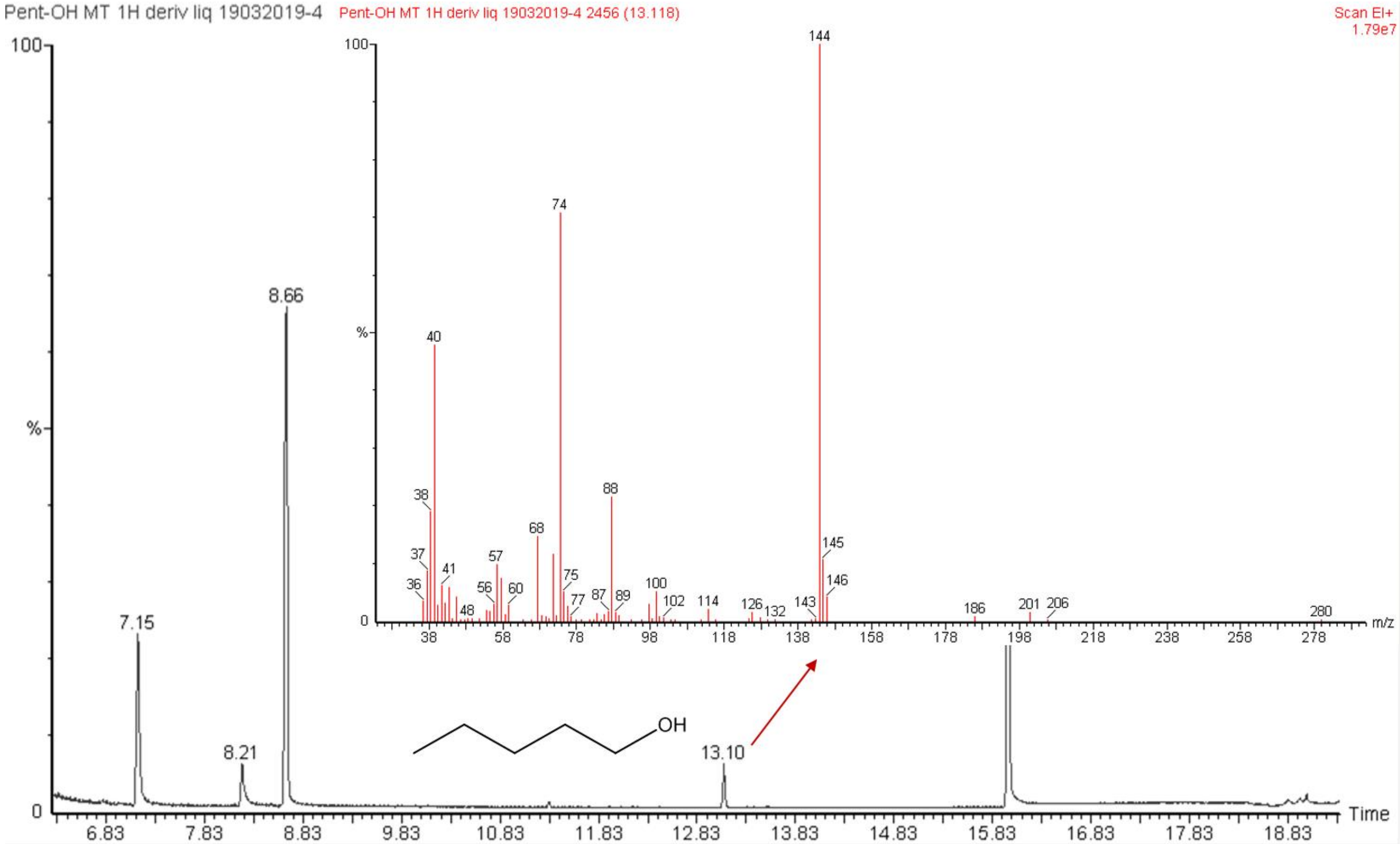
Pent-OH MT 1H deriv liq 19032019-4
Pent-OH MT 1H deriv liq 19032019-4 2456 (13.118)
Scan EI+
1.79e7
100
%
0
Time
m/z
7.15
8.21
8.66
13.10
OH
144
74
40
38
88
68
37
57
41
36
56
60
75
77
87
89
100
102
114
126
132
143
145
146
48
186
201
206
280

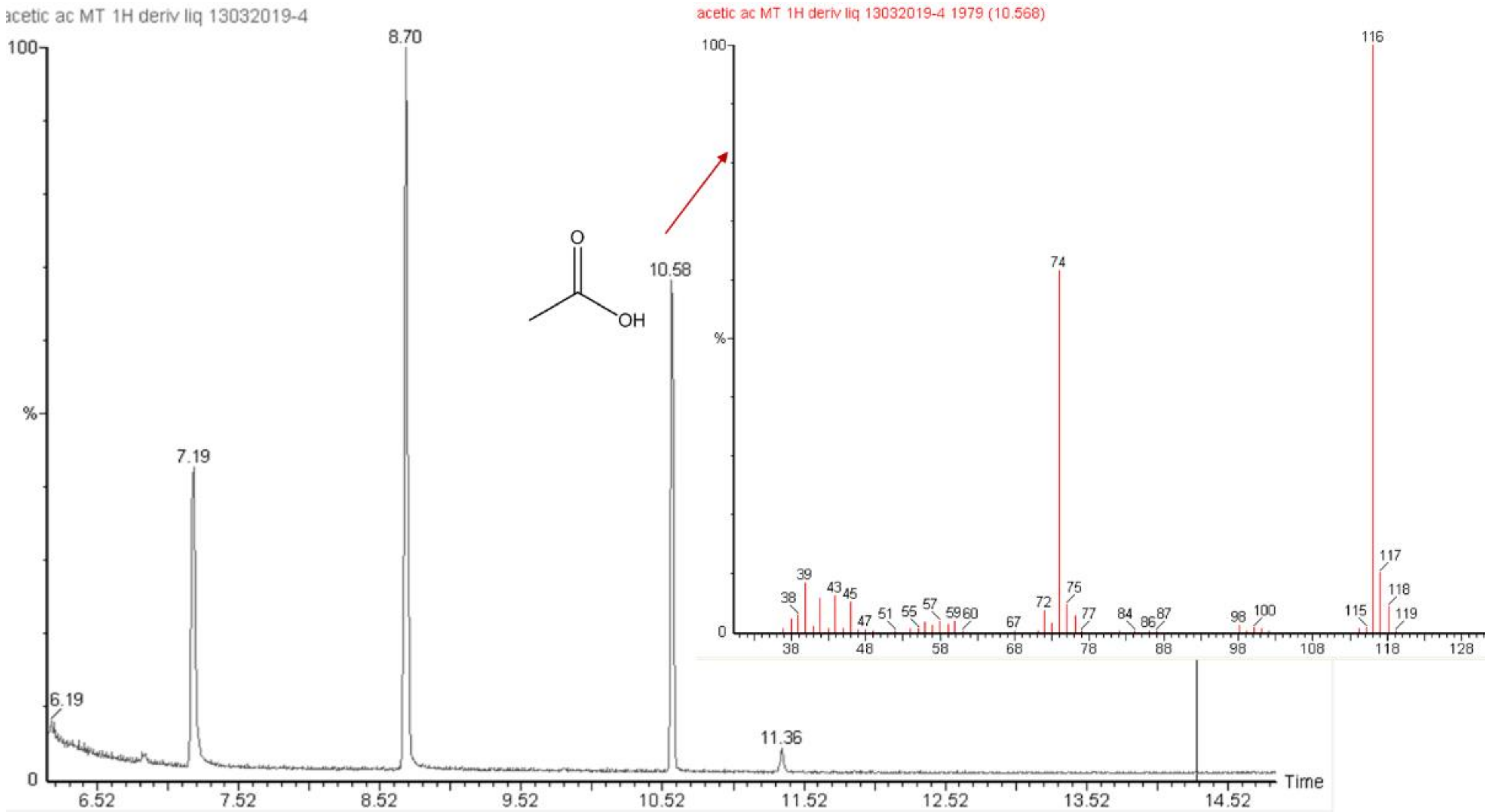

acetic ac MT 1H deriv liq 13032019-4
acetic ac MT 1H deriv liq 13032019-4 1979 (10.568)
8.70
10.58
7.19
6.19
11.36
OH
O
Time
116
74

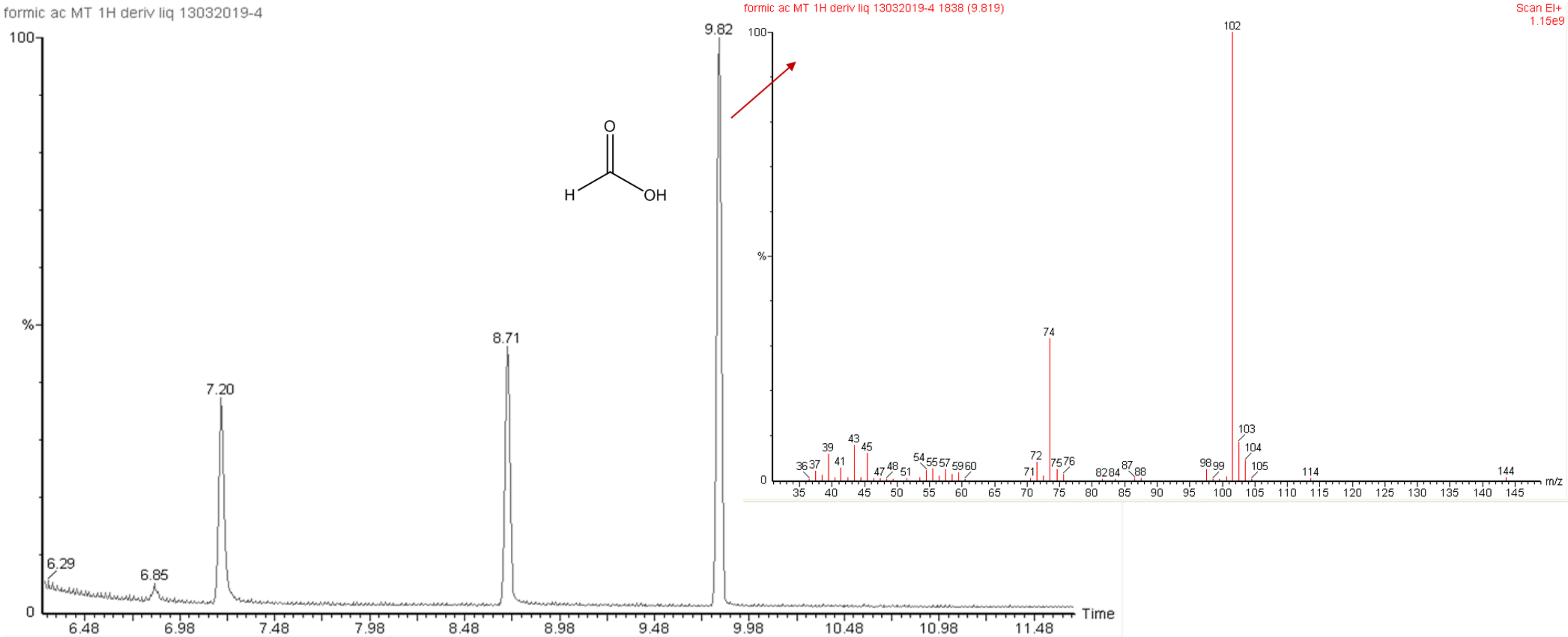
formic ac MT 1H deriv liq 13032019-4
100
%
0
9.82
8.71
7.20
6.29
6.85
6.48
6.98
7.48
7.98
8.48
8.98
9.48
9.98
10.48
10.98
11.48
Time
O
H
OH
formic ac MT 1H deriv liq 13032019-4 1838 (9.819)
Scan EI+
1.15e9
102
74
103
104
105
114
144
m/z

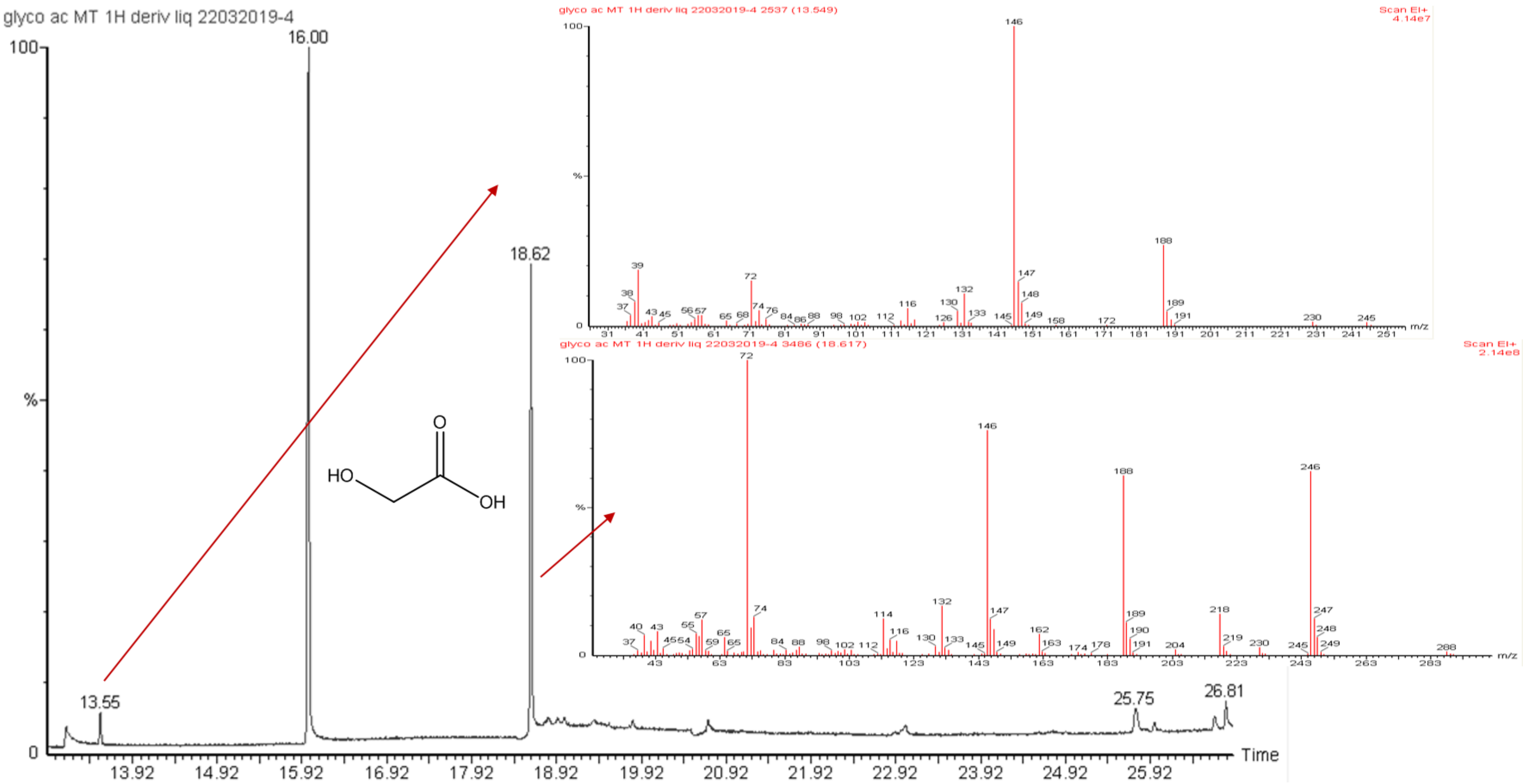
glyco ac MT 1H deriv liq 22032019-4
glyco ac MT 1H deriv liq 22032019-4 2537 (13.549)
Scan EI+
4.14e7
glyco ac MT 1H deriv liq 22032019-4 3486 (18.617)
Scan EI+
2.14e8
16.00
18.62
13.55
25.75
26.81
Time
HO
OH
O
m/z

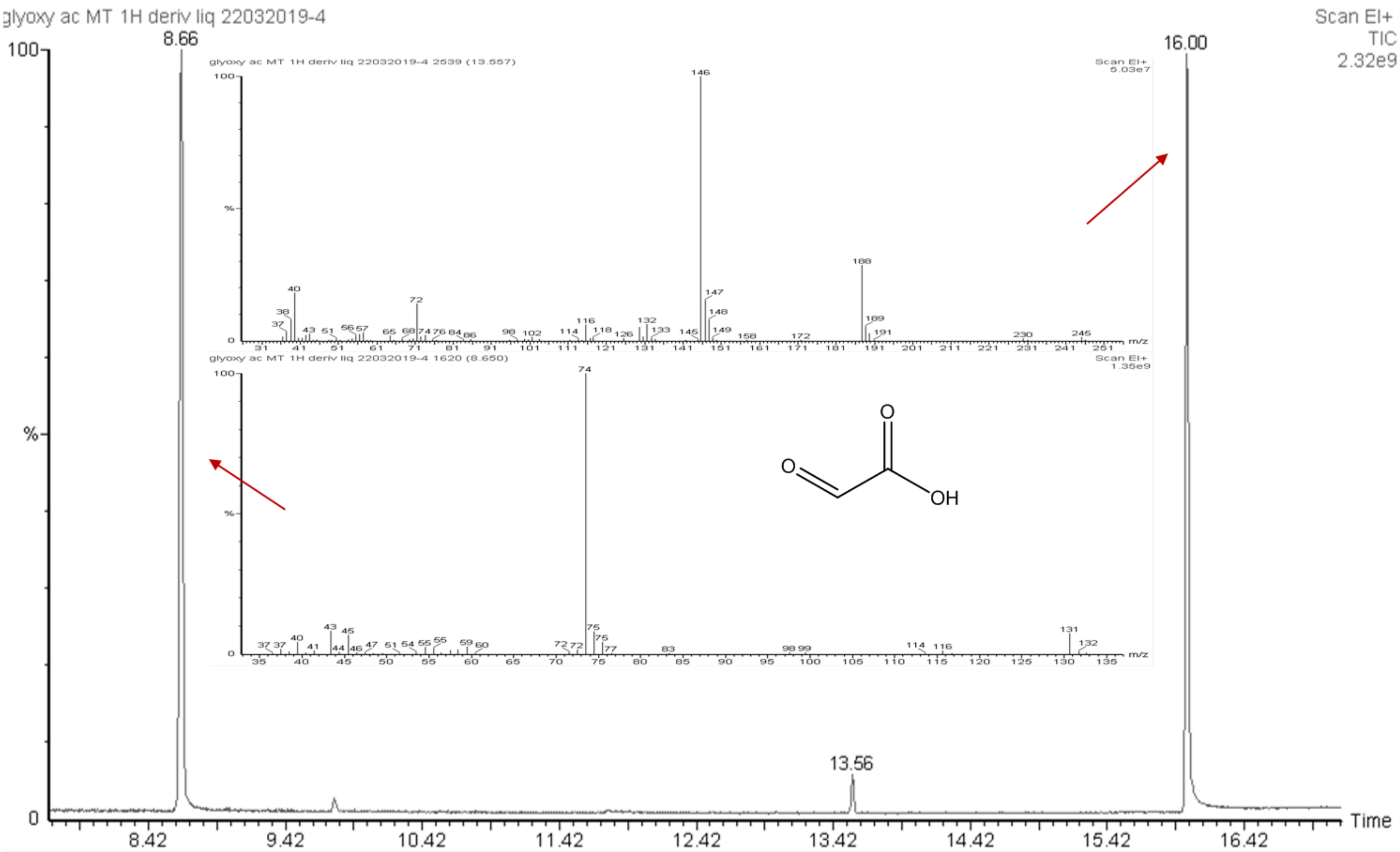

glyoxy ac MT 1H deriv liq 22032019-4
Scan EI+
TIC
2.32e9
8.66
16.00
13.56
glyoxy ac MT 1H deriv liq 22032019-4 2539 (13.557)
Scan EI+
5.03e7
glyoxy ac MT 1H deriv liq 22032019-4 1620 (8.650)
Scan EI+
1.35e9
m/z
Time
OH

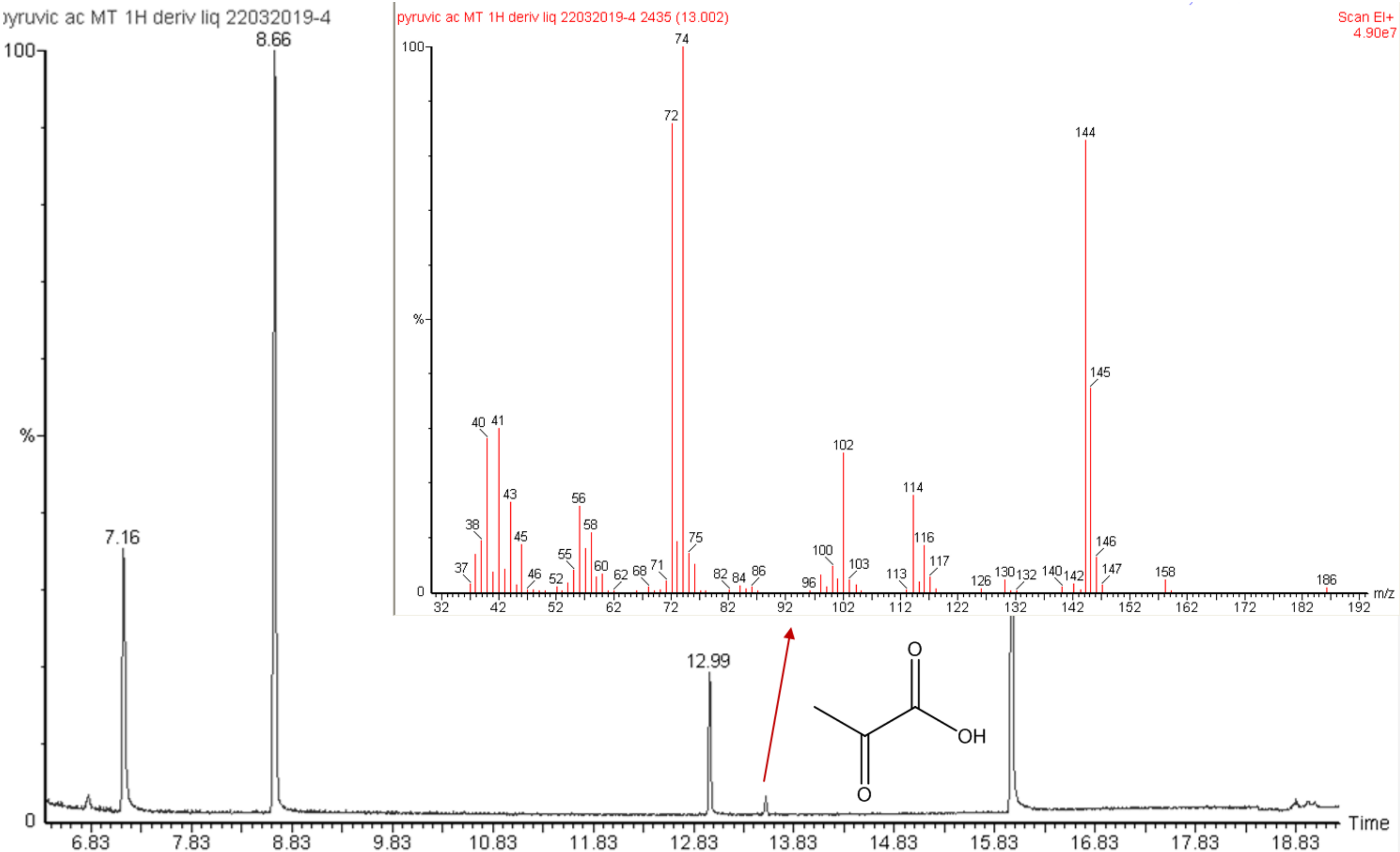

pyruvic ac MT 1H deriv liq 22032019-4
100
%
0
8.66
7.16
12.99
6.83 7.83 8.83 9.83 10.83 11.83 12.83 13.83 14.83 15.83 16.83 17.83 18.83
Time
pyruvic ac MT 1H deriv liq 22032019-4 2435 (13.002)
Scan EI+
4.90e7
74
72
144
145
40 41
102
43
56
114
38
58
45
75
116
146
55
60
100
103
117
37
46
52
62
68
71
82
84
86
96
113
126
130
132
140
142
147
158
186
m/z
32 42 52 62 72 82 92 102 112 122 132 142 152 162 172 182 192
O
OH
O

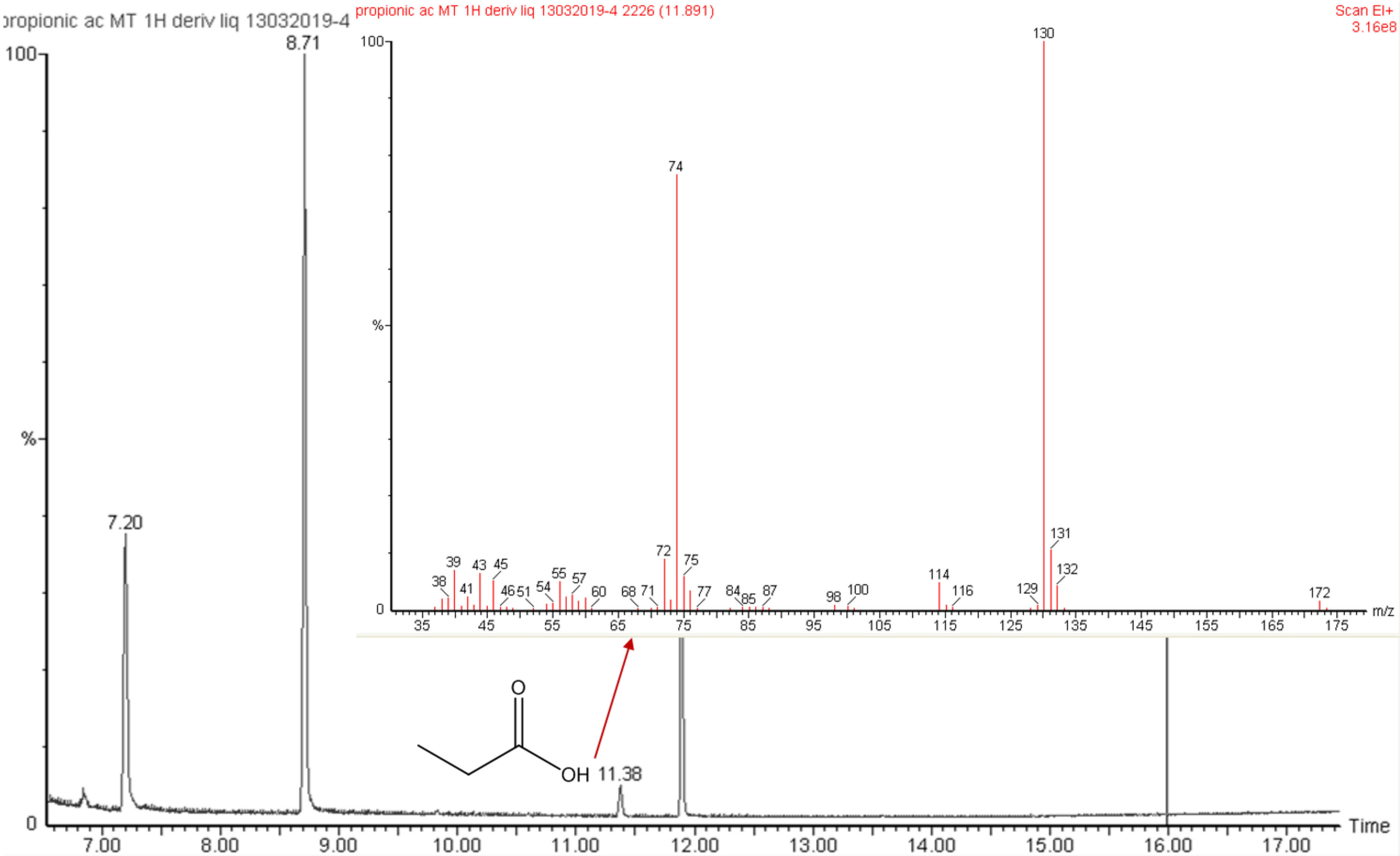

propionic ac MT 1H deriv liq 13032019-4
propionic ac MT 1H deriv liq 13032019-4 2226 (11.891)
Scan EI+
3.16e8
130
74
131
72
75
132
114
172
OH
7.20
8.71
11.38
Time
m/z
%

A.9 Comparison of VOC concentrations (min-max, mean value) in gaseous at PUY, HPB and CMN stations (pptv).

	PUY					
	Winter			Summer		
pptv	Min	Max	Mean	Min	Max	Mean
Isoprene	2.06	535.25	35.04	1.52	1391.81	124.65
Benzene	0.46	815.21	79.25	0.11	3287.97	176.55
n-Heptane	0.15	127.16	16.87	0.03	588.26	45.19
Toluene	0.49	774.95	31.56	0.47	1131.70	132.46
n-Octane	0.06	326.96	25.23	0.01	809.76	47.25
Ethylbenzene	0.06	38.45	7.00	0.02	762.71	61.18
m+p-Xylenes	0.09	117.37	14.05	0.08	1271.23	149.13
o-Xylene	0.09	98.96	0.013	0.02	1557.11	114.21
a-pinene	/	/	/	1.52	457.07	127.31
	HPB					
	Winter			Summer		
pptv	Min	Max	Mean	Min	Max	Mean
Isoprene	0	31.80	4.38	0.70	391.10	78.53
Benzene	0	999.65	297.04	0	105.60	36.21
n-Heptane	0	597.50	48.07	5.00	46.55	16.63
Toluene	0	1674.50	165.73	18.80	133.25	49.16
n-Octane	0	73.90	7.93	1.13	16.40	2.87
Ethylbenzene	0	276.40	29.77	0	24.40	9.04
m+p-Xylenes	0	1089.40	68.96	0	60.10	18.40
	CMN					
	Winter			Summer		
pptv	Min	Max	Winter	Min	Max	Summer
Isoprene	/	/	/	/	/	/
Benzene	39.48	702.23	171.46	21.62	63.88	37.62
n-Heptane	1.20	38.20	8.22	0.34	6.70	1.70
Toluene	9.05	387.00	76.62	7.84	81.62	29.59
n-Octane	0.46	10.48	2.98	0.48	2.92	1.23
Ethylbenzene	2.32	56.27	13.79	2.20	14.59	6.83
m+p-Xylenes	2.48	164.72	28.33	3.36	50.04	11.49
o-Xylene	0.46	29.23	5.94	0.47	10.02	2.31

A.10 Air mass backward-trajectories of the cloud events

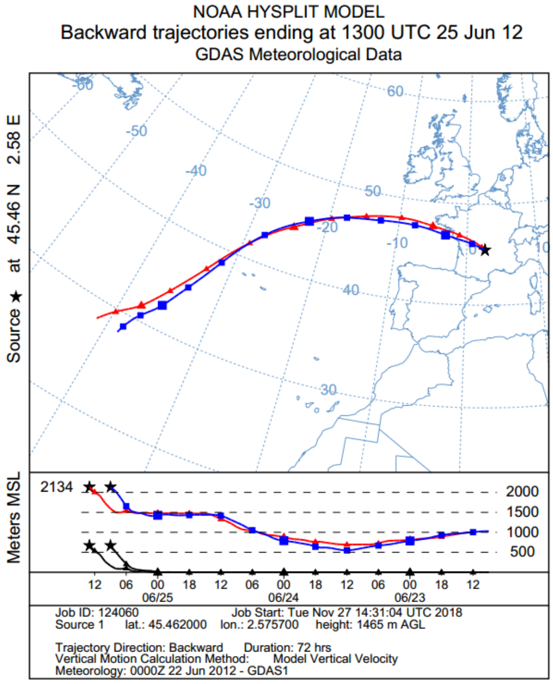

Cloud sample C1 06/25/2012

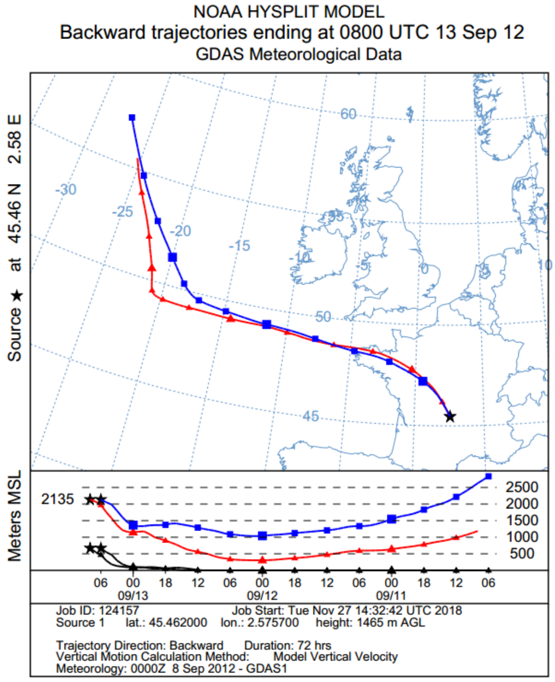

Cloud sample C2 09/13/2012

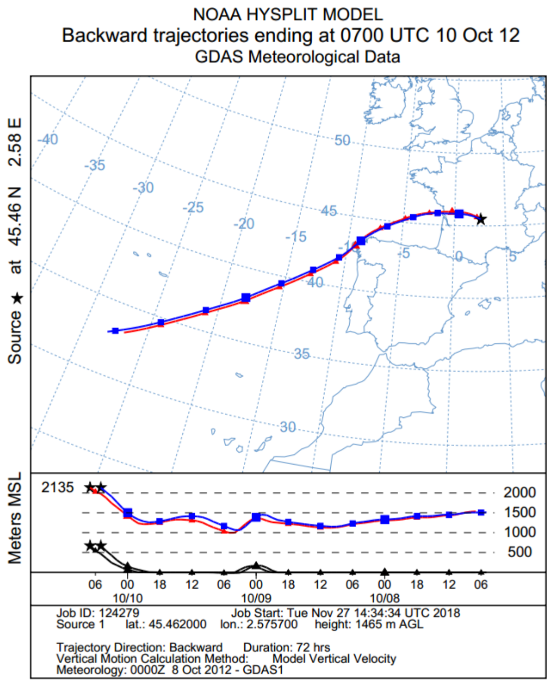

Cloud sample C3 10/10/2012

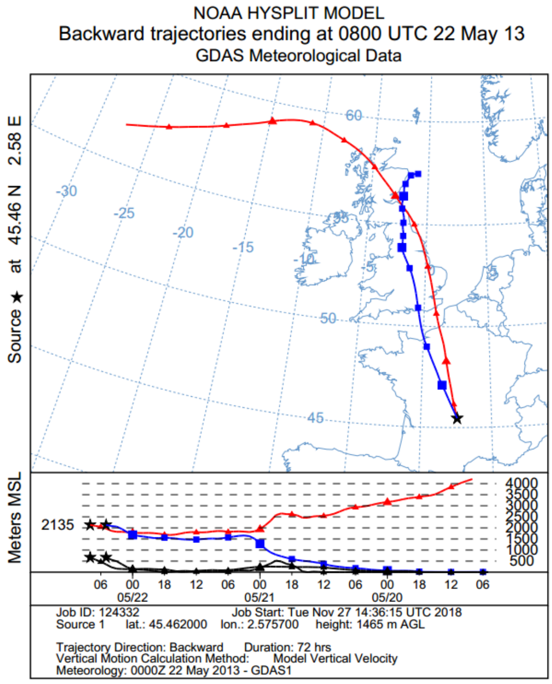

Cloud sample C4 05/22/2013

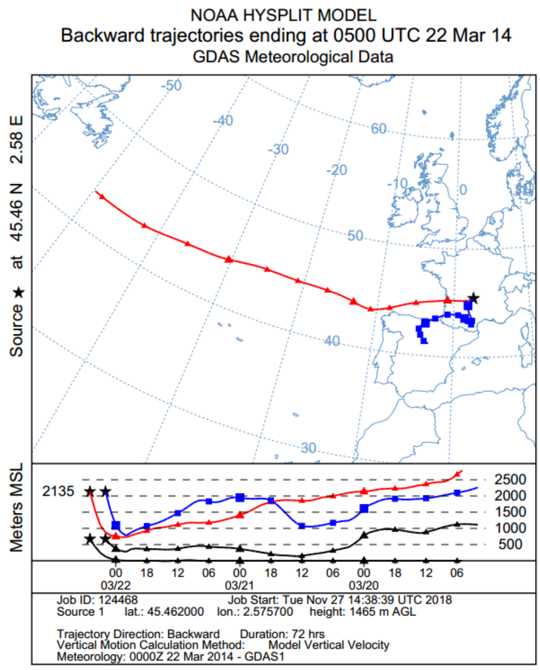

Cloud sample C5 S1 03/22/2014

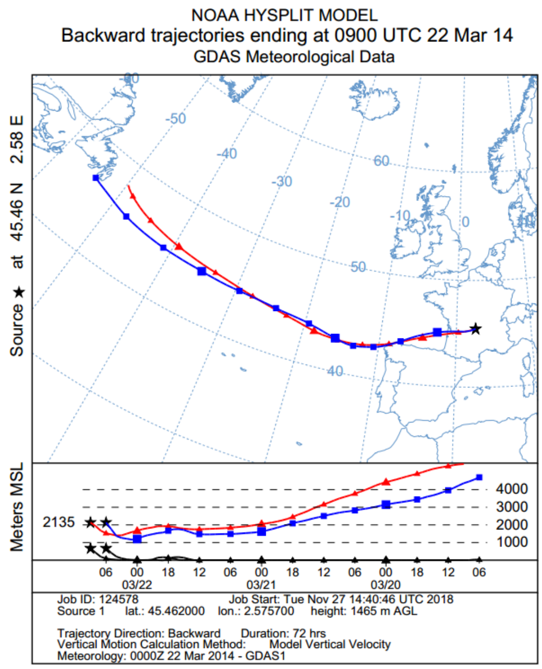

Cloud sample C5 S2 03/22/2014

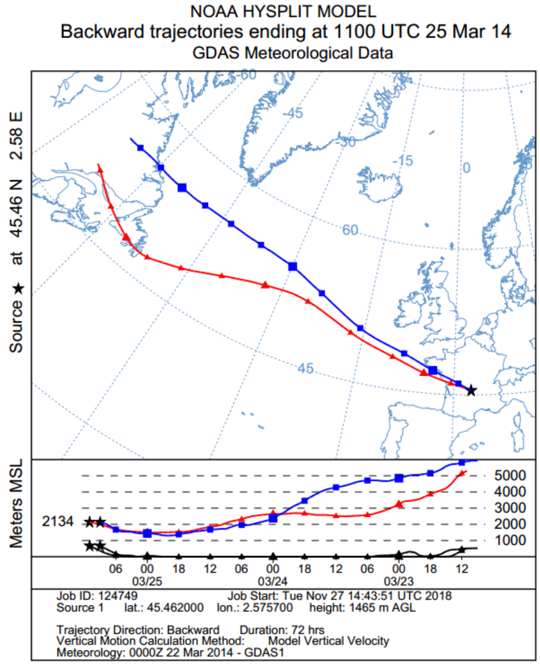

Cloud sample C6 S1 03/25/2014

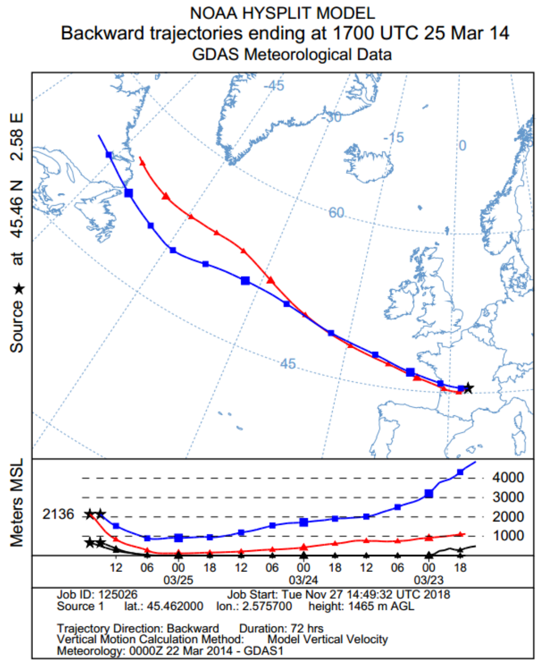

Cloud sample C6 S2 03/25/2014

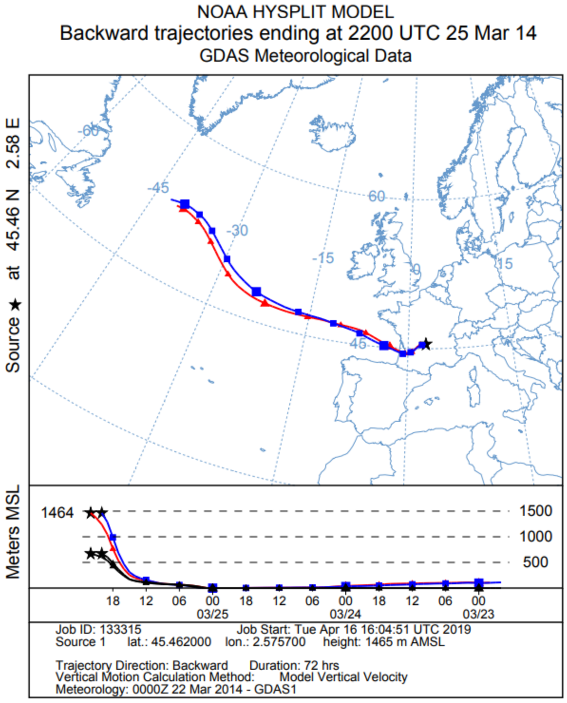

Cloud sample C6 S3 03/25/2014

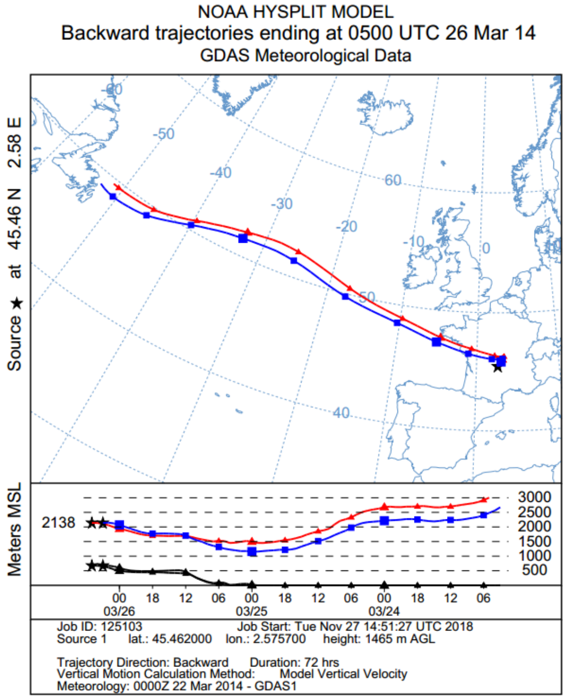

Cloud sample C7 S1 03/26/2014

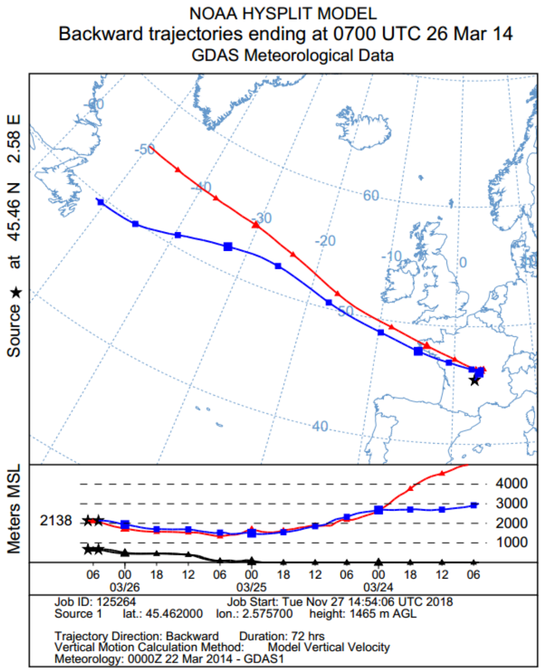

Cloud sample C7 S2 03/26/2014

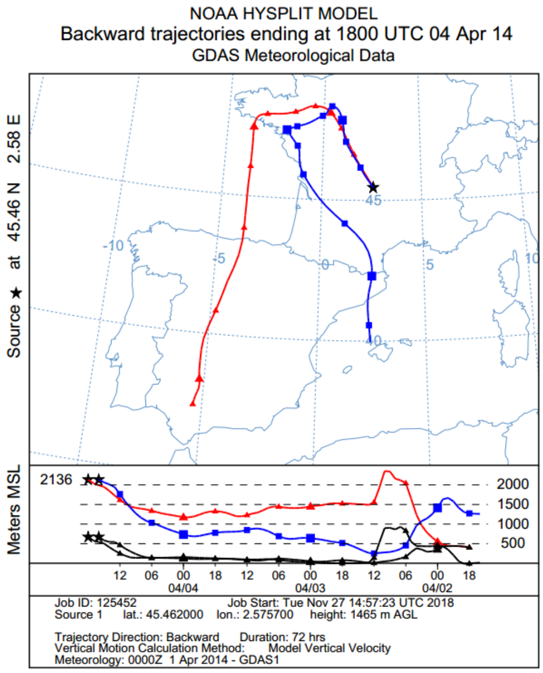

Cloud sample C8 S1 04/04/2014

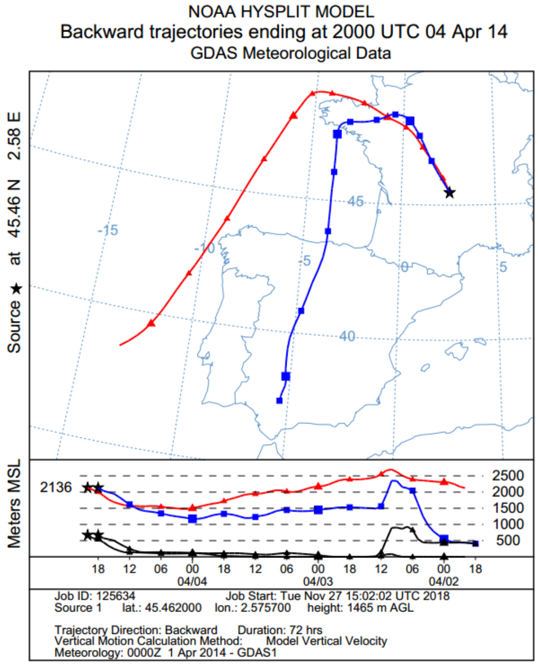

Cloud sample C8 S2 04/04/2014

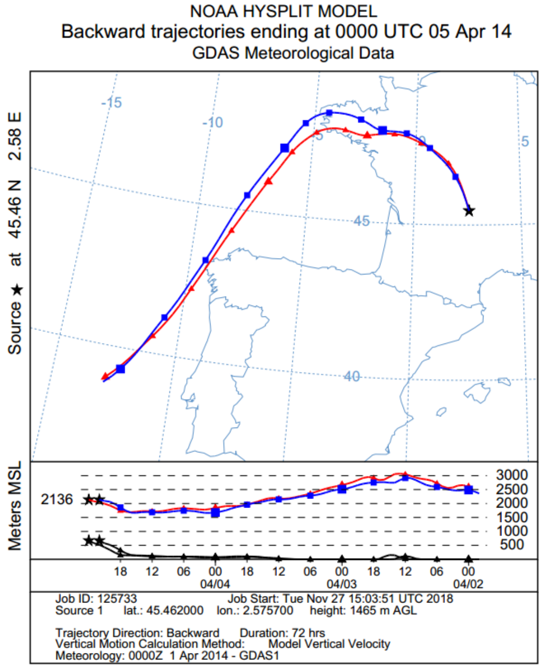

Cloud sample C9 S1 04/05/2014

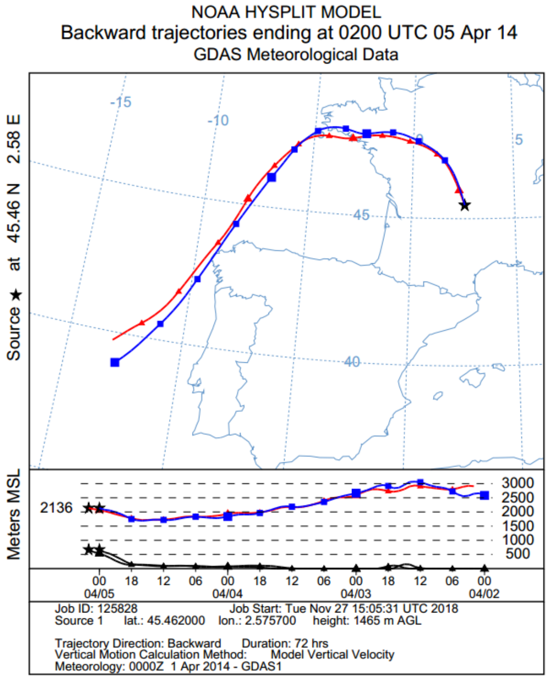

Cloud sample C9 S2 04/05/2014

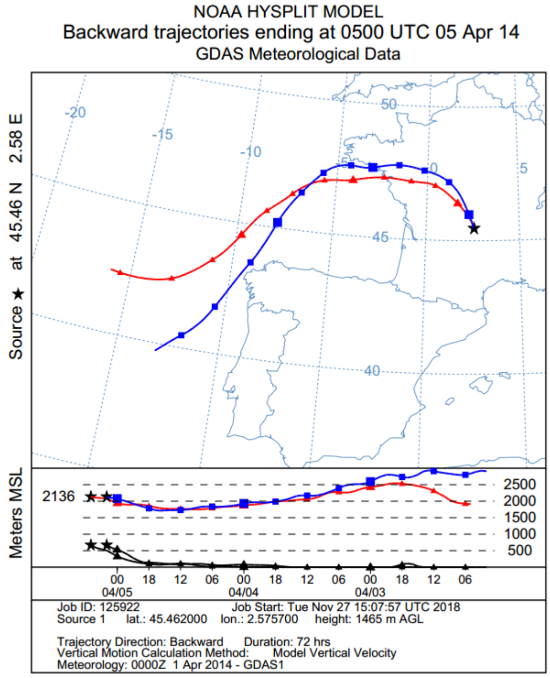

Cloud sample C9 S3 04/05/2014

A.11 Summary of the detected VOC concentrations (in ng mL^{-1} cloud water) measured in 11 cloud samples corresponding to 9 cloud events.

Cloud event / VOC (ng mL^{-1})	C1 Mar	C2 Mar	C3 Mar	C4 Mar	C5 S1 Mar	C6 S1 Mar	C7 S1 Cont	C8 S2 Mar	C9 S1 Mar	C9 S2 Mar	C9 S3 Mar
Isoprene	2.91	1.53	0.72	1.05	0.76	0.05	0.09	0.06	0.66	0.04	0.04
α-pinene	0.05	0.09	0.04	0.04	/	/	/	/	0.01	0.10	0.10
Benzene	0.71	0.47	0.45	0.40	0.32	0.02	0.63	1.62	0.88	0.93	0.70
Toluene	1.64	1.02	0.72	0.70	1.26	1.46	1.93	3.16	3.24	5.77	5.7
Ethylbenzene	0.28	0.20	0.11	0.11	0.16	0.10	0.14	0.13	0.01	0.15	0.17
m+p-xylene	0.61	0.40	0.26	0.24	0.47	0.45	0.57	0.27	0.05	0.41	0.44
o-xylene	0.39	0.31	0.24	0.15	0.59	0.74	1.04	0.36	0.14	0.74	0.79
Styrene	0.66	0.71	0.62	0.40	0.34	0.07	0.10	0.16	0.05	0.10	0.08
Isopropylbenzene (Cumene)	0.02	0.02	0.01	0.01	/	0.02	0.03	0.01	0.01	0.02	0.02
1,3,5-Trimethylbenzene	0.05	0.02	0.04	0.43	0.24	0.12	0.02	0.16	0.10	0.03	0.01
1,2,4-Trimethylbenzene	0.3	0.15	0.07	0.16	0.88	0.98	1.17	0.57	0.44	1.04	0.96
1,2,3-Trimethylbenzene	0.04	0.02	0.04	0.03	0.10	0.12	0.12	0.07	0.05	0.10	0.10
Naphtalene	0.07	0.09	0.03	0.09	0.02	0.07	0.19	0.05	0.01	0.02	0.10
n-propylbenzene	0.02	0.04	0.03	0.07	0.08	/	/	/	0.02	/	/
Limonene	0.1	0.06	0.04	0.08	/	/	/	/	/	/	/
Nopinone	5.26	0.56	0.81	0.77	1.99	1.05	1.71	0.50	0.51	/	0.13

A.12 Multi-component calibration mixture in nitrogen detailed with concentration, uncertainty and their CAS number.

Compounds	CAS#	Concentration (ppb)	Uncertainty
Formaldehyde	50-0-0	1072.6	±5%
Butane	106-97-8	178.9	±5%
Acetaldehyde	75-07-0	272.6	±5%
Methanol	67-56-1	305.5	±5%
Pentane	109-66-0	113.1	±5%
Ethanol	64-17-5	211.6	±5%
Propanal	123-38-6	166.1	±5%
Acetone	67-64-1	253.7	±5%
2-Propanol	67-63-0	110.8	±5%
Methacrolein	75-85-3	145.3	±5%
Butanal	123-72-8	117.0	±5%
Methyl vinyl ketone	78-94-4	190.2	±5%
Methyl ethyl ketone	78-93-3	109.2	±5%
2-Methyl,3-buten-2-ol	115-18-4	190.6	±5%
Toluene	108-88-3	100.1	±5%

Noted that the uncertainty is a conservative estimate of the combination of the uncertainties of the gravimetric preparation and analysis.

A.13 Calibration curve slope, linearity and Y-intercept of carbonyl compounds for on-sorbent-tube derivatization, in-solution derivatization and derivatization-SBSE (MVK: methyl vinyl ketone; MACR: methacrolein; GLY: glyoxal; MGLY: methl glyoxal; HA: hydroxyacetone).

	Compounds	Butanal	Pentanal	MVK	MACR	GLY	MGLY	Acetone	HA
In solution derivatization	Calibration curve slope	$1.0\ 10^{8}$	$8.0\ 10^{7}$	$1.0\ 10^{8}$	$6.0\ 10^{7}$	$7.0\ 10^{6}$	$9.0\ 10^{6}$	$7.0\ 10^{7}$	$3.0\ 10^{7}$
	Linearity	0.99	0.99	0.99	0.99	0.83	0.79	0.99	0.99
	Y-intercept	110147	90018	35771	7641.1	31695	45670	23766	5626.4
On-Tenax derivatization	Calibration curve slope	$2.0\ 10^{8}$	$1.0\ 10^{8}$	$4.0\ 10^{7}$	$7.0\ 10^{6}$	$7.0\ 10^{6}$	$6.0\ 10^{6}$	$1.0\ 10^{8}$	$8.0\ 10^{7}$
	Linearity	0.96	0.93	0.90	0.99	0.96	0.98	0.91	0.90
	Y-intercept	$1.0\ 10^{7}$	$2.0\ 10^{7}$	$9.0\ 10^{6}$	$1.0\ 10^{6}$	45678	7701.5	$2.0\ 10^{6}$	$8.0\ 10^{6}$
In solution derivatization SBSE	Calibration curve slope	$2.0\ 10^{8}$	$2.0\ 10^{8}$	$1.0\ 10^{8}$	$1.0\ 10^{8}$	$5.0\ 10^{7}$	$5.0\ 10^{7}$	$1.0\ 10^{8}$	$5.0\ 10^{7}$
	Linearity	0.99	0.99	0.99	0.99	0.80	0.75	0.99	0.99
	Y-intercept	277767	222809	9587.3	16384	61169	112623	69610	33362